CRANFIELD INSTITUTE OF TECHNOLOGY

DEPARTMENT OF FLUID ENGINEERING AND INSTRUMENTATION

PhD THESIS

Academic Year 1985-6

D.M.HALSEY

The character of swirl in turbulent pipe flow with reference to its effect on flowmeters

Supervisor Dr. J. Hemp

September 1986

ABSTRACT

A theoretical and experimental investigation of the character of swirl in turbulent pipe flow has been carried out and some implications for the use of flowmeters considered.

An extensive survey of industrial users of flowmeters has been made, involving the participation of over 70 companies, which provides information about current industrial practice, attitudes and understanding.

Axisymmetric perturbations of fully developed turbulent pipe flow have been studied using the mixing-length model of turbulence. A linearised theory finds the character of small perturbations, decaying exponentially in the axial direction, in which the tangential and axial motion are independent. A non-linear similarity theory finds the flow field at a particular cross-section of the pipe assuming it to be determined by the specification of the Reynolds number, the pipe's roughness and the swirl number at that cross-section.

Laser Doppler Anemometry was used to measure axial and tangential velocities on 4 equidistant cross-sections of a pipe following a double right-angle bend in two perpendicular planes. It was found that the tangential velocity had the form of a solid body rotation and decayed exponentially. The axial velocity profile after the bend was asymmetrical, having the form of a horseshoe which rotated with the swirl whilst returning to its fully developed form.

Theoretical studies of the effect of the measured axial velocity profiles on the accuracy of electromagnetic and ultrasonic flowmeters are presented.

It is suggested that the decay of the level of swirl in turbulent pipe flow after a double bend be modelled by the factor exp(-6fz/D) where f is the friction factor in fully developed flow and z/D the non-dimensionalised axial distance. The accuracy of flowmeters installed at particular locations downstream can then be predicted once the appropriate error characteristics of flowmeters are known. Some indications of these characteristics are presented.

For my parents

You hurled me into the deep, into the very heart
of the seas, and the currents swirled about me;
all your waves and breakers swept over me.

Jonah 2:3

Jesus said, 'Everyone who drinks this water will
be thirsty again, but whoever drinks the water I
give him will never thirst. Indeed, the water
I give him will become in him a spring of
water welling up to eternal life.'

John 4:13-14

For to me, to live is Christ
and to die is gain.

Philippians 1:21

LIST OF CONTENTS

LIST OF FIGURES

LIST OF PLATES

PRINCIPAL NOTATION

Symbol	Description	Section where first used or defined
Roman: Upper case		
D	Pipe diameter = 2a	3.5.1
ER	Maximum error permitted	5.1.1
F	Non-dimensionalising factor	4.3.1
G(r)	Radial part of U^{θ} in similarity theory	4.5
H(r)	Radial part of v in similarity theory	4.5
I	Measure of fully developed flow normalisation	5.1.1
K_M	Turbine meter factor	6.2.1
L	Mixing length	3.4
$\underline{Q}, Q_i$	Instantaneous velocity: vector and suffix forms	3.2
N	Number of samples	6.3.5
P	Instantaneous pressure,	3.2
	Modified mean perturbation pressure	4.2.1
Re	Reynolds number	3.3, 3.5.1
Ri	Gradient Richardson's number	3.7.2
R_τ	Friction Reynolds number	4.2.2
S	Swirl number	3.7.1
$\underline{U}$	Mean perturbation velocity	4.2.1
U_{av}	Average value of the mean axial velocity in a pipe	3.5.1
U_C	Centreline value of the mean axial velocity in a pipe	3.5.2
U_m	Velocity being measured	6.3.5
V(r)	Axial component of the mean velocity in fully developed flow	3.5.1

Symbol	Description	Section where first used or defined
Roman: lower case		
a	Pipe radius	3.5.1
f	Friction factor in fully developed flow	3.5.1
$f+f_e$	Friction factor in swirling flow	5.4
f_D	Doppler frequency	6.3.5
f_t	Frequency output of turbine meter	6.2.1
g(r)	Radial part of U^θ in linear theory	4.3.2
h(r)	Radial part of v in linear theory	4.3.3
k	Kinetic energy of turbulence,	3.4
	Prandtl's constant	3.5.2
$\underline{q}$	Fluctuating part of $\underline{Q}$	3.3
r	Radial component in cylindrical polar coordinates	3.5.1
t	Time	3.2
u_τ	Friction velocity	3.5.1
$\underline{x}$	Position vector	3.2
y	Distance from pipe wall = a - r	3.5.2
z	Axial component in cylindrical polar coordinates	3.5.1

Symbol	Description	Section where first used or defined
Greek		
β	Ratio of diameters of orifice and pipe	3.8
δ_{ij}	Kronecker delta (=1 if i=j, =0 if i≠j)	3.4
δ_f	Fringe separation	6.3.4
ϵ	Eddy viscosity	3.4
ϵ_o	Eddy viscosity in fully developed flow	3.5.1
ϵ_R	Roughness parameter	3.5.4
θ	Angular coordinate in cylindrical polar coordinates,	3.5.1
	Half angle between laser beams	6.3.4
λ	Exponential decay rate of tangential velocity in swirling flow,	3.7.3
	Wavelength	6.3.4
μ	Exponential decay rate of stream function,	4.3.3
	Mean of normal distribution	6.3.5
ν	Kinematic viscosity	3.2
ρ	Density	3.2
σ	Standard deviation of normal distribution	6.3.5
τ	Shear stress	3.5.2
τ_w	Value of τ at the pipe wall	3.5.1
ψ	Stream function	4.2.1
Superscripts		
$\bar{}$	Mean (time-averaged) value	3.3
*	Non-dimensionalised quantity	4.3.2
z,r,θ	Components in cylindical polar coordinates	4.2.1
'	Derivative with respect to r	4.3.2
Subscripts		
z,r,θ	Partial derivatives	4.2.1

1. INTRODUCTION

This thesis is principally concerned with a theoretical and experimental study of the character of swirling flow in pipes. It is also concerned with the effects of such flows on the accuracy of flowmeters and implications for industrial flow measurement. The thesis has this broad character because it is a Total Technology PhD (see Appendix A). Indeed, industrial needs have formed a significant part of the motivation for the work that has been carried out.

Chapter 2 starts with a review of industrial flow measurement, describing basic meter types and the purposes for which they are used. There is also a presentation of data arising out of a survey of the meters used in 72 different establishments; this information is then set into the context of more general knowledge concerning the industrial flowmeter market. The chapter goes on to explain the motivation for the work - that we desire a better knowledge of velocity profiles in pipes in order that we may be able to specify more appropriate installation conditions for flowmeters and provide information of use in their design.

Chapter 3 describes the background to the technical aspects of the work, presenting a literature survey covering various areas of interest such as turbulence modelling, pipe flows and swirling flows. The chapter sets the scene for the new approaches to the problem explained in chapter 4. Here we look at the theoretical part of the work, progressing from linearised equation methods to a fuller three-dimensional treatment of the decay of turbulent swirling flow. Chapter 5 is devoted to the computational work required to turn theory into numbers; the results obtained are also presented here.

Chapter 6 covers the experimental side of the work, describing the test facility and procedure which were used, and presents the results obtained. Some insights into the effects of these swirling flows on certain types of flowmeters are presented in chapter 7.

Chapter 8 concludes the work by discussing the relation between the theoretical and the experimental work in the light of the literature, and drawing conclusions. The implications of the work for flow measurement are also considered and recommendations are made for further work.

2. A SURVEY OF THE INDUSTRIAL FLOWMETER MARKET

2.1 Introduction

Mid way through the second year of the PhD, a letter was sent to 330 companies who use flowmeters, together with a questionnaire (see Appendix B).

There was a very considerable response: 72 replies were received, containing information regarding over 17000 flowmeters. Details of the results of the survey are also contained in Appendix B. In this chapter reference will be made to the tables in Appendix B simply by using the table number. Some of the comments which are made there merely duplicate those here; some add to them. In the remainder of this chapter we shall examine the purposes of flow measurement, discuss the main types of meters used both in terms of their principle of operation and their market niche, summarise the findings of the survey and identify those aspects of the industrial scene to which the technical work is relevant.

A summary of this market survey has already been reported (Halsey (1986)).

2.2 Purposes of flow measurement

It might well be thought obvious to remark that the purpose of flow measurement is to measure the flowrate of fluid in a pipeline. We seek, however, to understand what we wish to know the flowrate for, and so to determine whether this is in fact our real need.

By far the most common purpose of flow measurement (excluding those used in retailing) is to control a process (such as the refining of oil). The reading obtained is used to determine the required adjustment of a valve (for example) in order to bring about or maintain a particular process state. In this situation (called 'continuous flowrate/process control' in the survey), the prime concern is with repeatability and reliability. It is not so important whether the reading is actually accurate or not as long as it feeds the control loop (manual or automatic) with a repeatable signal. Since 83% of all flowmeters in the survey (see table 3) are employed for this purpose it is as well to note that although a measure of accuracy is needed, this is not in fact the paramount consideration

in most applications.

Of the remaining 17% of flowmeters, half (8% of the total) are used in batch processing. Theoretically this only requires the addition of a totaliser, but there are nevertheless some other points to bear in mind. If it is required to measure a relatively small amount of fluid, the start up and shut down times will contribute a significant proportion of the total bulk flow. Also, it is possible for a meter to be more accurate at some flowrates than others, and so the total reading may depend on the speed(s) used. It can be seen that accuracy is more important in this case; this is seen to be reflected in users' attitudes (see table 9).

Custody transfer accounts for 5% of the total; this concerns the fiscal transfer of fluid. If large quantities of oil are involved, the effect of an inaccurate meter could be very significant. It is clear that the overriding consideration is that of accuracy.

The remaining 4% ('other') are mainly used in research where accuracy (and probably accuracy at a range of flowrates) is also very important. Some of these 'others' are used as flow alarms where all that is required is that a reading is given if there is sufficient flow.

2.3 Types of flowmeters used in industry

The U.K. market in flowmeter purchases in recent years has been of the order of £40m. Of these, according to table 5, 45% are of the differential pressure type. At present, as can be seen from table 1, almost 60% of all meters in use are of this type; this is therefore the dominant meter type even though its relative numbers are in decline. The differential pressure (orifice) meter works by sensing the pressure drop across an orifice plate inserted into the flow; because the flow is constricted it loses pressure through the orifice, and this pressure drop is dependent (via some coefficient) on the square of the mean velocity. This, the industry's standard method, has been used because of its reliability and simplicity. There is a huge amount of accumulated experience, and it is also regarded as a relatively inexpensive method. There are problems, however, particularly with hostile fluids which destroy the sharp edge of the orifice plate and the lack of rangeability due to its

square law characteristic (most other types are linear), and users are turning towards the newer meter types in increasing numbers.

The other old, standard meter type is the variable area meter or rotameter which employs a little float sitting (supported by the flow) in a vertical, expanding pipe section - the faster the flow the higher the float sits. These account for 19% of all meters in the survey (table 1) and would seem to have a secure niche in the market since numbers do not appear to be changing over time. This is the bottom end of the flowmeter market - a reliable indication of the presence (and rough magnitude) of flow. For any degree of accuracy something rather better is required. It is not possible to use this type of meter to measure the full range of fluids.

Another common meter type with a stable market share is the positive displacment meter (9% of usage), which measures the flowrate by counting 'lumps' of fluid of known volume as they pass through the meter. This type of meter is very often used for custody transfer; it is very accurate.

The turbine meter is also frequently used for custody transfer as it too is accurate (the measurement here is obtained by counting the number of revolutions of the vanes as they are driven by the flow). The market niche for this type of meter would also appear to be full, since table 5 shows a stable usage over time, at around 7% of the total.

Of those meter types which are taking over from the differential pressure types, the electromagnetic meter has the largest market share (presently 4% of all usage). These meters measure the flowrate by detecting the voltage produced as the fluid flows through a magnetic field imposed from outside the pipe (this requires a conducting fluid). Since there is no intrusion into the flow, there is no extra pressure drop across this type of meter. It is suitable for any conducting fluid, no matter how inhomogeneous. As can be seen from table 5, the proportion of electromagnetic meters used is growing and now stands at 8% of purchases.

The vortex-shedding meter (1% of present usage) detects the frequency of the shedding of vortices behind a bluff body. This meter type, although not greatly used at present appears to be about to increase its market share significantly (tables 5,6).

Other meter types are the ultrasonic (doppler and transit time) and mass meters. Ultrasonic meters utilise the effect of the fluid motion on the passage of sound through the pipe. The doppler meter is relatively inaccurate and often used as an alarm; transit time meters are much more accurate. It would appear that the users in this survey use these two types much less than other information would lead us to believe is generally the case (see section 2.6). The mass meter, however, (an accurate meter) is relatively new and so still in the process of finding its niche. It actually measures mass flow rate directly, rather than via a calculation from the density and volume flow rate.

2.4 An overview of the results of the market survey

In the analysis of the questionnaire, the replies were divided into three groups depending on the number of meters recorded on the form: There were 25 'small' users having fewer than 61 meters each, 36 'medium-sized' users with between 61 and 600 meters and 11 'large' users owning more than 600 meters each. It should be noted that, in general, a 'user' corresponds to a particular site or to an individual's area of responsibility, rather than to an entire company.

The fact that the Foxboro Company gave substantial guidance in the selection of the users surveyed and that participation was voluntary clearly introduces unknown biases into the results; one way to get an indication of this is to examine table 2 to see what proportions of different kinds of fluids are being measured. There are, however, difficulties with this since (for example) a company whose line of business is the manufacture of food will use most of its flowmeters on anything but foodstuffs.

The relative numbers of the different types of flowmeters are presented in table 1 and have been discussed above in section 2.3. It is useful to note that although there are many types of meter having a small market share, these few are spread thinly right across the board, rather than being concentrated in just a handful of users.

It can be seen from table 5 that there has been a historical trend away from the orifice meter towards the electromagnetic and vortex-shedding types, and there is no reason to believe that this will cease. If we look at table 6 we see that although there will be

a good many orifice meters in service, the large users are looking towards the vortex-shedding meter in the future. (The question corresponding to table 6 was about usage rather than purchases). Table 5 would also seem to indicate an increase in the use of mass meters. An interesting statistic available from table 5 is that, on average, each of the last ten years has seen the acquisition of 4% of the meters presently in service with a company. This presumably means that there are meters in service which are over 25 years old.

Most meters (86%) are used to measure hydrocarbons, water, steam and chemicals. Table 2 also shows that two or three phase flows account for only 5% of the flow measurement covered in the survey.

We have already considered the purposes of flow measurement in section 2.2. It is useful to realise (table 3) that there are many users with a few meters employed on custody transfer duty.

The main range of line sizes (table 4) is from 2" to 6" although a significant amount of flow measurement is carried out in line sizes outside this range.

Opinions regarding meter performance and characteristics are very variable and so a simple averaging procedure has been used to give a feel for the overall perspective of the marketplace. If accuracy is not important at all, then table 7 indicates that the variable area meter is probably the one used since it is inexpensive. Excluding this type, it may be seen from table 10 that the electromagnetic, positive displacement and differential pressure types are regarded as the best overall, followed by turbine and vortex-shedding types. These form a group of standard, well regarded meter types with opinion depending very much on the particular application. Mass and ultrasonic meters are much less well regarded (the former are regarded as very accurate and expensive and so are not generally appropriate, the latter are regarded as unreliable).

The main influences on meter selection are accuracy, repeatability and reliability (see table 9); cost is apparently immaterial regardless of the purpose of the measurement. Users are considerably influenced by previous experience.

The installation lengths (lengths of straight piping upstream of a meter) used are varied (table 11), but are usually short whether compared with any standards which are available or with

manufacturer's guidance. They tend to be fixed crudely on the basis of 10 diameters regardless and even then only if there is room. We shall return to this matter later in this chapter.

2.5 Conclusions of the market survey

When the market survey was completed, a copy was sent to the participating companies. The conclusions reached then are given below with a few additional comments by way of explanation:

1. Differential pressure meters (almost all orifice meters) dominate the market both in usage and current sales, but are in decline.

2. Positive displacement, variable area and turbine meters have stable market shares.

3. Electromagnetic, vortex-shedding and mass meters are increasing their market shares.

4. Most meters are used for continuous flowrate measurement, on hydrocarbons, water, steam or chemicals and are between 2" and 6" in diameter.

5. Accuracy, reliability and repeatability are the key considerations in meter selection, not cost.

6. Installation lengths are usually short and are arrived at simplistically.

7. Large users are starting to use electromagnetic and vortex-shedding meters to replace their old orifice-plate meters; this will be a slow process.

8. Smaller users seem to experiment with new techniques more readily than large users.

2.6 An overview of the state of industrial flow measurement.

It is clear from the material contained in the previous sections that the industrial flowmeter market is complicated. In this section we seek to compare the findings of the present survey with other available data.

Information from Higham (1985) relating to the late seventies indicates that the relative numbers of the different types of flowmeters that were used then were not radically different from

those in the present survey. Differential pressure was still dominant (with 66%); electromagnetic (9%), variable area (8%), positive displacement (6%) and turbine (5%) were all present in reasonable quantities; vortex-shedding (2%) and ultrasonic (2%) made up most of the remainder.

Information from Furness (1985), dealing with the value of flowmeter purchases in the early eighties is rather different, giving differential pressure 40%, variable area 12%, positive displacement 16%, turbine 10%, electromagnetic 6%, ultrasonic 7%, mass meters 6% with the remainder as vortex-shedding (3%). Figure 2.1 shows both these sets of figures, together with those obtained in this survey, in the form of piecharts. The figures from the present survey are taken from table 5.

Comparing these sets of figures requires a knowledge of the relative costs of different systems. Basically, the differential pressure and variable area meters are less expensive and the electromagnetic, mass and positive displacement meters more expensive. With this in mind, there are rather fewer discrepancies, especially when it is realised that although the figure for differential pressure meters in the present survey is 61% of all usage (similar to Higham's data), the figure for purchases (48%) is also close to Furness's figure for the value of sales. The main reasons for the remaining differences (other than genuine changes in the patterns of usage) are that different parts of the flowmeter market were surveyed in each case. It would be reasonable to expect the present survey to follow on from Higham's information better than from Furness's figures since these surveys are both based on the kind of customers which Foxboro has. (Foxboro have relatively few customers in the utilities or customers using meters for custody transfer compared with what Furness regarded as typical, since their customers are mainly in the process industries).

It would seem, not only on the basis of these three surveys, but also on the basis of discussions with users that 'conclusion 7' in section 2.5 really is the case, and so we can expect to see the patterns of flowmeter usage change. It would seem likely too, that the ultrasonic meter will gradually gain acceptance along with mass meters; the fact that new technologies take a long time to realise

their potential can be seen in the fact that the vortex-shedding meter has been around for 20 years and is only now looking as if it will be generally accepted.

Other data is available in the article by Chowdhury (1982), concerning the United States market. He presents similar data to that of Furness, except for the much larger percentage of the market attributed to turbine meters (27%) at the expense of variable area and positive displacement meters which were not covered at all.

2.7 The motivation for the present work

We now turn to examine the status of those meter types whose reading is dependent on the flow profile present in the meter body, since it is these to which the theoretical and experimental work of this thesis will apply.

The meter types whose operation is dependent (at least indirectly) upon flow profile are the differential pressure, turbine, vortex-shedding, ultrasonic and electromagnetic types. It is clear that turbine meters (detecting the rate at which the flow drives the blades round) will be very sensitive to a swirling flow, that the vortex-shedding process can be significantly affected by the nature of the flow and that ultrasonic meters (depending on the value of an integral across one or two diameters) are also critically affected by the flow profile present. Orifice-plate meters are also affected by the velocity profile through the interaction of the flow with the obstructing plate. The electromagnetic meter, although less dependent than many by virtue of its intrinsic symmetry, is also affected though not by the swirling part of any flow.

The way in which the flow profile dependent nature of meters is dealt with is to calibrate all meters for use on a 'fully developed' flow. This is a flow in which the flow quantities do not change along the pipe axis. In other words, the flow has 'settled down' into its 'steady state' form. This is done because this is the only readily reproducible flow profile. It is, of course, possible to calibrate in any given situation. If a meter calibrated for fully developed conditions is presented with some other profile it will give an erroneous reading, at least to some degree. To ensure a satisfactory reading the meter must be offered a flow profile which

is sufficiently close to that of a fully developed one. After a bend, series of bends, valves or other perturbing pipe geometries there will be a disturbed profile of some kind (disturbed from the fully developed state which we are regarding as 'normal'). This disturbed profile will decay back to a fully developed profile if there is a sufficiently long straight section of pipe. The major problem is to determine what lengths are needed; these will depend on upstream pipe geometry and the type of meter being used.

The way in which the flowmeter user encounters these problems is in the specification of certain upstream installation lengths recommended by the manufacturer or contained in standards. Typical values for these (following a single right-angle bend - not the worst case) would be 5 diameters for an electromagnetic meter, 15 diameters for a turbine meter, 30 diameters for a vortex-shedding meter and 20 for an orifice-plate meter. As can be seen from table 10, these are not used by the vast majority of users - the usual approach being to use a 'standard' (arbitrary) length of 10 diameters regardless. For many purposes this will, in fact, be sufficient (see comments on the purposes of flowmeasurement in section 2.2), but this is certainly not the case for custody transfer metering. There were some notable cases in the survey of respondents who did use very long lengths for this reason. There is a relatively small volume (but high value) market for meters to be used for custody transfer purposes where recommended installation lengths will be adhered to, and so it would be useful to know what the decay patterns of flows are better than we do at present. At present the data supplied by manufacturers is not consistent and standards only exist for the orifice-plate meter. Even here installation length recommendations are beginning to be questioned.

The other motivation for seeking a better knowledge of the patterns of decaying flow profiles is that of flowmeter design. If we know the forms that decaying flows take, then we may be able to design flowmeters to be less sensitive to them or to compensate for them by using some of the information contained in the data which the device collects before it processes it to give a reading.

So far we have thought about accuracy. Although this is always important, it is repeatability which is always more important

(without repeatability there can be no accuracy) and is of overriding importance in the process industries where meter readings are used for control purposes. Were the presence of some kinds of flow profiles liable to render some kinds of meters significantly less repeatable it would be of great concern. This eventuality seems improbable, but should be borne in mind owing to the importance of the matter; if a problem did arise in this regard it would certainly warrant close examination.

3. TECHNICAL BACKGROUND AND LITERATURE SURVEY

3.1 Introduction

In this chapter we look first at the equations governing fluid motion, the nature of turbulence and the need for turbulence models. We then describe the fundamental forms of turbulence model and their merits and demerits. Sections follow presenting the state of knowledge regarding both fully developed flow and the flows found after various sorts of bends. Following this background, we examine the literature on swirling flows in some detail since it is the main area of the work. We conclude with a discussion of the literature regarding the effects of flow profile disturbances on flowmeters.

3.2 The governing equations

We restrict our attention to incompressible Newtonian fluids, governed by the Navier-Stokes equations

$$\frac{\partial Q_i}{\partial x_i} = 0 \qquad (3.1a)$$

$$\frac{\partial Q_i}{\partial t} + Q_j \frac{\partial Q_i}{\partial x_j} = -\frac{1}{\rho}\frac{\partial P}{\partial x_i} + \nu \frac{\partial^2 Q_i}{\partial x_j^2} \qquad (3.1b)$$

where ρ = density, ν = kinematic viscosity,

$\underline{Q}$ = instantaneous velocity and P = instantaneous pressure.

These equations can be found in any standard reference on basic fluid mechanics, such as Batchelor (1967) p174f.

3.3 The nature of turbulence and the need for turbulence modelling

It is not intended to present here anything approaching a comprehensive account of turbulence - such a task would not be in keeping with the emphasies of this work. It is necessary, however, to describe the fundamentals in order to see how and why a turbulent flow is modelled and analysed.

When fluid moves the manner of its motion can be characterised (at least in part) by a non-dimensional number called Reynolds number (Re). Reynolds number is the ratio of the inertia forces over the viscous forces and gives a measure of 'how fast' the fluid is moving. If a fluid moves 'slowly' (at Reynolds numbers less than 2000 say)

then it is observed that the fluid motion is laminar, meaning that the motion can be thought of as layers of fluid sliding past each other. If the fluid moves significantly faster than this (at Re = 10^4 or more for example) then it is found that there is an inherent instability in the physics which gives rise to velocities varying very rapidly in time and in space, albeit around a well defined time-average (called the mean flow). These velocities still satisfy equations (3.1), but vary so rapidly as to make any direct computational approach impossible owing to the massive storage requirements which would be needed (Rodi (1978)). This (turbulent) kind of flow is:

> ..an eddying motion which at the high Reynolds numbers usually prevailing has a wide spectrum of eddy sizes and a corresponding spectrum of fluctuation frequencies; its motion is always rotational and can be thought of as a tangle of vortex elements whose vorticity vectors can be aligned in all directions and are highly unsteady. The largest eddies, which are associated with the low frequency fluctuations, are determined by the boundary conditions of the flow and their size is of the same order of magnitude as the flow domain. The smallest eddies, associated with the high frequency fluctuations, are determined by viscous forces. .... The large eddies interact with the mean flow (because the scales of both are similar), thereby extracting energy from the mean motion and feeding it into the large-scale turbulent motion. The eddies can be considered as vortex elements which stretch each other. Due to this vortex stretching, which is an essential feature of the turbulent motion, the energy is passed on to smaller and smaller eddies until viscous forces become active and dissipate the energy. This process is called energy cascade. The rate at which mean-flow energy is fed into the turbulent motion is determined by the large-scale motion; only this amount of energy can be passed on to smaller scales and finally be dissipated. Therefore, the rate of energy dissipated is also determined by the large-scale motion

although dissipation is a viscous process and takes place at the smallest eddies. It is important to note that viscosity does not determine the amount of dissipated energy, but only the scale at which dissipation takes place. .... The mean flow often has preferred directons which are imposed also on the large-scale turbulent motion. .... During the cascade process ... the direction sensitivity is diminished. When the Reynolds number is high enough so that the large-scale and small-scale motions are sufficiently far apart in the spectrum, the direction sensitivity is lost entirely and the small-scale dissipative motion is isotropic. This phenomenon ... is called local isotropy and is an important concept in turbulence modelling." (Rodi (1978)).

The approach adopted by many over the decades has been to take the time-average of equations (3.1) since, for the most part, we seek the time-averaged values of the velocities. In order to do this we treat the instantaneous velocity $\underline{Q}$ as the sum of its time-averaged value $\overline{\underline{Q}}$ and a fluctuating component $\underline{q}$, so that $\underline{Q} = \overline{\underline{Q}} + \underline{q}$. It is, of course, possible for $\overline{\underline{Q}}$ to be time dependent, provided the time over which the time-average is taken is significantly smaller than the timescale over which the time-averaged value varies (Rodi 1978). In the work of this thesis we shall in fact be dealing with the case of steady flow, where the time-averaged velocities are time-independent. When we take the time-average of equations (3.1) we get

$$\frac{\partial \overline{Q}_i}{\partial x_i} = 0 \qquad (3.2a)$$

$$\overline{Q}_j \frac{\partial \overline{Q}_i}{\partial x_j} = -\frac{1}{\rho}\frac{\partial \overline{P}}{\partial x_i} + \nu \frac{\partial^2 \overline{Q}_i}{\partial x_j^2} - \frac{\partial}{\partial x_j}\left(\overline{q_i q_j}\right) \qquad (3.2b)$$

where overbars denote time-averages and we have incorporated the condition that the flow be steady.

The last term in equation (3.2b) involves the 'cross-correlation' of the turbulence fluctuations and is called the 'Reynolds stresses'. These arise because of the non-linearity of equations (3.1). Equations (3.2) are mathematically underdetermined, and so we have to

find some way of expressing the Reynolds stresses in terms of other quantities, such as the mean flow, in order to close the system.

It is this process of closure via some relationship between Reynolds stresses and the mean flow which is called (phenomelogical) turbulence modelling. The idea of a model is to deal with the large-scale turbulent motions which actually interact with the mean flow, leaving the energy cascade to 'come out in the wash'.

Many workers have sought a unified theory of turbulence, able to model its effects in as many situations as possible; in practice there are now a number of different types of model each with a different level of complexity and range of applications. Rodi (1978,1982) provides an excellent review of these as well as dealing with the material presented earlier in this chapter. Bradshaw (1972) is a delight for its entertaining style and additional treatments are given by Tennekes and Lumley (1972) and the lecture series by Launder and Spalding (1972). A brief overview follows, describing the main types of model; relevant areas will be pursued in chapter 4.

3.4 Turbulence models

A fundamental part of most turbulence models is the idea of relating the Reynolds stresses to the mean motion via an invented quantity called either the eddy viscosity or the turbulence viscosity. This system, due originally to Boussinesq (see Launder and Spalding (1972)), sets

$$- \overline{q_i q_j} = \epsilon \left[\frac{\partial \bar{Q}_i}{\partial x_j} + \frac{\partial \bar{Q}_j}{\partial x_i} \right] - \frac{2}{3} k \, \delta_{ij} \qquad (3.3)$$

where the eddy viscosity ϵ has yet to be prescribed and k is the turbulence kinetic energy; (k does not need to be determined since upon substitution into (3.2) the last term of (3.3) can be absorbed into the pressure term). The idea behind this approach was the supposition of an analogy between turbulent motion and the motion of molecules. This idea has since been exploded (Rodi 1978), but as the method has been sucessful it is still used as the basis of many models in use today. This 'eddy viscosity' concept, as it is known, says in effect that the damping of the turbulence on the mean flow is proportional to the local velocity gradient via some coefficient, ϵ,

which will itself be a function of position, and possibly of the mean flow as well. The next step is to decide how to choose ϵ. It is possible to take ϵ as constant, but this is not appropriate for dealing with flows close to walls. The simplest 'proper' turbulence models employ the concept of a 'mixing-length' L, which is a function of position supposedly relating to the size of the largest eddies present (L increases linearly away from a wall for example). L is used to relate the eddy viscosity and the mean flow velocities via the relationship

$$\epsilon = L^2 \left\{ \left[\frac{\partial \bar{Q}_i}{\partial x_j} + \frac{\partial \bar{Q}_j}{\partial x_i} \right] \frac{\partial \bar{Q}_i}{\partial x_j} \right\}^{1/2} \qquad (3.4)$$

and is a concept originally due to Prandtl (see Rodi (1978)). Empirical input is required to determine L; having done this the method has been shown to work well for shear layers and fully developed pipe and channel flows.

The main problems with the mixing-length model are that it takes no account of the convection or diffusion of turbulence (assuming it to be dissipated in the same place as it is generated), causes ϵ to be equal to zero whenever the velocity gradient is zero and requires L to be specified (which is impossible if the geometry of the flow domain is too complicated). It is not therefore suitable for a flow involving recirculation, rapid development or complicated geometries.

In order to deal with these problems, reseachers have invented more sophisticated models, many of which are still based on the eddy viscosity concept. The 'one-equation' model adds a transport equation for k, having replaced (3.4) with $\epsilon = c\sqrt{k}L$ where c is an empirical constant. This enables the model to deal with the transport of turbulence but still requires the specification of L. The 'two-equation' (k-ϵ) model adds a transport equation for L, which eliminates the need to specify L and has provided solutions to some recirculating flows although it cannot be regarded as omnipotent. It should be noted that these additional transport equations are obtained directly from the Navier-Stokes equations and that they also need to be modelled since they involve higher orders of cross-correlation fluctuations. The standard forms of the models

described so far assume that the turbulence is locally isotropic; there are adaptions available to cater for this not being the case. There are yet more complicated models dealing with a transport equation for each individual Reynolds stress component which are as yet largely untested but, since they do not employ the eddy viscosity concept, should be able to cater for situations where that concept breaks down such as complex flows with several velocity scales.

3.5 Fully developed turbulent pipe flow

3.5.1 Introduction

We shall be considering fully developed turbulent pipe flow as a reference state for the theory to be described in chapter 4 and so we discuss the background to this here, looking at the structure and character of the flow field.

The main difference between the profile of fully developed turbulent flow and that of the corresponding parabolic profile in laminar flow is that the turbulent profile is flatter in the central region of the pipe and much steeper near the wall. As the Reynolds number increases it approaches the appearance of a flat core and thin boundary layer.

There is a considerable literature relating to fully developed flow, treating it in a variety of ways. As a relatively simple flow, and as an important one due to its common occurance workers have tried to deal with practical matters (such as friction factors) as well as trying to develop a theoretical understanding of the turbulent flow mechanisms involved.

Some progress can be made theoretically just from equations (3.2); upon a substitution of $\overline{\underline{Q}} = (V(r),0,0)$ in cylindrical polar coordinates (z,r,θ), cross-correlation terms remain since the fluctuating velocity is non-zero in all components. To make further progress (beyond establishing the linearity of variation of the shear stress across the pipe section (see equation (3.7)) we have to introduce some modelling and empirical data. We consider (following Ward-Smith (1980)) the use of the eddy viscosity concept as outlined in section 3.3. When we substitute (3.3) into (3.2b) considering the fully developed flow field given as $\overline{\underline{Q}}$ above we get

$$0 = -\frac{1}{\rho}\frac{\partial \overline{P}}{\partial z} + \frac{1}{r}\frac{\partial}{\partial r}\left[r(\nu+\epsilon_o)\frac{\partial V}{\partial r}\right] \qquad (3.5a)$$

$$0 = -\frac{1}{\rho}\frac{\partial \overline{P}}{\partial r} \qquad (3.5b)$$

where $\overline{P}$ includes the term involving k from (3.3), and

ϵ_o is the value of ϵ in fully developed flow.

Various quantities have been defined in the literature (e.g. Ward-Smith (1980) p141) and will be used. They are

$$Re = \frac{DU_{av}}{\nu} \qquad (3.6a)$$

$$-\frac{a}{2\rho}\frac{\partial \overline{P}}{\partial z} = \frac{\tau_w}{\rho} = u_\tau^2 = U_{av}^2\left[\frac{f}{2}\right] \qquad (3.6b)$$

where $D = 2a$ = pipe diameter, τ_w = wall stress,

u_τ = friction velocity, U_{av} = average bulk flow velocity and

f = friction factor in fully developed flow.

It should be noted that the friction factors given by Ward-Smith (1980) and Miller (1971) differ by a factor of 4. We use Ward-Smith's definition. We simplify (3.5) to obtain

$$(\nu+\epsilon_o)\frac{dV}{dr} = -u_\tau^2\frac{r}{a} \qquad (3.7)$$

which states that the shear stress varies linearly with pipe radius.

3.5.2 Characteristic regions

Without employing any more assumptions, it is possible to characterise four regions of flow at different distances from the wall.

The first region (nearest to the wall) is called the viscous sublayer and is that region within which the effect of turbulent fluctuations is negligible so that the flow is entirely governed by the (molecular) viscosity ν. The velocity V is then a straight line, given by

$$\frac{V}{u_\tau} = \frac{u_\tau y}{\nu} \qquad (3.8)$$

where $y = a - r$. Measurements indicate that this law holds for values of $\alpha = \frac{u_\tau y}{\nu}$ up to about 5.

The second region, called the buffer layer, is that region in which the effects of the turbulent fluctuations become important and in which the effects of the viscosity ν remain significant. This region extends the value of α to about 30.

The third, much larger and more interesting region, called the logarithmic region is that region in which effects due to the wall still dominate, but the viscosity no longer affects the flow directly. We use the eddy viscosity ϵ_o to give us the following expression for the shear stress τ

$$\tau = \rho \, \epsilon_o \, \frac{dV}{dy} \tag{3.9}$$

Since ν is not involved directly, ϵ_o must (from dimensional considerations) be of the form $ky(\tau/\rho)^2$ thus giving us

$$\frac{dV}{dy} = \frac{u_\tau}{ky}$$

$$\rightarrow \quad \frac{V}{u_\tau} = \frac{1}{k} \ln(y) + \text{constant} \tag{3.10}$$

where k is Prandtl's constant.

This well-known logarithmic law, which applies up to values of y/a of about 0.2, is usually expressed in the form

$$\frac{V}{u_\tau} = A \ln\left[\frac{u_\tau y}{\nu}\right] + B \tag{3.11}$$

and has been tested using the measurements of Nikuradse, giving A = 2.5 and B = 5.5. Other very similar values have also been suggested.

The fourth region (the remainder of the pipe) is called the outer or core region and can be shown (dimensionally) to have a velocity profile of form

$$\frac{U_c - V}{u_\tau} = f\left[\frac{r}{a}\right] \tag{3.12}$$

where U_c is the maximum value of the velocity (occuring on the pipe axis), and f is an arbitrary function.

In practice it is possible to extend the logarithmic law across to the axis and use this to calculate friction factors; when this is done the values of A and B are changed from those given above in order to give the best fit with experimental measurements of the pressure drop, the form of the formula obtained is however entirely

satisfactory. See Ward-Smith (1980) for details.

Recent work by Afzal (1982) has examined an alternative treatment of these layers, using matched asymptotic expansions employing three distinct velocity scales as opposed to the two used above. Other velocity measurements have been carried out by Laufer (1954).

3.5.3 The use of mixing-length

We now turn to the use of a mixing-length L, to replace ϵ_o. In the case of fully developed flow, (3.4) becomes

$$\epsilon_o = L^2 \left|\frac{dV}{dr}\right| \tag{3.13}$$

and using this in (3.7) gives

$$\left[\nu + L^2 \left|\frac{dV}{dr}\right| \right] \left|\frac{dV}{dr}\right| = u_\tau^2 \frac{r}{a} \tag{3.14}$$

recognising that the velocity gradient is always negative.
It is interesting to note that if we consider a region close to the wall where the mixing-length L is proportional to y and ν is not important, then we obtain the logarithmic law as before.

We obtain L from the remarkable empirical fit of Nikuradse (see Schlichting (1979)) to a wide range of measurements at all Reynolds numbers and pipe roughnesses. His formula is

$$\frac{L}{a} = 0.14 - 0.08 \left[\frac{r}{a}\right]^2 - 0.06 \left[\frac{r}{a}\right]^4 \tag{3.15}$$

It will be seen that close to the wall (3.15) is linear in y, indicating a logarithmic law for the velocity. Since in fact the logarithmic region does not extend as far as the wall there is a need to smooth L off (in the buffer layer) in order to ensure a smooth transition from the logarithmic law modelled by L and the viscous sublayer. This has the effect of making the function $\nu + \epsilon_o$ have zero gradient on the wall. We use the wall correction devised by Van Driest (1956) (or see Launder and Spalding (1972)) for this purpose.

3.5.4 Friction factors in straight pipes

We summarise here the empirical formulae for friction factors in straight pipes as given by Ward-Smith (1980) p165f. We use the relative roughness parameter ϵ_R/D and have

for laminar flow:

$$f = 16/Re \qquad (3.16a)$$

for turbulent flow:

smooth regime

$$1/\sqrt{f} = 1.56\ln(Re/7) \qquad (3.16b)$$

intermediate regime

$$1/\sqrt{f} = 1.74[\ln(Re/5) - (1 - 1/Z)\ln(Z/2.30)]$$

$$\text{where } Z = \ln(Re/5) + (\epsilon_R/D)(Re/8.03) \qquad (3.16c)$$

rough regime

$$1/\sqrt{f} = 1.74\ln(3.7D/\epsilon_R) \qquad (3.16d)$$

where it can be shown that the boundary between the intermediate and rough regimes is at

$$Re = 172(D/\epsilon_R)\ln(3.7(D/\epsilon_R)) \qquad (3.16e)$$

Ward-Smith (1980) gives figures for the typical value of the roughness parameter ϵ_R; from these the relative roughness ϵ_R/D can be calculated.

3.6 Flows after bends

When fluid moving in a pipeline is forced round a bend, the faster moving fluid near the axis experiences a greater centrifugal force than the slower moving fluid near to the pipe walls. Consequently the fluid near the axis moves outwards (away from the centre of curvature of the bend) and the other moves inwards thus producing a pair of vortices superimposed on the axial flow. The resulting flow pattern is shown in schematically in figure 3.1. The non-axial part of such a flow pattern is called a secondary flow. If the bend is long enough a 'fully developed curved flow' can occur. In most practical situations this does not happen so we restrict our attention to 'short' bends. Ward-Smith (1980) provides a starting point in this area as does Miller (1971,1978).

We consider first the case as outlined above, of a single, swept, right-angle bend. An important parameter here, as in other bend flows, is that of 'radius ratio' (the ratio of the radius of curvature of the bend to the diameter of the pipe). Common values are 1 and 2, being fairly tight; a value of 4 is rarer, being somewhat looser. The fundamental form of the flow just downstream of such a

bend is characterised by the vortices described above and also by an axial flow whose equi-velocity contours form a horseshoe with the open end facing the inside of the bend. An example of this kind of profile is provided by the work of Murakami, Shimizu and Shiragami (1969). The flow field is, of course, symmetrical about the plane of the bend.

Early experimental work was done by Weske (1948) who used a wide variety of radius ratios, cross-sectional shapes and Reynolds numbers. More recent work has been carried out using laser-doppler anemometry (rather than pitot-tubes) by Moore and Kirouac (1981) who looked specifically at the case of a right-angle bend in a circular pipe. Other studies by Campbell (1960) and Blake (1973) have also considered mitre bends.

Extending the scope of our coverage to include double bends within one plane leads us back to the work of Murakami et al (1969) again. Hunt (1974) gives some measurements of the redevelopment of flow after a 180° bend as does Rowe (1970) who also measured the flow in the bend itself. It is found that the distance between the bends (spacer length) affects the interference between them. A separation of 10 diameters seems adequate to effectively elimenate any significant interaction.

Murakami et al (1969) also present data for the case of a double right-angle bend in two planes (not in perpendicular planes) which generates a powerful swirling motion rotating with the same sense as the handedness of the bend. The mechanism producing this effect may be understood in the following way. As the horseshoe profile of figure 3.1 approaches the second bend, it can be seen that the centrifugal action of the second bend is larger in the middle of the horseshoe than at its open end owing to its higher velocity (see figure 3.2). Accordingly, the angular momentum about the axis of the downstream piping is expressed as a rotating motion.

Mottram and Rawat (1986) present data for the case of a double right-angle bend in perpendicular planes following a Borda inlet which shows considerable asymmetry both in the axial and tangential velocity components close to the bend. There was also a very significant variation in the rate of decay of the swirl with pipe roughness. Nystrom and Padmanabhan (1985) have carried out tests on

double bends in two perpendicular planes with various radius ratios and spacer lengths following a 40 diameter inlet section. They found (using a swirl meter) that shorter spacer lengths and tighter bends each resulted in larger swirl levels. They found that a spacer length of 6 diameters was sufficient to reduce the swirl level after the bend to that resulting from a single bend. They also present values for the decay of swirl consistent with that of other workers.

Much effort has been expended finding the pressure drop through bends and combinations of bends. Miller (1971,1978) gives a large amount of such information. In general the pressure drop is higher for tighter bends than for looser ones and for mitre bends as opposed to swept bends. A greater proportion of the total loss occurs in the downstream tangent in the case of a looser bend. There is a corresponding effect on the redevelopment of the velocity as it develops in a shorter distance after a tighter bend.

Theoretical work in this area is limited. Rowe (1970) used an inviscid theory to investigate the flow in a bend and Rapier (1981) has done a very crude analysis of possible decay rates for general flows in pipes such as might be caused by bends. Owing to the extensive turbulence modelling required (especially in or near the separation regions close to bends) calculation is difficult. There is, however, a fuller literature concerning swirling flows and it is to this that we now turn our attention.

3.7 Swirling flow in pipes

3.7.1 Parameters used to characterise swirl

It will be useful to define at this stage some of the terms used in describing the level of swirl present in a pipe flow.

Early workers (e.g. Krieth and Sonju (1965)) measured the level of swirl directly using a 'swirlmeter' consisting of a disc mounted on a spindle positioned on the pipe axis. The rotational frequency provides the measure of swirl, and is in fact a weighted average (in some unknown way) of the tangential velocity distribution. Because of this it is difficult to relate readings obtained by this method to those obtained by any other.

A more satisfactory method for getting a value for the level of

swirl present at a particular cross-section of the pipe is to look at the ratio of the local tangential and axial momentum fluxes. This, as will be seen in section 4.2.1, is a method which arises directly out of the equations of motion.

We define

$$M_{ang} = 2\pi\rho\int_0^a Q^\theta Q^z r^2 dr \qquad (3.17a)$$

$$M_{ax} = 2\pi\rho\int_0^a \left[Q^z\right]^2 r\ dr \qquad (3.17b)$$

where superscripts denote the components of $\underline{\bar{Q}}$, and so we have (following Ward-Smith (1980)) the swirl number S defined by

$$S = \frac{M_{ang}}{aM_{ax}} = \frac{\int_0^a Q^\theta Q^z r^2 dr}{a\int_0^a \left[Q^z\right]^2 r\ dr} \qquad (3.18)$$

This parameter is related to a parameter which Ward-Smith calls W and is used by Kito and Kato (1984) under the name of Ω. These are defined via

$$\Omega = 2W = \frac{M_{ang}}{\pi\rho a^3\left[Q^z_{av}\right]^2} = \frac{2\int_0^a Q^\theta Q^z r^2 dr}{a^3\left[Q^z_{av}\right]^2} \qquad (3.19)$$

where Q^z_{av} is the average value of Q^z across the cross-section. The relation between Ω, W and S is

$$\frac{\Omega}{S} = \frac{2W}{S} = \frac{2}{a^2}\int_0^a \left[\frac{Q^z}{Q^z_{av}}\right]^2 r\ dr \equiv \beta_m \qquad (3.20)$$

where (3.20) defines β_m, the momentum coefficient. For small swirls, β_m is close to unity but as S increases β_m changes owing to the altering axial velocity profile. Although S describes the state of the flow as a whole, Ω is sometimes useful because it gives a measure just of the degree of angular motion, taking no account of the condition of the accompaning axial flow (which varies independently to some degree).

From the point of view of the theorist then, S is the useful measure if we seek to model the whole flow. An experimentalist may well use Ω, or may follow Yajnik and Subbaiah (1973) in using a pair

of values for Q^{Θ} and Q^{Z} at some reference radius to obtain a value for the local flow angle $\Phi = \arctan(Q^{\Theta}/Q^{Z})$ and then using this as the measure of swirl level. For the low levels of swirl which they had ($S < 0.075$) there was a linear relation between S and Φ, which was (approximately) $2S = \tan\Phi$.

Other methods used by experimentalists have been based on the apparatus used to generate the swirl. Many early workers used twisted tapes and therefore used the helix tip angle of the tape (e.g. Krieth and Margolis (1960), Smithberg and Landis (1964)). In later endeavours, some arrangement of vanes were used (e.g. Baker and Sayre (1974)) where the angle at which these vanes were set was used as the measure of the swirl level. In those cases where an initial swirl was generated by either of these methods and then allowed to decay, these measures will only be local just dowstream of the swirl generator and are therefore of limited value.

It should be observed, finally, that for any pair of values for Re and S, there will be many possible flow patterns and (in some sense) progressively more as we replace S with Ω, W or Φ.

3.7.2 The characteristics of a swirling flow field

We consider only the class of flows in which a swirling flow is introduced into a pipe and is allowed to decay. The different methods which can be used to generate this initial flow drastically affect the ensuing flow patterns, chiefly through the distribution of tangential velocity, but also through the associated axial velocity and pressure distributions. Baker and Sayre (1974) provide a useful starting point in describing the forced vortex ($Q^{\Theta} \propto r$) and free vortex ($Q^{\Theta} \propto 1/r$) regions which can occur (together with a wall layer) in the general case. Together with these, information is presented regarding the axial profile, which has its maximum value close to the wall and a concave shape in the core of the pipe rather than the usual convex curve of fully developed flow. They show the radial pressure distribution as well, based on the integral of $(Q^{\Theta})^{2}/r$.

Recent data from the paper by Kito and Kato (1984) supports this general picture, but seems to differ as to the manner of decay. Baker and Sayre found that the radius at which the forced vortex gave

way to the free vortex region decreased with the decay of swirl, while Kito and Kato found the reverse effect. This can, however, be explained by the fact that the swirl levels are higher in the paper by Baker and Sayre. Overall, the picture is that the changeover radius moves inwards and then outwards again, as the forced vortex region occupies the whole cross-section of the pipe for the final stages of the decay. Both of these pieces of work employed guide vanes to generate the swirl; this system produces a predominantly free vortex form of tangential velocity profile. (See also Wolf, Lavan and Fejer (1969) for flows with large swirl levels). Bradshaw (1973) gives an analysis of this area, and points out the differences in flow field due to the method of swirl generation.

In flows where the swirl has been generated by twisted tapes, the flow is of a forced vortex form (e.g. Musolf (1963) - see Krieth and Sonju (1965)); this is also the case for a flow coming out of a double bend in two planes (e.g. Murakami, Shimizu and Shiragami (1969)).

As Bradshaw (1973) declares, 'any device for generating strong swirl will cause large changes in the axial profile, whose return to 'full development' will be inseparable from the decay of the swirl'. The work of Yajnik and Subbaiah (1973) indicates that sufficiently far away from the swirl generator there may be a similarity region, within which there is just one possible flow field for a given pair of values for the Reynolds number and the swirl number. This region will start as soon as the swirl has decayed sufficiently for the initial conditions only to be affecting the flow through the local swirl level. Together with Bradshaw's statement then, we see that although there is a similarity form of axial and tangential velocity for a given swirl level, the flow emerging from a swirl generator will not be of this form and so a transition region exists in which the flow 'sorts itself out'. It is not clear for how long the effects of the initial forms of the axial and tangential velocities persist before similarity is reached. The decay of the radial pressure gradient (directly associated with the tangential profile) is the direct influence on the axial profile and persists in the similarity region, whereas the effects of the initial velocity profiles are governed by the non-linearities in the axial and tangential momentum

equations. Clearly the form of axial profile a little way downstream of a swirl generator owes as least as much to the axial profile set up by that generator as to any axial profile inherently associated with the level of swirl (as measured by Ω) which is present.

It is also clear that different swirl generators will affect the size and structure of the turbulence in significant ways and that the character of the turbulence of the incoming flow is also of importance. It is not surprising in view of these factors that disparate results have been reported.

Another important consideration is the effect of the swirling nature of the flow itself upon the structure of the turbulence. Bradshaw (1973) is a repository for a very thorough treatment of this issue, pointing out the twin effects of the radial pressure gradient and the curvature of the streamlines giving rise to stabilisation (less turbulence) near the axis and destabilisation near to the pipe wall. Various methods for modelling this effect via analogy with buoyancy employing a varient of the meteriological Richardson's number have been used and are discussed there. The gradient Richardson number (Ri) can be defined as:

$$Ri = \frac{2\,\frac{Q^\theta}{r^2}\,\frac{\partial}{\partial r}\left[rQ^\theta\right]}{\left[\frac{\partial Q^z}{\partial r}\right]^2 + \left[\frac{\partial Q^\theta}{\partial r} - \frac{Q^\theta}{r}\right]^2} \qquad (3.21)$$

3.7.3 Literature review

Having described the nature of a swirling flow in a pipe and its decay in phenomelogical terms we turn now to a broadly chronological review of the development of this understanding in the literature.

Talbot (1954) carried out a study of swirling laminar flow, using a linearised model suitable for the case when the axial velocity profile remains parabolic, and obtained good agreement with experimental measurements even though these were carried out at high swirl levels which were likely to have affected the axial velocity profile (Ward-Smith (1980)). The result which he obtained, namely that swirl decays exponentially and slowly, established the fundamental nature of the subject. The underlying decay rate (of his lowest order eigenfunction) was λ where $\lambda Re = 44.4$ and λ governs the decay through the factor $\exp(-\lambda z/D)$. Figure 3.3 shows this relation

between Re and λ together with those relationships found by other workers in a variety of situations.

An important branch of work on turbulent swirling flows (and one which started early) concerns friction factors and heat transfer coefficients. The paper by Krieth and Margolis (1960) is a good starting point for the earlier work and together with Smithberg and Landis (1964) provide ample data. Both these partnerships used twisted tapes to generate (and maintain) their swirl and report the considerable increases in friction which occur. Smithberg and Landis also measured the velocity distribution on a cross-section of the pipe; this has been utilised by many later workers. This area has been pursued over the years, and more recently by Sparrow and Chaboki (1984) who used a novel swirl generator and characterised the swirl level (in their decaying flow) by means of the wall swirl angle (evaluated on the edge of the wall layer).

Among those who used the velocity measurements of Smithberg and Landis were Krieth and Sonju (1965) (also using twisted tapes) who employed them as an initial condition for their linearised version of the tangential momentum equation. They used an eddy viscosity independent of position whose value was chosen in order to fit the experimental values for λ obtained by means of a swirl meter. The predictions for the tangential velocity itself were satisfactory for the early stages of decay when compared with measurements of Musolf (1963). This classic paper of Krieth and Sonju (1965), oft quoted in the literature, found that λ increases as Re falls and that λ did not change appreciably with S. (The maximum swirl level occuring in their experiments was about $S = 0.25$).

In 1969 three pieces of work were published, each bearing in a different way upon the picture. Wolf, Lavan and Fejer (1969) considered flows of air with large swirl levels ($S > 1$) generated by vanes. The swirl level was sufficiently high for the size of the free vortex region to increase with axial distance and for the axial velocity almost to exhibit flow reversal. An important observation made by Bradshaw (1973) is that the values of the eddy viscosity used by Krieth and Sonju (1965) and Wolf, Lavan and Fejer (1969) differ by a factor of 2, presumably as a result of their different methods of swirl generation. Rochino and Lavan (1969) carried out some

analytical investigations and compared these, with limited success, with some known experimental results. Murakami, Shimizu and Shiragami (1969) carried out pitot tube measurements of the flows in and after various bend configurations including a double right-angle bend in two planes at an angle of 60°. This is the bend combination angle which produces the most swirl (see also Miller (1978)) and they present tangential and a few axial velocity measurements. These show a solid body rotation and axisymmetric axial profile in the downstream part of the pipe (after 10 or 15 diameters).

Leestma (1972) (working with air) used hot wire anemometry to consider the development of a fully developed flow profile following the introduction of a swirling flow into a pipe, using a rotating honeycomb (used to establish parallel flow when stationary) to generate the swirl. His results, that the presence of (decaying) swirl slows down the normal flow development and that the swirl decayed fastest in the center of the pipe, provide evidence that the axial velocity has an important role in the flow as well as confirming the complicated nature of the interaction between the axial and tangential velocities in a decaying swirling flow. Wolf, Lavan and Fejer (1969) also stated that the decay of swirl resulting in a variation in the radial pressure gradient inhibits development of the axial velocity profile.

In 1973 and 1974 the papers by Yajnik and Subbaiah (1973) and Baker and Sayre (1974) were published. They both used vanes, and generated small and large swirls respectively. The local similarity established by Yajnik and Subbaiah (at significant axial distances from the generator, and values of $S < .075$) was expressed in terms of linear relations between swirl angle ϕ and the coefficients in both the axial velocity law of the wall and the friction factor formula. Baker and Sayre found (as Krieth and Sonju) that λ increases with a fall in Re but could not speak confidently about any dependence of λ upon S. Data concerning the dependence of the axial pressure gradient on S were presented, showing (for example) that the pressure drop doubles at a swirl level of $S = 0.4$.

Oosthuizen (1974) compared Baker and Sayre's measurements with the results of a modified mixing-length turbulence model and obtained superior results to those of Rochino and Lavan (1969) and others who

had used more complicated models. He utilised the idea of having the eddy viscosities in different directions differ by an empirical factor (to represent the non-isotropy of the turbulence). He also used a (non-standard) form of Richardson's number to modify the mixing length (to take account of the effects of streamline curvature) together with the standard value of the associated empirical constant (see Bradshaw (1973)). He predicts that λ will rise with a rise in S and/or a fall in Re. His work has the weakness that the same initial condition for the axial velocity was used regardless of the swirl level under consideration.

Ito, Ogawa and Kuroda (1979) used circulation to characterise swirl, and considered decay rates in the Re range $2x10^3$ - $5x10^3$, observing a transition between two different formulae for λ as Re increased. Their experimental apparatus consisted of a vertical pipe which was blanked off at the bottom, where two tubes fed the fluid in tangentially.

Janik and Padmanabthan (1980) examined the swirl (via a swirl meter) and the pressure drop in a large pipe close to swirl generating vanes, finding a striking increase of λ with decrease of the vane angle and/or Re. Velocity profiles downstream of the swirl generator were not measured.

Rapier (1981) carried out very crude analyses of decay rates of disturbances in pipe flows, finding that swirl was by far the longest lasting. His approach was similar to that of Youssef (1966) and has also been used by Mottram and Rawat (1986).

Both Nystrom and Padmanabhan (1985) and Mottram and Rawat (1986) have provided data concerning the decay rate of swirl in flows following double bends in two perpendicular planes.

The work described so far concerns stationary pipes. Although this is our only practical concern, it is useful to consider the methods and findings of reseachers who have looked at axially rotating ones. Lavan, Nielsen and Fejer (1969) considered laminar flow (analytically) in the region where a stationary and a rotating pipe join, in the case where the swirl level is high. Significant effects upon the axial profile were predicted (including flow reversal); these arose from the pressure term. Murakami, Kikuyama and Nishibori (1983) have studied turbulent flow in rotating pipes, using

Bradshaw's (1969) Richardson's number relation to modify their mixing length turbulence model; these modifications were supported by the experimental results which displyed marked turbulence stabilisation.

In 1984 two pieces of work by Kito were published. The first (by Kito alone) concerned the asymmetrical nature of most swirling flows (this had been observed by Baker and Sayre (1974)) and presented measurements of the flow field generated both by a symmetrical and an asymmetrical arrangement of vanes. The latter produced the more noticeable effects, but even in the supposedly axisymmetrical case a horseshoe shaped region of higher axial velocity surrounded an offset swirl center. As the horseshoe decays the axial profile becomes simply sheared across the pipe and the swirl becomes purely a solid body rotation. The whole flow pattern rotated with the swirl as it travelled along the pipe. The paper by Mottram and Rawat (1986) contains asymmetrical velocity profiles (measured on only one diameter) of similar form to those of Kito. It can be argued that a horseshoe profile is present which rotates with the swirl as it decays. This matter will be discussed more fully in chapter 7.

The other piece of work (Kito and Kato (1984)) concerned the flow close to the wall in a swirling pipe flow also generated by vanes. The measurements evidenced a change from a forced and free vortex mode towards the purely forced vortex mode (in the core of the pipe) as swirl decayed and showed that the axial velocity in the logarithmic region was only affected if $\Omega > 0.1$ (Ω is defined in equation 3.19). It seems likely that at this stage of the decay the flow was entirely of the forced vortex form. It is also the swirl level at which Bradshaw's (1969) criterion indicates flow instability near the wall. It was found that the flow became three-dimensional when Ω exceeded 0.186 and that the effect of swirl upon the axial velocity near the wall was saturated at $\Omega = 0.25$.

3.8 The effect of swirling flows on flowmeter readings

In this section we consider some of the literature relating to the effects of swirling flows on the accuracy of flowmeters. The intention is to give an overview of the nature of effects on different meter types and the sizes of swirl which cause appreciable errors rather than to give a manual dealing with all the practical

details.

The International Standard dealing with this area (ISO (1980)) is only applicable to differential pressure meters and contains two kinds of information of relevance here. Firstly, it gives minimum installation lengths of upstream and downstream piping for use following certain common pipe configurations in order to achieve the same accuracy as should be obtained in ideal (fully developed) conditions. For the swirl generating case of a double bend in two planes this table specifies (for an orifice meter) a length of 34 diameters when $\beta = 0.2$ rising to 80 diameters when $\beta = 0.8$. (β is the ratio of the diameters of the orifice and the pipe). These are the largest distances recommended for any of the situations dealt with. Secondly, the standard specifies that the flow profile may be regarded as satisfactory if the swirl angle is below 2° and if the ratio of the axial velocity at any point to its maximum value on the plane cross-section under consideration is within 5% of the corresponding value in fully developed flow.

The work of McHugh et al (1981,1984) has shown that the effects of swirl and of an asymmetrical axial velocity profile are in opposing directions (swirl increasing the discharge coefficient; the other reducing it). This means that situations involving different swirl generators and/or β ratios behave differently. In some tests with a double bend in two planes where the swirl angle was about 15° and the flow was asymmetrical there was a 3% increase in the discharge coefficient for $\beta = 0.31$ and a 3% fall for $\beta = 0.64$. The use of a flow straightener only removed the errors from the meter with $\beta = 0.31$, owing to the continued presence of asymmetry in the flow. In conditions of high swirl (60°) generated by vanes, they found increases in the discharge coefficient of up to 20%.

Mottram and Rawat (1986), experimenting with swirl generated by a double bend found increases in the discharge coefficient of up to 3% and a very significant variation in this effect with pipe roughness. Both McHugh et al and Mottram and Rawat used a Borda inlet as the first component of the flow loop, with only a short distance between it and the double bend. As a result of this the velocity profile at the inlet to the bend will not have been fully developed and may not even have been fully turbulent.

The turbine meter is clearly a meter sensitive to swirl. In a paper by Salami (1984) this is shown up well. In the absence of straighteners the reading obtained is a roughly linear function of the angle of the swirl generator, there being about a 1% increase in reading for each degree of swirl. Some straighteners consisting of a number of radial vanes were tested which reduced this percentage by various amounts. They were more effective if they were longer and/or had more vanes. It is clear that the 2° of swirl rule in the standard does not apply to turbine meters.

Work concerning electromagnetic flowmeters has been carried out by Tsachida, Tershima and Machiyama (1982). Following a double bend in two planes they plotted a graph of the percentage error against the axial distance between the bend and the meter for both horizontal and vertical meter orientations. They found that the curve for each orientation was qualitatively similar to a damped sine wave, the curves for the two different orientations being π out of phase. The maximum error was about 0.5% at a distance of 7 diameters from the bend. Deacon (1982) carried out a number of tests on electromagnetic meters following a double bend in two planes, concluding that the errors ranged between .23% and 1.97% depending on the make of meter and its postion (2½ or 5 diameters from the bend).

Cousins (1977) has investigated the effect of swirl on vortex-shedding meters by installing one 10 diameters after a double bend in two perpendicular planes. His results displayed no significant meter errors; nevertheless he observes that sufficient swirl can have a very significant effect on the mechanism of vortex-shedding.

Davies, Moore, Mattingly and Miller (1978) have carried out some numerical calculations using the k-ϵ model of turbulence concerning the effects of swirling flow on target flowmeters, which measure the flowrate by placing a 'target' disk in the flow and sensing the drag force on it. They used an inlet condition for the tangential velocity consisting of a region of forced vortex flow and a region of free vortex flow, and found errors of up to 50% when the flow was nearly all of the free vortex form even at a value of S as low as 0.25.

4. THE THEORETICAL WORK

4.1 The philosophy of the approach

We have already identified in section 2.7 some industrial motivations for an improved understanding of swirling pipe flows. We have also identified the governing equations and the form of available turbulence models in chapter 3, together with an understanding of the nature of the flow field. We also saw, in section 3.7.2 that following the generation of swirl (whether by bends or vanes), the tangential and axial velocities interact as the swirl decays. At large enough distances downstream there is a similarity solution (with the flow field depending only on Re and S). Further upstream the profiles depend more directly on the initial (entry) conditions.

The basic philosophy adopted in this work is to seek solutions which characterise the motion of the fluid in the case of axisymmetric swirling flow. To do this, we use both linear equations to obtain solutions for various different initial conditions and non-linear equations to find a similarity solution. Throughout, we regard the axial velocity as the fully developed velocity profile plus a perturbation velocity profile.

The reasoning behind this approach is threefold. Firstly, we shall obtain general forms for the velocity profiles which should be suitable for the purpose of analysing effects on flowmeters. Secondly, the predominantly solid-body rotation type of swirling flows which arise out of a double bend in two planes (the typical industrial situation in which swirl occurs) is also the far field form of all swirling flows regardless of the nature of their origin. We shall thus be dealing with situations of practical interest since the sizes of swirl commonly found after bends is not very large and so a perturbation approach should be valid. Thirdly, to deal with the relatively short region before these methods are applicable would involve solving the equations for each set of initial conditions separately. This is because the equations would need to be both non-linear and asymmetrical and would contain more complicated turbulence modelling terms. This process would be inefficient (not necessarily giving information of general applicability) and would

yield information of limited theoretical value or practical use since the details of flows close to bends of different geometries are likely to be noticeably different from each other.

In the subsequent sections (having first of all described the mathematical model) we consider first of all the linearised equations, giving rise to axial and tangential (perturbation) flows which do not interact in any way. We move on to a second-order linear theory dealing with the direct effect of the tangential motion on the axial motion (applicable to small swirl levels) and then, finally, we consider a set of non-linear coupled equations for the similarity solution. The region of applicability of the similarity solution is not only, or even primarily a question of swirl level, but of the character of the flow - whether or not it has attained this form or not (in different physical situations this could be expected to occur at different swirl levels).

4.2 The mathematical model

4.2.1 The basic equations

We return to equations (3.2),(3.3) and (3.4) which are (renumbering them):

$$\frac{\partial \bar{Q}_i}{\partial x_i} = 0 \tag{4.1a}$$

$$\bar{Q}_j \frac{\partial \bar{Q}_i}{\partial x_j} = -\frac{1}{\rho}\frac{\partial \bar{P}}{\partial x_i} + \nu \frac{\partial^2 \bar{Q}_i}{\partial x_j^2} - \frac{\partial}{\partial x_j}\left(\overline{q_i q_j}\right) \tag{4.1b}$$

$$-\overline{q_i q_j} = \epsilon \left[\frac{\partial \bar{Q}_i}{\partial x_j} + \frac{\partial \bar{Q}_j}{\partial x_i} \right] - \frac{2}{3} k \, \delta_{ij} \tag{4.1c}$$

$$\epsilon = L^2 \left\{ \left[\frac{\partial \bar{Q}_i}{\partial x_j} + \frac{\partial \bar{Q}_j}{\partial x_i} \right] \frac{\partial \bar{Q}_i}{\partial x_j} \right\}^{1/2} \tag{4.1d}$$

We now amalgamate (4.1b) and (4.1c) using (4.1a), absorbing the

term in k into the pressure term to obtain

$$\bar{Q}_j \frac{\partial \bar{Q}_i}{\partial x_j} = -\frac{1}{\rho}\frac{\partial \bar{P}}{\partial x_i} + (\nu + \epsilon)\frac{\partial^2 \bar{Q}_i}{\partial x_j^2} + \left[\frac{\partial \bar{Q}_i}{\partial x_j} + \frac{\partial \bar{Q}_j}{\partial x_i}\right]\frac{\partial}{\partial x_j}(\nu + \epsilon) \qquad (4.2)$$

We now employ cylindrical polar coordinates (z,r,Θ) and consider the case of axisymmetric flow obtaining

$$U^z_z + U^r_r + \frac{1}{r}U^r = 0 \qquad (4.3a)$$

$$(V + U^z)U^z_z + U^r(V_r + U^z_r) = -P_z + (\nu + \epsilon)\left[\frac{1}{r}\left[r(V_r + U^z_r)\right]_r + U^z_{zz}\right]$$

$$+ (\nu + \epsilon)_r(V_r + U^z_r + U^r_z) + 2U^z_z(\nu + \epsilon)_z + \frac{2}{a}u^2_\tau \qquad (4.3b)$$

$$(V + U^z)U^r_z + U^rU^r_r - \frac{[U^\Theta]^2}{r} = -P_r + (\nu + \epsilon)\left[\frac{1}{r}\left[rU^r_r\right]_r - \frac{1}{r^2}U^r + U^r_{zz}\right]$$

$$+ (\nu + \epsilon)_z(V_r + U^z_r + U^r_z) + 2U^r_r(\nu + \epsilon)_r \qquad (4.3c)$$

$$(V + U^z)U^\Theta_z + U^r(U^\Theta_r + \frac{1}{r}U^\Theta) = (\nu + \epsilon)\left[\frac{1}{r}\left[rU^\Theta_r\right]_r - \frac{1}{r^2}U^\Theta + U^\Theta_{zz}\right]$$

$$+ (\nu + \epsilon)_z U^\Theta_z + (\nu + \epsilon)_r r\left[\frac{U^\Theta}{r}\right]_r \qquad (4.3d)$$

where $U^z_r = \frac{\partial}{\partial r}$(z coordinate of $\underline{U}$),

$V = V(r)$ = mean fully developed axial velocity profile (3.7),

$\underline{U}$ = mean perturbation velocity (total flow = $(V(r),0,0) + \underline{U}$),

P = modified mean perturbation pressure = $\bar{P}/\rho - 2u_\tau^2 z/a$,

and u_τ, a and ρ are defined as in equation (3.6).

We now employ the standard assumption that second derivatives with respect to z are zero. This is the same as saying that the flow is a boundary layer, that the decay is slow or that the radial velocity is small compared with the axial velocity. We obtain

$$U^z_z + U^r_r + \frac{1}{r}U^r = 0 \qquad (4.4a)$$

$$(V + U^z)\,U^z_z + U^r(V_r + U^z_r) + P_z = \frac{1}{r}\left[r(\nu + \epsilon)\left[V_r + U^z_r\right]\right]_r + \frac{2}{a}u^2_\tau \qquad (4.4b)$$

$$- \frac{[U^\Theta]^2}{r} + P_r = 0 \qquad (4.4c)$$

$$(V + U^z)\, U^\Theta_z + U^r(U^\Theta_r + \frac{1}{r}\, U^\Theta) = \frac{1}{r^2}\left[r^2(\nu + \epsilon)\left[U^\Theta_r - \frac{U^\Theta}{r}\right]\right]_r \qquad (4.4d)$$

This has been acheived by observing that the continuity equation (4.4a) implies that if $U^z_{zz} \ll U^z_{rr}$ then $U^r_z \ll U^z_r$. This accounts for the lack of terms in the radial equation (4.4c).

It can be seen at this point, that the first terms of equations (4.4b,d) give rise to the z-derivative of the numerator and denominator of the expression for the swirl level S (see equation (3.18)), simply by multiplying by appropriate powers of r and ignoring second derivatives with respect to z.

We now consider equation (4.1d). On examining a full expansion of the bracket ignoring terms involving either a derivative with respect to Θ or a second derivative with respect to z we obtain

$$\epsilon = L^2 \left[\left[V_r + U^z_r\right]^2 + \left[U^\Theta_r - \frac{U^\Theta}{r}\right]^2 \right]^{1/2} \qquad (4.5)$$

which can be recast as

$$\epsilon = \epsilon_0 \left[\left[1 + \frac{U^z_r}{V_r}\right]^2 + \left[\frac{U^\Theta_r - \frac{U^\Theta}{r}}{V_r}\right]^2 \right]^{1/2} \qquad (4.6)$$

where $$\epsilon_o = L^2 |V_r| \qquad (4.7)$$

which is the formula for ϵ in fully developed flow. We express ϵ in this form in order to facilitate the use of different descriptions of the fully developed flow variables. It also makes the difference due to the perturbation flow easier to see.

We shall use the stream function ψ to remove equation (4.4a). ψ is defined by the equations

$$\psi_z = -rU^r \quad , \quad \psi_r = rU^z \qquad (4.8)$$

The flow field is thus represented by the three scalars ψ, U^Θ and P each of these being a function of r and z. We turn now to the

question of boundary conditions. These may most easily be understood by imagining the pressure terms to have been eliminated by differentiation. The remaining two parabolic equations in ψ and U^Θ have the boundary conditions

In r (for all z):

$$\text{At } r = 0 \qquad \frac{\psi_z}{r} = \left[\frac{\psi_r}{r}\right]_r = U^\Theta = 0, \tag{4.9a}$$

$$\text{At } r = a \qquad \frac{\psi_z}{r} = \frac{\psi_r}{r} = U^\Theta = 0, \tag{4.9b}$$

$$\text{and} \qquad \psi(r=0) = \psi(r=a) = \text{constant} \tag{4.9c}$$

In z (for all r)

$$\text{At } z = 0 \qquad \psi \text{ and } U^\Theta \text{ specified} \tag{4.9d}$$

The conditions in r ensure that there is no slip on the wall and that the solution is non-singular on the axis (4.9a,b) and that the perturbation flow does not contribute to the bulk flow along the pipe (4.9c). The (constant) value of ψ on pipe axis and wall will be taken (without loss of generality) to be zero. (Boundary conditions on the pressure P are determined by the above conditions and the equations. They are that $P_r(r=0) = 0$ and that $P(z=0)$ be specified).

Thus the set of equations with which we work is (4.4),(4.6) and (4.8) together with the boundary conditions (4.9). We also employ formulae for V and ϵ_o; these are described in the next section.

It will be seen that no allowance is made for the effect of rotation on the turbulence using Richardson's number Ri (3.21). This is because we deal with swirl levels sufficiently small for this effect to be unimportant (it's inclusion would multiply L by a factor of 1-2.5Ri (Bradshaw (1973)), Ri being of the order of 0.01 when S=0.1 since Ri involves the square of U^Θ).

4.2.2 Formulae for fully developed flow

We use two different descriptions, one based around the log law of the wall and the other based on the Nikuradse mixing-length formula. In both cases we ensure that our formulae for V and ϵ_o satisfy equation (3.7). The fundamental difference between the methods is that the first method starts by defining V predominantly

on theoretical grounds and then obtains ϵ_o from (3.7), whereas the second method starts by defining ϵ_o on the grounds of experimental results and then finds V from (3.7). However, both methods use an empirical polynomial for ϵ_o as their starting point in a region near the pipe axis (a precedent set by Reichardt (1951)).

(i) Method 'A' (based on the log law)

The logarithmic law of the wall described in section 3.5.2 only truly applies in the region close to the wall where $30\nu/u_\tau < y < 0.2a$ where $y = a - r$. We define the friction Reynolds number $R_\tau = au_\tau/\nu$. In the region closer to the wall than this, we use a 'merger' of this law (as Hinze (1975) p721) and a logarithmic law of approximately twice the slope, following empirical fits to data (see Afzal (1982)), together with a linear law for the velocity in the viscous sublayer. We do not use Afzal's 'composite velocity profile' because it is not smooth at $y/a = 5/R_\tau$ owing to its aysymptotic nature. In the central region we use a polynomial in r^4 for ϵ_o chosen so that ϵ_o takes the value $0.07au_\tau$ on the axis (as suggested by Hinze (1975) on the basis of Laufer's (1954) measurements), and so that there is a smooth transition of value and slope at $r = 0.8a$. The expressions are:

For $1 \geq r/a \geq 1-5/R_\tau$:

$$V = \frac{yu_\tau}{aR_\tau} \qquad (4.10a)$$

For $1-5/R_\tau \geq r/a \geq 1-30/R_\tau$:

$$\frac{V - U_c}{u_\tau} = \left[1 - \alpha\left[\frac{y}{a}\right]\right]\left[2.44 \ln\left[\frac{y}{a}\right] - 0.8\right] + \alpha\left[\frac{y}{a}\right]\left[5 \ln\left[\frac{y}{a}\right] - 3.05\right] \qquad (4.10b)$$

where $\alpha(y/a) = (2 - 3q + q^3)/4$, $q = y/a - 17.5/R_\tau$.

For $1-30/R_\tau \geq r/a \geq 0.8$:

$$\frac{V - U_c}{u_\tau} = 2.44 \ln\left[\frac{y}{a}\right] - 0.8 \qquad (4.10c)$$

For $0.8 \geq r/a \geq 0$:

$$\frac{\epsilon_o + \nu}{au_\tau} = 0.07\left[1 + \beta\left[\frac{r}{a}\right]^4 + \gamma\left[\frac{r}{a}\right]^8\right] \qquad (4.10d)$$

where we use equation (3.7) to find ϵ_o or V as appropriate and choose β, γ to ensure a smooth fit at $r/a = 0.8$.

(ii) Method 'B' (based on Nikuradse)

We use the idea of a mixing length as discussed in section 3.5.3. We modify the empirical formula due to Nikuradse via the buffer layer correction devised by Van Driest as mentioned there. This multiplies the L given in equation (3.15) by an exponential factor resulting in the formula

$$\frac{L}{a} = \left[0.14 - 0.08 \left[\frac{r}{a}\right]^2 - 0.06 \left[\frac{r}{a}\right]^4 \right] \left[1 - \exp\left[- \frac{yR_\tau}{26a} \right] \right] \qquad (4.11)$$

With L specified we can calculate dV/dr from (3.14) and integrate it from the wall where V = 0 to find V. Close to the axis of the pipe, L is constant and dV/dr = 0, giving $\epsilon_0 = 0$. This is clearly wrong physically (since there are turbulent fluctuations there) and a direct comparison with values of ϵ_0 calculated from Nikuradse's measurements (see Schlichting (1979) p609) shows that $\epsilon_0 \neq 0$ on the axis. The discrepancy arises as a result of fitting L to data rather than fitting ϵ_0 directly. Although L is a useful concept it fails on the axis (since it would need an infinite value of L to give a non-zero value of ϵ_0). Accordingly, we use a polynomial for ϵ_0 in this region ($r < 0.1a$), based on the graph given in Schlichting, making a smooth join with the formula in the rest of the pipe. It takes the form

$$\frac{\epsilon_0}{au_\tau} = .0125 + \zeta\left[\frac{r}{a}\right] + \eta\left[\frac{r}{a}\right]^2 \qquad (4.12)$$

We are able to extend this method to the case of a rough pipe quite easily by following the method of Van Driest (1956) by changing the multiplier in equation (4.11) so that it becomes

$$1 - \exp\left[- \frac{yR_\tau}{26a}\right] + \exp\left[- \frac{35y\ D}{26a\ \epsilon_R}\right] \qquad (4.13)$$

for values of ϵ_R/D satisfying $0 \leq \epsilon_R/D \leq 35/R_\tau$, and just 1 for $\epsilon_R/D \geq 35/R_\tau$. The figure of 35 used here is different from the figure of 30 that Van Driest used; we follow Ward-Smith here because we are also using his expressions for the friction factor.

In practise, these profiles need small adjustments in order to ensure that the mean velocity is normalised. This is done by multiplying U_c and L by a factor close to unity in methods (i) and (ii) respectively so that

$$2\pi \int_0^a rV(r)\, dr = \pi a^2 U_{av} \qquad (4.14)$$

Figures 4.1 and 4.2 show the fully developed flow velocity and eddy viscosity in various cases. Figure 4.1 is a comparison between methods 'A' and 'B' and also shows the profiles obtained with method 'B' in a pipe of relative roughness $\epsilon_R/D = 0.0026$. This corresponds to a typical 3" steel pipe. Figure 4.2 is a comparison between the Reynolds numbers $10^4, 10^5$ and 10^6 for the case of method 'B' in a smooth pipe.

4.3 The linearised theory

4.3.1 Introduction

We consider the case where $|\underline{U}|$ is small compared with $|V|$, and linearise the set of equations we obtained at the end of section 4.2.1. For equation (4.6) we obtain

$$\epsilon = \epsilon_o \left| \left[1 + \frac{U_r^z}{V_r} \right] \right| \qquad (4.15)$$

On substitution into (4.4) using (4.8) we have

$$\frac{1}{r} V \psi_{rz} - \frac{1}{r} V_r \psi_z + P_z = \frac{1}{r} \left[r(\nu + 2\epsilon_0) \left[\frac{\psi_r}{r} \right]_r \right]_r \qquad (4.16a)$$

$$P_r = 0 \qquad (4.16b)$$

$$V U_z^\Theta = \frac{1}{r^2} \left[r^2(\nu + \epsilon_0) \left[U_r^\Theta - \frac{U^\Theta}{r} \right] \right]_r \qquad (4.16c)$$

We have ignored the modulus signs in (4.15) because we are working with a small perturbation, thus ensuring that the value of the bracket is always positive.

It can be seen that the equations (4.16) form two groups; one consisting of two equations for ψ and P, the other a single equation for U^Θ. This linearised theory then, deals only with perturbations in which the axial and tangential velocity are independent. Hence we cannot deal with the interactions between these velocity components using this method.

4.3.2 The tangential motion

We consider first the tangential momentum equation (4.16c). We try a separated solution of the form

$$U^{\Theta} = g(r^*) \exp(-\lambda z^*) \qquad (4.17)$$

where $r^* = r/a$ and $z^* = z/D$.

On substitution into (4.16c) and non-dimensionalising we have

$$\frac{1}{r^*}(r^*(\nu^* + \epsilon_0^*)\, g')' - \frac{1}{r^{*2}}(r^*(\nu^* + \epsilon_0^*))'g + \lambda F V^* g = 0 \qquad (4.18a)$$

where $\nu^* = \frac{\nu}{au_\tau}$, $\epsilon_0^* = \frac{\epsilon_0}{au_\tau}$, $V^* = \frac{V}{U_{av}}$, $\frac{1}{F} = \frac{u_\tau}{2U_{av}}$ and $g' = \frac{dg}{dr}$ (4.18b)

From henceforth we shall drop the superscript '*' indicating a non-dimensionalised variable.

It can be seen that (4.18a) together with the boundary conditions that g(r=0) = g(r=1) = 0 form a Sturm-Louville system with eigenvalues λ_n and eigenfunctions $g_n(r)$ which can be normalised to satisfy the orthonormality condition

$$\int_0^1 rV(r)\, g_m(r)\, g_n(r)\, dr = \delta_{mn} \qquad (4.19)$$

It can be shown that these eigenfunctions form a complete set (e.g. Morse and Feschbach (1953) p719f). This means that any function for $U^{\Theta}(r)$ on z=0 can be expressed as a linear combination of the $g_n(r)$'s and that we therefore have the solution to the problem. The values of the coefficients can be calculated easily owing to the orthogonality of the eigenfunctions. The formula for $U^{\Theta}(r,z)$ is

$$U^{\Theta}(r,z) = \sum_{n=0}^{\infty} a_n g_n(r)\, e^{-\lambda_n z} \qquad (4.20)$$

where $$a_n = \int_0^1 rV(r)\, g_n(r)\, U^{\Theta}_{z=0}(r)\, dr \qquad (4.21)$$

It is found (see section 5.2) that the lowest eigenvalue λ_o is of the order of 0.02, corresponding to a decay rate of a factor of 10 in 115 diameters and that the other λ_n's are at least 10 times higher. The function $g_o(r)$ has the form of a solid body rotation except in a thin layer near the wall; the function $g_n(r)$ has n zeros other than the end-points.

4.3.3 The axial motion

We turn now to the axial motion and try the following expressions for the stream function and pressure

$$\psi(r,z) = h(r)\ \exp(-\mu z)\ ,\quad P(z) = p\ \exp(-\mu z) \tag{4.22}$$

When these are used in (4.16a,b) we obtain

$$\frac{1}{r}\left[\ r(\nu + 2\epsilon_0)\left[\frac{h'}{r}\right]'\ \right]' = \mu F\left[\ p + \frac{1}{r}(Vh' - V'h)\ \right] \tag{4.23}$$

together with the boundary conditions of (4.9). This can be solved (see section 5.3) to give a collection of eigenvalues μ_n and eigenfunctions $h_n(r)$. The lowest eigenvalue μ_o is of the order of 0.2 corresponding to a decay rate of a factor of 10 in 12 diameters. The function $h_n(r)$ has n zeros other than those at the end-points. The function $h_o(r)$ corresponds to a perturbation axial velocity which is (say) negative in the central region of the pipe and positive near the wall, it being of zero magnitude at a radius of about 0.7. Unfortunately, these $h_n(r)$'s are not directly orthogonal and moreover it is not possible to prove completeness in the same way as before (the operator is not self-adjoint). However, it is possible to approximate an initial condition closely using them so that for all practical purposes this is a solution to the problem. We should use a weighting function in the same manner as before, chosen (with regard to the equations) to be $(V'/r)'$. The precise choice is unimportant since we should be solving a matrix equation for the coefficients in any case.

4.4 The second-order linear theory

We now consider an extension of the linear theory discussed above in section 4.3, in order to deal with the interactions between the tangential and axial motion. We substitute the most slowly decaying term in the eigenfunction expansion obtained for the tangential velocity back into the non-linear terms in the equations for the stream function. In other words, we take equations (4.4a-c),(4.6) and (4.8), non-dimensionalise them and substitute the expressions

$$\psi = A^2 t_0(r) e^{-2\lambda_0} \tag{4.24a}$$

$$P = A^2 q_0(r) e^{-2\lambda_0 z} \tag{4.24b}$$

$$U^\Theta = A\, g_0(r) e^{-\lambda_0 z} \tag{4.24c}$$

where A is an arbitrary constant factor. We remove terms involving powers of A greater than two, and in particular we find that (4.6) becomes

$$\epsilon = \epsilon_0\left[1 + \frac{U_r^z}{V'} + \frac{1}{2}\left[\frac{U_r^\Theta - U^\Theta/r}{V'}\right]^2\right] \tag{4.25}$$

It will be seen that the equation for U^Θ is that of the linear theory and that we have the following equation for t_0:

$$\frac{2\lambda_0 F}{r}(Vt_0' - V't_0) - \frac{1}{r}\left[r(\nu + 2\epsilon)\left[\frac{t_0'}{r}\right]'\right]' = 2\lambda_0 F q_0(r) + P_f(r) \tag{4.26a}$$

where $P_f(r) = \frac{(g_0' - g_0/r)}{V'}\left[\epsilon_0\left[g_0'' - \frac{g_0'}{r} + \frac{g_0}{r^2}\right]\right.$

$$\left. + \frac{(g_0' - g_0/r)}{2}\left[\epsilon_0\left[\frac{1}{r} - \frac{V''}{V'}\right] + \epsilon_0'\right]\right] \tag{4.26b}$$

and $q_0(r) = K_0 + \int_0^r \frac{g_0^2(r)}{r}\, dr$. (4.26c)

We have the boundary conditions of (4.9), and can obtain (see section 5.4) a solution for the stream function forced by the tangential velocity. The basic form of the result is similar to that of the eigenfunction h_0.

4.5 The similarity theory

We consider now an approach similar in form to the linear theory in that exponential decays are used, but which is fundamentally different in that the flow is to be entirely determined by the specification of the swirl level S. This similarity solution, endeavours to determine the magnitude and form of axial profile inherently associated with a particular level of swirl. Evidence to suggest that such a form may exist is provided by the experimental work of Yajnik and Subbaiah (1973).

We return to the equations (4.4), (4.6) and (4.8) and make the assumption that

$$U^\Theta = G(r)\exp(-\lambda z), \qquad \psi = H(r)\exp(-2\lambda z) \tag{4.27}$$

on the grounds of the form of equation (4.4c) and linear theories. We absorb the radial momentum equation (4.4c) into the axial momentum equation by an integration with constant K as in section 4.4 to obtain the equations

$$-2\lambda F\left[\left[V+\frac{H'}{r}e^{-2\lambda z}\right]\frac{H'}{r}-\frac{H}{r}\left[V+\frac{H'}{r}e^{-2\lambda z}\right]'+\left[K+\int_0^r\frac{G^2}{r}\,dr\right]\right]e^{-2\lambda z}$$

$$=\frac{1}{r}\left[r(\nu+\epsilon)\left[V+\frac{H'}{r}e^{-2\lambda z}\right]'\right]'+1 \qquad (4.28a)$$

$$-\lambda F\left[\left[V+\frac{H'}{r}e^{-2\lambda z}\right]Ge^{-\lambda z}+2\frac{H}{r}\left[G'+\frac{G}{r}\right]e^{-3\lambda z}\right]$$

$$=\frac{1}{r^2}\left[r^2(\nu+\epsilon)\left[G'-\frac{G}{r}\right]\right]'e^{-\lambda z} \qquad (4.28b)$$

$$\epsilon=\epsilon_0\left[\left[1+\frac{(H'/r)'}{V'}e^{-2\lambda z}\right]^2+\left[\frac{(G'-G/r)}{V'}e^{-\lambda z}\right]^2\right]^{1/2} \qquad (4.28c)$$

We now consider a particular plane cross-section of the pipe at which the swirl level is defined. Defining the z-origin to be at this plane removes all of the exponentials in (4.25), leaving us with the problem specified by the equations

$$-2\lambda F\left[\left[V+\frac{H'}{r}\right]\frac{H'}{r}-\frac{H}{r}\left[V+\frac{H'}{r}\right]'+K+\int_0^r\frac{G^2}{r}\,dr\right]$$

$$=\frac{1}{r}\left[r(\nu+\epsilon)\left[V+\frac{H'}{r}\right]\right]'+1 \qquad (4.29a)$$

$$-\lambda F\left[\left[V+\frac{H'}{r}\right]G+2\frac{H}{r}\left[G'+\frac{G}{r}\right]\right]=\frac{1}{r^2}\left[r^2(\nu+\epsilon)\left[G'-\frac{G}{r}\right]\right]' \qquad (4.29b)$$

$$\epsilon=\epsilon_0\left[\left[1+\frac{(H'/r)'}{V'}\right]^2+\left[\frac{G'-G/r}{V'}\right]^2\right]^{1/2} \qquad (4.29c)$$

with the boundary conditions

$$G(0)=G(1)=H(0)=H(1)=0 \qquad (4.30a)$$

$$\left[\frac{H'}{r}\right]'(0)=\frac{H}{r}(0)=\frac{H}{r}(1)=\frac{H'}{r}(1)=0 \qquad (4.30b)$$

with the swirl level defined by

$$S=\frac{\int_0^1\left[V+\frac{H'}{r}\right]Gr^2dr}{\int_0^1\left[V+\frac{H'}{r}\right]^2 r\,dr} \qquad (4.31)$$

This problem is solved separately for each value of S, to give the similarity solution for that particular swirl level (see section 5.5). Solutions at different values of S can be strung together using the decay rates contained in the solution; this then gives the full solution. It can be seen that for small swirl levels the solutions of these equations will be the same as those obtained on the basis of the second-order linear theory of section 4.4.

5. THE COMPUTATIONAL WORK

5.1 The numerical method

5.1.1 Finding the fully developed flow quantities

We use the quantities V and ϵ_o (and various of their derivatives) in the coefficients of the differential equations we wish to solve. Expressions for these quantities, based on two different methods, are given in section 4.2.2. It was observed there that slight modifications were needed to ensure that the bulk flow velocity found by integrating V/U_{av} is equal to unity. A searching routine was used to achieve this that was also used to help solve the main equations; it is discussed here. As an example, we take method 'A' of section 4.2.2 where the value of U_c is to be found.

Once a value of U_c has been prescribed, it is possible to calculate everything else and then to evaluate the expression

$$I = 2 \int_0^1 r \left[\frac{V}{U_{av}}\right] dr - 1 \qquad (5.1)$$

which should ideally give the result I = 0, though in fact it will be slightly different. If we make two different initial guesses for U_c called U_{c1} and U_{c2} and these provide corresponding values I_1 and I_2 then the searching procedure for the value of U_c which gives $|I| \leq ER$ (where ER is the maximum error permitted) is as follows. If I_1 and I_2 are of the same sign, linear extrapolation is used to find the value of U_c where I would be zero. This new value of U_c and the nearest of U_{c1} and U_{c2} to it are renamed U_{c1} and U_{c2} respectively. The appropriate value of I is renamed I_2 (this is the smaller of the original I_1 and I_2). The (new) value of U_{c1} produces a (new) value for I_1. This process is repeated until I_1 and I_2 are of opposite sign, or until $|I| \leq ER$. If and when I_1 and I_2 are of opposite sign the method of finding the new value of U_c is the same (now interpolation, obviously) but we ensure that we retain at each stage the closest pair of values of U_c which have corresponding values of I of opposite sign. We continue until $|I| \leq ER$. The flowchart in figure 5.1 illustrates this searching routine. Typically, in all the applications of this searching routine no more than 10 iterations were required. In this particular application we set ER = 10^{-5}.

5.1.2 The method used to solve the equations

The linearised equations of sections 4.3 and 4.4 can be expressed in the form

$$Y_1' = Y_2 \qquad (5.2a)$$

$$Y_2' = Y_3 \qquad (5.2b)$$

.....

$$Y_m' = f(x, Y_1, Y_2, \ldots, Y_m) \qquad (5.2c)$$

where m = 2,3 respectively, and Y' = dY/dx. (In the case of the linear equation for the tangential velocity x, Y_1, Y_2 correspond to r, U^θ, U^θ_r. We shall use the (x,Y) formulation whilst describing the general method.) The similarity theory of section 4.5 can be expressed as a coupled pair of such systems. At the outset therefore, we consider our method for dealing with a set of equations like this. The method we adopt is the standard 4th order Runge-Kutta method, a description of which can be found in any standard reference on numerical methods such as Isaacson and Keller (1966) p400f. The equations (5.2) are a special case of the general form to which the method can be applied. The general form is for a set of equations

$$Y_r' = f_r(x, Y_1, Y_2, \ldots, Y_m) \qquad r = 1, \ldots, m \qquad (5.3)$$

solved on a grid $x_1, x_2, \ldots, x_n, \ldots, x_N$
where $x_{n+1} = x_n + H$ by using the relations

$$Y_r(x_{n+1}) = Y_r(x_n) + (k_{r1} + 2k_{r2} + 2k_{r3} + k_{r4})/6 \qquad (5.4)$$

where

$$k_{r1} = Hf_r(x_n, Y_1(x_n), \ldots, Y_m(x_n)) \qquad (5.5a)$$

$$k_{r2} = Hf_r(x_n+H/2, Y_1(x_n)+k_{11}/2, \ldots, Y_m(x_n)+k_{m1}/2) \qquad (5.5b)$$

$$k_{r3} = Hf_r(x_n+H/2, Y_1(x_n)+k_{12}/2, \ldots, Y_m(x_n)+k_{m2}/2) \qquad (5.5c)$$

$$k_{r4} = Hf_r(x_n+H, Y_1(x_n)+k_{13}, \ldots, Y_m(x_n)+k_{m3}) \qquad (5.5d)$$

In order to start off the integration from the grid point x_1 it is necessary to specify the $Y_r(x_1)$. The method produces values of each Y_r to 4th-order accuracy; that is to say that the error term at each step is of the order of H^5. The grid that we use is not of

entirely uniform spacing owing to the presence of a wall layer in which many of the quantities involved have high gradients with respect to x. The grid adopted is as follows. The spacing between grid points is 0.01 from x_1 = 0.00 to x_{91} = 0.90, 0.001 from x_{91} to x_{181} = 0.990, and is 0.0001 from x_{181} to x_{281} = 1.0000. This grid has been chosen so that we integrate right across the pipe including all effects, even those in the viscous sublayer. Even at Re = 10^6 we still have 3 grid points within the viscous sublayer, since in this case $R_T = 1.91 \times 10^4$ and so $1-5/R_T = 0.99974$. We choose to integrate from the axis to the wall. In order to be able to evaluate (5.4c,d) it is necessary to know the values of V and ϵ_0 (and their derivatives) on a grid twice as fine as that used for the Y_r. These values are calculated at the beginning of the program in the way described in section 5.1.1.

Because half of the boundary conditions (in x) are specified at each end of the interval, it is necessary to guess the 'missing' boundary conditions at x_1 and to shoot to the postion x_{281} (that is to integrate across the pipe on the basis of the guess). The task then is to improve the original guess by a process of iteration until the values for the appropriate $Y_r(x_{281})$ correspond sufficiently closely to the boundary conditions specified at x_{281}. This is done using the searching routine described in section 5.1.1.

A number of checks on the overall accuracy of the method by increasing the number of grid points, working in the double precision mode of the VAX 8650 used and integrating in the opposite direction were carried out. None of these changes altered the results in any significant way. The integration was performed in the radial direction because the searching process converged faster when this was done.

5.2 The linear theory for the tangential velocity

5.2.1 The method

The equations, following section 4.3.2 and writing g_1 for g and g_2 for g' are

$$g_1' = g_2 \qquad (5.6a)$$

$$g_2' = -\left[\frac{1}{r} + \frac{\epsilon_o}{(\nu + \epsilon_o)}\right]\left[g_2 - \frac{g_1}{r}\right] - \frac{\lambda FV}{(\nu + \epsilon_o)} g_1 \qquad (5.6b)$$

together with the boundary conditions

$$g_1(0) = 0, \quad g_1(1) = 0 \qquad (5.6c)$$

In order to start off an integration from the grid position $x_1 = 0$, we have to specify $g_2(0)$ as well as putting $g_1(0) = 0$ in accordance with (5.6c). Because we are finding eigensolutions, the solution we find can be multiplied by any constant. This means that we can specify $g_2(0)$ to be any arbitrary value A_0 (say). However, we shall need to specify λ as well, and it is this quantity that we shall find via the searching routine of section 5.1.1 in such a way as to satisfy $g_1(1) = 0$. By choosing our initial pair of values for λ appropriately we can find whichever eigensolution we wish.

There is however one matter remaining to be explained. Having specified $g_1(0) = 0$ and $g_2(0) = A_0$ and prescribed a value for λ, the program should be able to solve the equation. In order to do so, however, it has to find $g_2'(0)$ by evaluating equation (5.6b) at $r = 0$. Because $1/r$ is singular at $r = 0$, this has to be done by hand using a power series for g, as follows. Putting $g \equiv g_1 = A_0 r + A_1 r^2 + A_2 r^3 + \ldots$. we find that $g_2 = A_0 + 2A_1 r + 3A_2 r^2 + \ldots$. and so (5.6b) becomes

$$2A_1 + 6A_2 r = -\left[\frac{1}{r} + \frac{\epsilon_o}{(\nu + \epsilon_o)}\right]\left[A_1 r + 2A_2 r^2\right] - \frac{\lambda FV}{(\nu + \epsilon_o)}\left[A_1 r\right] \qquad (5.7)$$

when terms in r^2 are ignored. It can be seen from section 4.2.2 that whichever method has been used to obtain V and ϵ_o that they have the forms

$$V = a_o + a_1 r^2 + a_2 r^3 + \ldots . \quad , \quad \epsilon_o = b_o + b_1 r + b_2 r^2 + \ldots . \qquad (5.8)$$

near $r = 0$. Therefore the terms in r^0 in (5.7) imply that $A_1 = 0$. We therefore specify $g_2'(0) = 0$ resulting in a set of initial conditions at $r = 0$ of

$$g_1(x_1) = 0, \quad g_2(x_1) = A_0, \quad g_2'(x_1) = 0 \qquad (5.9)$$

A process similar to this is required for each set of equations that we shall be considering.

When we use the searching routine to find λ we define the error

condition as $|g_1(1)/A_0| \leq ER = 10^{-5}$ to ensure that the boundary condition is approximated to within the chosen fraction of the typical size of the quantity concerned (in this case g). This principle is also applied to the other sets of equations discussed in later sections.

5.2.2 The results

Table 5.1 contains the values of λ_0, λ_1 and λ_2 obtained at each of the Reynolds numbers 10^4, 10^5 and 10^6 using each of 3 formulations of the fully developed flow quantities: method 'A' (for a smooth pipe) and method 'B' both for a smooth pipe and for a pipe with ϵ_R/D = 0.0026. This value of ϵ_R/D corresponds to a typical steel pipe of 3" diameter. Method 'B' with this roughness parameter is henceforth termed method 'B' rough.

Table 5.1

Reynolds Number	Fully developed flow formulation	λ_0	λ_1	λ_2
10^4	Method 'A' smooth	0.0316	0.2586	0.6156
	Method 'B' smooth	0.0320	0.2600	0.5816
	Method 'B' rough	0.0355	0.3025	0.6786
10^5	Method 'A' smooth	0.0192	0.1896	0.4442
	Method 'B' smooth	0.0196	0.1944	0.4462
	Method 'B' rough	0.0286	0.2635	0.6018
10^6	Method 'A' smooth	0.0126	0.1502	0.3510
	Method 'B' smooth	0.0126	0.1532	0.3540
	Method 'B' rough	0.0271	0.2710	0.6205

We see from this table that the two methods 'A' and 'B' (for smooth pipes) produce very similar results (as would be expected from the profiles of velocity and eddy viscosity shown in figures 4.1). We see that there is a significant dependence of λ_1 upon pipe roughness and upon Reynolds number.

Figure 5.2 is a graph of λ_o against Re for different values of ϵ_R/D, using method 'B'. It can be seen that the graph is very similar in form to the Moody diagram for the friction factor (e.g. Ward-Smith (1980) p164). In fact, in line with Rapier's crude analysis, the relation

$$\lambda_o = 4f \tag{5.10}$$

is satisfied by these results to within 10%.

In figure 5.3 we present graphs of a typical pair of velocity profiles arising from these calculations, corresponding to the eigenvalues λ_o and λ_1 at Re = 10^5, plotted both on a linear and a logarithmic scale. The latter scale reveals the fact that the behaviour close to the wall of the pipe is of the same form as that of the fully developed profile. The profiles are normalised in the sense of equation (4.19) and are given for the case of a smooth pipe using method 'B'.

Figure 5.4 shows the profile corresponding to the eigenvalue λ_o for each of the three formulations of the fully developed flow quantities described above at a Reynolds number of 10^5. It can be seen that they are very similar.

5.3 The linear theory for the stream function

5.3.1 The method

The equations, following section 4.3.3 and writing $h = r^2R$, $R_1 = R$, $R_2 = R'$, $R_3 = R''$ are

$$R_1' = R_2 \tag{5.10a}$$

$$R_2' = R_3 \tag{5.10b}$$

$$R_3' = -\frac{1}{r}\left[5R_3 + \frac{3R_2}{r}\right] - \frac{2\epsilon_o'}{(\nu + 2\epsilon_o)}\left[R_3 + \frac{3R_2}{r}\right] + \frac{\mu F}{(\nu + 2\epsilon_o)}\left[V'R_1 - V\left[R_2 + \frac{2R_1}{r}\right] - \frac{p}{r}\right] \tag{5.10c}$$

together with the boundary conditions

$$R'(0) = 0 \text{ ; with } R(0) \text{ and } R''(0) \text{ constants} \tag{5.11a}$$

$$R(1) = R'(1) = 0 \tag{5.11b}$$

If we specify $R_1(0) = B_0$, $R_2(0) = 0$ and $R_3(0) = 2B_1$ then putting the expression $R = B_0 + B_1r^2 + B_2r^3 + \ldots.$ in (5.10c) implies that for values of r near zero we have

$$6B_2 = -\frac{1}{r}(16B_1 + 39B_2r) - \frac{16\epsilon_0'B_1}{(\nu + 2\epsilon_0)} - \frac{\mu F}{(\nu + 2\epsilon_0)}\left[\frac{2VB_0}{r} + \frac{p}{r}\right] \qquad (5.12)$$

which results, upon the substitution of the forms for V and ϵ_0 in (5.8) and some algebraic manipulation, in the following initial conditions at r = 0

$$R_1(x_1) = B_0 \qquad (5.13a)$$

$$R_2(x_1) = 0 \qquad (5.13b)$$

$$R_3(x_1) = 2B_1 \qquad (5.13c)$$

$$R_3'(x_1) = -\frac{96B_1\epsilon_0'(0)}{15(\nu + 2\epsilon_0(0))} \qquad (5.13d)$$

$$p = -2V(0)B_0 - \frac{16(\nu + 2\epsilon_0(0))B_1}{\mu F} \qquad (5.13e)$$

When we use the searching routine of section 5.1.1 we fix B_0 and then choose B_1 and μ in order to satisfy the boundary conditions (5.11b). We do this by nesting two searching routines each of which are identical to the one already discussed. We make an initial guess for μ and then, using this value of μ, we use a searching routine to find the value of B_1 which satisfies the boundary condition $R_1(1) = 0$. We then make our second initial guess for μ and find the corresponding value for B_1. This second searching routine (for μ) continues in exactly the same way as the other one, finding that value of μ for which $R_2(1) = 0$. When we come to find B_1 for a particular value of μ, we use the values of B_1 associated with the two previous values of μ as our initial guesses for B_1. The error conditions employed were $|R_1(1)/(B_0\mu)| \leq 10^{-4}$ and $|R_2(1)/B_0| \leq 10^{-4}$.

5.3.2 The results

Table 5.2 contains the values of μ_0, μ_1 and μ_2 obtained for each of the Reynolds numbers 10^4, 10^5 and 10^6 for method 'B' smooth and method 'B' rough as defined in section 5.2.2.

Table 5.2

Reynolds Number	Fully developed flow formulation	μ_0	μ_1	μ_2
10^4	Method 'B' smooth	0.2768	0.7710	1.4734
	Method 'B' rough	0.3253	0.9059	1.1731
10^5	Method 'B' smooth	0.2176	0.6074	1.1720
	Method 'B' rough	0.2961	0.8237	1.5860
10^6	Method 'B' smooth	0.1754	0.4872	0.9376
	Method 'B' rough	0.3097	0.8581	1.6475

We see in the graph in figure 5.5 a comparison between the axial velocity profiles corresponding to the eigenvalue μ_0 at Re = 10^5 obtained with different pipe roughnesses. The axial velocities on the pipe axis are chosen to be the same in both cases. The form of profile near the wall is similar to that of the fully developed flow as was the linearised solution for the tangential velocity.

5.4 The second-order linear theory

5.4.1 The method

The equations, following section 4.4 and writing $t_0 = r^2 Z$ with $Z_1 = Z$, $Z_2 = Z'$ and $Z_3 = Z''$ are

$$Z_1' = Z_2 \tag{5.14a}$$

$$Z_2' = Z_3 \tag{5.14b}$$

$$Z_3' = -\frac{1}{r}\left[5Z_3 + \frac{3Z_2}{r}\right] - \frac{2\epsilon_0'}{(\nu + 2\epsilon_0)}\left[Z_3 + \frac{3Z_2}{r}\right]$$

$$+ \frac{1}{(\nu + 2\epsilon_0)}\left[2\lambda_0 F\left[V'Z_1 - V\left[Z_2 + \frac{2Z_1}{r}\right] - \frac{q_0(r)}{r}\right] - \frac{P_f(r)}{r}\right] \tag{5.14c}$$

together with the boundary conditions

$$Z'(0) = 0; \text{ with } Z(0) \text{ and } Z''(0) \text{ constants} \tag{5.15a}$$

$$Z(1) = Z'(1) = 0 \tag{5.15b}$$

This is an identical problem to that of section 5.3.1 except that the pressure term q_0 is a function of r and $P_f(r)$ is also present, these two combining to form a forcing term.

The initial conditions at r = 0 become

$$Z_1(x_1) = C_0 \tag{5.16a}$$

$$Z_2(x_1) = 0 \tag{5.16b}$$

$$Z_3(x_1) = 2C_1 \tag{5.16c}$$

$$Z_3'(x_1) = -\frac{96C_1\epsilon_0'(0)}{15(\nu + 2\epsilon_0(0))} \tag{5.16d}$$

$$q_0(x_1) = -2V(0)C_0 - \frac{8(\nu + 2\epsilon_0(0))C_1}{\lambda_0 F} \tag{5.16e}$$

We fix C_0 and find the value of C_1 which causes $R_1(1) = 0$ using a searching routine. The outer searching routine then finds C_0 such that $R_2(1) = 0$. We use the same error conditions as before. This process is different from the preceding ones in that we find the size of the function as well as its form, it being a forced solution.

It will be seen that there is a need to know the values of g_1, g_2 and $g_3 = g_2'$ both on the grid points x_1 to x_{2s1} and at the points half way between these points, because these values are used by the Runge-Kutta method. We also need to calculate $q_0(r)$ on these points. The methods used to achieve this are now described.

We know the values of g_1, g_2 and g_3 on the x_n to 4th order. (We can calculate g_3 using the differential equation without losing accuracy in this sense.) In order to obtain the values of these quantities on the half way points between grid points we fit (for each interval between adjacent grid points) a 5th-order polynomial to the 6 pieces of information we have for that interval. This gives us expressions for g_1 and g_2 on the half way points to 4th order. We then calculate g_3 (also to 4th order) from the differential equation.

In order to obtain $q_0(r)$ on these half way points, we proceed as follows. We have the integrand at each grid point and the points half way between these points. We fit parabolas through the three points we have in each grid point interval and integrate by the standard Simpson's rule. We also integrate these same parabolas half way across the interval, obtaining the value there.

5.4.2 The results

Table 5.3 shows the size of the axial velocity perturbation on the pipe axis and the addition (f_e) to the fully developed flow friction factor (f) in both smooth and rough pipes at each of three Reynolds numbers at a swirl level of S = 0.1.

Table 5.3

Reynolds Number	Fully developed flow formulation	f_e	$U^z(r=0)$
10^4	Method B smooth	0.000869	0.00946
	Method B rough	0.001360	0.00842
10^5	Method B smooth	0.000634	0.00498
	Method B rough	0.001030	0.00517
10^6	Method B smooth	0.000474	0.00325
	Method B rough	0.000988	0.00396

Figure 5.6 shows the axial velocity profile corresponding to the Re = 10^5 case for both smooth and rough pipes, again at S = 0.1. It should be noted that, owing to the nature of this second-order linear theory, values of the axial velocity at other swirl numbers can be calculated directly, by multiplying by the square of the ratio of the swirl numbers. It can be seen that the value of the axial perturbation is greater for the case of a rough pipe; this is related to the fact that the fully developed profile is flatter in a smooth pipe.

5.5 The similarity theory

5.5.1 The method

The two, coupled, equations (one each for the tangential velocity and the stream function) of section 4.5 are no different in principle from those that we have already considered. The only difference is that the two equations are solved by an iterative scheme. Once a (preliminary) solution for the tangential velocity has been found (taking the stream function as zero) which satisifies the condition on the swirl level, it is substituted into the equation for the stream function. The resulting (preliminary) solution for the stream function is then obtained. This ends one cycle of the iteration. The stream function obtained is then substituted into the equation for the tangential velocity and the iteration proceeds. It is terminated when the solutions obtained after n and n+1 iterations are sufficiently close to each other. The details are as follows.

We write $H = r^2T$, $T = T_1$, $T' = T_2$, $T'' = T_3$, $T''' = T_4$ together with $G = G_1$, $G' = G_2$, $G'' = G_3$ and obtain (for the equation for the tangential velocity)

$$G_1' = G_2 \tag{5.17a}$$

$$G_2' = \frac{-\lambda F[(V + rT_2 + 2T_1) - 2rT_1(G_2 - G_1/r)] - Q_3}{(\nu + \epsilon_0(Q_0 + Q_1^2/Q_0))} \tag{5.17b}$$

where

$$Q_0 = \left[Q_2^2 + Q_1^2\right]^{1/2}, \quad Q_1 = \frac{G_2 - G_1/r}{V'}, \quad Q_2 = 1 + \frac{rT_3 + 3T_2}{V'},$$

$$Q_3 = Q_2\left[\frac{rT_4 + 4T_3 - (Q_2 - 1)V''}{V'}\right] - Q_1^2\left[\frac{1}{r^2} + \frac{V''}{V'}\right] \tag{5.17c}$$

together with usual boundary conditions on G of $G(0) = G(1) = 0$. It can be seen that if we substitute the form $G = D_0r + D_1r^2 + D_2r^3$ into the equations together with $T = E_0 + E_1r^2 + E_2r^3$, then we find that we need to have $D_1 = 0$ in order to avoid the last term in the expression for Q_3 being singular. We therefore have the initial conditions at $r = 0$

$$G_1(x_1) = 0, \quad G_2(x_1) = D_0, \quad G_2'(x_1) = 0 \ . \tag{5.18}$$

In order to calculate the values of G_i and T_i on the points half

way between the grid points the same procedure was followed as in section 5.4.1 in order to obtain the G_i and the integral for the pressure. For the T_i, a 5th-order polynomial was set up for each interval using T_1, T_2 and T_3 at both end points of the interval which was then used to calculate T_1 on the half way point. Another 5th-order polynomial was set up using T_2, T_3 and T_4 in the same way. This polynomial was used to determine T_2 and T_3 on the half way point. T_4 was calculated from the differential equation as before, all these values then being known to 4th-order accuracy.

In order to solve this equation for the tangential velocity, a process like that used for the linear theory of section 5.2.1 was employed. First, a value of D_0 was chosen and then, using this value of D_0, λ was found so as to satisfy the boundary condition $G_1(1) = 0$ using a searching routine with error condition $|G_1(1)/D_0| \leq ER = 10^{-5}$. This solution was then integrated together with the most recently calculated version of the stream function using equation (4.28) to obtain S, the swirl level. A second searching routine was then used to find that value of D_0 for which the S obtained matched the value specified at the outset (S_0). The error condition was $|S/S_0-1| \leq ER = 10^{-4}$. A solution was thus obtained which had the required swirl level, and this was then substituted into the equation for the stream function which is now discussed.

The differential equation for the stream function is expressed as

$$T_1' = T_2 \tag{5.19a}$$

$$T_2' = T_3 \tag{5.19b}$$

$$T_3' = \frac{Q_4 - Q_5 - Q_6}{Q_7} \tag{5.19c}$$

where

$$Q_4 = -2\lambda F\Big[(V + rT_2 + 2T_1)(rT_2 + 2T_1) - rT_1(V' + rT_3 + 3T_2) + K + \int_0^r \frac{G_1^2}{r}\,dr\Big] ,$$

$$Q_5 = (\nu + \epsilon_0 Q_0)\Big[5T_3 + \frac{3T_2}{r}\Big] + \epsilon_0' Q_0 (rT_3 + 3T_2) + \frac{(Q_0 - 1)}{r}(r\epsilon_0 V')' ,$$

$$Q_6 = \frac{\epsilon_0 Q_2}{Q_0}\Big[Q_1\Big[G_3 - Q_1\Big[V'' + \frac{V'}{r}\Big]\Big] + Q_2\Big[4T_3 - (Q_2 - 1)V''\Big]\Big] ,$$

$$Q_7 = r\Big[\nu + \epsilon_0\Big[Q_0 + \frac{Q_2^2}{Q_0}\Big]\Big] \tag{5.19d}$$

together with the usual boundary conditions that T(0), T"(0) are constants and that T'(0) = T(1) = T'(1) = 0. The substitution of the polynomials already specified for the T_i and the G_i near r = 0 together with the forms for V and ϵ_0 in (5.8) into (5.19d) results in

$$Q_0 = \left|1 + \frac{8E_1}{2a_1}\left[1 + \left[\frac{15E_2}{8E_1} - \frac{3a_2}{2a_1}\right]r\right]\right| + O(r^2)$$

$$= I_s(1 + \alpha + \alpha\beta r) + O(r^2) \qquad (5.20a)$$

where $I_s = \pm 1$ as appropriate and (5.20a) defines α and β. Also

$$Q_4 = -2\lambda F[(a_0 + 2E_0)2E_0 + K] + O(r^2) \qquad (5.20b)$$

$$Q_5 = [\nu + (b_0 + b_1 r)I_s(1 + \alpha + \alpha\beta r)](16E_1 + 39E_2 r)$$
$$+ [I_s(1 + \alpha + \alpha\beta r) - 1][4a_1 b_0 + (6a_1 b_1 + 9a_2 b_0)r]$$
$$+ 8I_s(1 + \alpha)b_1 E_1 r + O(r^2) \qquad (5.20c)$$

$$Q_6 = b_0 I_s(1 + \alpha)[9E_2 - 12E_1 a_2/a_1]r + O(r^2) \qquad (5.20d)$$

$$Q_7 = [\nu + 2b_0 I_s(1 + \alpha)]r + O(r^2) \qquad (5.20e)$$

which means that the term in r^{-1} in (5.19c) gives

$$K = -2E_0(a_0 + 2E_0) - \frac{2a_1}{\lambda F}\left[\nu\alpha + b_0[\gamma(1 + \alpha) - 1]\right] \qquad (5.21a)$$

where $\gamma = I_s(1 + \alpha)$ and the term in r^0 gives

$$E_2 = \frac{\alpha\gamma(9b_0 a_2 - 6b_1 a_1) - (\gamma - 1)(6a_1 b_1 + 9a_2 b_0)}{45(\nu + 2b_0\gamma)} . \qquad (5.21b)$$

We therefore have the following initial conditions at r = 0

$$T_1(x_1) = E_0 \qquad (5.22a)$$

$$T_2(x_1) = 0 \qquad (5.22b)$$

$$T_3(x_1) = 2E_1 \qquad (5.22c)$$

$$T_3'(x_1) = \frac{\epsilon_0(0)V'''(0)(\alpha\gamma - \gamma + 1) + 2\epsilon_0'(0)V''(0)(1 - \gamma - \alpha\gamma)}{5(\nu + 2\gamma\epsilon_0(0))} \qquad (5.22d)$$

$$K = -2E_0(V(0) + 2E_0) - \frac{V''(0)}{\lambda F}\left[\nu\alpha + \epsilon_0(0)(\gamma(1 + \alpha) - 1)\right] \qquad (5.22e)$$

where $\alpha = 8E_1/V''(0)$ and $\gamma = I_s(1 + \alpha)$. (5.22f)

We solve the equations in the same way as described in section 5.4.1, employing the most recently calculated version of the G_i and the associated value of λ. As soon as two cycles of the iteration have been completed we compare the results of successive iterations in order to determine whether it has yet converged. The error

condition we use is as follows. We find the maximum difference in the values of G_1 between the two versions and divide it by the maximum value of G_1 in the latest version. We do the same for T_1. We also find the ratio of the difference between the two values for λ and the present value. We do the same for K. These four error ratios are squared, averaged and the result square rooted to give an overall measure of the difference between the two versions. We require this final figure to be less than 10^{-3}.

If we wish to solve the entire system of equations for a number of values of S_0, we solve for them in ascending order, using the previous solution as a first guess at the next solution, to make the iteration as fast as possible. Typically, no more than 5 cycles of the iteration were needed to solve for one value of S_0.

5.5.2 The results

Figures 5.7 and 5.8 show the values of λ over a range of Reynolds numbers and swirl numbers in smooth and rough pipes respectively. It is clear that the effects of Reynolds number and swirl number on λ are related, and that swirl increases λ more in flows with higher Reynolds numbers in rougher pipes.

Figures 5.9 and 5.10 show the values of the friction factor $(f+f_e)$ relative to that in fully developed flow (f) for smooth and rough pipes respectively. It can be seen that here the effects of Reynolds number and swirl number are broadly independent, the effect of Reynolds number being very limited.

Figures 5.11 and 5.12 show the values of the axial perturbation at the pipe axis for smooth and rough pipes respectively. The corresponding deviation of the fully developed profile is shown for comparison.

Figures 5.13 and 5.14 show the tangential and axial velocity profiles obtained at a swirl level of 0.1 in both smooth and rough pipes at Re = 10^5. In figures 5.15 to 5.18 examples of the solutions for tangential and axial velocities in smooth and rough pipes are presented at a number of swirl levels at a Reynolds number of 10^5.

5.6 Discussion

We present in figures 5.19 to 5.25 a number of comparisons between the theories discussed earlier in this chapter.

In figure 5.19 we present the ratio of the decay rate λ found using the similarity theory to that of the linear theory for a number of swirl numbers at Re = 10^5 for the smooth and rough pipe cases. We see that λ increases more in rough pipes, just as we observed when considering figures 5.7 and 5.8. The predominant effect is that λ increases linearly with swirl once the swirl number is greater than about 0.2. This is the swirl level at which the axial perturbation becomes non-negligible.

In figure 5.20 we present the ratio of the friction factor found using both the second-order linear theory and the similarity theory for both smooth and rough pipes. We see that there is no significant difference between any of these even at high swirl levels.

When we consider figure 5.21 however, there is a difference between the theoretical methods. Figure 5.21 shows the size of the axial velocity at the pipe axis for a number of swirl levels at Re = 10^5 for smooth and rough pipes. We see that when $S \lesssim 0.2$ there is no significant difference, although the similarity theory does produce a higher value. When $S \gtrsim 0.2$ however, a gap opens up between the two theories, as the effects of the other non-linear terms is felt. We see that our previous observation (figures 5.6,5.17 and 5.18) that there is a bigger perturbation in the case of a rough pipe applies throughout the graph.

Figure 5.22 shows tangential velocity profiles according to both the linear and the similarity theory for S = 0.1 and Re = 10^5 in a smooth pipe. The results of the two theories are effectively the same.

Figure 5.23 shows axial velocity profiles also at S = 0.1 and Re = 10^5 in a smooth pipe for all three theoretical methods. The profile obtained from the linear method has been normalised so that its value on the axis is the same as that of the profile obtained from the similarity theory. We see that the difference of note is between the linear theory and the other two, each of which contains the effect of the high tangential velocity gradients near the wall on the eddy viscosity. Figures 5.24 and 5.25 correspond to figures 5.22 and 5.23 and are for the case when S = 0.4.

6. THE EXPERIMENTAL WORK

6.1 Nature, purpose and scope of the experiments

The experimental work carried out consisted of the measurement of axial and tangential components of the velocity of water flowing in a long straight pipe following a left-handed double right-angle bend in two perpendicular planes (away from an observer, down and to the right), together with some measurements of wall pressure.

Laser Doppler Anemometry was used for the velocity measurements because of its non-intrusive character and its high accuracy. Although some information concerning the turbulent intensities in the flow was collected as a result of using this measurement system (and are presented), this was not the prime concern of the work.

The purpose of the experiments was twofold. Firstly, a thorough description of the flow field following this sort of double bend was desired, there being (to the author's knowledge) no comprehensive set of such measurements reported in the literature. Secondly, it was intended to use this body of data to test the theoretical work described in chapters 4 and 5. We seek then, an enhanced knowledge and understanding of the swirling flow field generated by a double right-angle bend in two perpendicular planes and to establish its size and form, together with its manner and rate of decay.

Accordingly, velocities were measured on a plane preceding the double bend to establish the form of flow field there, and on 5 sections following the double bend. Sufficient measurements were made to establish the nature of the flow.

6.2 A description of the test facility and the measurements made

6.2.1 An overall description of the flow loop

The test facility was designed in order to enable the measurements described in section 6.1 to be made; it is shown in diagramatic form in figure 6.1 and also in plates 1-4. The fibreglass tank made with 4ft square panels contained about 1900 gallons ($\triangleq$ $7m^3$). The water was drawn out of one side of the tank close to one end through a bellmouth and was returned (eventually) to the other end. In the middle of the tank a perforated screen, dividing the tank

in two, ensured that no air was entrained into the pump and that adequate mixing took place to provide steady and uniform flow conditions at the pump inlet. A drain was fitted at the end of the tank furthest from the pump inlet. Periodically the tank was drained, cleaned and refilled in order to provide a sufficiently clean water supply for the measurements. To lengthen the life of a tankful of water wooden covers were placed over the tank to reduce the amount of dust entering the water. They also supported the returning pipelines. A dipping thermometer capable of measuring temperature to within 0.5°C was hung in the tank at the end to which water returned.

On leaving the tank, water passed through a section made of 6" diameter steel pipe round a 90° bend, through a fully open gate valve and into a 30 hp centrifugal pump whose duty point was a flowrate of 40000 gal/hour and a total head of 95ft of water. The outlet from the pump had a 5" diameter; a (steel) reducer to a pipe diameter of 4" then led into a 'tee' junction made from ABS as was the rest of the flowloop excluding the test sections. This 'tee' junction supplied another flow loop and was shut off with a gate valve throughout the course of the experiments. A reducer to a pipe diameter of 3" (the rest of the flowloop was of this size) and another 'tee' junction followed providing one line which went through a ball valve and on into the test section and another which passed through a 5μm filter and a ball valve before rejoining the first line before the test section. A bypass line controlled with a diaphragm valve returning immediately into the far end of the tank was taken off the subsidiary line before the filter; this was not in use whilst measurements were being taken. The filter was available either to help determine whether the water needed changing or to lengthen its life. It was not used when measurements were being taken.

After these preliminaries came the test sections. The inlet to the test section (shown in plate 4) was a 90° mitred elbow preceded by about 10 diameters of (vertical) straight pipe intended to eliminate the possibility of swirl arising from bend interactions (e.g. Murakami, Shimizu and Shiragami (1969)). After the elbow, 40 diameters of (horizontal) straight pipe preceded the double bend under test. This was intended to provide it with a reasonably fully developed flow, and is a sufficient distance as far as the standards

for orifice plate flow measurement (ISO (1980)) are concerned. Measurements of this 'inlet' flow are given later in this chapter. The double bend itself was followed by 140 diameters of (horizontal) straight pipe forming the main test section. Details of the nature of the test sections (made of perspex) are given in section 6.2.2. At the downstream end of the test section a drain was fitted, this being a low point of the loop.

A 180° bend brought the returning water back along a (horizontal) line vertically above the main test section which contained a turbine meter used to control the flow rate. The meter had been calibrated at the Central Electricity Generating Board (traceable to standards) and was provided with its own bypass with ball valves. There were over 65 diameters of straight piping preceding it, ensuring a reading as accurate as the calibration made possible (individual measurements were certified to be within ±0.2% to 95% confidence). The meter factor (K_M) was 19015 ± 15 within the range of flowrates used in the experiments, an error bound of ±0.1%. (The flowrate given by the relation f_t/K_M is given in m^3/s where f_t is the frequency of the turbine meter).

Finally, the water was taken up and over the middle of the test area, down onto the tank at the end nearest the pump and through a diaphragm valve which was used in conjuntion with the turbine meter to maintain the desired flowrate. The pipeline then ran along the top of the tank and down into it at the far end.

Measurements were taken with the flow loop operating at two different flowrates. These were defined to be the flowrates present when the frequency output of the turbine meter was f_t = 190 Hz and f_t = 475 Hz. (The faster of these flowrates was the maximum that could be obtained whilst avoiding cavitation in the turbine meter and the bends in the pipework). These flowrates were maintained to within an accuracy of ± 1 Hz at all times which is an error of 0.5% at the slower flowrate and an error of 0.2% at the faster flowrate. The faster flowrate was achieved by opening the ball valve to the main loop fully and controlling the flow with the diaphragm valve at the downstream end of the main loop. The pressure in the perspex section just after the double bend was 37 PSI. The slower flowrate was achieved by throttling the flow with the ball valve and controlling

it as before with the downstream diaphragm valve. This was done in such a way as to cause the pressure in the perspex section just after the double bend to be 30 PSI; this ensured that there was no cavitation in the loop. The reading of the turbine meter was steady after an initial period lasting about half an hour during which it read up to 1% high. It was not measurably sensitive to the temperature range used (10°C to 25°C) although the Reynolds number was, this being a function of the kinematic viscosity of water, ν. The averge axial velocities at the two flowrates were 5.35m/s and 2.14m/s based on the formula

$$U_{av} = \frac{4f_t}{\pi D^2 K_M} \qquad (6.1)$$

and an average internal pipe diameter of 77.1mm (see section 6.2.2). The Reynolds numbers of the two flowrates (based on a nominal value of 1×10^{-6} m^2/s for ν) were 4.13×10^5 and 1.65×10^5.

The time taken (nominally) for the tankful of water to have recirculated once was almost 5 minutes at the faster flowrate and almost 12 minutes at the slower flowrate.

6.2.2 The test sections

The test sections on either side of the double bend at the centre of the experiments were constructed out of sections of extruded perspex pipe. As shown in figure 6.2, each section was flanged (flush at the end) with PVC flanges. These flanges had been concentrically turned on the inside and the outside to facilitate alignment between consecutive test sections. Each test section was 2m long except for one test section 1m long which formed part of the pipework preceding the double bend. A special tool was used to join the sections together; it consisted of the two halves of an annulus which bolted together around a pair of abutting flanges. Because the outer rims of the flanges were aligned by the annulus, the inner rims were also aligned. Therefore the pipes were aligned.

The only imperfections in the geometry of the straight sections was the slight gap owing to the gasket between flanges (3mm) and the non-circularity of the pipe itself. The degree of circularity of the piping was determined by measuring the external and internal diameter of the pipe sections. Of a large number of such measurements in

different orientations (made using callipers to an accuracy of ±0.1mm) the resulting averages were 90.1mm for the external diameter, 77.1mm for the internal diameter and 6.5mm for the wall thickness. The figure for the internal diameter varied by 1%. The 2m section immediately after the double bend was found to be slightly smaller than the others and to be less circular than them; the internal diameter of this section was measured to be within 3% of a mean value of 76.0mm. The ABS pipe used for the rest of the flowloop had a nominal internal diameter of 78mm.

The main test section also had pairs of pressure tappings in the walls of the pipe postioned at the ends of a diameter. These were aligned with the bolt holes in the flanges and were 3.2mm in diameter. A shaped piece of perspex rod was glued to the exterior of the pipe providing anchorage for copper fittings to which were connected pieces of ¼" flexible plastic tubing. Dimensions are shown in figure 6.3. Once the main test section was built into the flowloop, the line joining two adjacent bolts was at a clockwise angle of 11° ± 1° to the vertical (looking downstream). This was determined by measuring the vertical height of the lower bolt above the floor (81.0cm) and the distance of the lower bolt from the floor along the (slanting) line joining the two bolts (82.5cm) with a tape measure. The plane containing the pressure tappings was therefore at a clockwise angle (looking downstream) of 56° ± 1° to the horizontal.

The double bend under test is shown in figure 6.4 and in plate 5. The right angle between the two component bends was obtained by glueing them together whilst holding them against a right-angled block. The connexions to the flanges involve small, unknown imperfections in wall regularity, as indicated. It should be noted that despite the fact that the two 90° bends were directly abutted, there was an effective spacer length of 1 diameter between them. The radius ratio of each of the component bends was 2.3.

The test sections and double bend were not dismantled or adjusted in any way during the course of the experiments. The geometry was therefore constant.

6.2.3 The pressure measurements

A Bourdon gauge was attached to the pressure tapping just after

the double bend as an aid to fixing the same flow conditions on different occasions and to ensure that that no excessive pressure was exerted on the perspex pipe.

The measurement of differential pressure between two tappings was carried out in two different ways. A mercury manometer and a differential pressure transducer with an electronic filter to eliminate the effects of vibrations of the supporting structure were each used to determine the pressure difference between each tapping and a reference tapping. The two systems were each accurate to within 2% of the maximum differential pressures measured, and they agreed to within 2%. The locations of the pressure tappings are shown in figure 6.5.

6.2.4 The velocity measurements

The following measurements were made, using Laser Doppler Anemometry (see section 6.3). Axial velocities were measured on the horizontal diameter and two offset chords about half a radius above and below it on sections 1 and 2 as shown in figure 6.6; figure 6.7 shows the locations of the sections where measurements were made. Axial velocities were measured on the horizontal diameter only of sections 3 to 5. Tangential (vertical) velocities were measured on sections 1 to 4 on the horizontal diameter. All of these measurements were made at the two different flowrates/Reynolds numbers as described in section 6.2.1. Various measurements were made on section 0 at the faster flowrate only. Sections 1 to 4 were equidistant, being separated by 2.03 m (26.3 diameters).

6.3 Laser Doppler Anemometry

6.3.1 Introduction

Laser Doppler Anemometry (LDA) is based on the fact that if two laser beams cross in a flow, forming an interference pattern, then a dust particle following the flow which passes through these fringes provides a photomultiplier with an oscillating signal the frequency of which is proportional to the speed of the fluid in the direction perpendicular to the fringes.

An LDA system manufactured by DANTEC was used, consisting of a

15mW He-Ne laser, beam splitter, Bragg cell frequency shifter and focusing lens (focal length 300mm) which produce the intersecting beams and a photomultiplier (focal length 150mm) situated on the other side of the pipe to receive forward scattered light providing the signal for analysis. Natural seeding was used.

The Bragg cell is used to shift the frequency of one of the beams by 40 MHz in order to make the fringe pattern a moving one. This lessens the effect of various error inducing phenomena such as low velocity particles and particles crossing the intersection volume at shallow angles to the fringes; it also removes the possibility of sign ambiguity.

The entire apparatus is shown in figure 6.8 and in plates 7-9; it can be seen that the components producing the beams form a unit supported on three screws one at the rear and two (one on each side) at the front. These screws are used to orientate the laser beams. In the subsequent sections we examine in turn the methods of signal processing used, the alignment procedure, the methods of calibration and allowance for refractive effects, the procedure followed when taking measurements and a summary of the errors involved. The detailed error analysis is contained within appropriate sections. For a fuller description of the LDA method the reader is referred to the book by Durst, Melling and Whitelaw (1976) and the lecture notes by Adrian and Fingerson.

6.3.2 Signal processing

When the signal is received the electronics carry out the following procedure. First, the 40 MHz shift is removed and then replaced with a small shift of 1 MHz or 2 MHz which separates the relatively high frequency signal arising from particles from the lower frequency due to the variation in intensity of the beams across their cross-section (called the pedestal). Electronic filters then isolate the flow signal and remove most of the noise. Then, individual 'doppler bursts' corresponding to particles are analysed to establish that they are sufficiently distinguishable from the noise; those that are accepted give rise to a validation rate as a fraction of the data rate of 'bursts' considered. Allowance is made for the fact that there is a bias towards particles with higher

velocity by using the inverse averaging method. These values are then transferred to an Apple computer which calculates the mean and standard deviation of the data collected within a range specified by the operator using a standard program supplied by DANTEC.

6.3.3 The alignment procedure

A matter of considerable importance was the positioning of the beams' intersection in the right place. In order to facilitate knowledge of the location of the beams' intersection a perspex box was made in two parts (see figure 6.9) which could be placed around the pipe at any chosen section, the join being made watertight with a sealant. The box was filled with water, thus almost entirely removing distortions due to the different refractive indices involved. A small amount of clear detergent was added to the water in the box to inhibit the formation of air bubbles on either the walls of the box or of the pipe itself. The laser was positioned on a free-standing traversing table the legs of which were adjusted so as to make the table horizontal in the direction perpendicular to the pipe and to be aligned with the pipe axis in the other direction. This was achieved by means of a spirit level to within ± 0.1°. It was important to level the table in the cross-pipe direction in order to ensure that measurements would be made on a horizontal line, rather than one at an angle to the horizontal. It was important to level the table in the direction parallel to the pipe axis because it was this levelling which formed the basis for the aligning of the laser parallel to the pipe. The traversing gear consisted of a screw thread of pitch 2mm in the cross pipe direction and a similar traversing thread in the flow direction. The photomultiplier was positioned on a similar table placed on the other side of the pipe. This table had no screw traverses but did enable continuous movement of the optics in both directions in the horizontal plane.

The alignment of the laser was achieved as follows. Having levelled the table as described so that it was aligned with the pipe, the laser was placed on it resting on a few pieces of hardboard the size of the laser's baseplate (and in line with it) and one piece of aluminium at right angles to these supporting the laser's side screws (see plate 7). Initially the laser rested directly on the face of its

baseplate. Then the side screws and rear screw were wound down until they began to take the laser's weight. (The side screws were always moved together, by the same number of turns, thus maintaining the angle previously set by the spirit level). The laser beams were then positioned in the horizontal plane (they could be rotated about their centreline to an accuracy of ± 0.1° by lining up a marked spot on the rotating part with a particular position on a scale in degrees marked on the stationary part). The laser was then traversed until the beams intersected on the outside of the perspex box. (The box had previously been aligned with a spirit level so that the face nearest the laser was vertical to within ± 0.1°). The laser's position was then altered until the returning beams coincided exactly with the outgoing ones. This was determined by holding a piece of paper in front of one of the beams and establishing that the spots due to the incoming and outgoing beams coincided. This ensured that the laser's axis was perpendicular to the face of the box to within ± 0.1° since a deflection of 0.1° gives rise to a lateral movement of 1mm in the relative beam positions on the face of the laser's front lens which is readily discernable. The laser was then traversed inwards (towards the pipe axis) until the beams met on the outside wall of the pipe. Further adjustments were made using the laser's supports until the beams reflected off the nearest wall of the pipe and those reflected off the nearest wall of the box were all in a common plane (parallel to the pipe axis) together with the outgoing beams. This ensured that the beams' intersection was on the horizontal diameter rather than a displaced chord. This was achieved to within ± 0.5mm. Finally, as a check on the possibility of 'twist' about the beams' axis the laser was traversed much further into the pipe (so that the laser beams passed through the nearest pipe wall at least 20mm apart from each other) to ensure that the beams continued to stay in the same plane. Were the laser misaligned by as much as 0.1°, the curvature of the pipe would cause the beams reflected off it to depart from the plane by 0.5mm as seen on the face of the laser's front lens. This process ensured that the laser was aligned to within ± 0.1° of the desired location, on the horizontal diameter.

When measurements were taken on horizontal chords offset from the horizontal diameter, the alignment was based only on the reflections

from the front of the box and on the levelling of the traversing table but was still within ± 0.3°. The height was determined by measuring the different vertical distances between the intersection of the beams and a fixed point on the front of the perspex box in the different positions. This was done with a tape measure to within ± 0.5mm.

Measurements were taken with the beams in this horizontal position (axial velocity) and, when on the horizontal diameter, also in the vertical position (tangential velocity) simply by rotating the beams round without further alignment of the laser. This was done to within ± 0.1° as we have seen. The importance of having the beams aligned in a direction perpendicular to the pipe axis when measuring the tangential velocity is considerable - if the plane of the beams were misaligned by 1° then there is an addition to the tangential velocity readings of around 0.1 m/s when the average axial velocity is 6 m/s. The accuracy of the alignment was about ± 0.3° when all the various elements are combined. If a mistake were made, the error would always be of one sign, shifting the zero point of the tangential velocity distribution and would therefore be obvious if it were significant. There is no significant effect on the axial velocity measurements due to slight misalignment.

6.3.4 Calibration and allowance for the effects of refraction

The basic calibration required is the measurement of the angle between the laser beams. If this angle is called 2θ and the wavelength of the light λ then the fringe separation is δ_f where

$$\delta_f = \frac{\lambda}{2\sin(\theta)} \qquad (6.2)$$

and the velocity being measured is given by the product of δ_f and the doppler frequency f_D. The angle θ was measured by traversing the aligned laser right through the pipe so that the beams' intersection was positioned on the far side of the perspex box and placing a vertical screen about 1m away from it. The distance from the spot where the beams intersected and the screen was measured with a tape measure to be 80.20cm (± 0.05cm) and the distance between the spots where the beams hit the screen was measured (in the same way) to be 15.35cm (± 0.1cm). The inaccuracy is not only due to the tape measure

but also to the fact that the spots caused by the beams hitting the screen were of finite size. These measurements result in a value for θ of 5.47° and a value for δ_f of 3.32μm to an accuracy of 1%, based upon the value for λ of 632.8nm. These measurements refer to the values in air. There is no need in general to change the value of δ_f when the beams meet in the water because although $\sin(\theta)$ changes by the ratio of the refractive indices, the wavelength of the light λ changes similarly, these effects cancelling.

We turn now to the twin questions of the effects of refraction at the pipe walls on the linearity of the traverse and upon the calibration factor.

In the case of the measurement of the axial velocity on the horizontal diameter it is clear that the position of the beams' intersection is a linear function of the position of the traversing table. The beams always intersect at the same angle with two parallel surfaces and so the calibration constant δ_f does not change across a traverse.

Figure 6.10 shows the configuration present when the axial velocity is being measured on one of the horizontal chords offset from the horizontal diameter. We ignore the small refractions which occur as a result of the small angle between the beams and the direction perpendicluar to the pipe axis. It can easily be seen (using the law of refraction) that the angles ψ,ϕ,$\delta\theta$ and $d\theta$ defined in the figure are related by the equation

$$\sin(\phi)\sin(\psi + \delta\theta + d\theta) = \sin(\psi)\sin(\phi + \delta\theta) \qquad (6.3)$$

which simplifies for small $\delta\theta$ and $d\theta$ to the relation

$$d\theta = (1 - \tan(\psi)/\tan(\phi))\delta\theta \qquad (6.4)$$

which means that for $\sin(\psi) = 21/45$ as shown in the figure we have ψ = 27.82° and ϕ = 24.97°. Using the mean value for the wall thickness it can be seen that $\tan(\delta\theta) = 6.5\tan(\phi)/38.5$ which means that $\delta\theta$ = 4.50° and $d\theta$ = -0.60°. This means that (in the orientation in the figure) the beams in the pipe fall at an angle 0.60° to the horizontal by 0.68mm over the length of the chord along which they are traversed (64.5mm). It can also be seen that the beams drop below their original horizontal line as a result of entering the pipe by an amount equal to $6.5\sin(\psi-\phi)/\cos(\phi)$ = 0.35mm, and that it is from this lower position that they fall. The maximum deviation from the

horizontal line 0.5mm below that which is set is no more than 0.5mm, which is within the accuracy of the setting process. This deviation is ignored. The 0.5mm adjustment to the set height is, of course, taken into account. The calibration constant is unchanged as in the case of the axial velocity measurements on the horizontal diameter.

In the case of the measurements of the tangential velocity however (always on the horizontal diameter), adjustments are needed owing to the refraction at the wall of the pipe. We see in figure 6.11 the configuration present in this situation (only one of beams is drawn since they are symmetrical about the horizontal diameter). The beam has been drawn in a general position. If we consider the situation where the beam is just touching the far inside wall of the pipe we have the relationship $\psi + \delta\theta + d\theta = \theta - d\theta$. On the assumption that $\delta\theta$ and $d\theta$ are small, we see that we may take $\psi = \theta$. Using the value of $\theta = 5.47°$ we find that $\phi = 4.95°$ (using the refractive indices 1.33 and 1.47 for water and perspex respectively). By the same analysis as in the previous (axial velocity) case and employing an iteration to take account of the relationship between ψ and θ, we find that $\delta\theta = 0.75°$ and $d\theta = -0.080°$, an increase in θ of about 1½%. It is clear that the position of the beams' intersection will be decreased by the same amount below that given by the linear method and that these effects are of the opposite sign on the other side of the pipe. (It should be noted that when the beams pass through the pipe axis, $d\theta = 0$ since the beams form radii of the pipe and meet the pipe walls perpendicularly). These alterations are in fact well within the precision bounds for the tangential velocity measurements and are ignored.

As a check upon these calculations, recourse was made to the computer program of Peacock (1984) which confirmed the above findings.

6.3.5 The measurement procedure

The procedure for taking the measurements was as follows. The table was traversed so that the beams intersected on the inside wall of the pipe and was then traversed whole numbers of turns of the thread across the pipe, a measurement being taken every 2 turns. When measuring on the horizontal diameter it took 29 turns to traverse the pipe when the beams were in the horizontal plane, and 27½ turns when

in the vertical plane. Therefore measurements in each direction were made quite separately, on different traverses. 24 turns were needed for a corresponding traverse on the offset chords. 29 turns outside the pipe corresponds to a theoretical 77.1mm (= 29x2x1.33) inside compared with the measured average of 77.1mm; clearly this exactitude is fortuitous but nevertheless indicative of a satisfactory level of consistency.

The errors in positioning the laser for measurements consisted of the error in positioning the beams' intersection on the wall of the pipe at the start of a traverse (about one quarter of one revolution of the thread ≙ 0.65 mm inside the pipe) plus half the beamwise length of the spot (0.35 mm) making an error of ± 0.8mm.

At each measurement point the photomultiplier was positioned symmetrically between the beams and to one side of the plane containing them in such a way as to be focused onto the beams' intersection. The angle between the axis of the beams and that of the photomultiplier was always kept small (∠ 10°) in order to obtain a strong signal. The voltage applied increased until a signal was obtained, and the focusing and precise positioning of the photomultiplier were adjusted to maximise the data rate obtained. The applied voltage was reduced until the data rate was only 500 Hz. The flow signal was deemed to be satisfactory if the validation rate was over 30%. Normally it was as much as 50%.

The extra frequency shift used to facilitate the filtering of the signal was 1 MHz for axial velocity measurements and 2 MHz for tangential measurements, the filters being fixed at 1 MHz and 4 MHz regardless. The relationship between the doppler frequency f_D , the velocity being measured U_m and the fringe separation δ_f is

$$f_D = \frac{U_m}{\delta_f} \qquad (6.5)$$

where δ_f was found to be 3.32 μm (see section 6.3.4), and typical values of U_m were 2 m/s and 6 m/s (axial velocity) and -1 m/s to 1 m/s (tangential velocity). The values of f_D were therefore 2/3 MHz and 2 MHz (axial velocity) and -1/3 MHz to 1/3 MHz (tangential velocity). The values corresponding to the filter readings (taking into account the shift supplied) were therefore between 1⅓ and 3 MHz (axial velocity) and between 1⅓ and 2⅔ MHz (tangential velocity).

The procedure for making a measurement was to provide the computer with upper and lower bounds of acceptability for the data and then to take 500 individual velocity measurements. The computer then eliminated those measurements lying outside the specified bounds and calculated the mean (μ) and standard deviation (σ) of the 'accepted' measurements which remained. The number of measurements 'accepted' out of the 500 which were taken was typically 400-450 for the axial velocity measurements and 350-400 for the tangential velocity measurements. The bounds used were then reset using a mixture of trial and error and iteration until the bounds used coincided with the values $\mu \pm 2\sigma$ as calculated from the measurements made using those bounds. The lack of precision owing to this procedure (as distinct from the entirely separate error in the basic calibration) is a function of the quality of the signal received, of the turbulence intensity and of the proximity of the measuring position to the wall of the pipe. These factors are closely linked. An overall measure of the precision may be regarded to be the greater of ½% of the reading and ± 0.02m/s, which is consistent with the formula of Yanta and Smith (1973).

The standard deviation thus obtained is a measure of the turbulence intensity in the measuring direction. The turbulent intensities measured in this way are the normal stresses in the z and θ directions. The accuracy of these values for the turbulent intensities can be estimated, following Yanta and Smith (1973), by the number of data points used to obtain each measurement. Their formula says that if N samples were taken then we can be 95% confident that the standard deviation lies within $200/(2N)^{½}$% of the measured value. They also observe that this error estimate is independent of the flow conditions, although it does assume a signal of perfect quality. For N = 400 (a typical value for all the measurements made in this work), this works out to be very nearly 7%. Taking into account the fact that the signal quality, although good, is imperfect we may regard the accuracy of these measurements as 10%.

The temperature of the water in the tank was recorded at regular intervals of half an hour. It usually rose by about 0.75°C in that time. Measurements were not taken outside the range 10°C to 25°C; most measurements were in the middle of this range. Tests were

carried out to determine whether the change in Reynolds number due to the change in ν with temperature were significant. It was found that they were not, the change in Reynolds number being no more than 10% and the volume flowrate being the same.

6.4 A summary of the errors involved

Temperature of water		± 0.5°C
Volume flowrate		0.5%
Reynolds number		10% (due to ν)
Pipe circularity		1%
Pressure measurements		2%
Velocity measurements		
	Calibration	1%
	Location - horizontal	± 0.8mm
	- vertical	± 0.5mm
	Alignment	± 0.3°
	Imprecision	± 0.02m/s or ½% if greater
Turbulence Intensity		10%

The axial velocity measurements taken on the later planes where the flow was more closely axisymmetric were integrated to give a figure for the bulk flowrate for comparison with that given by the turbine meter. Results of this procedure given later in this chapter showed a relative error of no more than 2%.

Having measured profiles on all of the measurement sections, the apparatus was moved back to section 2 two months after the original measurements were made there (the whole measurement programme lasted

about 4 months). A traverse of axial velocity was made which corresponded with the previous measurements within 2% (except for one point close to the wall) demonstrating the long term consistency of the apparatus. Some measurements of the tangential velocity were also made which were within ±0.03m/s of the original measurements, thus confirming the validity of the error analysis of the alignment procedure. The effect of the error in horizontal location (±0.8mm) is obviously more important near the wall where the velocity gradients are higher. The figure of 2% may be regarded as the overall accuracy of the measurements.

6.5 The results of the velocity measurements

6.5.1 Reference measurements, on sections 0 and 5

The measurements of axial velocity at both Reynolds numbers on section 5, at a distance of 125 diameters from the outlet of the bend are tabulated in table 10 of appendix C. It is clear from the small size and decreasing character of the tangential velocities on preceding sections that the swirl level here is negligible, being too small to measure accurately. It would seem, from the measurements presented later in this chapter that the swirl angle was of the order of 0.5°. We would expect, therefore, that the axial profile be fully developed, and consequently to be suitable as a reference profile for the measurements made on preceding sections. We also have measurements of the axial profile at the higher Reynolds number on section 0, at a distance of 39 diameters from the preceding mitred right angle bend and 4 diameters upstream of the double bend under test.

Figure 6.12 shows the experimental measurements made on sections 0 and 5 at the higher Reynolds number, together with the corresponding theoretical curve using method 'B' of section 4.2.2. Negative radial positions are on the left hand side of the pipe when looking downstream. The agreement between the theory and the measurements, and particularly those on section 5, is very good. Figure 6.13 shows the same information as that in figure 6.12, but taken with reference to the centreline velocities rather than the average velocities. Curves corresponding to 95% and 105% of the

theoretical curve are also drawn, showing that the measurements of the axial velocity on section 0 lie within this range. This means that the inlet flow is within the specification of the standard (ISO (1980)) for orifice plate flow measurement, as would be expected from the upstream geometry. It can be seen from table 1 of appendix C that the swirl angle at section 0 is less than 1°, thus being well within the 2° limit prescribed. We can see therefore that the flow entering the bend is very nearly fully developed.

Figures 6.14 and 6.15 show the results of the axial velocity measurements on section 5 at the lower Reynolds number presented in the same ways as before. Again, it can be seen that the profile is very close to the theoretical profile and, in general, well within the 5% band just as before. No measurements were taken of the axial velocity on section 0 at this Reynolds number; it can be assumed that the inlet profile will be at least as well developed as it is for the case of the higher Reynolds number.

A calculation was carried out, to determine whether the velocity measurements on section 5 and the turbine meter agreed as to the bulk flowrate, using the following procedure. The two velocity measurements nearest the wall on each side of the pipe were used to obtain an 'effective' value for the velocity on the wall by means of linear extrapolation. The resulting profile was then integrated using the trapezium rule to obtain the bulk flow. It was found that the proportionate error between this value and the reading of the turbine meter was 0.1% and 0.7% in the case of the higher and lower Reynolds numbers respectively. It should be noted that the difference between the result obtained using linear extrapolation near the wall and that obtained using a logarithmic relation chosen both to fit the value and slope at the point nearest to the wall and to be equal to zero on the wall is no more than 1% of the flowrate. We see then that although there is difficulty in carrying this calculation out with high accuracy, it is possible to say that the turbine meter and the laser measurements are in agreement to within 2%.

6.5.2 Tangential velocity measurements

Figures 6.16 and 6.17 show the tangential velocity measurements on sections 1 to 4 for the higher and lower Reynolds numbers

respectively. They are presented as proportions of the average axial velocity. Negative radial positions are on the left hand side of the pipe looking downstream. The swirl levels shown in the key were calculated using the trapezium rule, integrating right across the pipe. The value of U^{Θ} on the wall of the pipe was put equal to that at the nearest point to the wall where a measurement was made. If x represents the (signed) distance from the axis then the formula used to find an approximate value of S was

$$\tan\phi \triangleq 2S \approx \frac{2}{U_{av}}\int_{-1}^{1} x^2 |U^{\Theta}| \, dx \qquad (6.6)$$

It can be seen that the profiles become progressively more linear and more symmetrical about the centerline at the sections further downstream. Figure 6.18 is a comparison between the two Reynolds numbers, showing the tangential velocity measurements on sections 1 and 2. The marginally slower decay at the higher Reynolds number is discernable, the swirl levels being very similar on section 1. The values for the swirl level give rise to values for λ, the exponential decay rate of the swirl. The four values of swirl level on the four sections were used to obtain values of A and λ for each Reynolds number using a linear regression analysis of the logarithm of a supposed relationship of the form

$$S = A\exp(-\lambda z/D) \qquad (6.7)$$

The values obtained were A = 0.0730 and λ = 0.0217 for the higher Reynolds number and A = 0.0635 and λ = 0.0254 for the lower Reynolds number. The correlation coefficients were -0.997 and -0.995 respectively. These relationships, together with the experimentally determined levels of swirl giving rise to them are shown in figure 6.19.

6.5.3 Axial velocity measurements

Figures 6.20 and 6.21 show the axial velocity measurements on the horizontal diameter on sections 1 to 5 at the two Reynolds numbers. We see that the velocities on sections 3 to 5 are very similar, but that there are significant deviations from the fully developed flow on sections 1 and 2. Figures 6.22 to 6.25 show the axial velocity measurements made on all three chords on sections 1 and 2 at both the

Reynolds numbers. The asymmetry present on section 1 can be seen to be of the form of a horseshoe of high velocity on the higher chord and the right hand end of the lower chord surrounding a region of lower velocity on the left hand end of the lower chord. In chapter 7, in the context of considering the effects of these profiles on flowmeters, an algorithm is presented which gives a formula for the velocity profile over the whole cross-section based on the experimental results. The contour plots resulting from this (figures 7.1 to 7.4) display the horseshoe character of the profiles on section 1 and show that on section 2 the deviation from a fully developed profile is much less pronounced. It is also shown in chapter 7 that the axial profile rotates around with the swirl, in the same way as the profiles of Kito (1984) did.

6.6 The results of the pressure measurements

Figure 6.26 shows the pressure measurements for both Reynolds numbers, taken with reference to the readings at the higher tapping at the downstream end of the test section. Straight lines have been drawn, corresponding to the expected pressures in fully developed flow in smooth pipes at the same Reynolds numbers. The formula used to generate these lines was

$$\Delta P = - 2U_{av}^2 f \Delta z / 9.807 \qquad (6.8)$$

where f is calculated from equation (3.16b) and Δ indicates a difference in the quantity. The factor 9.807 arises from the conversion from bar to metres of water. The experimental results lie very close to this theoretical line, but at the upstream end of the test section the pressure drop is marginally higher than that in fully developed flow. There are also variations between the pressures at the two tappings at each section owing to the asymmetric nature of the flow (c.f. Kito (1984)).

Figure 6.27 shows the relationship between the swirl level and the local friction factor. The effects of the variations owing to asymmetry were minimised by the following procedure. The 10 stations at which pressure was measured were paired off into 5 pairs of successive stations. For each Reynolds number the four values of pressure in each pair were averaged and then the differential

pressure was formed from the averaged values obtained from two successive pairs of stations. Appropriate values of Δz were used to calculate the local friction factor $f+f_e$, equations (6.7) being used to provide the values of the swirl level S at the mid point of the interval Δz.

7. THE EFFECT OF THE MEASURED VELOCITY PROFILES ON ELECTROMAGNETIC AND ULTRASONIC FLOWMETERS

7.1 Introduction

In this chapter we consider the effects of the measured axial velocity profiles on electromagnetic and both single and dual beam ultrasonic flowmeters. In order to do this we first represent the axial velocity data (on 36 points on each section as shown in figure 6.6) using an algorithm described in section 7.2. We are then able to carry out simple integrations appropriate to each kind of flowmeter in order to obtain the expected errors as a proportion of the result obtained for fully developed flow (as defined by the theoretical method 'B' in a smooth pipe) passing through the flowmeter in question.

7.2 Representation of axial velocity profiles by polynomials

In this section we describe an algorithm used to represent the experimentally measured axial velocity profiles on sections 1 and 2 at each of the Reynolds numbers.

It was decided to use a general quartic polynomial in the cartesian coordinates x and y and to choose the coefficients by means of a least squares regression analysis. We use a quartic polynomial (having 14 coefficients) because the profile has, in general, the form of a 4th-order polynomial on any diameter. If we use many more or many fewer terms, trials showed a less satisfactory outcome, both in terms of the degree of fit at the data points and in the behaviour of the resulting formula far from the data points. In order to guide the shape of the resulting formula at the top and bottom of the pipe, furthest from any experimental data points, 6 additional values were specified and treated as extra data points, making 42 in all. These extra data points were at $x = 0$, $y = \pm 0.95$ and at $x = \pm 1$, $y = \pm 1$ where x and y are the cartesian coordinates of the axes in figures 7.1 to 7.4. The values used were 0.9 at the first two and 0.25 at the other four, all velocity data being normalised to the average velocity. Clearly there is an element of arbitrariness in this procedure. A number of trials were carried out which indicated that the effect of using different values at different points was not very

significant, when it is recognised that the figures obtained here are only an approximate guide to these effects in any case. The accuracy of the integration models of the flowmeters will be discussed for each flowmeter separately in later sections.

The formula used was a polynomial of the form

$$
\begin{aligned}
Q^z/Q_{av} = 1 + & \\
& a_1x + a_2y + \\
& b_1(x^2 - 1/4) + b_2xy + b_3(y^2 - 1/4) + \\
& c_1x^3 + c_2x^2y + c_3xy^2 + c_4y^3 + \\
& d_1(x^4 - 1/8) + d_2x^3y + d_3(x^2y^2 - 1/24) + d_4xy^3 + d_5(y^4 - 1/8)
\end{aligned}
\qquad (7.1)
$$

where it can be seen that the first term is the average bulk velocity of 1, and that each of the other terms have no net flow. We therefore satisfy the condition that the bulk flow be 1, regardless of the choice of the coefficients.

Figures 7.1 to 7.4 show axial velocity contours obtained using this algorithm which represent the data shown in figures 6.22 to 6.25. The sense of the diagrams is that we are looking downstream. The figures show that the axial velocity is in the form of a horseshoe on section 1, and that by the time the flow reaches section 2 this horseshoe has decayed considerably, whilst rotating with the swirl. That the axial velocity profile rotates with the swirl can be seen by means of the lines of symmetry drawn on the figures. These lines are postioned in such a way as to make the bulk flow through each of the two semicircles the same as each other; their postion was determined by carrying out a large number of integrations of the bulk flow through such semicircles and finding the diameter which split the bulk flow in half. The direction of the swirl is anticlockwise, and it is possible to compare the angle through which the profiles have rotated as determined from these lines of symmetry and as determined by carrying out the integrals in z of equations (6.7) between the two planes. These result in 0.93 and 0.78 of a revolution for the higher and lower Reynolds numbers according to the integrals of equations (6.7), and 0.91 and 0.86 as determined by the postion of the lines of symmetry. These are very close to each other.

7.3 The electromagnetic flowmeter

Electromagnetic flowmeters measure the flowrate by detecting the potential difference between two electrodes at opposite ends of a diameter of the pipe resulting from the flow of the (conducting) fluid in the pipe through an externally applied magnetic field. The flow signal measured in this way (using the two-dimensional model of an integral over a plane cross-section) is found to be

$$\text{Flowrate} = \int_0^{2\pi}\int_0^1 W(r,\theta)Q^z(r,\theta)\ r\,dr\,d\theta \qquad (7.2)$$

where $W(r,\theta)$ is a weight function depending on the nature of the applied magnetic field and the geometry of the meter etc. Actually, the flow signal from the meter is the value of a volume integral of the scalar product of the velocity vector and a weight vector in a section of pipe (normally about 1 or 2 diameters long). This two-dimensional model will be very close to this because the change in flow profile changes slowly with axial distance. We consider the case of an electromagnetic flowmeter with a uniform magnetic field applied across it. This means that the weight function is given by the expression

$$W(r,\theta) = \frac{1 + r^2\cos 2\theta}{1 + 2r^2\cos 2\theta + r^4} \qquad (7.3)$$

as given by Shercliff (1962) p28 who also describes the basics of electromagnetic flow measurement.

In order to overcome any possible problems arising from the singularity of W at $\theta = \pm\pi/2$, we use the fact that the value of the flowrate as calculated by equation (7.2) is 1 for the case of a uniform profile $Q^z(r,\theta) = 1$. Since W is symmetrical in the lines along which $\theta = 0,\pi$ and $\theta = \pm\pi/2$, the values of Q^z in the four quadrants were summed in the appropriate way giving a total Q_t^z. Equation (7.2) can then be expressed as

$$\text{Flowrate} = \frac{1}{4}Q_t^z(r=1,\theta=\pi/2) + \int_0^{\pi/2}\int_0^1 rW\left[Q_t^z - Q_t^z(r=1,\theta=\pi/2)\right]\ dr\,d\theta \qquad (7.4)$$

This intgral was then evaluated using a grid consisting of 101 radial points and 25 tangential points. Integrations were performed for each of the 25 possible relative positions of the flowmeter (weight function) and flow (Q^z). Integrations were carried out for the case

of the theoretical profile of method 'B' in a smooth pipe at the appropriate Reynolds numbers; these results were used as a calibration to determine the relative error caused by the perturbed profiles.

Having obtained these results on each of the two measurement sections, figure 7.5 (which shows meter errors at all points between the sections) was prepared in the following way. We saw in figures 7.1 to 7.4 that the swirling nature of the flow causes the whole axial profile to rotate around with the flow as it travels down the pipe and decays towards its fully developed form. The diametrical lines of symmetry in those figures define the angle of rotation between the planes. Assuming a constant rate of rotation, we can specify the position of the line of symmetry at any axial location. We are then able to determine the angular displacement of the line of symmetry from the fixed postion of the electrodes (we consider the cases where the electrodes are either in the vertical or horizontal plane). We know the error at this angular displacement on each of the sections. We use linear interpolation in the axial direction to find our estimate of the error of the meter were it placed at that axial position. We see in figure 7.5 that the error oscillates in the manner of a damped sine wave as did the results of Tsuchida, Terashima and Machiyama (1982). There is no appreciable difference between the true flowrate and the overall level of the predicted readings. This is because the configuration used (that of a uniform magnetic field with point electrodes) is ideal for axisymmetric flows.

7.4 Ultrasonic flowmeters

We consider the effects of the measured profiles on both single beam and dual beam ultrasonic flowmeters. These meters operate by measuring the time of flight of a beam of ultrasound passing across the flow in a pipe. The component of the flow in the direction of the beam affects the speed of the beam, thus determining the measured time. In general therefore, the beams have to pass diagonally across the pipe, so as not only to cross the pipe but also to cover some distance downstream as well (usually this distance is about 1 diameter). This applies whether or not there is more than one beam. Some profile development will occur in this downstream length, but we

ignore this since it is small as we observed in the previous section. We also ignore the effects of the radial and tangential components of velocity; these depend upon the precise arrangement of the beams in the meter body. We know that the radial velocity is small because the redevelopment of the flow profile is slow; it therefore has little effect. The tangential velocity, although of the same order of magnitude as the deviations in the axial velocity profile from its fully developed form, has little effect on the types of ultrasonic flowmeters considered: In the case of the single beam ultrasonic flowmeter the beam is at right angles to the tangential direction; in the dual beam case the effects on the two beams cancel. We therefore calculate integrals in the plane at right angles to the pipe axis.

For the case of the single beam meter, the beam is positioned along a diameter and so the integral we calculate is

$$\text{Flowrate} = \int_0^1 \left[Q^z(\theta=\theta_o) + Q^z(\theta=\theta_o+\pi) \right] dr \qquad (7.5)$$

We calculate this using the same grid sizes as before, and for each of the 48 postions required to evaluate it at all the relevant angular postions. Figure 7.6 was prepared in the same way as figure 7.5; the errors were calculated from a calibration integral performed using the theoretical fully developed profile.

In the case of the dual beam meter the two beams are positioned on two parallel chords of the pipe each at a distance of half the pipe radius from the centre. Integrals of the same form as that in equation (7.5) were evaluated and the results from the two chords averaged. Figure 7.7 is the result of these integrals and has been prepared in the same way as the other figures.

We see that in both cases there is damped oscillatory behaviour as in figure 7.5. We also see that the results in figure 7.6 display a negative shift from the true value, owing to the relatively high importance that a single beam ultrasonic flowmeter attaches to the central region of the pipe and to the fact that the profile under consideration is flatter, overall, than in fully developed flow.

8. DISCUSSION, CONCLUSIONS AND RECOMMENDATIONS

8.1 Consideration of the theoretical and experimental work

8.1.1 Discussion

We said in section 4.1 that in the theoretical part of the work we would consider those swirling flows in pipes which have the form of a solid body rotation. We said this because this is the kind of swirling flow most often experienced by flowmeters and is also the kind of swirling flow into which all swirling flows eventually decay. We consider in this section the relation between the theoretical calculations, the experimental results and our understanding of the nature of the flow (gained both from this work and our survey of the literature in chapter 3).

Firstly, we consider the decay rate of swirl λ, as a function of Reynolds number Re, and Swirl number S. We saw in figure 3.3 that λ falls with a rise in Re. Although the precise form of the relationship is uncertain, there is no doubt as to the universal nature of this finding of so many workers. Physically it means that although in a flow with a higher Re there will be a higher eddy viscosity which increases the rate of decay of swirl as seen by itself, this is more than compensated for by the faster speed at which the 'lump of fluid' under consideration is travelling downstream. The experiments described in this thesis also support this general finding, despite the relative proximity of the two values of Re used.

We saw in chapter 5 that the linear theory also predicts this behaviour, as well as revealing the profound influence of the pipe roughness through the friction factor. The crude theory of Youssef (1966), Rapier (1981) and Mottram and Rawat (1986) points to the relationship $\lambda = 4f$; this agrees with the linear theory of this work to within 10%. However, the experimental results presented in chapter 6 and those of other workers indicate that this formula sometimes underestimates the rate of decay. Figure 8.1 shows some relevant information, where the theoretical curve drawn is that for the case of a smooth pipe, according to the linear theory of this thesis (method B).

Mottram and Rawat (1986), whose experiments (with air and at two different pipe roughnesses) broadly support the $\lambda = 4f$ formula, used a double bend preceded by a Borda inlet. Nystrom and Padmanabhan (1985) also used a double bend (in a smooth pipe) but provided it with a 40 diameter inlet section (as did the author in the experiments described in chapter 6) which ensured a reasonably fully developed profile at the inlet to the bend. It may well be that significant differences exist between the turbulence intensities present in these studies; this would have an influence on decay rates. Whilst the author was carrying out the computations described in chapter 5, experience was gained indicating that the decay rate λ is a parameter which is relatively sensitive to changes in the character of the wall layer, this being the location of the high tangential velocity gradients which are involved in the mechanism of turbulence. It would seem plausible that the swirl after a double bend decay slower if the preceding flow is not fully turbulent (as is the case a short distance after a Borda inlet) than if the double bend be preceded by an inlet section long enough to render the inlet flow reasonably fully developed.

In view of this, and of the good agreement between the decay rates obtained as a result of the experiments described in this work and those of Nystrom and Padmanabhan (1985) (both in smooth pipes, and after a double bend provided with an inlet section), it would seem that these results are an accurate reflection of typical decay rates in swirling flows following double bends in pipelines. This view is in line with the findings of Krieth and Sonju (1965) who used twisted tapes to generate swirl having the form of a solid body rotation.

As we have seen, the theories which suggest $\lambda = 4f$ would appear to underestimate the true decay in swirling flows following double bends in pipelines. The form of the relationship would seem to be right however, since we can see that it varies with Re in the right way. The author suggests therefore that the empirical relationship $\lambda = 6f$ be used, in line with the results of Nystrom and Padamanbhan (1985) and those reported in this thesis.

In chapter 5 we saw that the similarity theory predicts a rise in λ with S, albeit a small one. Although Ward-Smith (1980) observes

that Youssef (1966) (working with high swirls) found higher rates of decay than other workers, there is no very direct connexion between these facts since the similarity theory is only valid in situations where the tangential velocity profile has the form of a solid body rotation. The workers who obtained the high decay rates on the graph in figure 3.3 (lines 3,5,9 and 10) either used vanes or tangential entry tubes to generate a large amount of swirl. Both these methods produce a tangential velocity profile having the form of a free vortex in a region near the wall and tend to result in a region of reverse axial flow around the pipe axis. This may be presumed to account for the differences between the results obtained by these workers and those of Baker and Sayre (1974).

Secondly, we consider the friction factor in swirling flow. We see in figure 8.2 that the similarity theory is in reasonable agreement with the work of both Baker and Sayre (1974) and that of Janik and Padmanabhan (1980) as well as that of Yajnik and Subbaiah (1973) for sufficiently low swirl levels ($S \lesssim 0.2$). At higher swirl levels, the theory predicts a higher value than these workers do. This may be partly due to the fact that the theory deals with the local values of swirl and friction factor whereas the experimental results of Baker and Sayre (1974) (for example) deal with measurements of the pressure drop over a significant length of pipe. The linearised formula given by Yajnik and Subbaiah (1973) can be reformulated as the line shown in figure 8.2, whose equation is $f + f_e = f(1 + 1.56S)$. The curve corresponding to the region of agreement on the graph can be expressed as $f + f_e = \exp(1.65S)$. The attempt to consider the relationship between f and S using the author's pressure measurements (described in chapter 6) was not particularly successful, owing to the very small variations involved, and the hazards of asymmetry.

Thirdly, we consider the nature and form of the velocity profiles described by the theory. We have seen that theoretical and experimental work of this thesis have both produced swirling flow having the form of a solid body rotation. The point of particular interest is the degree to which this rotation affects the axial velocity profile. The similarity theory shows relatively little effect compared with many observed phenomena, but this is to be

expected since we exclude from consideration the effects of the swirl generator (or bend) being used. The theory considers the 'far field' effect where there is no free vortex part to the tangential velocity profile. The theory is consistent with the experiments described in this thesis in the weak sense that once the asymmetries near to the double bend have decayed (measurement section 3), the swirl level (2°) is such that the theory would predict no measurable axial velocity perturbation as indeed was the case. This is also consistent with the work of Yajnik and Subbaiah (1973) and (implicitly) with the standard (ISO (1980)) which says that 2° of swirl is acceptable for flow measurement purposes. The theoretical work of this thesis is unable to make any statement about the flow field close to swirl generators or bends, or indeed any swirling flow which does not have the form of a solid body rotation. It may be that were an axisymmetric flow generated with a large swirl having the form of a solid body rotation, the predictions of the theory at higher swirl levels could be tested. It should be noted that there is a significant difference between the form of the axial velocity profile close to the wall predicted by the similarity theory and that predicted by the linear theory, owing to the formulation of the eddy viscosity ϵ. The linear theory (as it stands) could not, in any case, be applied to situations where the maximum value of the axial velocity was no longer on the pipe axis.

Finally, we consider the form of velocity profiles found to exist after a double right angle bend in two perpendicular planes. We see that the asymmetry that was observed is consistent with the rotating horseshoe profiles of Kito (1984) and with the more restricted measurements of Mottram and Rawat (1986). It would seem that a double bend inherently generates this asymmetry as indicated in the sketch in figure 8.3, following on from the ideas of figures 3.1 and 3.2: As a result of the swirling motion starting in the second bend, the region of higher axial velocity and the region of lower axial velocity retain their identity (to some degree) resulting in the asymmetrical profiles which were observed. The work of chapter 7 indirectly supports this, showing that upon the assumption that profiles of this kind were present in the experiments of Tsuchida, Terashima and Machiyama (1982), the qualitative nature of their

results can be predicted. It is clear however that the effects of slightly different spacer lengths between the two component bends and bend radius ratios are of importance and are by no means fully understood.

8.1.2 Conclusions

1. In pipe flows with swirl in the form of a solid body rotation, an empirical approximation to the exponential decay rate of the swirl λ, is given by the formula $\lambda = 6f$.

2. The decay rate λ, rises both with a fall in Re and with a rise in S, and is also dependent on the origin of the swirl. It is normally higher if there is a region of recirculating flow or if vanes have been used, resulting in the outer part of the flow having the form of a free vortex.

3. The friction factor in swirling flow ($f + f_e$), relative to that in non-swirling flow (f) at the same Re and pipe roughness, can be found from the formula $f + f_e = f\exp(1.65S)$ at least for values of S less than 0.2.

4. In pipe flows in which swirl decays, whatever its origin, there is a significant region of the flow (downstream) in which although the swirl level remains measurable, the axial velocity profile is effectively fully developed. There is, however, no reason to believe that the turbulent intensities are the same as that in fully developed flow.

5. The behaviour of the axial velocity in swirling flows upstream of this region is almost entirely dependent on the inlet conditions.

6. Swirling flows tend to preserve whatever axial velocity profile is initially present, rotating it around as it travels downstream.

7. The double bend used in the experiments described in this thesis gave rise to asymmetrical axial velocity profiles having the form of a horseshoe close to the bend. The swirl number (S) 9 diameters downstream from the bend was about 0.07, corresponding to a swirl angle (Φ) of 8°.

8.2 Implications of the work for flow measurement

8.2.1 Discussion

We see from the conclusions in section 8.1.2 that it is vital when considering the effects of swirling flow on flow meters that the Reynolds number and pipe roughness be known, in order that the friction factor f and hence the decay rate λ be known. Apart from this, the other vital piece of information that is needed is the initial size and form of the swirl present.

Flows arising from double bends of the form described in this thesis are the most common swirling flows in piping systems, along with similar flows produced by the combination of a 'Tee' junction or half open gate valve with a single bend. We can see from the experiments described in chapter 6 and from the work of Mottram and Rawat (1986), that if a flowmeter is close to a double bend of this kind (within 40 diameters say) then the axial velocity profile is liable to be noticeably different from that in a fully developed flow, even in rough pipes. For the case of a relatively smooth pipe Mottram and Rawat (1986) found that this was the case even for distances as high as 70 diameters. In the experiments described in this thesis, in a smooth pipe and with lower swirl levels than those of Mottram and Rawat (1986), the position of measurement section 3 (60 diameters) is a fair measure of this distance. It would seem then, that the requirement of the standard ISO (1980) that the swirl angle be no more than 2° is a satisfactory measure of the state of the axial profile, at least in situations of this type.

Two areas of interest emerge. One is the effect on flow meters of swirl angles of less than 2°, even when the axial velocity profile is very nearly that of a fully developed flow. The other is the effect of the asymmetrical axial velocity profiles which were observed in the experiments to be caused by double bends.

We have already seen, in section 3.8 that a swirl angle of 2° is liable to cause a turbine meter to be in error by 2%. It can also be seen from the work of Mottram and Rawat (1986) regarding orifice plate meters that the swirl level is a parameter which can be used to determine the required distance between the bend and the meter. Their results, together with those of McHugh, Kinghorn and Dyet (1984) do

not contradict the 2° figure. Electromagnetic and ultrasonic meters would not be measurably affected by a swirling flow (having a small value of S) in which the axial velocity profile had the fully developed shape. It is not clear at what swirl level the accuracy of vortex-shedding meters is affected; it would (however) seem unlikely that small swirl levels such as 2° are significant in view of the work of Cousins (1977).

The effect of the asymmetrical profiles following a double bend is to cause the error of flowmeters to oscillate as the distance between them and the bend changes. This has been shown to be the case for both electromagnetic and ultrasonic meters in chapter 7 and would seem to be the likely explanation of the results of Tsuchida, Terashima and Machiyama (1982) concerning electromagnetic meters. The orifice plate meters of Mottram and Rawat (1986) seem less sensitive to this asymmetry. It is clear the qualitative form of the results in chapter 7 is genuine, but that because it is not possible at present to predict the precise locations of the oscillations, distances at which flowmeters should be positioned must be determined from the envelope of the oscillations. For the electromagnetic flowmeter, the results of Tsuchida, Terashima and Machiyama (1982) are that the maximum error is 0.5%, falling to 0.1% in 25 diameters. The results of the author would suggest that the magnitude of the error be higher (1%) and that it be higher for longer. Deacon (1982) also found errors of the order of 1% in electromagnetic flowmeters close to a double bend. Clearly, experiments performed with real flowmeters must be the basis for firm figures, rather than those of chapter 7, even though these are a reasonable guide. The results of the calculations in chapter 7 show that ultrasonic meters behave similarly, and that the maximum errors associated with them are of the order of 6% and 2% for the single and dual beam versions respectively.

8.2.2 Conclusions

1. The initial swirl angle Φ, the friction factor f, and the manner by which the swirl has been generated are the pieces of information needed when considering the expected accuracy of a flowmeter positioned in a swirling flow, in order that the swirl angle and the form of the axial velocity profile present in the meter

body may be determined.

2. If it is desired to place a meter far downstream of a double bend, then the distance required can be calculated (approximately) from $\Phi = \Phi_0 \exp(-6fz/D)$ where it be required that Φ be less than 2° for an orifice plate, electromagnetic or ultrasonic meter, or that Φ be determined according to the relation that 1° of swirl causes a turbine meter to be in error by 1%. As a rough guide, Φ_0 may be taken as 10° at a distance 10 diameters downstream from the double bend. Typical values resulting from these figures as applied at a Reynolds number of 10^5 are as follows. In a smooth pipe ($f = 0.0045$) $\Phi \angle 2°$ at $z/D = 70$ diameters downstream of the bend, and $\Phi \angle 0.25°$ at 147 diameters. In a rough pipe ($f = 0.0066$ based on $\epsilon_R/D = 0.0026$) $\Phi \angle 2°$ at $z/D = 51$ diameters and $\Phi \angle 0.25°$ at 104 diameters.

3. If it is desired to place a meter relatively close to a double bend, then the errors vary considerably with meter type, and decay from a maximum value near to the bend (at 5 diameters say) in the manner of a damped sine wave whose envelope may be regarded as following the decay law given in conclusion 2. The figures 10 diameters after the double bend seem to be 3% for an orifice plate meter, 1% for the electromagnetic meter, 6% for a single beam ultrasonic meter and 2% for a dual beam ultrasonic meter.

4. Users of flowmeters need to decide what their purpose is in measuring the flowrate and to use an appropriate meter type in adequate installation conditions (these will depend on that purpose). There may be situations in custody transfer applications in which a flow straightener would be appropriate, even though this would require a not inconsiderable straight length between it and the flowmeter. It should be noted that owing to the asymmetry of the flow after a double bend it is likely that similar installations may display quite different errors from each other, since the horseshoes need only be in slightly different places for this to be the case.

8.3 Recommendations for further work

1. Double bends of the kind used in the experiments described in this thesis are many and various. A study investigating the effects of spacer length and radius ratio is in order so as to investigate the physics of the formation of the horseshoe profiles. It would be particularly interesting to be able to predict the initial orientation of the horseshoe as it emerges from the bend.

2. Theoretical work aimed at modelling the asymmetrical profiles and the preserving effect of swirl upon axial profiles would be both interesting and useful, serving to improve understanding of the character of this kind of swirling flow.

3. A series of tests on flowmeters placed downstream of a double bend in order to establish the magnitudes of the effects described and predicted in this work is necessary in order to further confirm (or deny) the conclusions presented in this chapter, and to give a firm experimental basis for action by flowmeter users. Such tests would need to be carried out over a representative range of Reynolds numbers and pipe roughnesses, and should investigate the effects of various bend geometries. It is important to ensure that the flow preceding the bends be fully turbulent as is the case in the vast majority of flowmeter installations in real pipelines. Nevertheless, it may be necessary to consider inlet flow conditions other than that of a fully developed flow, such as the flow after bends or valves.

4. Theoretical work modelling the effect of swirling flows on flowmeters of various types would be a useful adjunct to the experimental tests recommended above. The theoretical and experimental work of this thesis provides evidence as to the form of velocity profiles which should be considered as initial conditions for such studies. In particular, the vortex-shedding meter is one for which no simple model such as those used in chapter 7 exists and for which a detailed analysis would be useful.

5. Standards need to be adjusted and/or written to take account of the differing behaviour of the various types of flowmeter now in use. They should deal with the important influence of the friction factor (depending, in general, both on pipe roughness and Reynolds number), the installation lengths required to remove errors and the likely errors in their absence.

ACKNOWLEDGEMENTS

The author owes a debt of gratitude to the Science and Engineering Research Council and to the Foxboro company who, between them, sponsored the work. Without this sponsorship the work could not have been achieved. In particular, thanks are due to Mr E.H. Higham and other employees of the Foxboro company who gave up a considerable amount of time to discuss matters with the author and, thereby, to provide some invaluable information.

The author has a special desire to thank the members of the support panel (see Appendix A), all of whom have made significant contributions to the successful completion of the work. Professor R.C. Baker and Dr J. Hemp, between them, gave the project its initial direction and kept it on a steady course whilst giving the author considerable freedom to pursue his own lines of inquiry. Professor C. New had a particular role in bringing the market survey into being; the author received much detailed assistance with this from Dr R.A. Furness and Mr E.H. Higham both in its execution and in the drafting of chapter 2.

As the chairman of the support panel, Professor R.C. Baker carried out the roles of strategist, referee and diplomat most effectively; the author is very grateful to him for the energy which he put into this. Without his input this thesis could have not have been as broad or comprehensive as it is.

As academic supervisor, Dr J. Hemp proved perenially accessible and continually helpful. The author wishes to thank him particularly for his patient and thorough manner, not least in the preparation of the final thesis.

Especial thanks are also due to Dr A. Goulas who gave considerable assistance to the author with the Laser Doppler Anemometry. Without his wisdom and experience this important part of the work would have been very much more difficult. Mr H.K. Versteeg also proved an invaluable source of information, guidance and practical help in this regard and offered many helpful comments upon the draft of chapter 6, as well as being a valuable source of help in a multitude of other ways.

The author is more than somewhat grateful for the encouragement he received at the hands of Dr J.R. Heritage, particularly during

lean periods which were experienced during each of the first and second years. He proved a valuable sounding board, particularly with regard to the formulation of the similarity theory.

The author wishes to thank Mr H.K. Versteeg, Dr J.R. Heritage and Dr A. Goulas for their assistance with aspects of the computational work including the numerical methods used, the author's learning of Fortran and the gentle art of persuading the computer to give of its best.

The author also wishes to thank Mrs J.E. Heritage, Dr R.A. Furness, Dr A. Goulas and others for their assistance with the design and operation of the experimental facility.

Thanks are also due to Dr C.P. Lenn, who provided the electronic filter used for making some of the pressure measurements.

The author wishes to thank Mr J. Parker for his expert assistance in the construction of the experimental facility as well as to Mr D. Wallace for the help he gave on a number of occasions. The author is also thankful for the assistance he received from various members of the staff (past and present) of the British Hydromechanics Research Association.

The author is very thankful that the powers that be in the Department of Fluid Engineering and Instrumentation decided to purchase word processors, and that he has been able to use one of these to produce the text of this thesis.

In addition, thanks are due to every member of the Department of Fluid Engineering and Instrumentation for making the author's task a pleasant one and for helping both to make this thesis what it is and its author more nearly what he should be.

Finally, the author would like to pay tribute to Mr A. Hull with whom he lodged throughout the time of the PhD. The stable home base which he provided and the Christian fellowship which the author enjoyed both with him and many others both at St. John's Church in Bedford and at the Institute formed a firm foundation and are much appreciated.

REFERENCES

ADRIAN R.J.
FINGERSON L.M.
Laser anemometry theory, application and techniques.
TSI Short course notes.

AFZAL N.
Fully developed turbulent flow in a pipe: An intermediate layer.
Ingenieur-Archiv vol 52, 1982, pp355-377

BAKER D.W.
SAYRE C.L.
Decay of swirling turbulent flow of incompressible fluids in long pipes.
In: Proc. of Symp. on Flow: Its measurement and control in science and industry vol 1 pp301-312
Editor R.B.Dowdell, Indust. Soc. of America. 1974

BATCHELOR G.K.
An introduction to fluid dynamics.
Cambridge University Press 1967

BLAKE K.A.
The development of velocity profiles downstream of swept and simple mitre bends.
Flowmeasurement memo No. 107 NEL April 1973

BRADSHAW P.
The analogy between streamline curvature and bouyancy in turbulent shear flow.
Jnl Fluid Mechanics vol 36, 1, 1969, pp177-191

BRADSHAW P.
Understanding and prediction of turbulent flow.
Aeronautical Journal vol 76, 1972, pp403-418

BRADSHAW P.
Effects of streamline curvature on turbulent flow.
Agardograph No. 169, 1973

CAMPBELL J.M.S.
Development of a pipe bend having a good outlet velocity distribution, and the effect of subsequent contractions.
BHRA RR658 1960

CHOWDHURY J. Electronics, flowmeters: a winning combination.
Chemical Engineering vol 89, 13, June 1982 pp39-43
McGraw-Hill

COUSINS T. Vortex meters.
Transducer 1977 conference,
paper in day 3, session flow measurement.

DAVIES R.W.
MOORE E.F.
MATTINGLEY G.E.
MILLER R.W. Numerical Solutions for turbulent, swirling flow through target flowmeters.
ASME Paper 78-WA/FM-4 1978

DEACON J.E. Electromagnetic flowmeter tests
Flowmeko 1983, 3rd Conference of the IMEKO
Technical Committee on flow measurement, Budapest,
Hungary, 20-22 Sept. 1983. Editor: A. Szilvassy.

DURST F.
MELLING A.
WHITELAW J.H. Principles and practice of laser-doppler anemometry.
Academic Press 1976

FURNESS R.A. Private communications 1985

HALSEY D.M. A survey of industrial usage of flowmeters.
Measurement and Control vol 19, 5, June 1986,
pp52-55

HIGHAM E.H. Private communications 1985, but see
Measurement and instrumentation for control
Edited by M.G. Mylroi and G. Calvert, IEE control
engineering series No. 26, Peter Peregrinus 1984

HINZE J.O. Turbulence.
2nd edition McGraw-Hill 1975

HUNT J.D. — An experimental study of the redevelopment of a distorted pipe flow. PhD Thesis, Dept. Engng. Mechs., Raleigh, North Carolina, USA, 1974

INTERNATIONAL STANDARDS ORGANISATION — Measurement of fluid flow by means of orifice plates, nozzles and venturi tubes inserted in circular cross-section conduits running full. ISO 5167-1980(E)

ISAACSON E. KELLER H.B. — Analysis of numerical methods John Wiley and Sons Inc. 1966

ITO S. OGAWA K. KURODA C. — Decay process of swirling flow in a circular pipe. International Chemical Engineering vol 19, 4, 1979 pp600-605

JANIK C.R. PADMANABHAN M. — Effect of swirling flow on pipe friction losses. ARL-ALden Research Labs. Feb 1980, 26-81/M296KF

KITO O. — Axi-asymmetric character of turbulent swirling flow in a straight circular pipe. Bull. JSME vol 27, 226, April 1984, pp683-690

KITO O. KATO T. — Near wall velocity distribution of turbulent swirling flow in a circular pipe. Bull. JSME vol 27, 230, Aug. 1984, pp1659-1666

KRIETH F. MARGOLIS D. — Heat transfer and friction in turbulent vortex flow. Applied Science Research section A vol 8, 1959, pp457-473

KRIETH F. SONJU O.K. — The decay of a turbulent swirl in a pipe. Jnl Fluid Mechanics vol 22, 2, 1965, pp257-271

LAUFER J.
The structure of turbulence in fully developed pipe flow.
NACA Report No. 1174, 1954

LAUNDER B.E.
SPALDING D.B.
Lectures on mathematical models of turbulence.
Academic Press 1972

LAVAN Z.
NIELSEN H.
FEJER A.A.
Separation and flow reversal in swirling flows in circular ducts.
Physics of Fluids vol 12, 9, Sept. 1969 pp1747-1757

LEESTMA D.C.
An experimental investigation of the effects of swirling and pulsing the flow through an axisymmetric duct.
MSc Thesis, Naval Postgraduate School, 1971,
US Naval Academy.

McHUGH A.
DYET D.
KINGHORN F.C.
Prediction of the effect of swirling flows on orifice plate measurements.
NEL Report No. 676 July 1981

McHUGH A.
KINGHORN F.C.
DYET W.D.
Efficiency of an etoile flow straightener in non-symmetric swirling flow upstream of orifice plates.
NEL Report No. 692 August 1984

MILLER D.
Internal fluid flow - a guide to pipe losses and duct systems.
BHRA 1971

MILLER D.
Internal flow systems.
BHRA Fluid engineering series 4, 1978

MOORE W.E.
KIROUAC G.J.
Measurements of turbulent flow induced by a 90-degree cylindrical elbow.
Knolls atomic power laboratory - 4142
American Physical Society, Division of fluid mechanics 22/11/1981

MORSE P.M.
FESCHBACH H.
Methods of theoretical physics
Int. Student Edition, McGraw-Hill 1953

MOTTRAM R.C.
RAWAT M.S.
The swirl damping properties of pipe roughness and the implications for orifice meter installation
Paper 6.1 of Int. Conf. on flow measurement in the mid-eighties, 9-12 June 1986 at NEL Glasgow.

MURAKAMI M.
SHIMIZU Y.
SHIRAGAMI H.
Studies on fluid flow in three dimensional bend conduits.
Bull. of JSME vol 12, 54, 1969, pp1369-1379

MURAKAMI M.
KIKAYAMA K.
NISHIBORI K.
Flow in axially rotating pipes.
Memoirs of the Facalty of Engng., Nagoya Univ. vol 35, 1, 1983

MUSOLF A.O.
An experimental investigation of the decay of a turbulent swirling flow in a pipe.
Thesis, Univ. of Colarado, 1963

NISSAN A.H.
BRESAN V.P.
Swirling flow in cylinders.
A.I.Ch.E. Jnl. vol 7, 4, Dec 1961, pp543-547

NYSTROM J.B.
PADMANABHAN M.
Swirl due to combined pipe bends.
Paper 2 pp9-24 of International conference on the hydraulics of pumping stations, held at UMIST, England 17-19 Sept. 1985. Organised and sponsored by BHRA.

OOSTHUIZEN P.H. — A numerical study of swirling pipe flow using a modified mixing length model. ASME-CSME Fluids Engng. Conf. Montreal, Quebec May 13-15, 1974. CSME Paper No. 73-CSME-82

PEACOCK G. — The effect of asymmetric inlet flow on the hydraulic forces in a centifugal pump. MSc Thesis, School of Mechanical Engineering, Cranfield Institute of Technology, Sept 1984.

RAPIER A.C. — The effect of upstream flow conditions on flow meters. Paper C2 in Int. Conf. on advances in flow measurement techniques, 9-11 Sept. 1981 at Warwick University. Sponsored by BHRA Fluid Engineering.

REICHARDT H. — Vollstandige Darstellung der turbulenten Geschwindigkeitsverteilung in glatten leitungen. Z. angew. Math. Mech. vol 31, pp208-219 1951

ROCHINO A. LAVAN Z. — Analytical investigations of incompressible turbulent swirling flow in stationary ducts. Trans ASME: Jnl of Appl. Mech. June 1969 pp151-158

RODI W. — Turbulence models and their application in hydraulics - a state of the art review. Book publication of the international association for hydraulic research, Delft, Netherlands 1978

RODI W. — Examples of turbulence models for incompressible flows. AIAA Jnl vol 20, 7, 1982, pp872-879

ROWE M. — Measurements and computations of flow in pipe bends. Jnl Fluid Mechanics vol 43, 4, 1970, pp771-783

SALAMI L.A. Effect of upstream velocity profile and integral flow straighteners on turbine flowmeters. Int. Jnl. Heat and Fluid Flow vol 5, 3, Sept 1984 pp155-165

SCHLICHTING H. Boundary layer theory. 7th edition McGraw-Hill 1979

SHERCLIFF J.A. The theory of electromagnetic flow-measurement. Cambridge University Press 1962

SMITHBERG E. LANDIS F. Friction and forced convection heat-transfer characteristics in tubes with twisted tape swirl generators. Trans ASME: Jnl of Heat Transfer vol 86, 2, 1964, pp39-49

SPARROW E.M. CHABOKI A. Swirl affected turbulent fluid low and heat transfer in a cicular tube. Trans ASME: Jnl of Heat Transfer vol 106, Nov. 1984 pp766-773

TALBOT L. Laminar swirling pipe flow. Trans ASME: Jnl of Applied Mech. vol 21, pp1-7 1954

TENNEKES H. LUMLEY J.L. A first course in turbulence. MIT Press 1972

TSUCHIDA T. TERASHIMA Y. The effects of flow velocity profile on the electromagnetic flowmeters. Reprinted from Report of Researches, Nippon Inst. of Tech. 1982 (most of text in Japanese).

VAN DRIEST E.R. On turbulent flow near a wall. Jnl of the Aeronautical Sciences Nov. 1956 pp1007-1011,1036

WARD-SMITH A.J. Internal fluid flow - the fluid dynamics of flow in pipes and ducts.
Clarendon Press, Oxford 1980

WESKE J.R. Experimental investigation of velocity distributions downstream of single duct bends.
NACA Technical Note No. 1471, 1948

WOLF L.
LAVAN Z.
FEJER A.A. Measurements of the decay of swirl in turbulent flow.
AIAA Jnl. vol 7, 5, May 1969 pp971-973

YAJNIK K.S.
SUBBAIAH M.V. Experiments on swirling turbulent flows part 1: Similarity in swirling flows.
Jnl Fluid Mechanics vol 60, 4, 1973, pp665-687

YANTA W.J.
SMITH R.A. Measurements of turbulence transport properties with a laser doppler velocimeter.
AIAA Paper 73-169, 1973

YOUSSEF T.E.A. Some investigations on the rotating flow with a recirculation core in straight pipes.
ASME Paper 66-WA/FE-36 1966

APPENDIX A: The role and composition of the support panel

The PhD was supervised by a support panel of supervisors under the chairmanship of Professor R.C. Baker. The purpose of the panel was to give general guidance and support to the author during the course of the work, particularly with regard to the 'non-technical' aspects of the work concerned with the industrial marketplace which characterise a Total Technology PhD. It also sought to be a forum in which the many different aspects of the work could be discussed in conjunction with each other and was responsible for ensuring that all these aspects were covered in a satisfactory manner. In particular, the panel encouraged the author to attend the 'Young Managers Programme' at the CIT Management School during the summer of the first year, and played an important part in the formulation of the ideas that led to the market survey described in chapter 2.

Initially, the panel consisted of Dr J. Hemp (Academic supervisor), Professor C. New (Management supervisor) and Mr E.H. Higham of the Foxboro company (Industrial supervisor). Later, the panel was joined by Dr R.A. Furness, who took a particular interest in some aspects of the experimental work, the market survey and the implications of the work for flow measurement. Dr J. Hemp had responsibility for the theoretical aspects of the work as well as 'running' the PhD on a day to day basis. Professor C. New had particular responsibility for ensuring that the work gave an appropriate emphasis to the needs of the industrial marketplace. Mr E.H. Higham, on behalf of the Foxboro company who sponsored the work, provided a means for their voice to be heard and had a particularly important role regarding the non-technical aspects of the work.

APPENDIX B: THE MARKET SURVEY

B1 The questionnaire and accompanying letter

The letter which accompanied the questionnaire is given below. It was addressed to the Technical Manager of the organisation concerned unless the author knew of an appropriate individuals details. It is as follows:

I am a Total Technology PhD student in the Department of Fluid Engineering and Instrumentation at the Cranfield Institute of Technology. My PhD project involves a theoretical and experimental investigation of the decay of swirling perturbations of fully developed flow in pipes, together with an assessment of the implications for the industrial flowmeter market. To achieve this I am sending the enclosed questionnaire to a large number of flowmeter users in order to obtain information about current industrial practice, attitudes and understanding. The Foxboro Company (who provided me with your address) are sponsoring my work and have given me some relevant insights from the standpoint of a manufacturer. However, I am particularly interested in your reply as I am primarily concerned with the users' point of view. I should be very pleased if you were able to assist me by completing this questionnaire.

I realise that it may be difficult to lay hands on all the information requested, in which case I should be most grateful for best estimates. In return for your labour I shall be happy to make a summary of my findings available to you, thus giving you information about the practices and opinions of other users; information from individual contributers will, of course, be treated confidentially.

The questionnaire follows.

	Differential Pressure:		Electro-magnetic	Turbine	Vortex-shedding	Ultrasonic:		Positive Displace-ment	Variable Area	Mass	Others
	Orifice	Others				Doppler	Transit Time				

Numbers of installed meters of different types

Over 10 years old											
4-10 years old											
1-3 years old											
Under 1 year old											
Total currently installed											

Your rating of each meter type for (please use 0=Don't know 1=Very low 2=Low 3=Medium 4=High 5=Very high)

Overall cost											
Accuracy											
Reliability											
Stringency of installation requirements											
Ease of maintenance											

Installation lengths you use (meter types you have) and future usage expectations (all types)

Typical number of pipe diameters of straight piping upstream of meter (before bend/valve etc.)											
Expected long term usage of meter type (please use 1=none 2=some 3=a lot)											

How do you determine appropriate installation lengths for your meters?

Please tick box(es)

BSI Standards/ISO Standards	
ANSI Standards/AGA Standards	
Manufacturer's recommendations	
Your own company's code of practice	

Please specify any other methods that you use

Numbers of meters of all types classified according to

(A) fluid being measured

Liquids	Water	
	Hydrocarbons	
	Chemicals	
	Foodstuffs	
	Others	
Gases	Steam	
	Air	
	Hydrocarbons	
	Chemicals	
	Others	
Fluid Mixtures	Liquid/Solid	
	Liquid/Gas	
	Liquid/Liquid	
	Gas/Solid	

(B) purpose of measurement

Continuous flowrate (process control)	
Batch processing	
Custody transfer	
Any others	

(C) line size

½"	
1"	
1½"	
2"	
3"	
4"	
6"	
8"	
Others:	

Additional comments and/or explanations

Your rating of the importance of various influences on your flowmeter selection decisions regarding
(please use 1=Very low 2=Low 3=Medium 4=High 5=Very high)

(A) each purpose for which you measure flow

	Continuous flowrate	Batch processing	Custody transfer
Overall cost			
Accuracy			
Reliability			
Stringency of installation requirements			
Ease of maintenance			
Repeatability			
Rangeability			

(B) your flowmeasurement as a whole

Previous experience of manufacturer/meter type	
Guidance offered by manufacturers	
Recommendations from sources other than maufacturers	

How do you ensure the accuracy of installed meters?

Please tick box(es)

Not at all		
Regular calibration	externally	
	in situ	
Plant/material balance		

Please specify other methods that you use

Describe nature of business at site(s) to which data refer

B2 A tabular presentation of the results

List of Tables

Nomenclature

The following abbreviations for the names of meter types are used throughout this appendix both in the tables and the text:

Differential Pressure (Orifice)	= DP_{or}
Differential Pressure (Other)	= DP_{ot}
Electromagnetic	= EM
Turbine	= TU
Vortex-shedding	= VS
Ultrasonic (doppler)	= US_d
Ultrasonic (transit time)	= US_t
Positive Displacement	= PD
Variable Area	= VA
Mass	= MS
Other	= OT

Table 1: Numbers of meters of different types and their users, (divided up into user size groups)

DP_{or}	DP_{ot}	EM	TU	VS	US_d	US_t	PD	VA	MS	OT	TOTAL

1a: Numbers of meters

1-60	193	28	62	108	6	7	0	100	112	1	4	621
61-600	2030	253	515	475	101	49	3	747	1018	79	8	5278
601+	7393	264	135	703	50	9	5	637	2200	28	15	11439
TOTAL	**9616**	**545**	**712**	**1286**	**157**	**65**	**8**	**1484**	**3300**	**108**	**27**	**17338**

1b: Percentage of meters of different types within size groups

1-60	31	5	10	17	1	1	0	16	18	0	1	100
61-600	38	5	10	9	2	1	0	14	19	2	0	100
601+	66	2	1	6	0	0	0	6	19	0	0	100
TOTAL	**56**	**3**	**4**	**7**	**1**	**0**	**0**	**9**	**19**	**1**	**0**	**100**

1c: Numbers of users (corresponding to the numbers in table 1a)

1-60	19	5	11	16	3	5	0	13	12	1	2	25
61-600	34	18	22	25	12	11	3	28	26	10	3	36
601+	11	7	6	10	7	4	3	9	10	5	1	11
TOTAL	**64**	**30**	**39**	**51**	**22**	**20**	**6**	**50**	**48**	**16**	**6**	**72**

Example

There are 25 users having between 1 and 60 meters. Of these, 19 have some DP_{or} meters. These 19 users have 193 DP_{or} meters between them. These 193 DP_{or} meters form 31% of all the meters owned by the members of this, the smallest size group.

Comments

Generally, larger users have a greater diversity of meter types (3.6 types on average for small users, 6.6 for large).

It is clear that DP_{or} dominate the market, though this is particularly true of the large users. The other users have more of the four 'modern' meter types (EM,TU,VS and US) and also of PD. VA meters are distributed remarkably uniformly across the size groups.

There are a number of meter types which form a small proportion of the total; they are spread thinly amonst a large number of users.

It should be noted that 66% of all the meters in the survey are held by the 11 large users, and 4% by the 25 small users. The range of numbers of meters owned by a single user was from 5 to 1500 meters.

Table 2: Fluids being measured (numbers of meters)

		1-60	61-600	601+	TOTAL	% of GRAND TOTAL
Liquids	Water	186	1087	1349	2622	18
	Hydrocarbons	109	707	3183	3999	28
	Chemicals	56	628	1304	1987	14
	Foodstuffs	16	324	30	370	3
	Other	15	5	0	20	0
TOTAL		381	2751	5866	8998	63
Gases	Steam	53	723	1052	1828	12
	Air	42	453	247	742	5
	Hydrocarbons	59	470	1155	1684	12
	Chemicals	4	122	95	221	2
	Other	32	83	0	115	1
TOTAL		190	1851	2549	4588	32
Fluid Mixtures	Liquid/Solid	2	173	100	275	2
	Liquid/Gas	0	12	192	204	1
	Liquid/Liquid	0	50	135	185	1
	Gas/Solid	0	6	61	67	1
TOTAL		2	241	488	731	5
GRAND TOTAL		573	4843	8903	14319	100

Comments

The major applications are hydrocarbons (40%), water (18%) and steam (12%) together with chemicals (16%) which make up 86% of the Grand Total.

It is important to realise that there is a complicated and indirect relationship between the nature of the business in a plant and the numbers of meters used on different fluids. For example, even in a company which makes food, the majority of flow measurement is carried out in the four areas listed above rather than on foodstuffs.

The larger users have more meters measuring hydrocarbons, while most of the foodstuff measurement is carried out by medium sized operators.

Table 3: Purpose of measurements

3a: Numbers of meters

	1-60	61-600	601+	TOTAL	% of TOTAL
Continuous Flowrate	293	3619	6713	10625	83
Batch Processing	56	477	524	1057	8
Custody Transfer	33	195	499	677	5
Others	145	320	0	465	4
TOTAL	527	4611	7686	12824	100

3b: Numbers of users

Continuous Flowrate	15	31	8	54
Batch Processing	8	16	2	26
Custody Transfer	4	10	5	19
Others	9	10	0	19
TOTAL	21	34	8	63

Comments

Although the vast bulk of measurements were for continuous flowrate/process control purposes, a good number of users (of all sizes) engage in some batch processing and some custody transfer measurements. The 'other' measurements were often for reseach and development purposes and sometimes for flow alarms (using US_d meters). This just means that there are many users employing a few meters on custody transfer duty.

Table 4: Line sizes (numbers of meters)

	½"	1"	1½"	2"	3"	4"	6"	8"	Other	TOTAL
1-60	43	60	42	84	86	37	25	39	38	454
61-600	255	507	411	681	397	395	266	159	101	3172
601+	150	377	272	846	1166	1191	1602	628	691	6923
TOTAL	**488**	**944**	**725**	**1611**	**1694**	**1623**	**1893**	**826**	**830**	**10549**

Comments

Fewer users were able to complete this table than were able to give details of fluids being measured. There is a marked tendency for smaller users to have smaller line sizes. Overall, however, the distribution is uniform between line sizes of 2" and 6", falling away at each end. The largest line size recorded was 60".

Table 5: History of meter usage
(% of meters in use of a given age in years)

	DP_{or}	DP_{ot}	EM	TU	VS	US_d	US_t	PD	VA	MS	TOTAL	Meter
>10	61	4	1	8	0	0	0	8	18	0	100	9098
4-10	57	2	5	6	1	0	0	8	21	0	100	4651
1-3	43	3	9	7	4	1	0	8	23	2	100	2014
<1	45	3	8	7	6	0	0	9	20	2	100	860
TOTAL	57	4	4	7	1	0	0	8	19	0	100	16623

Comments

Age is measured in years; for example the number of DP_{or} meters in the survey as a whole which are over 10 years old is 61% of 9098.

The information above is that for the survey as a whole; differences between the size groups are that TU meters are rising in all but the largest users and that smaller users tend to lead the way in changes of usage patterns.

It is clear that the basic trend has been one of a gradual reduction in the use of DP_{or} types in favour of EM and VS types, and more lately MS types also. There has been an increase in the use of US types, albeit a very small one.

At present, 55% of the meters in use are over 10 years old, 28% between 4 and 10 years, 12% between 1 and 3 years and 5% under 1 year. It is roughly true to say that in each of the last ten years 4% of the meters presently in use were acquired. Extrapolating backwards would suggest that there are meters in service which are over 25 years old.

Table 6: Future usage expectations

The ratings obtained from the questionnaire (1 = none, 2 = some, 3 = a lot) were averaged to give each meter type an overall position on a scale from 1 to 3. The following key is used:

DP_{or} = 0, DP_{ot} = 1, EM = 2, TU = 3, VS = 4,
US_d = 5, US_t = 6, PD = 7, VA = 8, MS = 9.

	LEAST				MOST
	1	1.5	2	2.5	3
1-60	65941	2	78	3	0
61-600	6 59	1 4	237	8	0
601+	65 9	13	2	784	0
TOTAL	6 59	1 4	2378		0

Comments

In cases where users only filled in numbers for the types of meters they already had, the blank entries were treated as '1's. The total gives each user equal weight.

Overall, it is clear that the DP_{or} meter will continue to be dominant although the use of VS and PD meters will increase. There is evidence of wider usage of both VS and EM meters when the positions above are compared with those in table 1. The historical trend towards EM and VS types can thus be detected in the future intentions shown above, albeit a slow one. MS meters and VS meters will continue to be minority usage meters for some time. Since at present both VS and MS meters have the same proportion of the market in this survey, we may expect VS to improve their relative position significantly in the future. It is interesting to notice that the order of the different meter types here is very similar to that in shown in table 1 for the present usage.

Table 7: Users' opinions about meter types

The ratings obtained from the questionnaire (from 1 to 5) were averaged, the mean adjusted (by subtracting 3) to be equal to zero, and the sign changed (if necessary) so that a positive value is 'good' in all cases. For example, if the average value for the cost was 4, then adjusting the mean gives 1, and changing the sense gives -1 since a low cost is 'good'. The same key is used as in table 6. The totals give each user equal weight, as before.

		WORST -2 -1 0 1 2 BEST
Cost	1-60	1 247 03 5 8
	61-600	9 2 746135 0 8
	601+	9 2 7 56 3 1 4 0 8
TOTAL		9 2 761435 0 8
Accuracy	1-60	85 34 17 02
	61-600	5 6 8 0 413 72 9
	601+	5 8 6 0 1 4 9 32 7
TOTAL		56 8 0 41 37 29
Reliability	1-60	4 538072 1
	61-600	6 493 71 80 2
	601+	5 6 3 98 7 2 10 4
TOTAL		6 5 493 78 01 2
Installation Requirements	1-60	10 5 7 24 3 8
	61-600	9 6 04 1 53 2 78
	601+	346012 9 5 87
TOTAL		960 14 532 7 8
Maintenance	1-60	42573 0 8 1
	61-600	69 473 12580
	601+	93 7 5 46 2 10 8
TOTAL		96 734 25 081

Comments

All the data used in this table refer to views based on experience. VA meters generally score highly since they are entirely satisfactory unless some degree of accuracy is needed. It is usual for some degree of accuracy to be desired, and so other types are normally used. The four types regarded as most accurate (EM, PD, DP and TU) are all fairly accurate and are reasonably established in the marketplace. Since choosing between them will depend on the precise nature of the task there is considerable competition between them. VS meters are also fairly accurate and are on the edge of this area; as we have already seen we expect VS meters to be more widely used in future. The MS meter is regarded as very expensive; it is not a meter of wide, general application although it most certainly will have an increasing role as it gains acceptance. The US meters get a very poor showing, mainly due to the very small number of users in the survey all having found theirs to be unreliable.

Table 8: Methods used to ensure meter accuracy (numbers of users)

		1-60	61-600	601+	TOTAL
None		1	7	0	8
Regular calibration	In situ	11	17	7	35
	External	19	25	8	52
Plant/Material Balance		14	23	8	45
TOTAL		25	36	11	72

Comments

It is not surprising that so many users choose an indirect method. There are a good many calibrations recorded however, although it should be noted that when a user says that he uses a particular method this reveals nothing about the proportion of his meters tested in this way or how often it is done.

Table 9: Users' opinions about the selection of meters

The ratings given on the questionnaires (from 1 to 5) were averaged, and had 3 subtracted from them in order to make zero the 'medium' point. The totals give users equal weight, as before. A key is used in the same manner as before. It is:

Cost = 0, Accuracy = 1, Reliability = 2, Installation = 3, Maintenance = 4, Repeatability = 5, Rangeability = 6

a). For each measurement purpose

		LEAST IMPORTANT → MOST IMPORTANT
		-1 0 1 2
Continuous Flowrate	1-60	3 06 4 1 5 2
	61-600	6 30 1 4 5 2
	601+	4 3 601 5 2
TOTAL		3 60 4 1 5 2
Batch processing	1-60	3 0 6 4 1 2 5
	61-600	6 0 3 4 1 2 5
	601+	3 0 6 4 2 15
TOTAL		63 0 4 1 2 5
Custody transfer	1-60	3 06 4 2 15
	61-600	6 0 34 2 1 5
	601+	0 4 6 3 25 1
TOTAL		0 6 34 2 15

Comments

Regardless of the purpose of measurement, accuracy, repeatability and reliability would seem to be the most important attributes of a flowmeter. The importance of cost is on a level with that of rangeability or installation and all these are very considerably lower in importance than the top three. It is remarkable that cost is not regarded as of more importance than it is for continuous flowrate. It is also questionnable whether accuracy is actually as important as it seems to be for this usage, although repeatability certainly is.

b). Overall (average values minus 3)

	1-60	61-600	601+	TOTAL
Previous experience	1.38	0.97	1.10	1.11
Manufacturer's Guidance	0.38	0.17	-0.20	0.16
Guidance from elsewhere	0.53	0.08	-0.30	0.13

Comments

It is not surprising that previous experience is so important, or that larger users are more independent than smaller ones.

Table 10: An evaluation of meter types

An attempt has been made here to combine some of the information in Tables 7 and 9a in order to evaluate the various meter types. This is a process fraught with danger owing to the variable quality and significance of the data, but which sheds some light upon the situation. We add together the rating for each meter type for cost, accuracy and reliability for each measurement purpose, weighting them according to the perceived importance of these characteristics for that purpose. We use the same key as for Table 6.

		WORST -12 -6 0 6 BEST 12
Continuous Flowrate	1-60	4 371 802
	61-600	6 5 9 43 17028
	601+	5 6 98 3 2107 4
TOTAL		6 5 9 4 317802
Batch processing	1-60	4 5 37 1802
	61-600	6 5 9 43 1 078 2
	601+	5 6 89 3102 74
TOTAL		6 5 9 4 381702
Custody transfer	1-60	4 5 371 8 02
	61-600	6 5 943 1087 2
	601+	5 6 8 9 0 31 247
TOTAL		6 5 94 83107 2

Comments

There is clearly a wide disparity between the views of the different size groups regarding the VS meter and the VA meter. Beyond this it is possible to say that EM, PD, DP_{or} and TU meters seem to be generally favoured and that US meters are very unpopular.

Table 11: Installation lengths used (diameters)

	DP_{or}	DP_{ot}	EM	TU	VS	US_d	US_t	PD	VA	MS
a): Mean values										
1-60	20	10	10	10	9	6	-	8	3	-
61-600	14	13	8	8	13	10	8	4	4	3
601+	14	12	9	13	18	17	10	3	8	8
TOTAL	16	13	9	10	14	10	9	5	4	4
b). Extremes used										
1-60	1-69	1-30	0-30	0-40	8-10	1-10	-	0-30	0-10	-
61-600	2-40	5-30	2-20	2-20	5-25	3-20	5-10	0-10	0-10	0-6
601+	5-40	10-20	0-25	5-20	10-20	0-40	10-10	0-5	0-20	1-15
TOTAL	1-69	1-30	0-30	0-40	5-25	0-40	5-10	0-30	0-20	0-15

Table 12: Methods used to determine installation lengths (number of users)

	0-60	61-600	601+	TOTAL
BSI/ISO Standards	13	21	6	40
AGA/ANSI Standards	1	3	4	8
Manufacturers' Recommendations	19	34	6	59
Companies own code of practice	6	10	3	19

Comments (for tables 11 and 12)

The general attitude is summed up by one respondent who said that his organisation always use 10 diameters (more if possible) because it will normally suffice and is a simple rule which does not confuse personnel! Frequently, the installation precludes the use of even as many as 10 diameters. Very few users actually follow the standards (for orifice-plate meters); those doing so are normally engaging in custody transfer. The manufacturers' recommendations are clearly of importance in governing practice - they rarely ask for more than the upper ends of the ranges found in the survey. However, most installation lengths in use are well below that, and are (in a sense) unsatisfactory. This is especially true of DP, TU, VS, and US meters. PD and VA meters not needing many straight upstream diameters, are not generally being given them. A few users recognised the importance of removing swirling motions, and would expect to use the lengths given above after having done this.

APPENDIX C: THE RESULTS OF THE EXPERIMENTAL MEASUREMENTS

List of Tables

C1 The velocity measurements

All the traverse positions given use the convention that the negative direction is towards the outside of the test area. This means that the positive direction is from left to right as an observer looks downstream. They are corrected for the effects of refraction as appropriate. The zero position is on the vertical diameter both for the case of measurements on the horizontal diameter and those on the offset chords. In both cases the distances given have been non-dimensionalised using the pipe radius. The distances corresponding to the pipe wall are also given.

All velocity and turbulence intensity measurements are given in m/s and are corrected for the effects of refraction where that is appropriate. The turbulence intensity as given here is the root mean square of the fluctuations in the flow direction under consideration. The sign of the tangential velocity measurements as given here is such that as an observer looks downstream, a positive sign for the tangential velocity on the left hand side of the vertical diameter means that the tangential flow is downwards there. It can be seen

that this refers to a rotation in the anti-clockwise direction, the same direction as that of a left handed screw thread.

Table 1: Velocity measurements on section 0 at Re = 4.13×10^5

Horizontal diameter:

Traverse Position	Axial Velocity	Turbulence Intensity
-1.00	Pipe wall	
-0.86	4.98	0.35
-0.72	5.46	0.27
-0.59	5.64	0.27
-0.45	5.80	0.24
-0.31	6.01	0.20
-0.17	6.05	0.21
-0.03	6.05	0.21
0.10	6.04	0.19
0.38	5.93	0.25
0.71	5.60	0.27
0.93	4.90	0.39
1.00	Pipe wall	

Traverse Position	Tangengential Velocity	Turbulence Intensity
-1.00	Pipe wall	
-0.94	-0.02	0.21
-0.72	-0.06	0.22
0.00	-0.00	0.12
0.72	0.03	0.20
0.94	0.00	0.21
1.00	Pipe wall	

Vertical Diameter:

Height above horizontal diameter	-21mm	26mm
Non-dimensional radius	-0.55	0.67
Axial Velocity	5.74	5.60
Turbulent Intensity	0.27	0.27

Table 2: Axial Velocity measurements on Section 1

Horizontal diameter:

	Re = 4.13×10^5		Re = 1.65×10^5	
Traverse Position	Axial Velocity	Turbulence Intensity	Axial Velocity	Turbulence Intensity
-1.00	Pipe wall			
-0.86	5.58	0.29	2.22	0.15
-0.72	5.65	0.29	2.27	0.15
-0.58	5.66	0.28	2.28	0.12
-0.44	5.68	0.28	2.28	0.12
-0.30	5.63	0.26	2.26	0.12
-0.16	5.68	0.24	2.29	0.13
-0.02	5.70	0.22	2.31	0.11
0.12	5.72	0.23	2.36	0.11
0.26	5.76	0.23	2.37	0.12
0.40	5.83	0.23	2.40	0.10
0.54	5.89	0.23	2.42	0.09
0.68	5.94	0.25	2.44	0.09
0.82	5.93	0.24	2.39	0.10
0.96	5.55	0.26	2.18	0.13
1.00	Pipe wall			

Horizontal chord 21.5mm above horizontal diameter:

	Re = 4.13×10^5		Re = 1.65×10^5	
Traverse Position	Axial Velocity	Turbulence Intensity	Axial Velocity	Turbulence Intensity
-0.82	Pipe wall			
-0.68	5.84	0.37	2.43	0.13
-0.54	6.10	0.34	2.45	0.13
-0.40	6.14	0.33	2.49	0.12
-0.26	6.14	0.31	2.47	0.12
-0.12	6.17	0.30	2.43	0.11
0.02	6.11	0.28	2.47	0.10
0.16	6.04	0.30	2.45	0.12
0.30	6.04	0.29	2.43	0.10
0.44	5.98	0.31	2.39	0.11
0.58	5.90	0.29	2.36	0.12
0.72	5.53	0.32	2.15	0.16
0.82	Pipe wall			

Horizontal chord 20.5mm below horizontal diameter:

	Re = 4.13×10^5		Re = 1.65×10^5	
Traverse Position	Axial Velocity	Turbulence Intensity	Axial Velocity	Turbulence Intensity
-0.82	Pipe wall			
-0.68	5.36	0.28	1.98	0.14
-0.54	5.37	0.32	2.06	0.14
-0.40	5.51	0.33	2.13	0.14
-0.26	5.51	0.31	2.20	0.17
-0.12	5.58	0.33	2.27	0.16
0.02	5.78	0.25	2.33	0.10
0.16	5.82	0.24	2.35	0.12
0.30	5.82	0.23	2.38	0.10
0.44	5.83	0.23	2.39	0.10
0.58	5.83	0.24	2.41	0.10
0.72	5.57	0.25	2.11	0.10
0.82	Pipe wall			

Table 3: Tangential Velocity measurements on Section 1

Horizontal diameter:

	$Re = 4.13x10^5$		$Re = 1.65x10^5$	
Traverse Position	Tangengential Velocity	Turbulence Intensity	Tangential Velocity	Turbulence Intensity
-1.00	Pipe wall			
-0.93	0.93	0.28	0.38	0.14
-0.85	0.82	0.27	0.34	0.12
-0.71	0.58	0.25	0.24	0.12
-0.56	0.33	0.26	0.15	0.13
-0.41	0.16	0.26	0.06	0.11
-0.26	0.07	0.27	0.05	0.10
-0.11	-0.03	0.29	0.02	0.11
0.04	-0.05	0.25	0.00	0.10
0.19	-0.08	0.28	0.00	0.09
0.34	-0.13	0.26	-0.01	0.08
0.49	-0.24	0.24	-0.02	0.08
0.64	-0.41	0.21	-0.13	0.09
0.79	-0.56	0.21	-0.19	0.09
0.93	-0.65	0.23	-0.16	0.09
1.00	Pipe wall			

Table 4: Axial Velocity measurements on section 2

Horizontal diameter:

	$Re = 4.13x10^5$		$Re = 1.65x10^5$	
Traverse Position	Axial Velocity	Turbulence Intensity	Axial Velocity	Turbulence Intensity
-1.00	Pipe wall			
-0.86	5.00	0.37	1.95	0.20
-0.72	5.46	0.32	2.16	0.17
-0.59	5.56	0.30	2.23	0.12
-0.45	5.71	0.29	2.32	0.11
-0.31	5.83	0.28	2.41	0.10
-0.17	5.88	0.22	2.39	0.09
-0.03	5.87	0.24	2.42	0.08
0.10	5.93	0.21	2.40	0.09
0.24	5.94	0.21	2.42	0.07
0.38	5.91	0.20	2.41	0.07
0.52	5.87	0.22	2.38	0.09
0.66	5.76	0.23	2.18	0.15
0.79	5.47	0.28	2.13	0.17
0.93	4.78	0.42	1.88	0.17
1.00	Pipe wall			

Horizontal chord 21.5mm above horizontal diameter:

	Re = 4.13×10^5		Re = 1.65×10^5	
Traverse Position	Axial Velocity	Turbulence Intensity	Axial Velocity	Turbulence Intensity
-0.83	Pipe wall			
-0.69	5.12	0.37	1.98	0.14
-0.55	5.34	0.33	2.12	0.14
-0.41	5.53	0.28	2.22	0.14
-0.28	5.64	0.26	2.25	0.13
-0.14	5.70	0.24	2.30	0.10
0.00	5.72	0.23	2.31	0.14
0.14	5.72	0.23	2.34	0.11
0.28	5.66	0.24	2.28	0.12
0.41	5.57	0.26	2.23	0.13
0.55	5.43	0.25	2.11	0.14
0.69	4.92	0.40	1.98	0.18
0.83	Pipe wall			

Horizontal chord 20.5mm below horizontal diameter:

	$Re = 4.13x10^5$		$Re = 1.65x10^5$	
Traverse Position	Axial Velocity	Turbulence Intensity	Axial Velocity	Turbulence Intensity
-0.83	Pipe wall			
-0.69	4.79	0.40	1.93	0.13
-0.55	5.23	0.34	2.06	0.12
-0.41	5.46	0.33	2.19	0.17
-0.28	5.60	0.32	2.32	0.15
-0.14	5.59	0.30	2.32	0.14
0.00	5.71	0.30	2.35	0.12
0.14	5.70	0.26	2.37	0.11
0.28	5.73	0.29	2.36	0.10
0.41	5.63	0.31	2.32	0.11
0.55	5.43	0.32	2.16	0.17
0.69	5.20	0.38	2.03	0.16
0.83	Pipe wall			

Table 5: Tangential Velocity measurements on Section 2

Horizontal diameter:

	$Re = 4.13x10^5$		$Re = 1.65x10^5$	
Traverse Position	Tangengential Velocity	Turbulence Intensity	Tangential Velocity	Turbulence Intensity
-1.00	Pipe wall			
-0.93	0.42	0.23	0.13	0.10
-0.85	0.36	0.22	0.12	0.08
-0.71	0.29	0.20	0.10	0.09
-0.56	0.20	0.15	0.07	0.08
-0.42	0.15	0.15	0.05	0.07
-0.27	0.08	0.11	0.03	0.06
-0.13	0.03	0.10	0.02	0.06
0.02	0.00	0.09	0.01	0.05
0.16	-0.08	0.10	-0.01	0.05
0.31	-0.18	0.11	-0.03	0.05
0.45	-0.25	0.11	-0.03	0.06
0.60	-0.30	0.12	-0.06	0.06
0.75	-0.37	0.13	-0.08	0.07
0.89	-0.39	0.18	-0.11	0.10
1.00	Pipe wall			

Table 6: Axial Velocity measurements on section 3

Horizontal diameter:

	Re = 4.13×10^5		Re = 1.65×10^5	
Traverse Position	Axial Velocity	Turbulence Intensity	Axial Velocity	Turbulence Intensity
-1.00	Pipe wall			
-0.86	5.11	0.35	1.96	0.17
-0.72	5.63	0.30	2.25	0.13
-0.59	5.82	0.31	2.40	0.11
-0.45	6.06	0.28	2.50	0.09
-0.31	6.27	0.18	2.54	0.08
-0.17	6.22	0.18	2.54	0.07
-0.03	6.26	0.19	2.52	0.06
0.10	6.25	0.19	2.52	0.07
0.24	6.24	0.20	2.53	0.09
0.38	6.16	0.22	2.50	0.10
0.52	5.91	0.29	2.40	0.11
0.66	5.77	0.29	2.37	0.10
0.79	5.34	0.36	2.12	0.14
0.93	4.68	0.38	1.88	0.18
1.00	Pipe wall			

Table 7: Tangential Velocity measurements on Section 3

Horizontal diameter:

	$Re = 4.13x10^5$		$Re = 1.65x10^5$	
Traverse Position	Tangengential Velocity	Turbulence Intensity	Tangential Velocity	Turbulence Intensity
-1.00	Pipe wall			
-0.93	0.25	0.19	0.08	0.09
-0.85	0.22	0.17	0.07	0.10
-0.71	0.19	0.17	0.07	0.08
-0.56	0.15	0.17	0.04	0.06
-0.42	0.10	0.13	0.02	0.06
-0.27	0.06	0.11	0.01	0.06
-0.13	0.03	0.11	0.01	0.06
0.02	0.00	0.12	0.00	0.05
0.16	-0.03	0.13	0.00	0.05
0.31	-0.07	0.14	-0.01	0.05
0.45	-0.11	0.15	-0.02	0.06
0.60	-0.14	0.17	-0.02	0.06
0.75	-0.19	0.18	-0.04	0.07
0.89	-0.25	0.18	-0.06	0.09
1.00	Pipe wall			

Table 8: Axial Velocity measurements on section 4

Horizontal diameter:

	$Re = 4.13x10^5$		$Re = 1.65x10^5$	
Traverse Position	Axial Velocity	Turbulence Intensity	Axial Velocity	Turbulence Intensity
-1.00	Pipe wall			
-0.86	4.93	0.38	1.93	0.14
-0.72	5.40	0.31	2.15	0.13
-0.59	5.70	0.26	2.29	0.14
-0.45	5.93	0.27	2.41	0.10
-0.31	6.08	0.23	2.45	0.08
-0.17	6.19	0.20	2.53	0.07
-0.03	6.23	0.18	2.52	0.08
0.10	6.21	0.18	2.51	0.07
0.24	6.18	0.19	2.53	0.08
0.38	6.07	0.23	2.45	0.09
0.52	5.86	0.25	2.38	0.10
0.66	5.59	0.27	2.32	0.11
0.79	5.36	0.31	2.18	0.13
0.93	4.83	0.35	1.86	0.17
1.00	Pipe wall			

Table 9: Tangential Velocity measurements on Section 4

Horizontal diameter:

	$Re = 4.13x10^5$		$Re = 1.65x10^5$	
Traverse Position	Tangengential Velocity	Turbulence Intensity	Tangential Velocity	Turbulence Intensity
-1.00	Pipe wall			
-0.93	0.13	0.15	0.05	0.07
-0.85	0.11	0.15	0.05	0.07
-0.71	0.09	0.14	0.04	0.07
-0.56	0.07	0.12	0.03	0.06
-0.42	0.05	0.11	0.02	0.06
-0.27	0.03	0.11	0.01	0.06
-0.13	0.00	0.11	0.00	0.05
0.02	-0.01	0.10	0.00	0.05
0.16	-0.02	0.11	0.00	0.05
0.31	-0.03	0.13	-0.01	0.05
0.45	-0.03	0.12	-0.01	0.06
0.60	-0.06	0.14	-0.01	0.06
0.75	-0.10	0.17	-0.01	0.06
0.89	-0.13	0.20	-0.03	0.06
1.00	Pipe wall			

Table 10: Axial Velocity measurements on section 5

Horizontal diameter:

	$Re = 4.13x10^5$		$Re = 1.65x10^5$	
Traverse Position	Axial Velocity	Turbulence Intensity	Axial Velocity	Turbulence Intensity
-1.00	Pipe wall			
-0.86	4.93	0.35	1.89	0.12
-0.72	5.31	0.27	2.13	0.15
-0.59	5.60	0.24	2.27	0.12
-0.45	5.80	0.23	2.40	0.09
-0.31	6.01	0.23	2.45	0.08
-0.17	6.17	0.20	2.48	0.08
-0.03	6.22	0.18	2.51	0.07
0.10	6.22	0.19	2.51	0.07
0.24	6.17	0.19	2.48	0.09
0.38	6.04	0.20	2.43	0.09
0.52	5.78	0.27	2.36	0.11
0.66	5.61	0.27	2.22	0.12
0.79	5.33	0.28	2.12	0.16
0.93	4.67	0.38	1.83	0.17
1.00	Pipe wall			

Table 11: Measurements on section 2, as a check, at Re = 4.13×10^5

Axial Velocity on the horizontal diameter:

Traverse Position	Axial Velocity	Turbulence Intensity
-1.00	Pipe wall	
-0.86	5.04	0.38
-0.72	5.47	0.30
-0.59	5.58	0.25
-0.31	5.71	0.24
-0.03	5.86	0.23
0.24	5.94	0.19
0.52	5.88	0.20
0.79	5.47	0.31
0.93	4.95	0.36
1.00	Pipe wall	

Tangential Velocity on the horizontal diameter:

Traverse Position	Tangential Velocity	Turbulence Intensity
-1.00	Pipe wall	
-0.93	0.43	0.24
0.02	-0.01	0.09
0.89	-0.41	0.20
1.00	Pipe wall	

C2 The pressure measurements

The axial positions of the pressure measurements are specified by their distance from the start of the first test section (measured in metres) and by whether the higher or lower tapping was being used. At each of the two Reynolds numbers the differential pressures are given relative to the pressure at the higher tapping furthest downstream. All measurements are given in metres of water. Measurements were made by two different techniques; a differential pressure cell and a mercury manometer.

Table 12: Pressure measurements (differential pressure cell)

Measurements were made using the differential pressure cell with an electronic filter. The zero error of 0.004bar has been removed, and the results rescaled by dividing them by 9.807 in order to convert the results from bar to metres of water.

	$Re = 4.13 \times 10^5$		$Re = 1.65 \times 10^5$	
Axial Distance	Higher Tapping	Lower Tapping	Higher Tapping	Lower Tapping
0.110	2.55	2.52	0.47	0.46
1.110	2.27	2.16	0.41	0.40
2.123	1.87	1.78	0.35	0.34
3.123	1.61	1.64	0.30	0.30
4.133	1.31	1.27	0.24	0.24
5.133	1.07	1.10	0.19	0.20
6.143	0.72	0.84	0.13	0.15
7.143	0.60	0.59	0.10	0.10
8.153	0.32	0.34	0.05	0.06
9.153	0.00	0.06	0.00	0.01

Table 13: Pressure measurements (mercury manometer)

Measurements were made with the mercury manometer (which was calibrated so as to measure in metres of water) at Re = 4.13×10^5.

Axial Distance	Higher Tapping	Lower Tapping
0.110	2.54	2.51
1.110	2.26	2.14
3.123	1.60	1.63
5.133	1.05	1.08
7.143	0.60	0.57
9.153	0.00	0.03

HIGHAM (Numbers 1975-80)

FURNESS (Sales Value 1984)

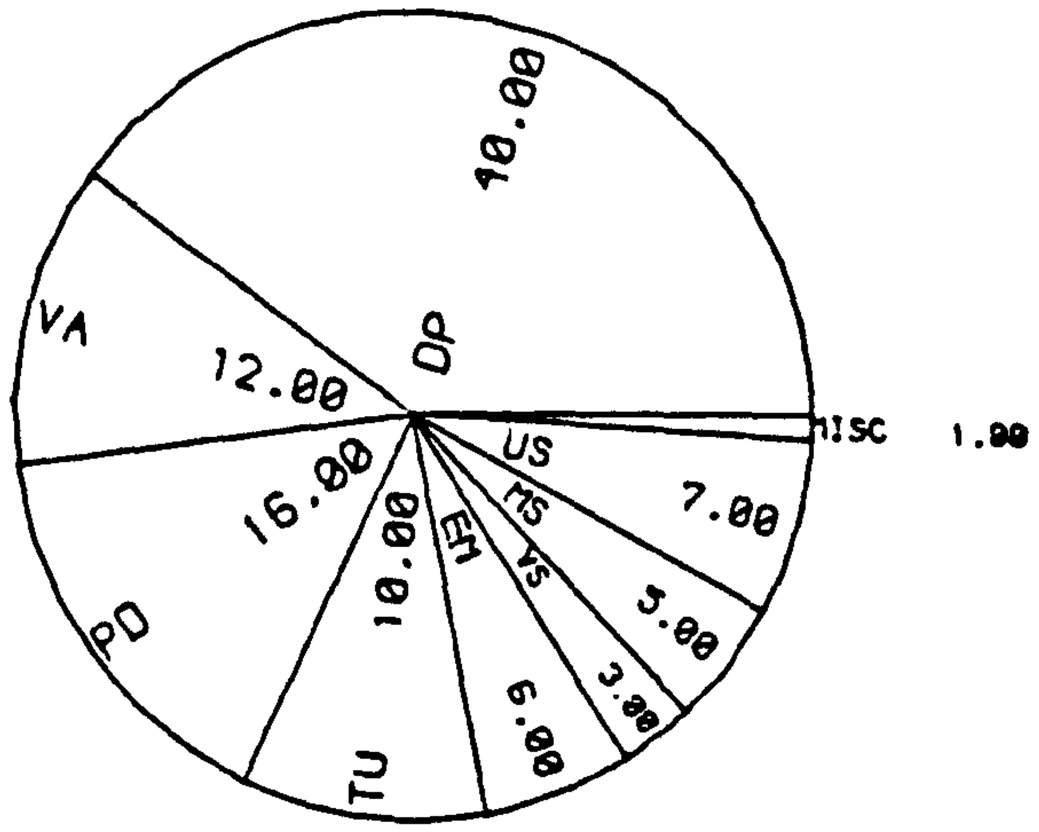

HALSEY 1985

Numbers in Use

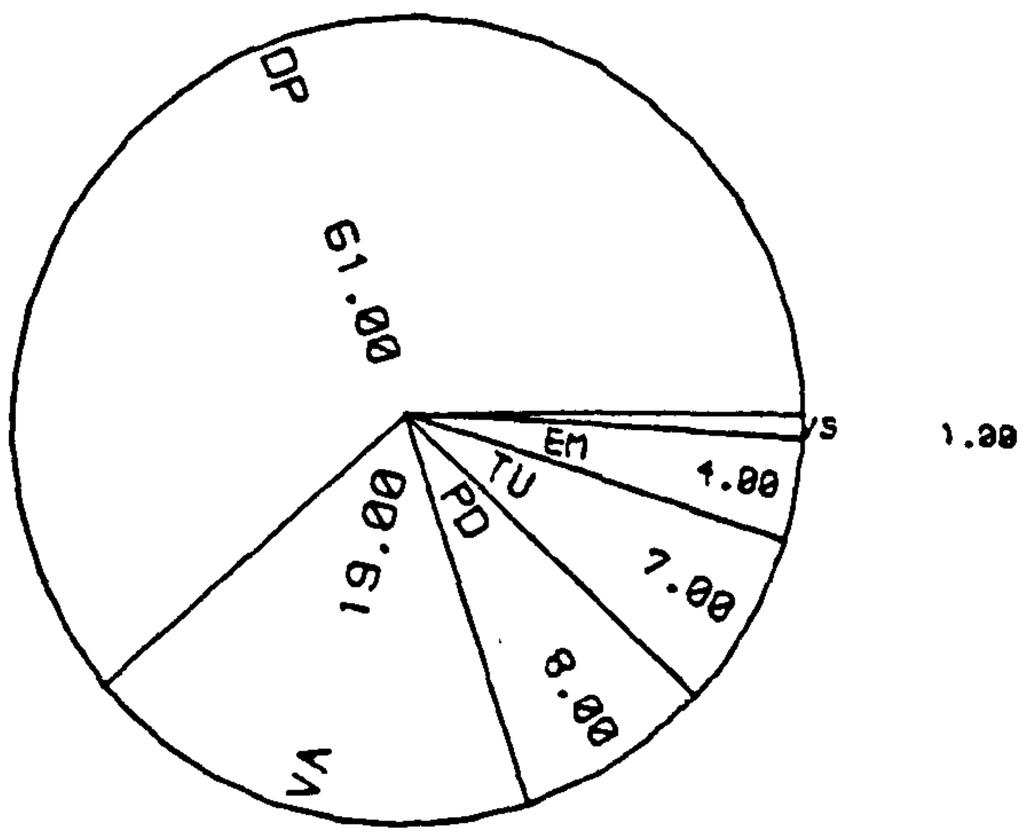

Sales Numbers

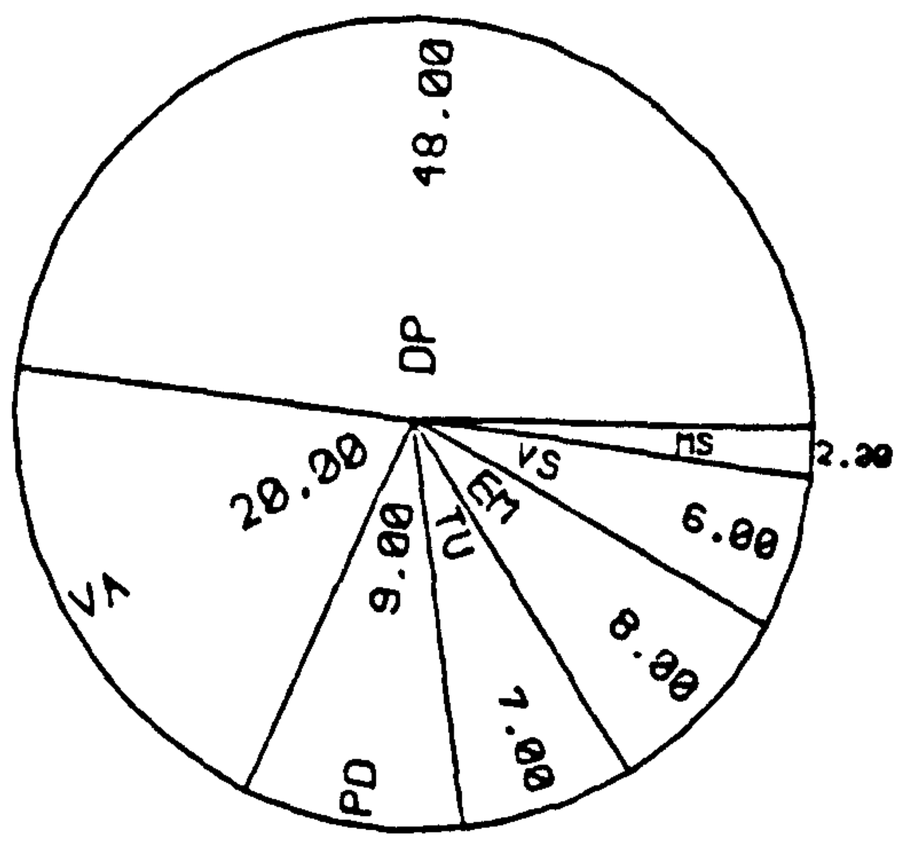

Figure 2.1: Relative proportions of different flowmeters used in industry

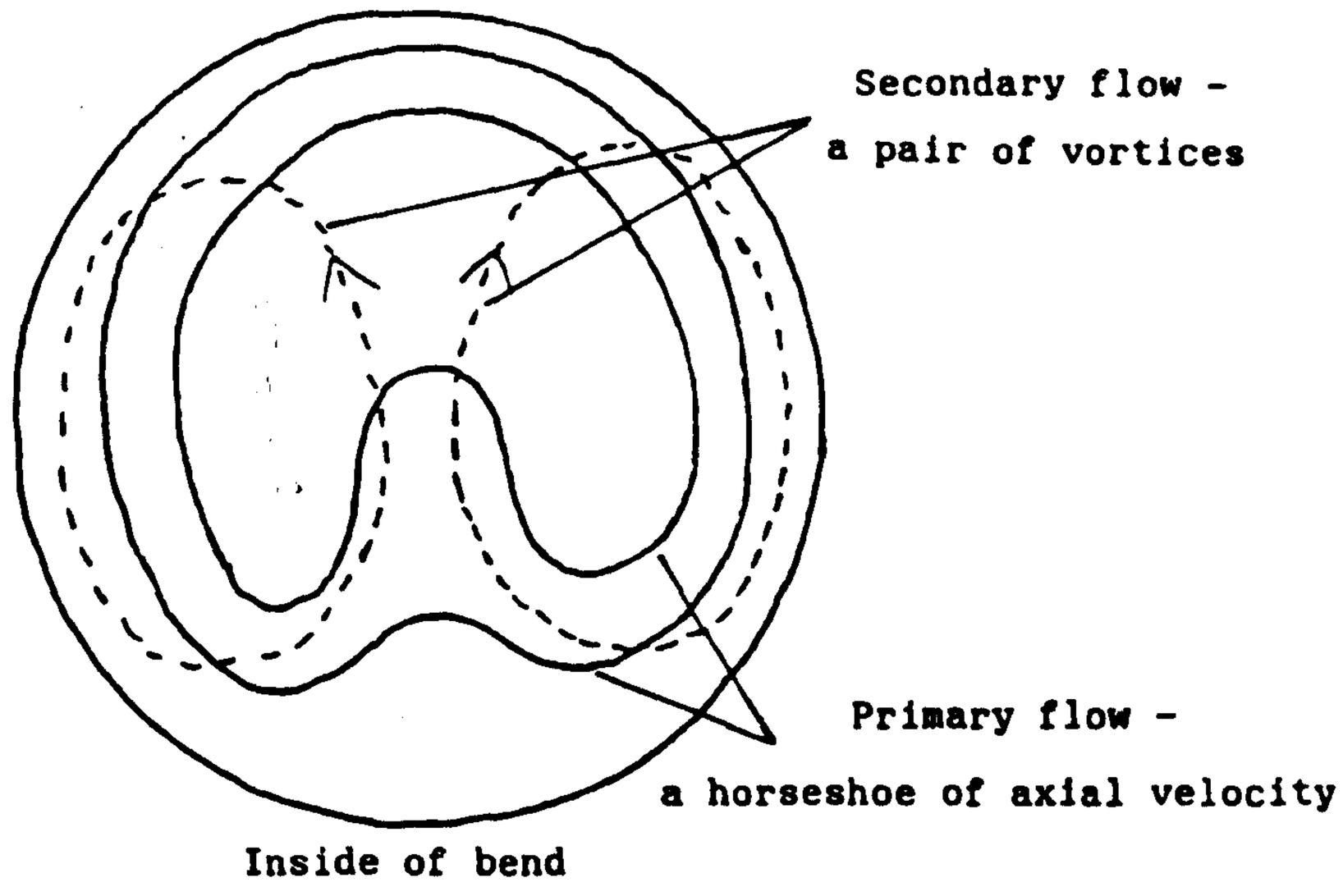

Figure 3.1: Motion of fluid after a single right-angle bend in a pipe

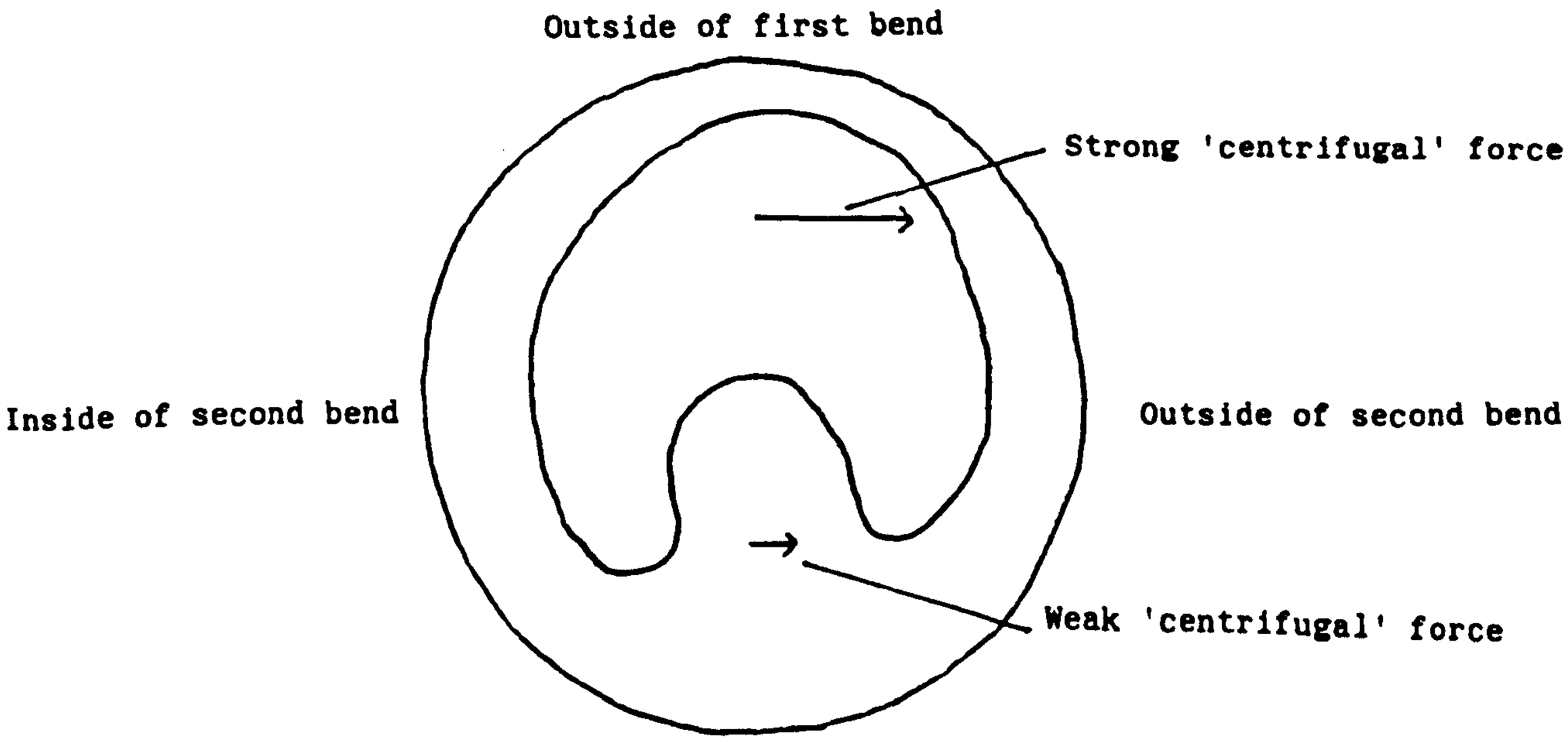

Figure 3.2: The effect of a second bend, at right-angles to the first

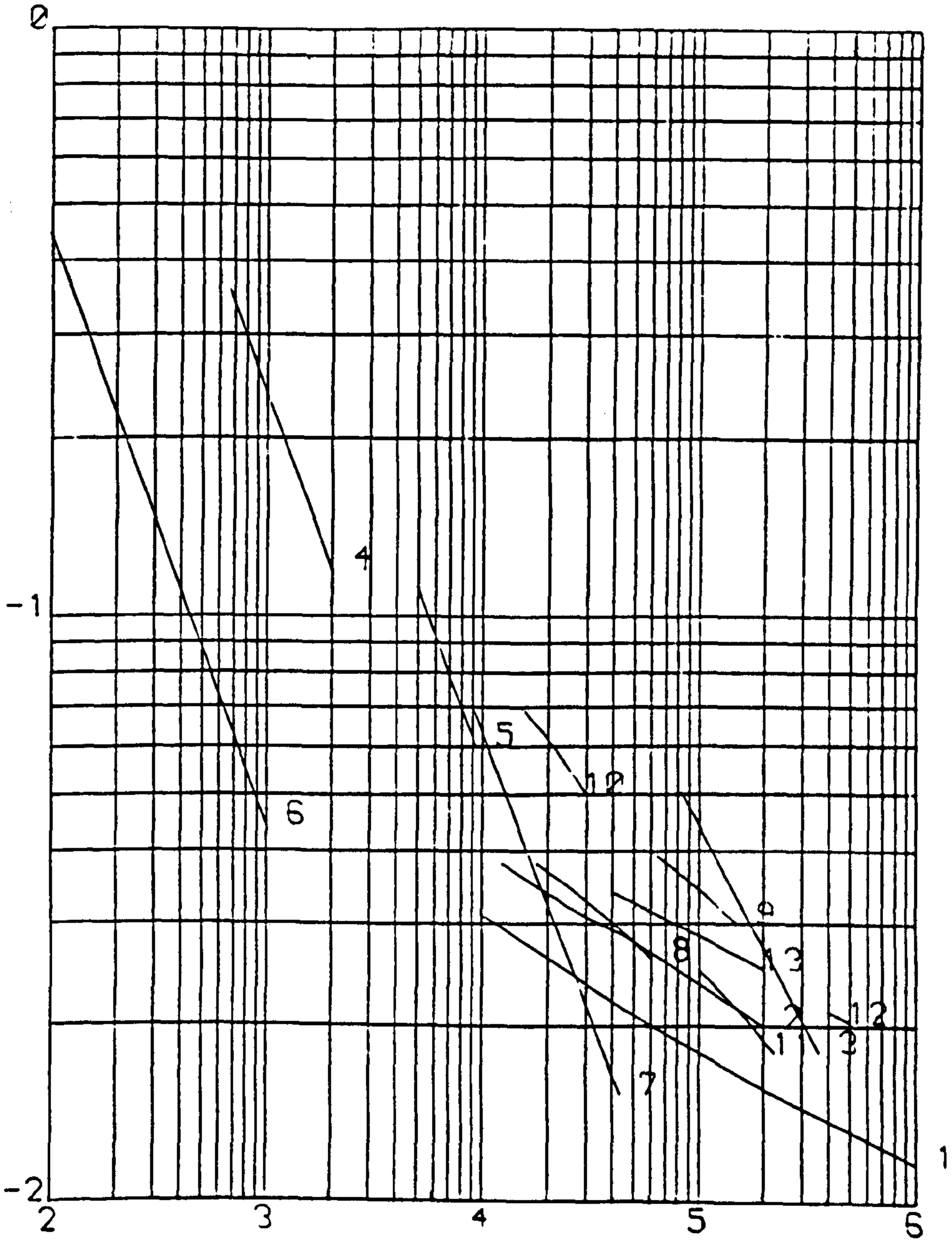

Figure 3.3: Relationships between the reynolds number and the decay rate of swirl, obtained from many sources

Key overleaf

Key for figure 3.3.

Line number and Author	Method of swirl generation and measurement	Formulae for λ and notes	
1 Rapier (1981)	Theory	4f	Smooth pipe
2 Baker and Sayre (1974)	Vanes, Swirl meter		
3 Wolf, Lavan and Fejer (1969)	Radial entry vanes, point velocities	$140/Re^{0.7}$	High swirl
4 Ito, Ogawa and & Kuroda (1979) 5	Tangential entry tubes at blanked off end of pipe, point velocities	240/Re	Laminar
		560/Re	Turbulent
6 Talbot (1954)	Theory	44.4/Re	Laminar
7 Sparrow and Chaboki (1984)	Swirl chamber, wall swirl angle	$483/Re^{0.97}$	Special apparatus
8 Krieth and Sonju (1965)	Twisted tapes, swirl meter		
9 Youssef (1966)	Vanes, point velocities		High swirl
10 Nissan and Bresan (1961)	Tangential entry tubes at blanked off end of pipe, point velocities		High swirl

Line number and Author	Method of swirl generation and measurement	Notes
11 Janik and Padmanabhan (1980)	Vanes, swirl meter	Measurements made close to the swirl generator
12 Nystrom and Padmanabhan (1985)	Double bend, swirl meter	40 diameter inlet section, smooth pipe
13 Mottram and Rawat (1986)	Double bend, point velocities	Double bend preceded by a Borda inlet, rough pipe

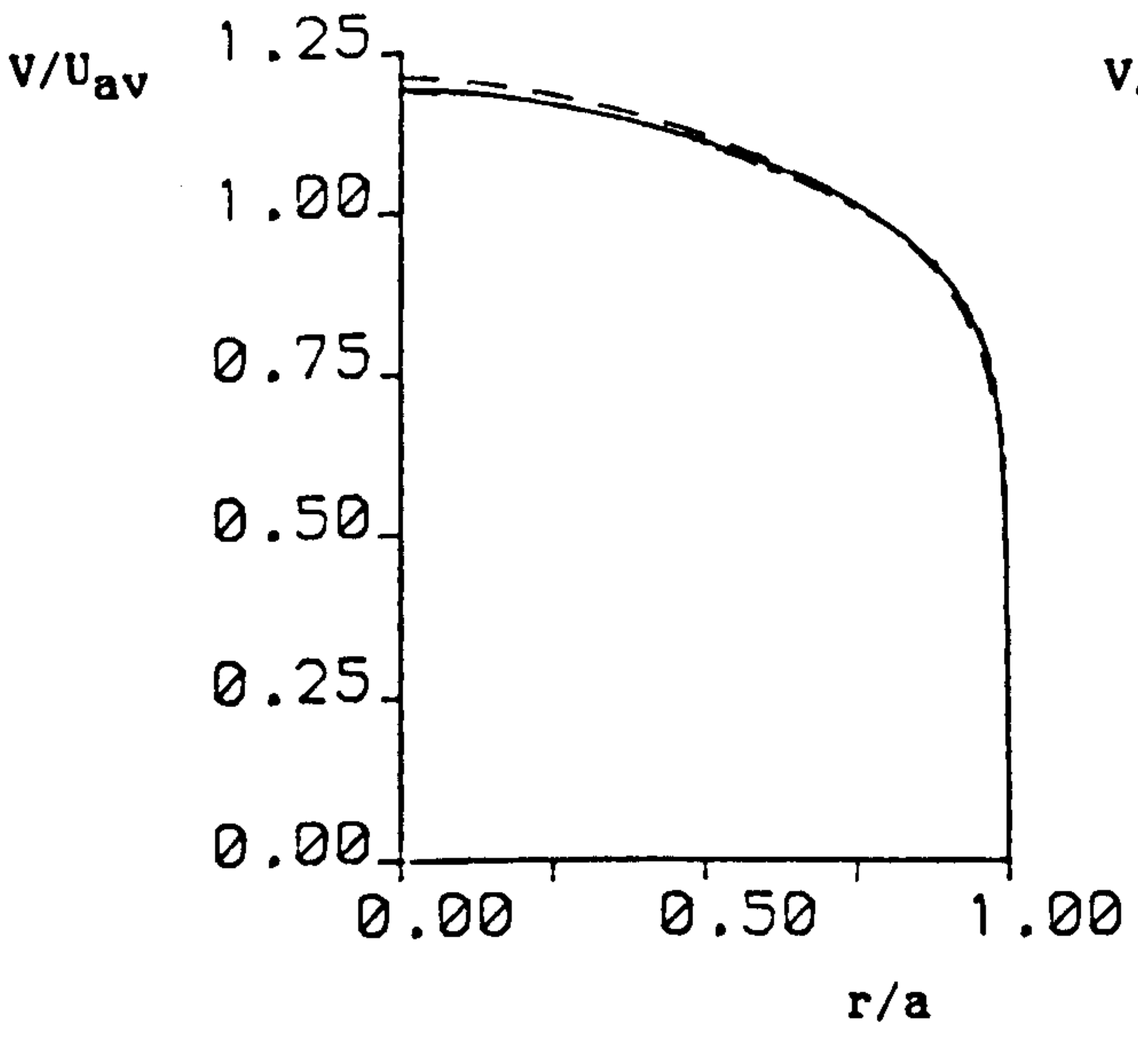

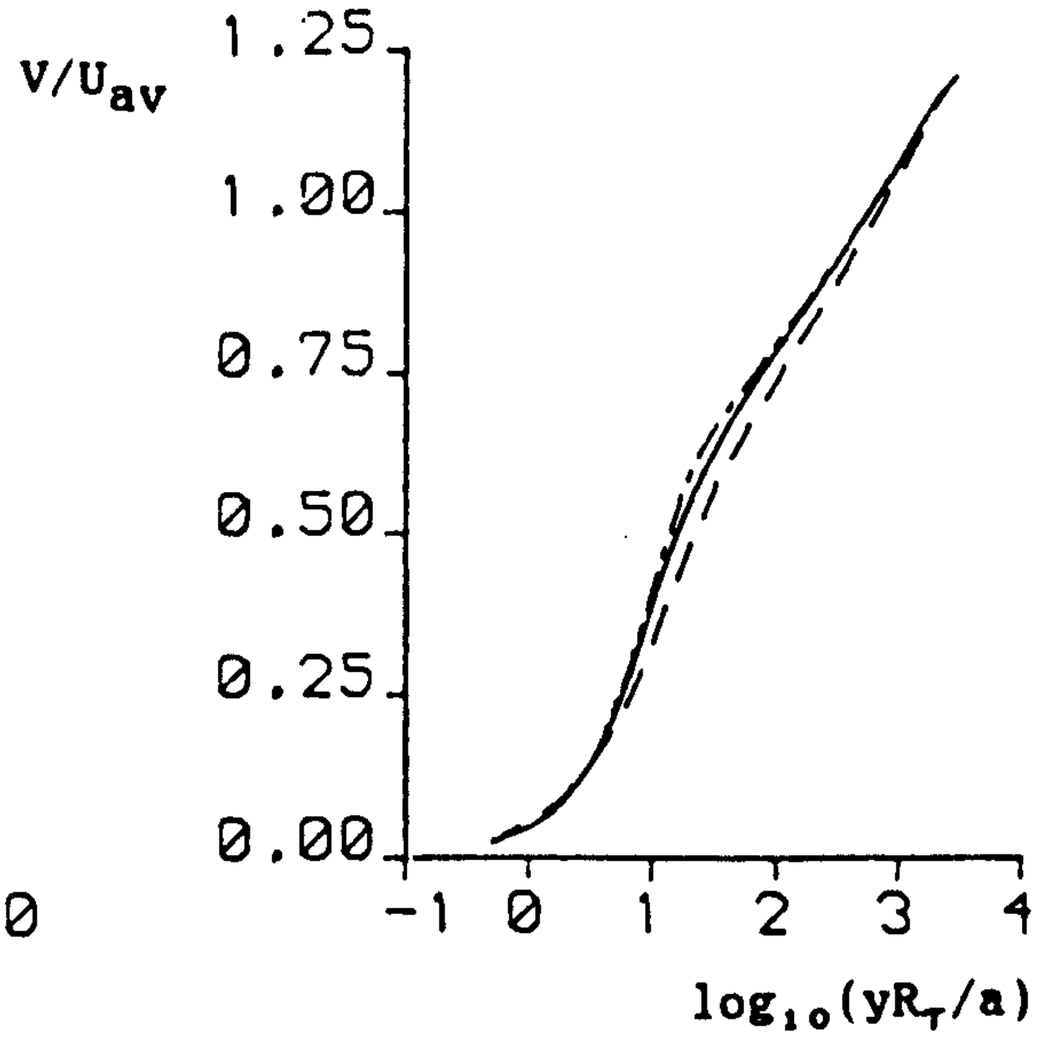

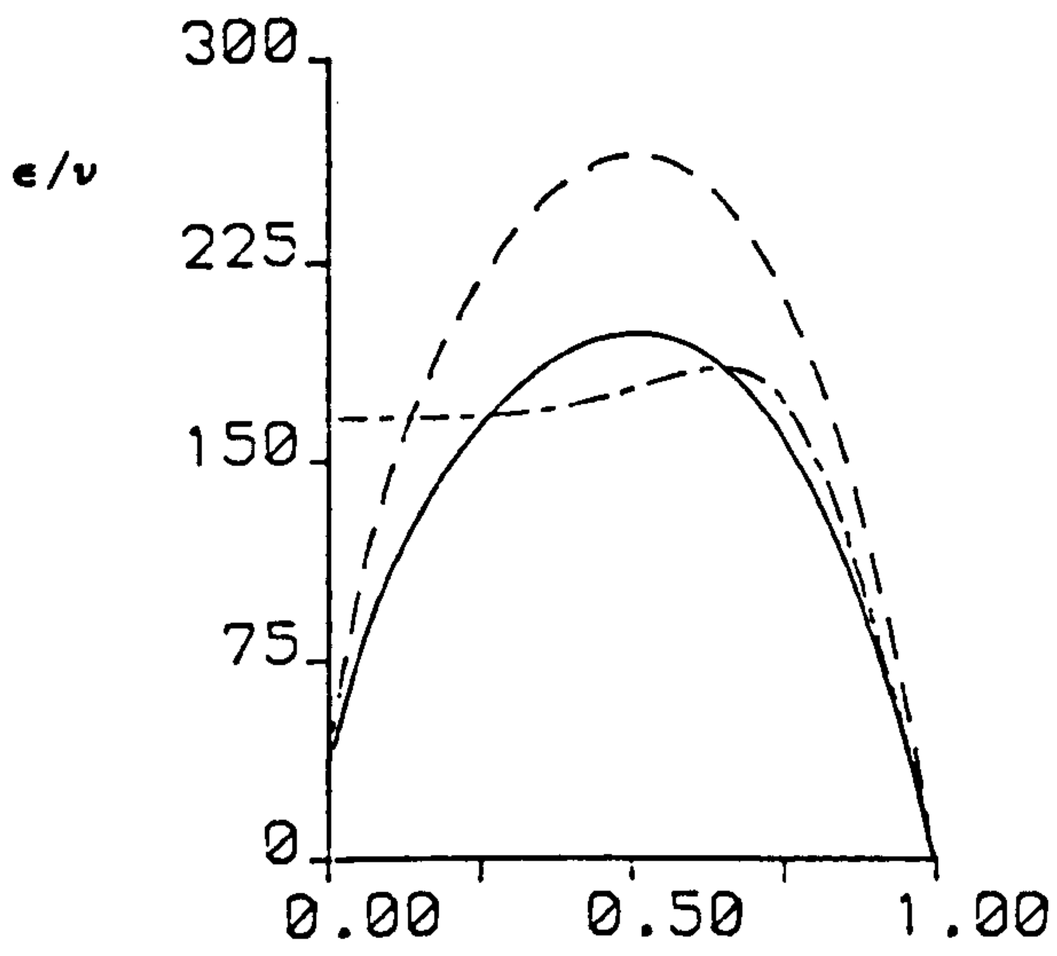

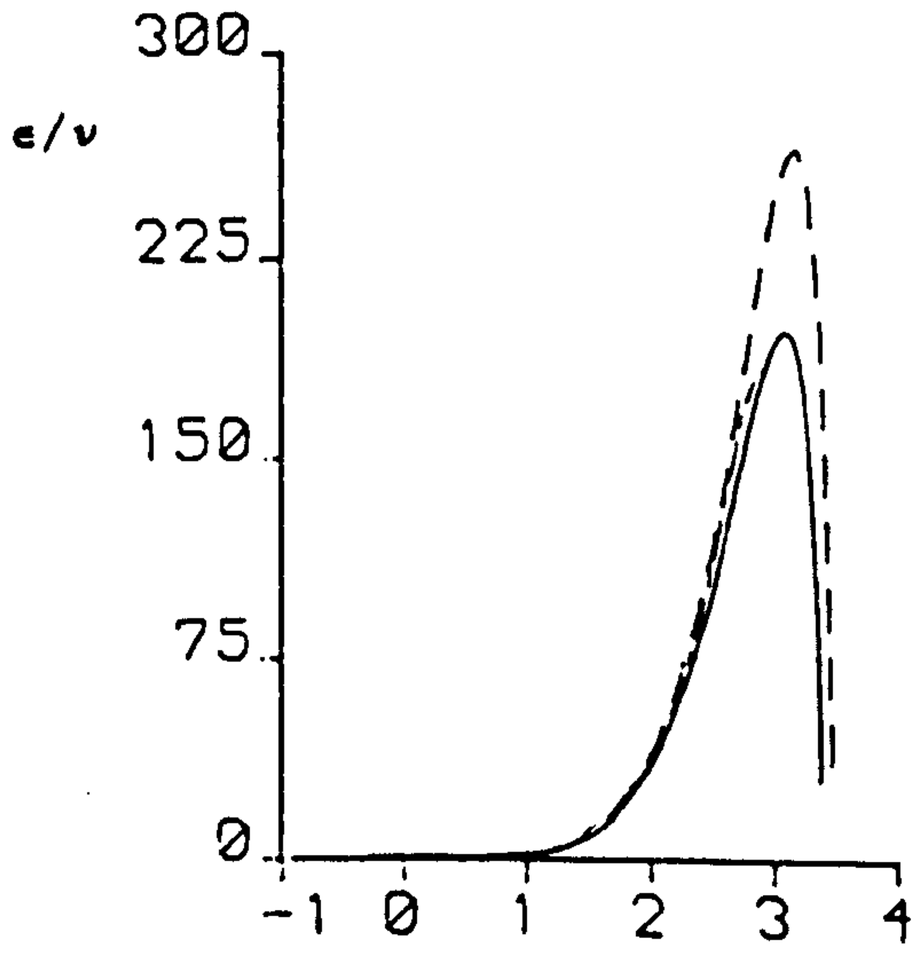

Figure 4.1: Theoretical Fully developed velocity and eddy viscosity at Re = 100000

_ _ _ _ _ _ Method B in a smooth pipe

_ _ _ _ . Method B in a rough pipe

_ . _ . _ . _ Method A in a smooth pipe

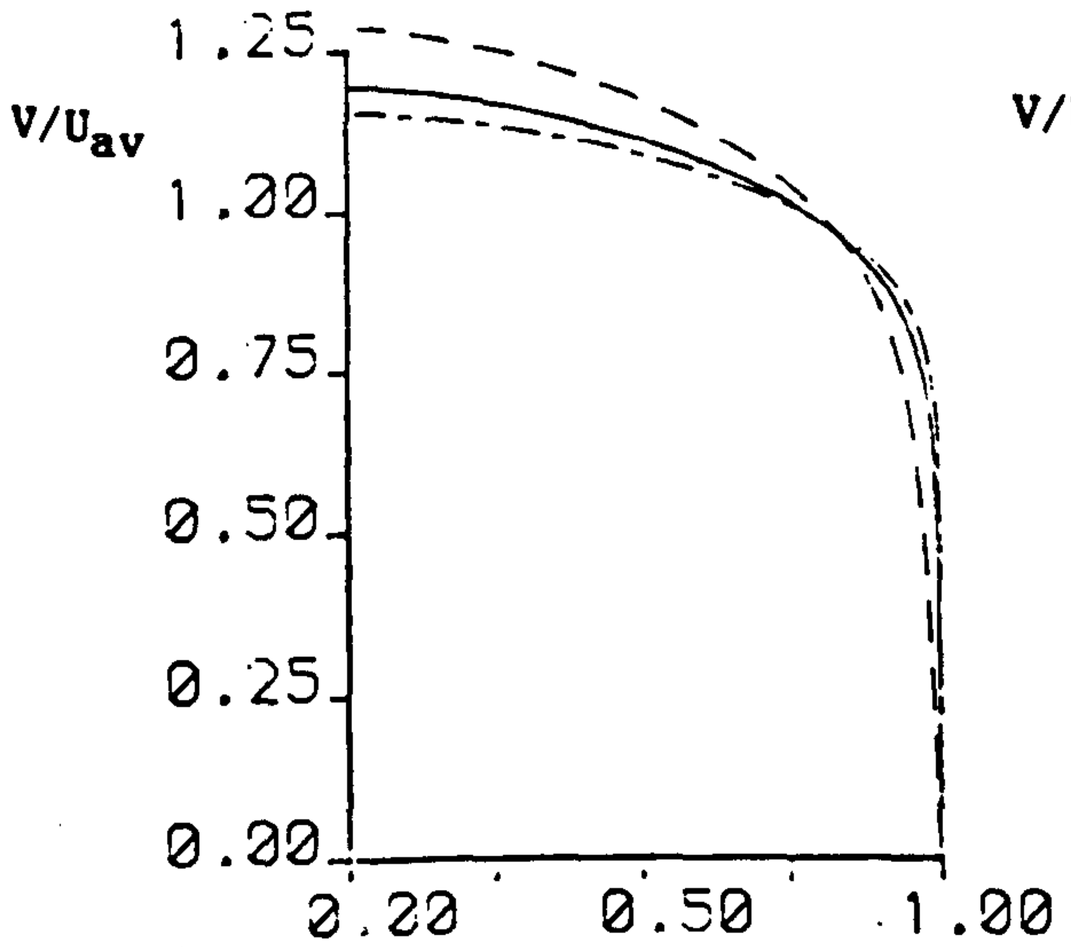

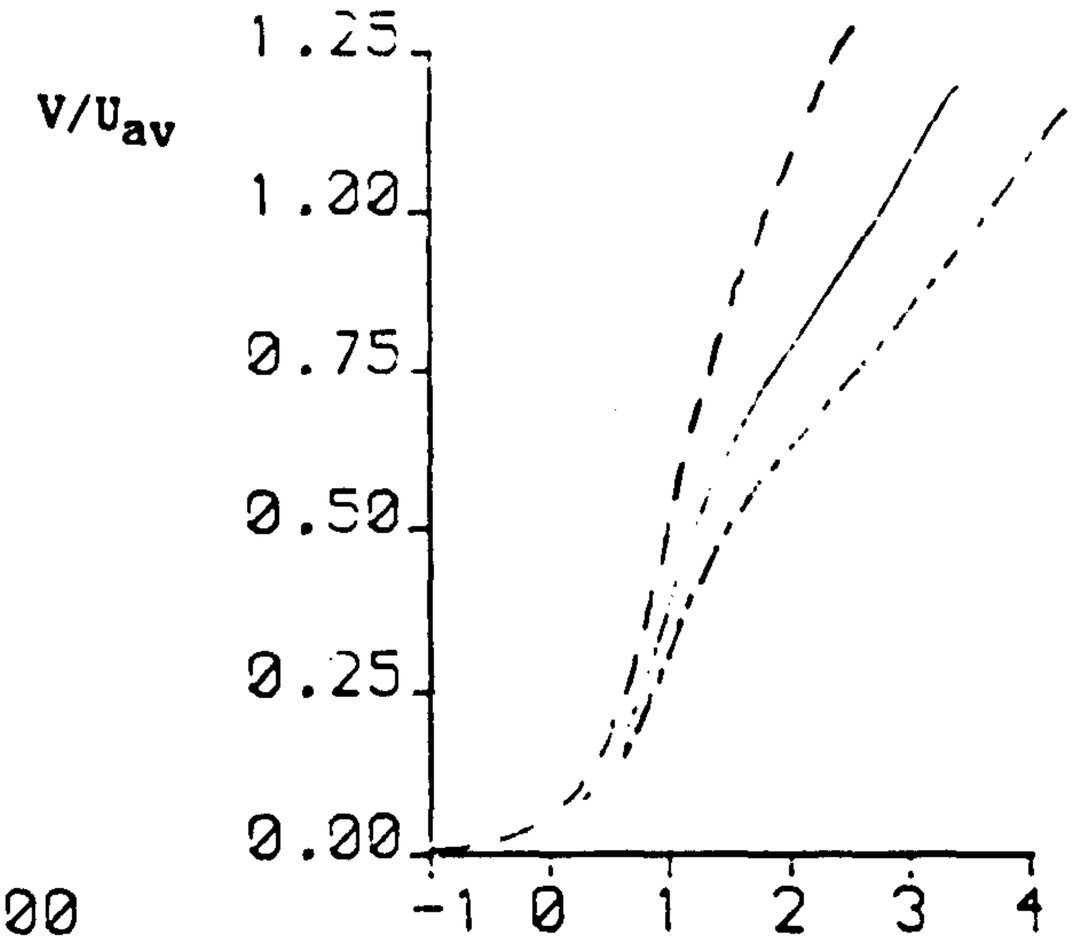

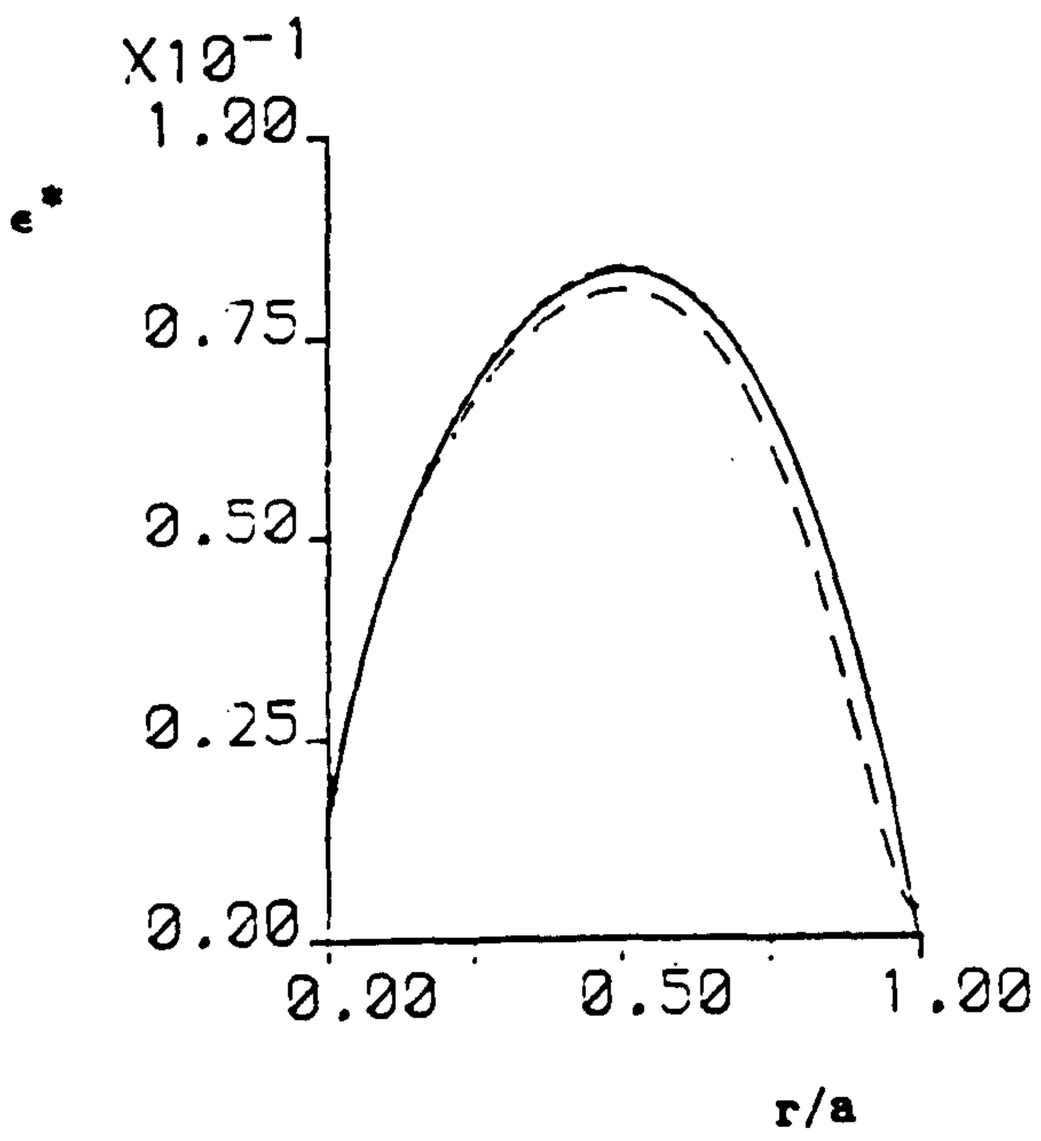

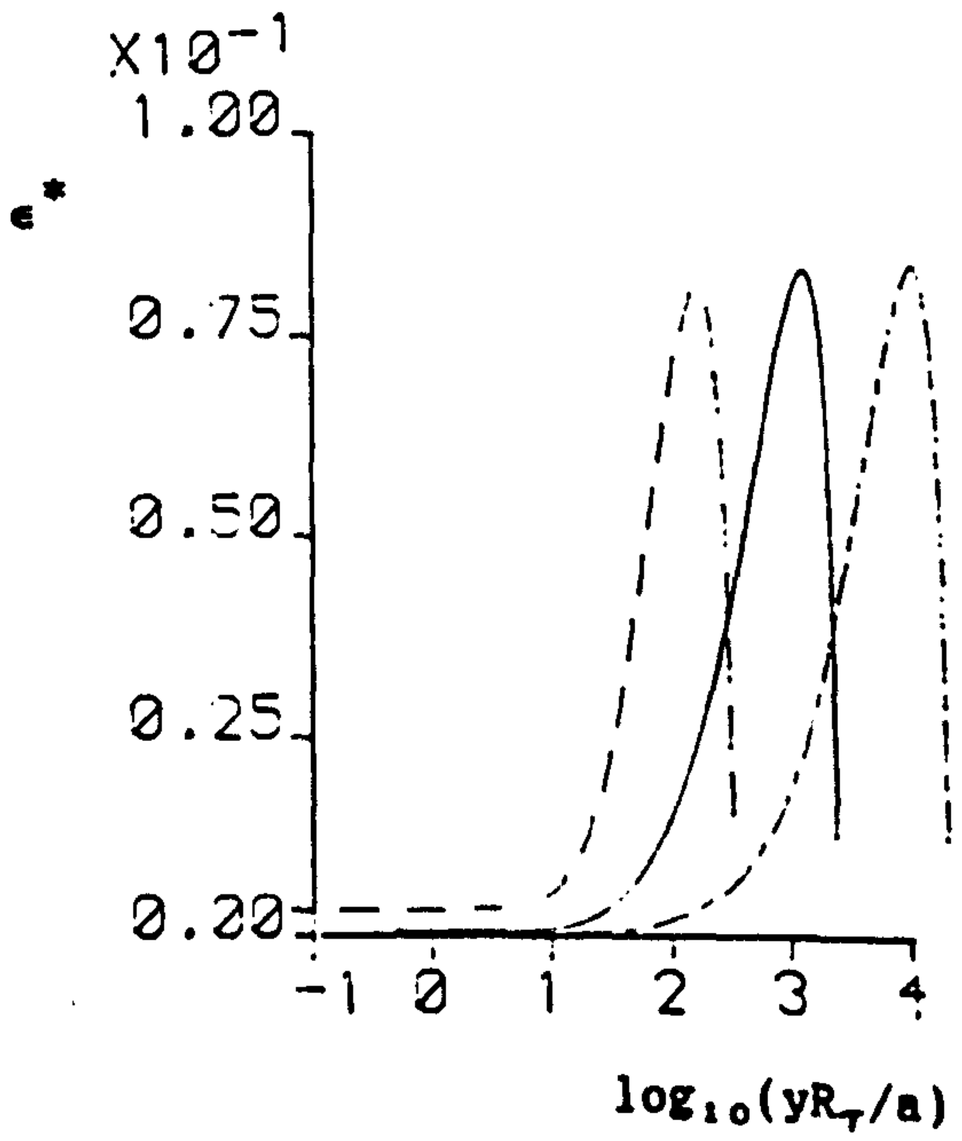

Figure 4.2: Theoretical Fully developed velocity and eddy viscosity: Method B smooth

_ _ _ _ . Reynolds number = 10000

_____ Reynolds number = 100200

_ . _ . _ . Reynolds number = 1000000

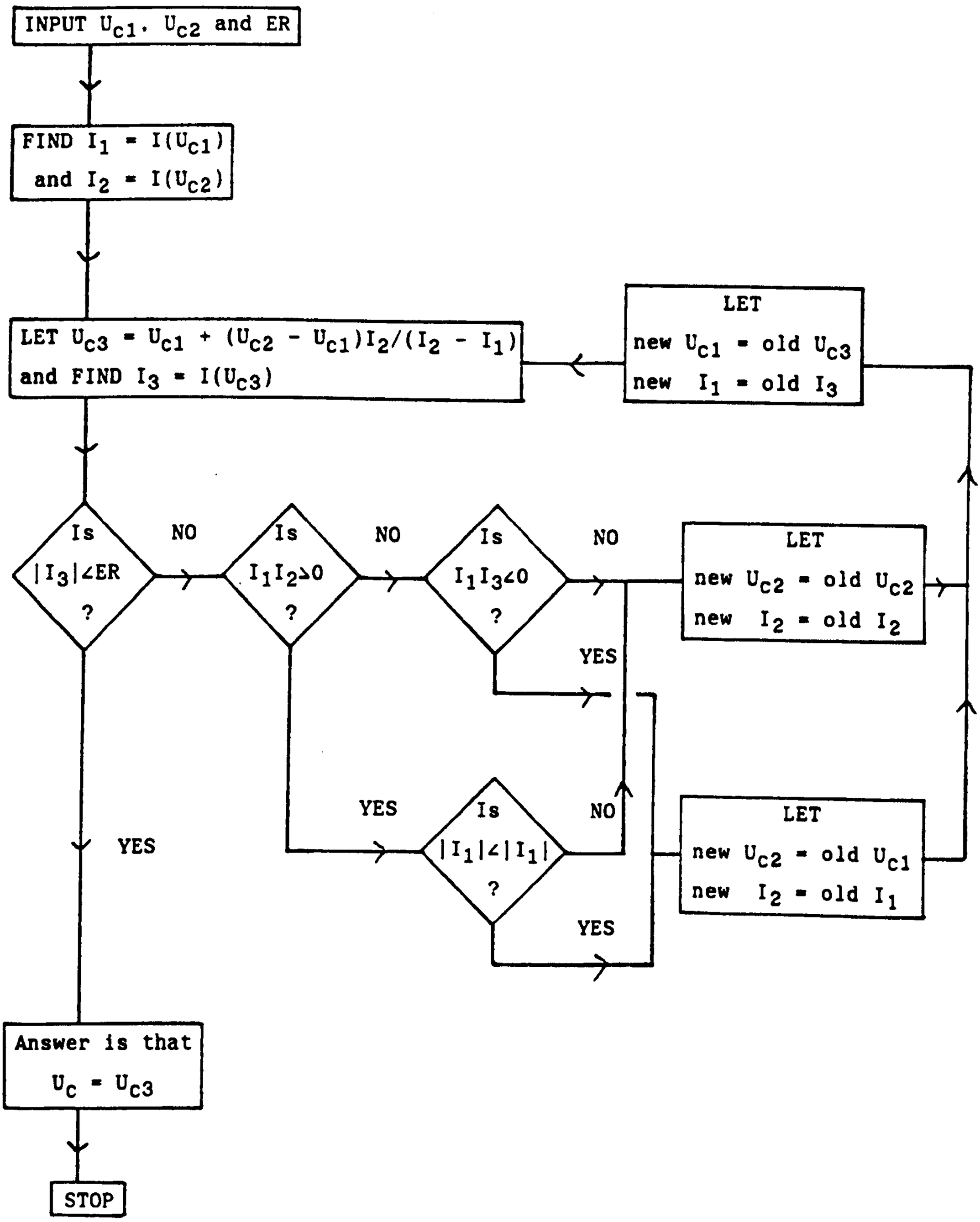

Figure 5.1: Flowchart for the searching routine

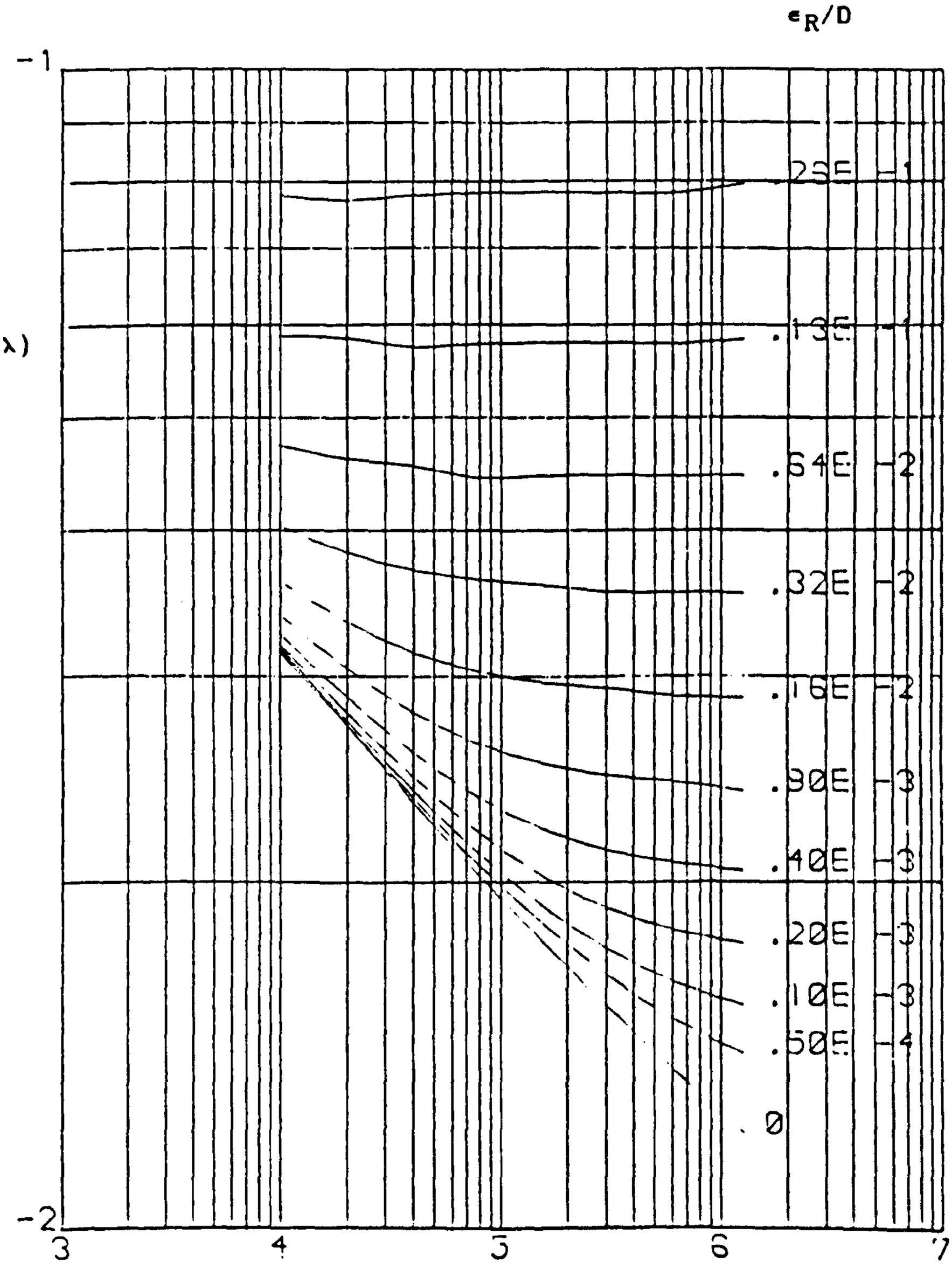

Figure 5.2: Relationships between the reynolds number and the decay rate of swirl at different roughnesses using Method B and the linear theory

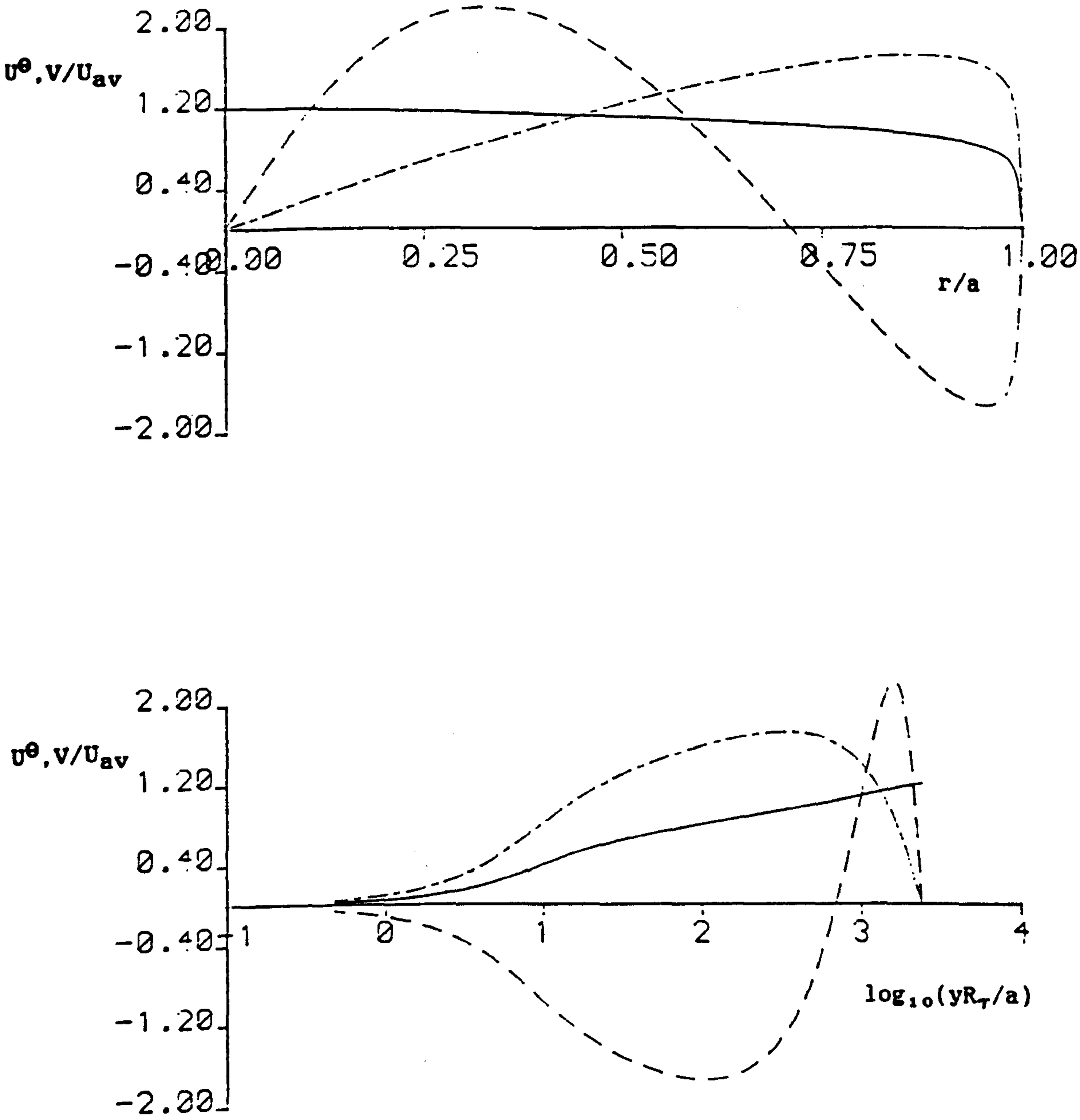

Figure 5.3: Tangential velocity eigenfunctions at Re = 100000 obtained using Method B smooth and the linear theory

——— Fully developed axial velocity

– – – – First eigenfunction

– – – – . Second eigenfunction

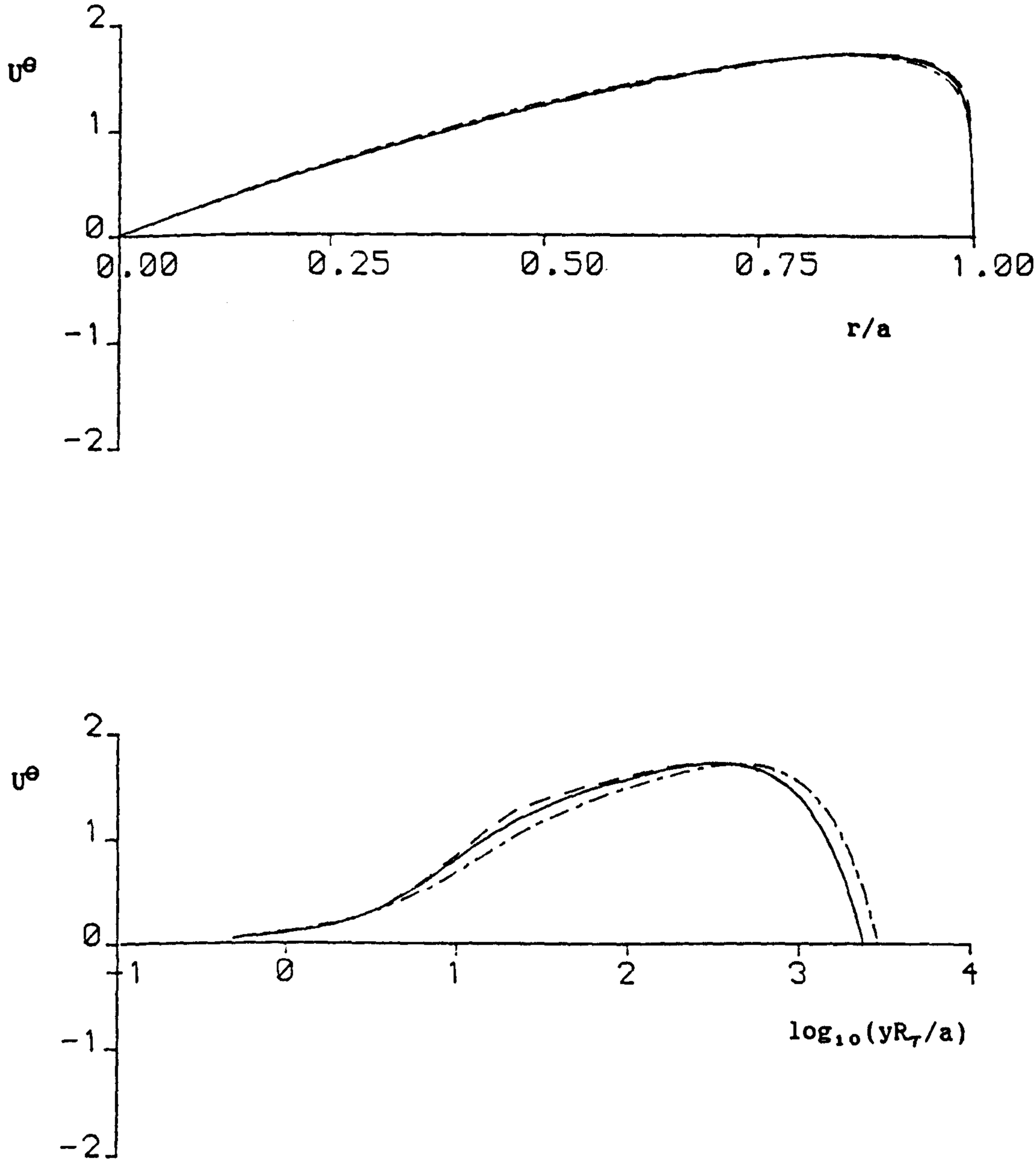

Figure 5.4: Tangential velocity eigenfunctions at Re = 100000 obtained using the linear theory

_____ Method B smooth

_ _ _ _ _ Method B rough

_ _ _ _ . Method A smooth

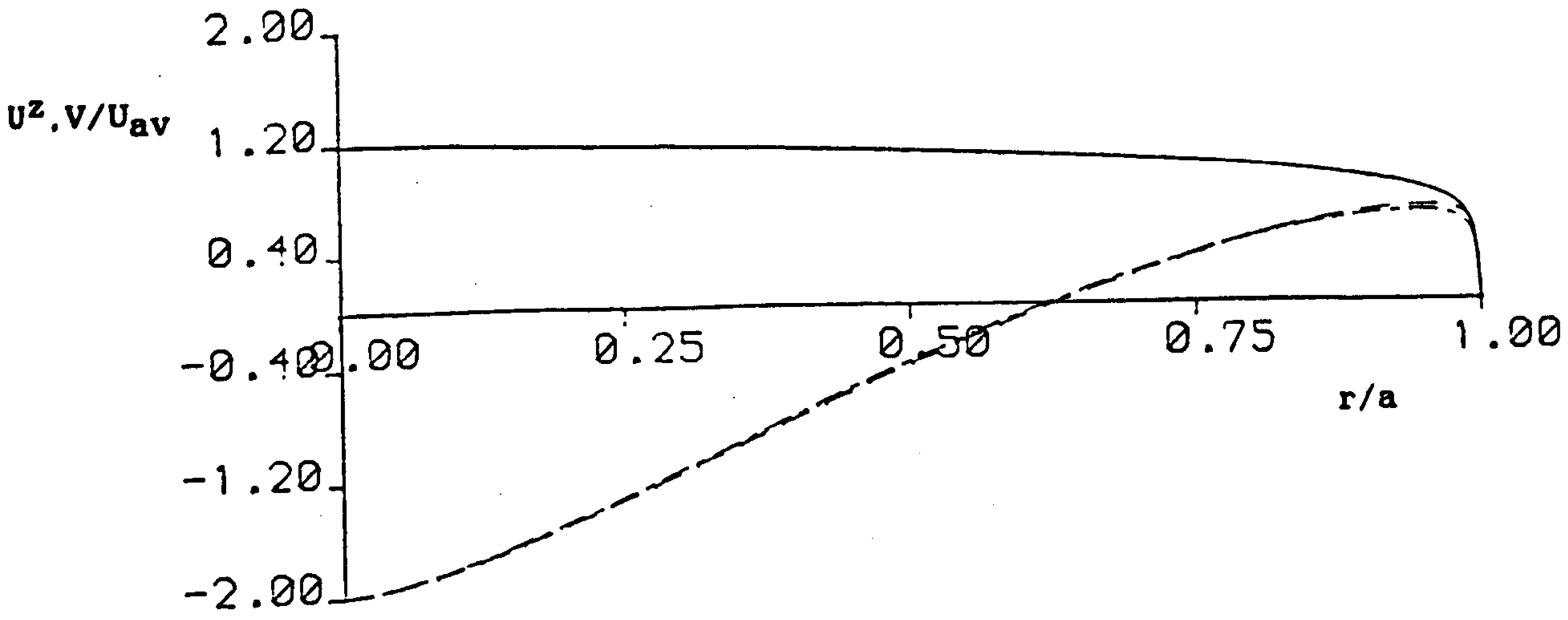

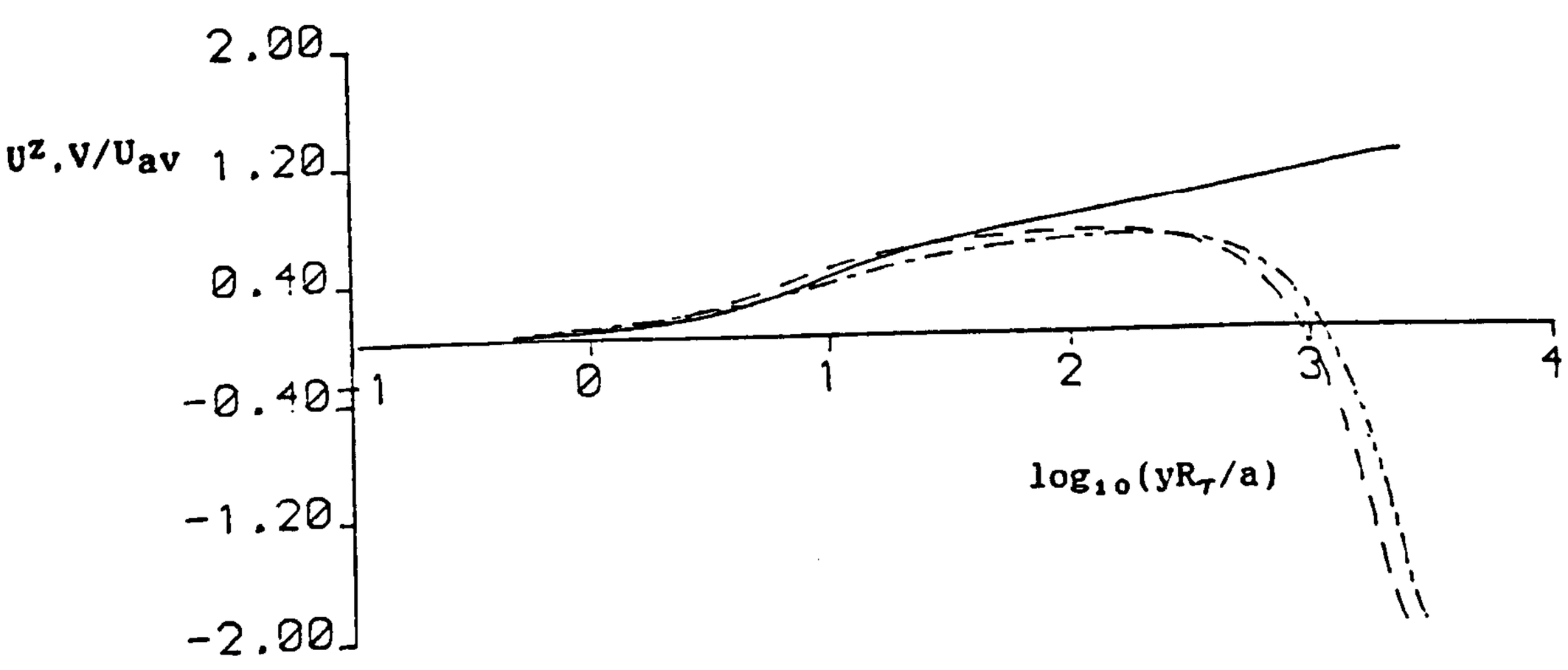

Figure 5.5: Axial velocity eigenfunctions at Re = 100000 obtained using the linear theory

———— Fully developed axial velocity (Method B smooth)

– – – – Method B smooth

– – – – – – Method B rough

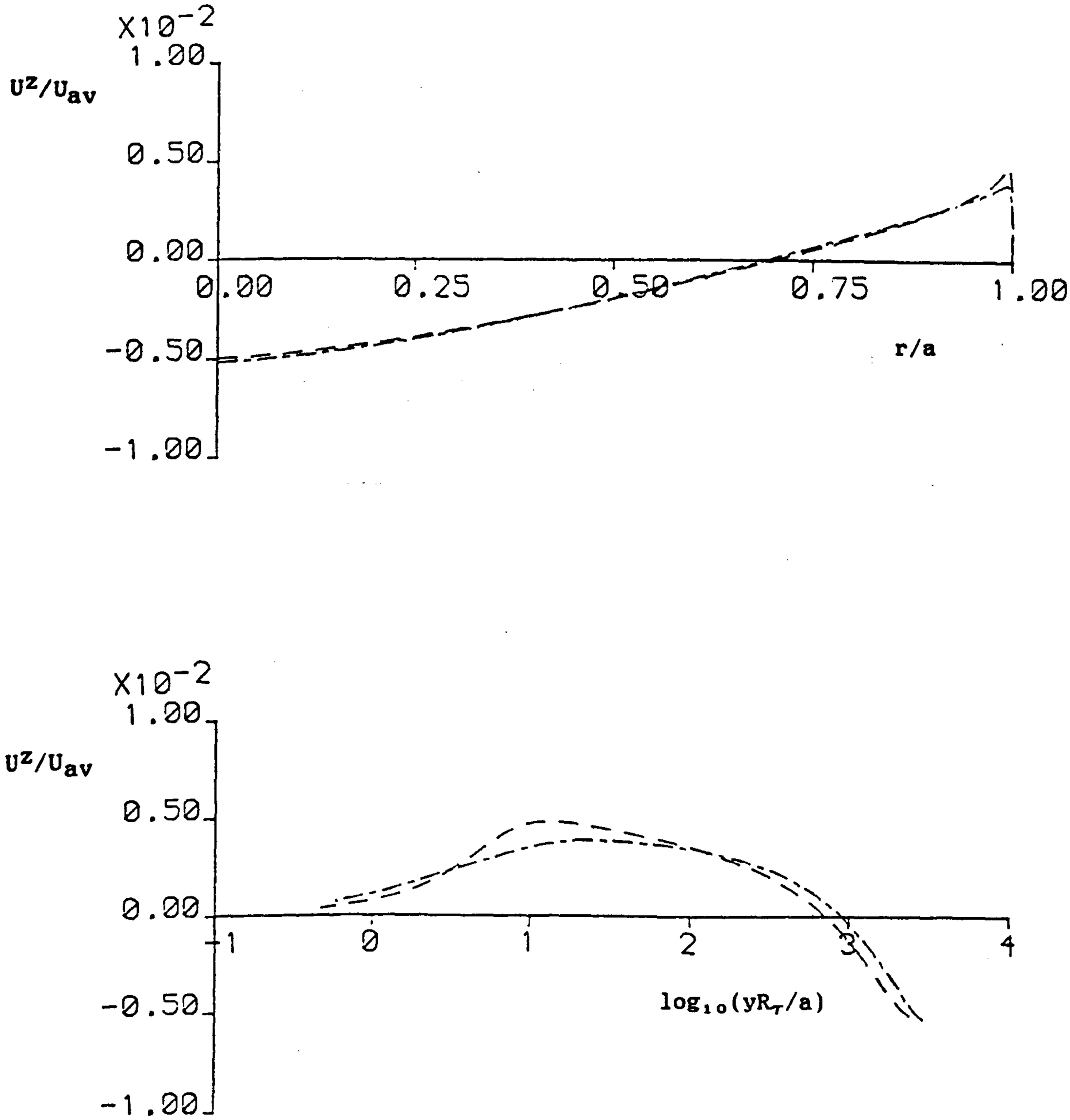

Figure 5.6: Axial velocity perturbation according to the second order linear theory at Re = 100000 and S = 0.1

_ _ _ _ . Meihod B smooth

_ . _ . _ . _ Meihod B rough

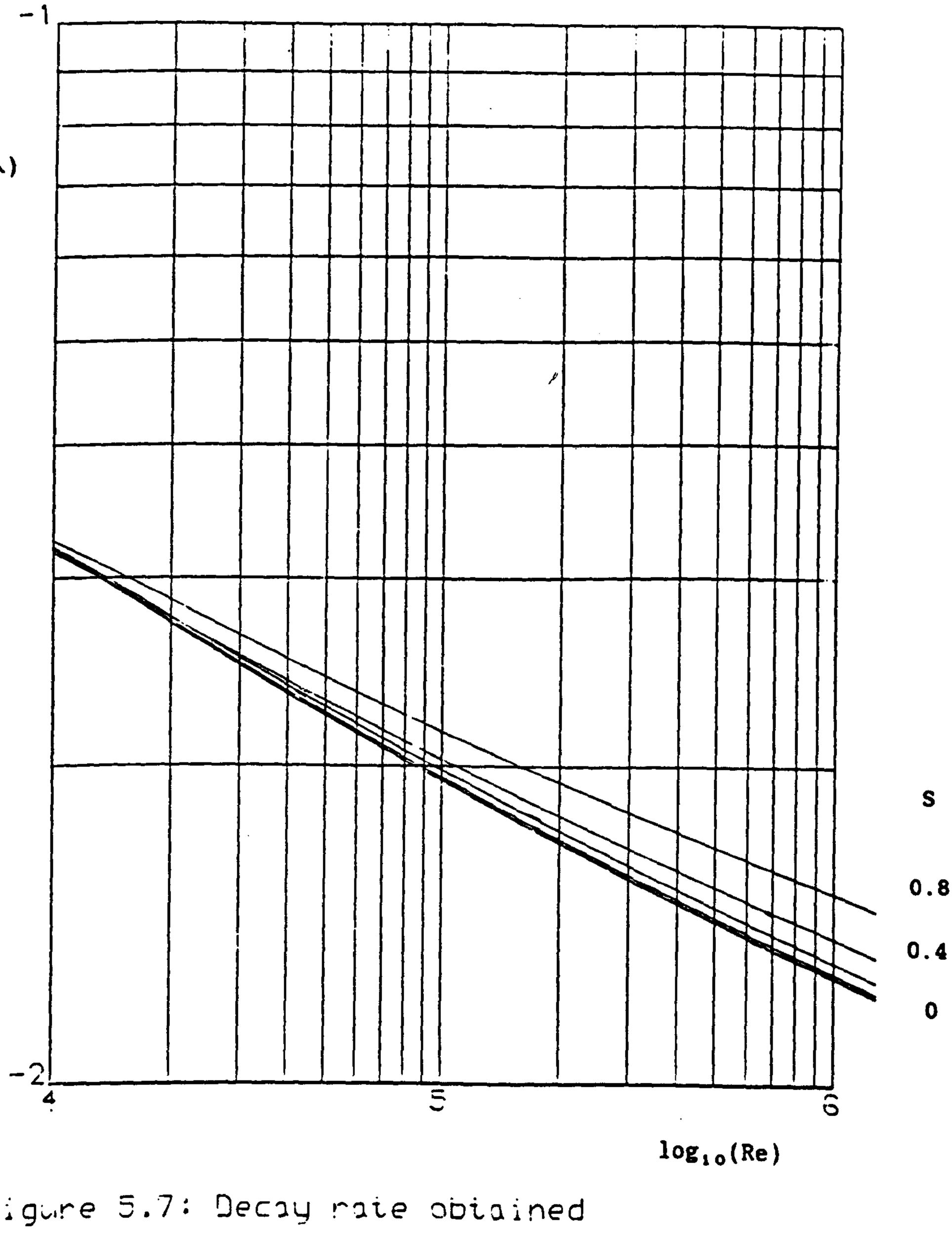

Figure 5.7: Decay rate obtained using the similarity theory with Method B smooth

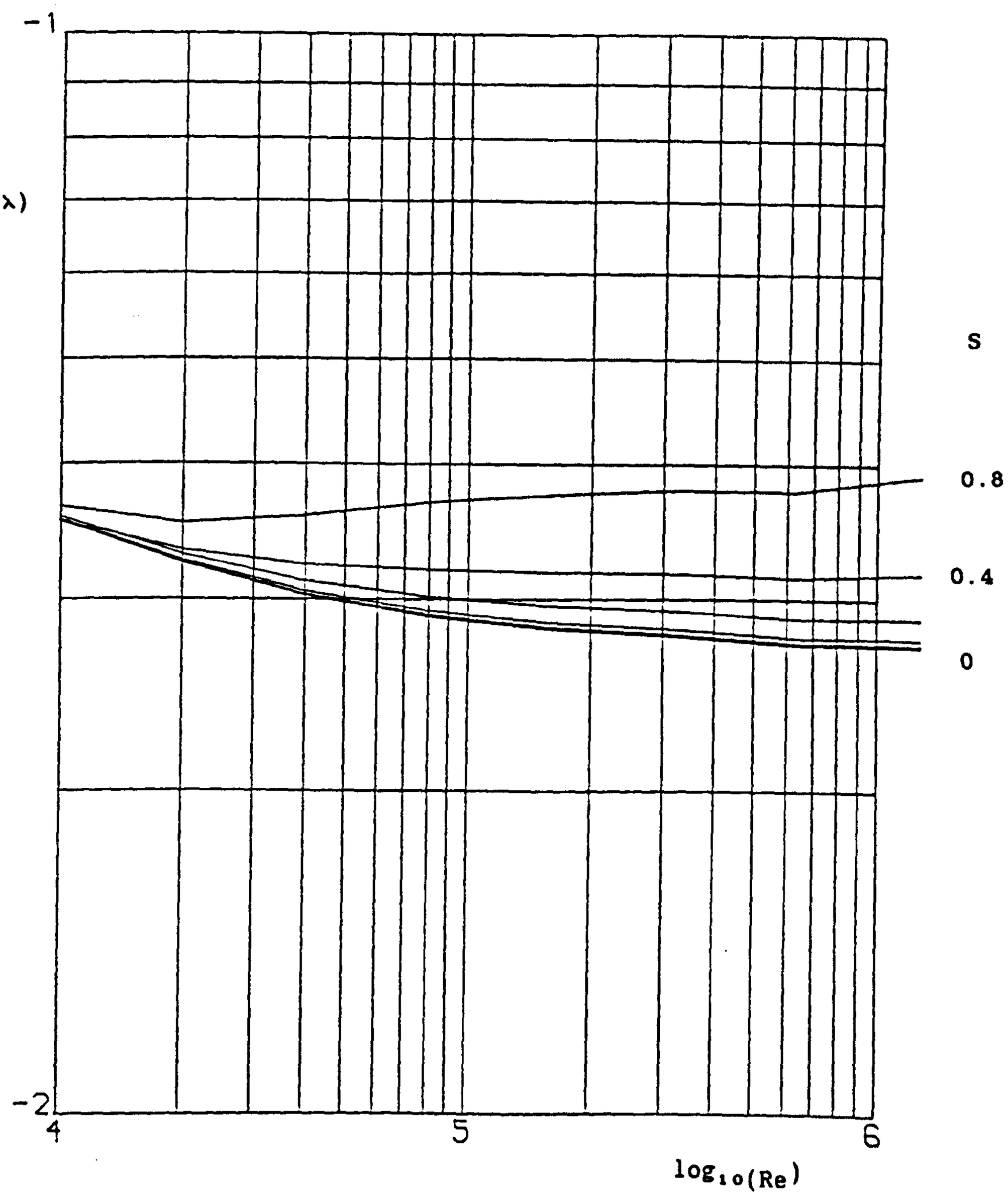

Figure 5.8: Decay rate obtained using the similarity theory with Method B rough

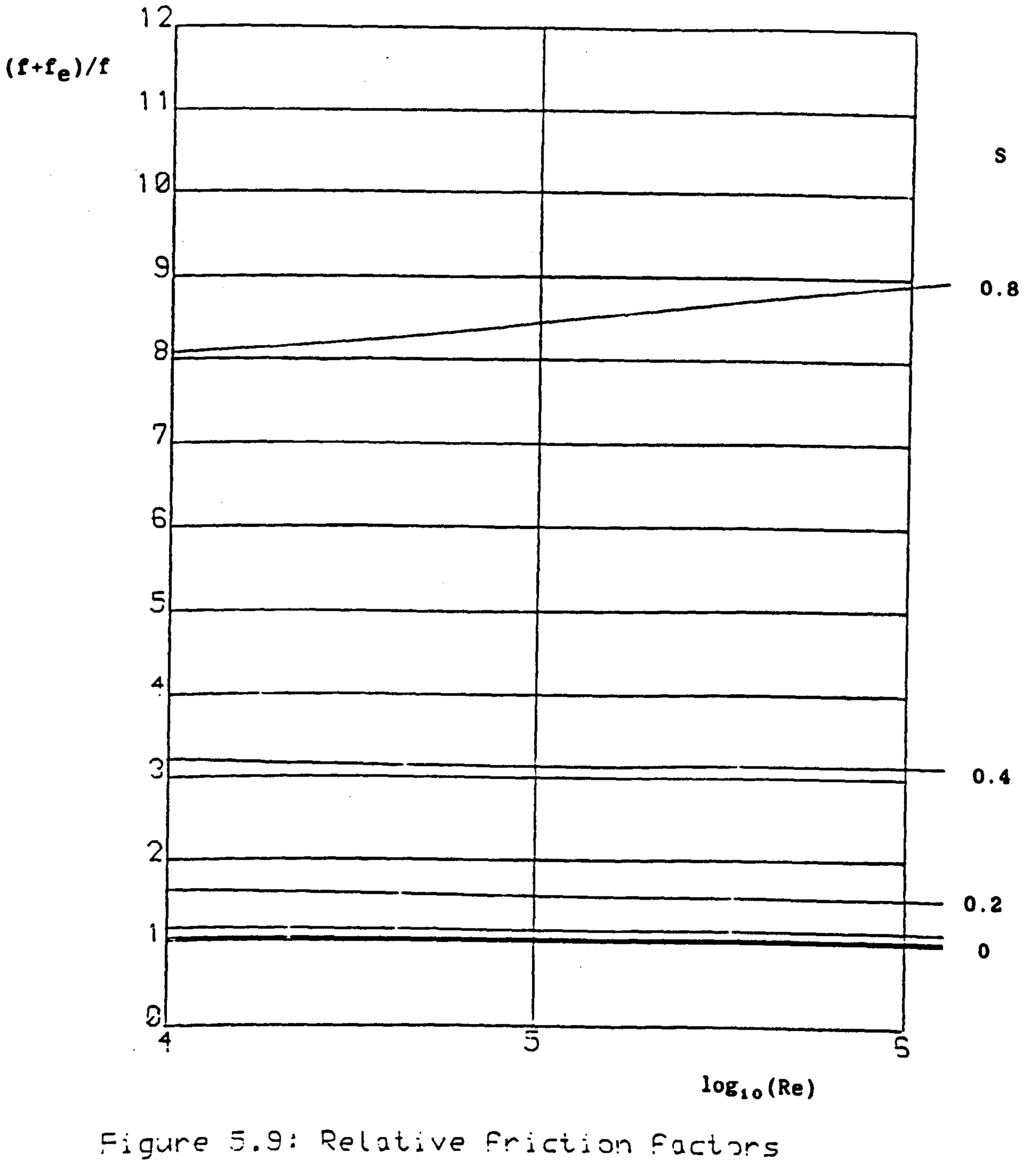

Figure 5.9: Relative Friction Factors obtained using the similarity theory with Method 3 smooth

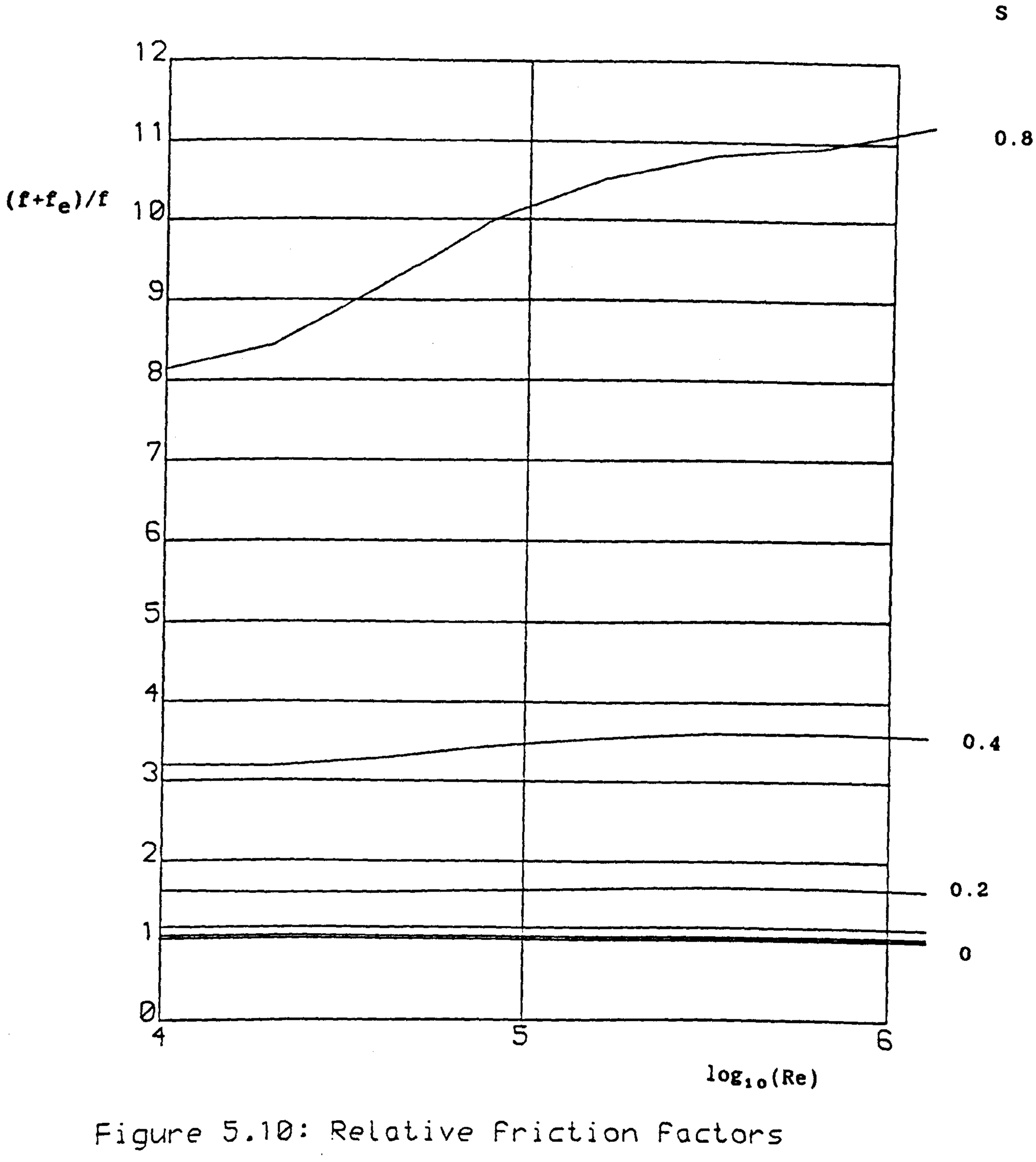

Figure 5.10: Relative friction factors obtained using the similarity theory with Method B rough

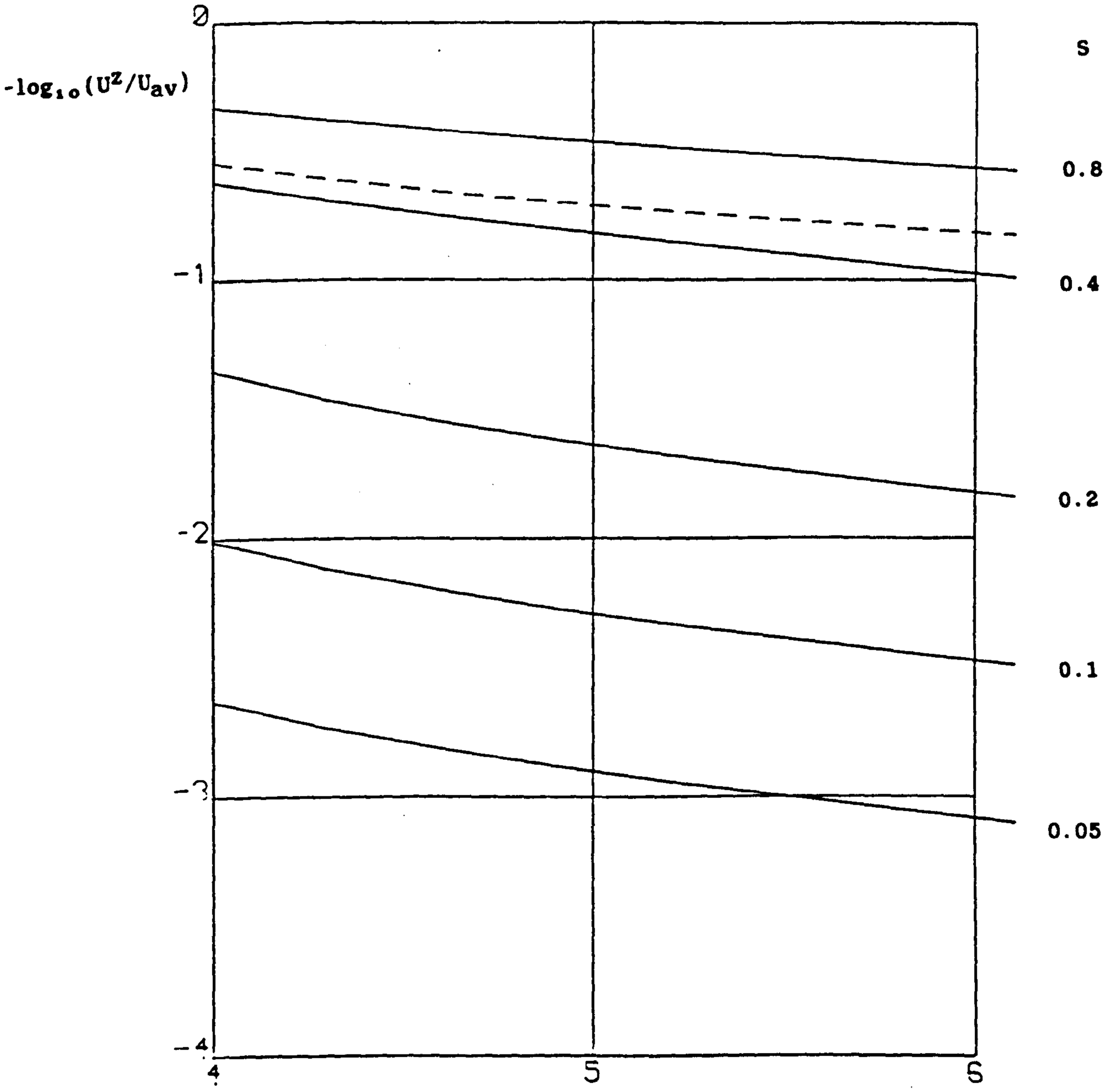

Figure 5.11: Axial velocity perturbation at r=0 obtained using the similarity theory with Method B smooth

— — — — $(U_c-U_{av})/U_{av}$

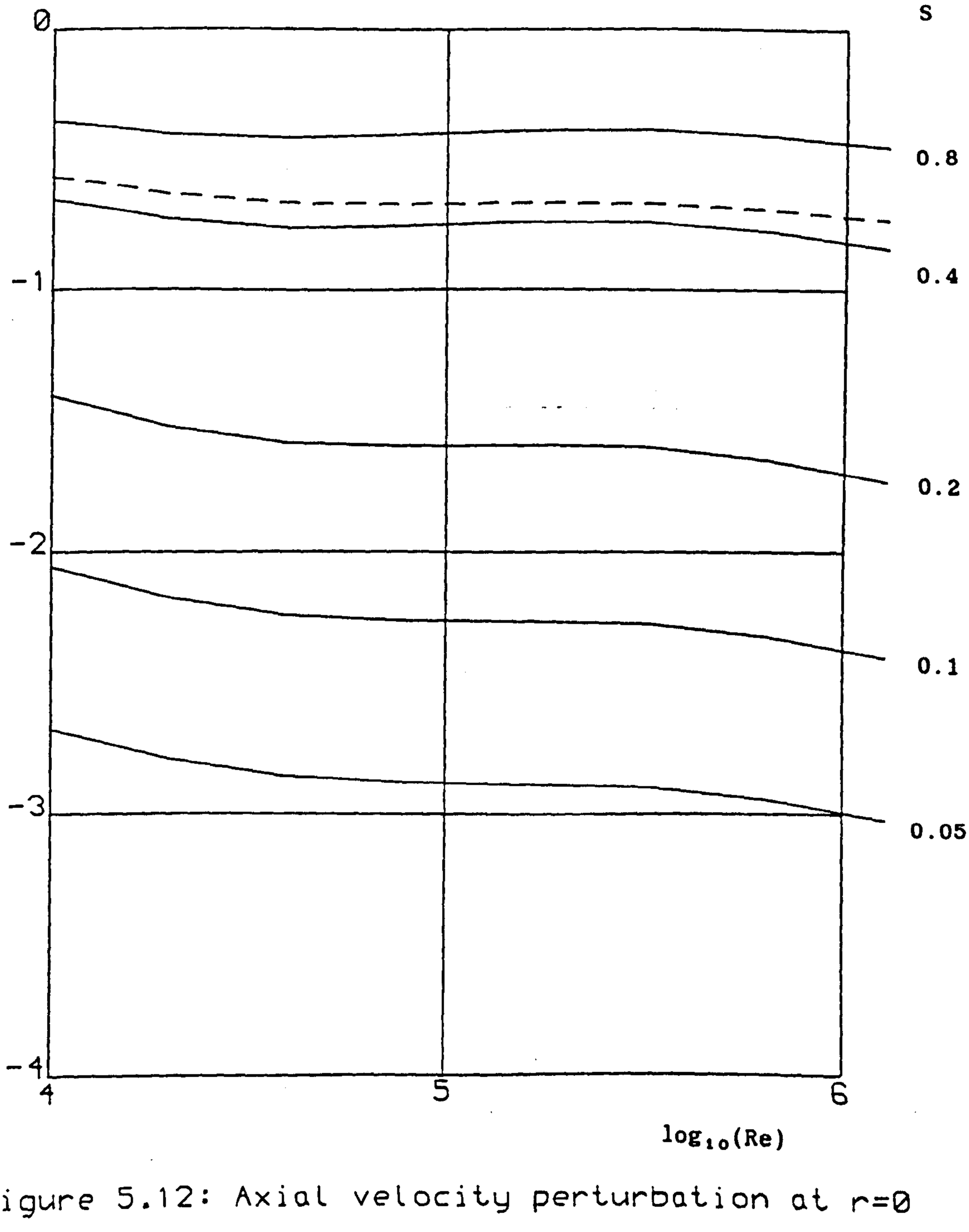

Figure 5.12: Axial velocity perturbation at r=0 obtained using the similarity theory with Method B rough

— — — — $(U_c-U_{av})/U_{av}$

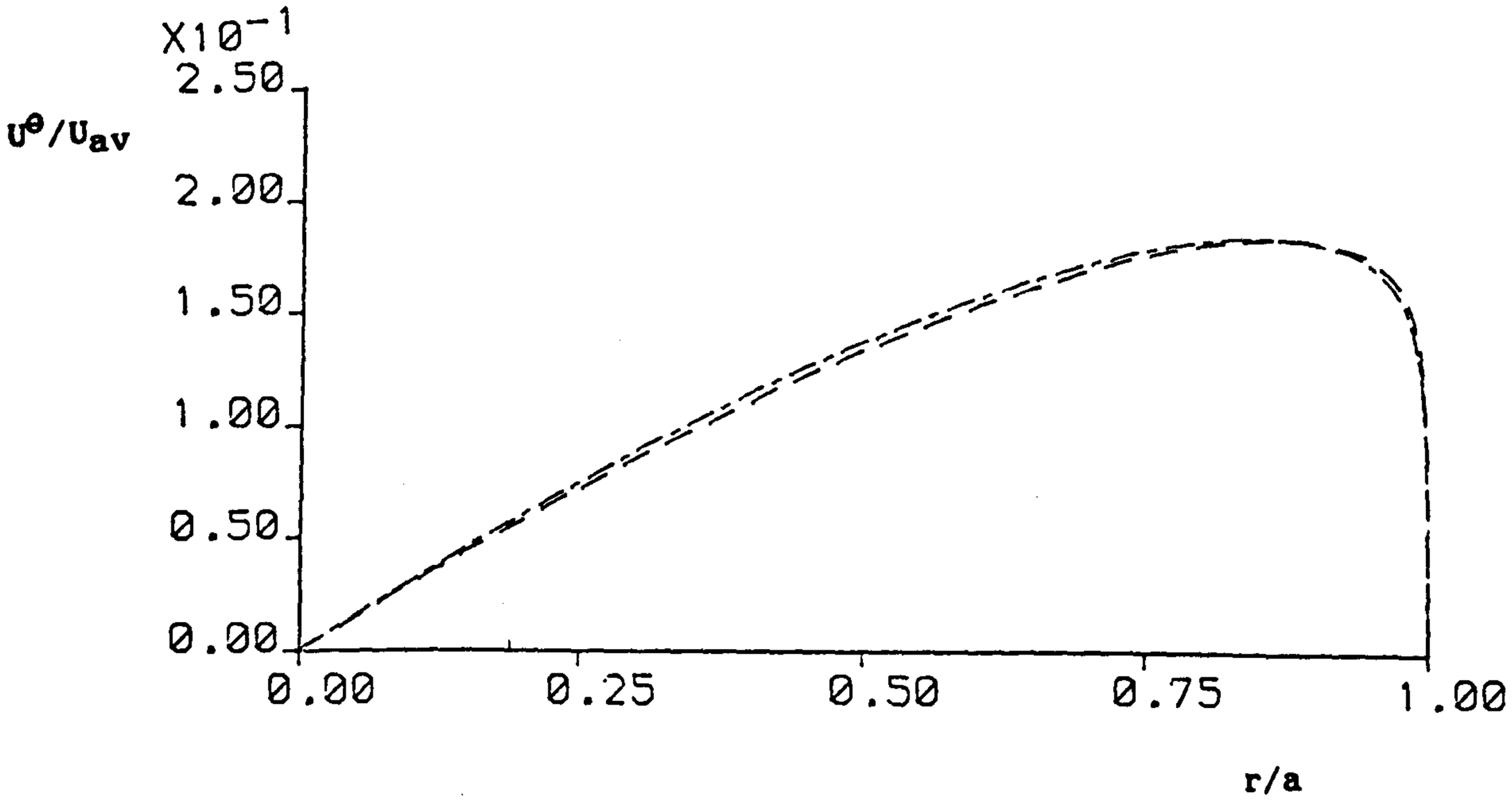

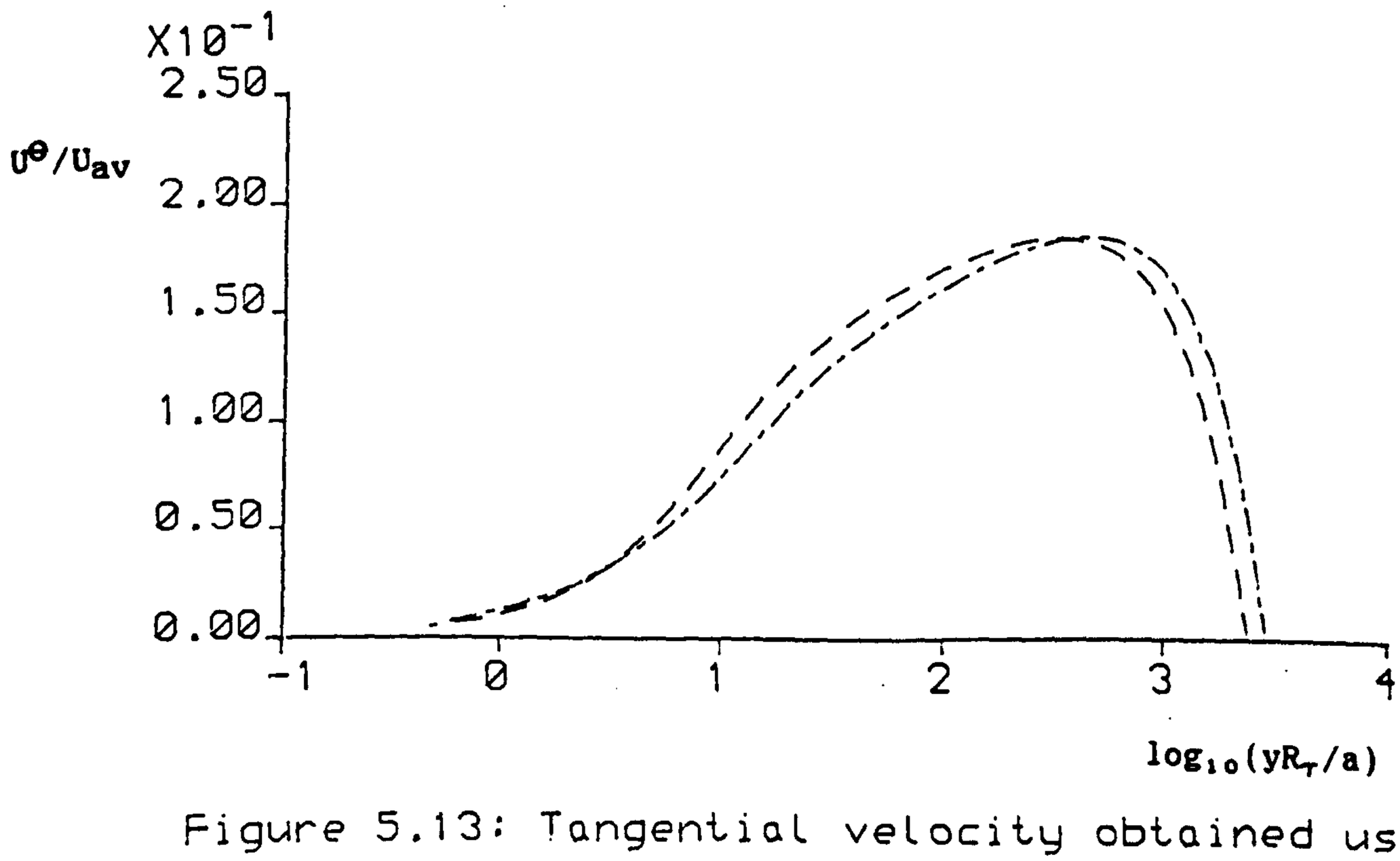

Figure 5.13: Tangential velocity obtained using the similarity theory at Re = 100000 and S = 0.1

_ _ _ _ . Method B smooth

_ _ _ _ _ _ Method B rough

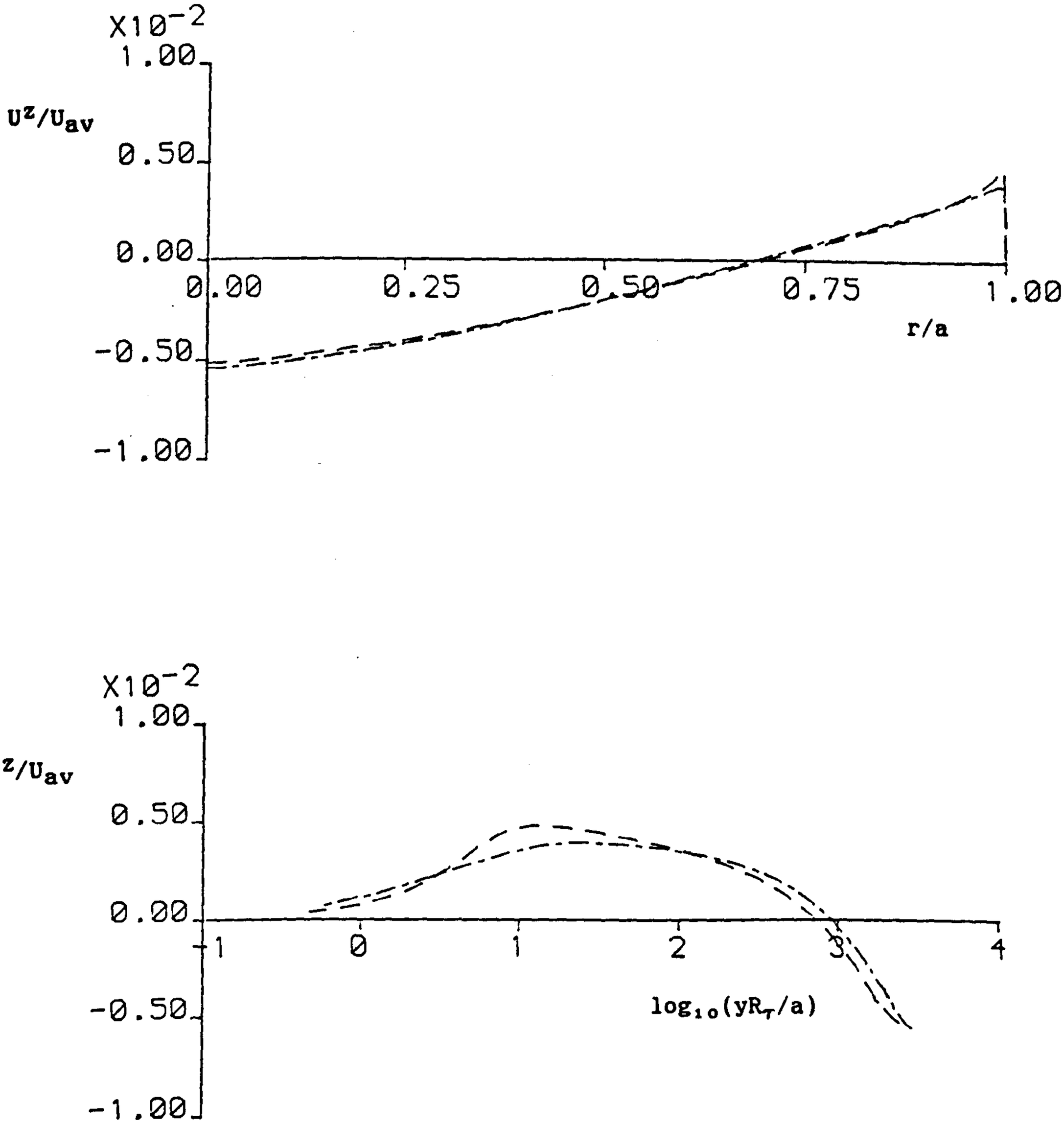

Figure 5.14: Axial velocity obtained using the similarity theory at Re = 100000 and S = 0.1

_ _ _ _ . Method B smooth

_ _ _ _ _ _ Method B rough

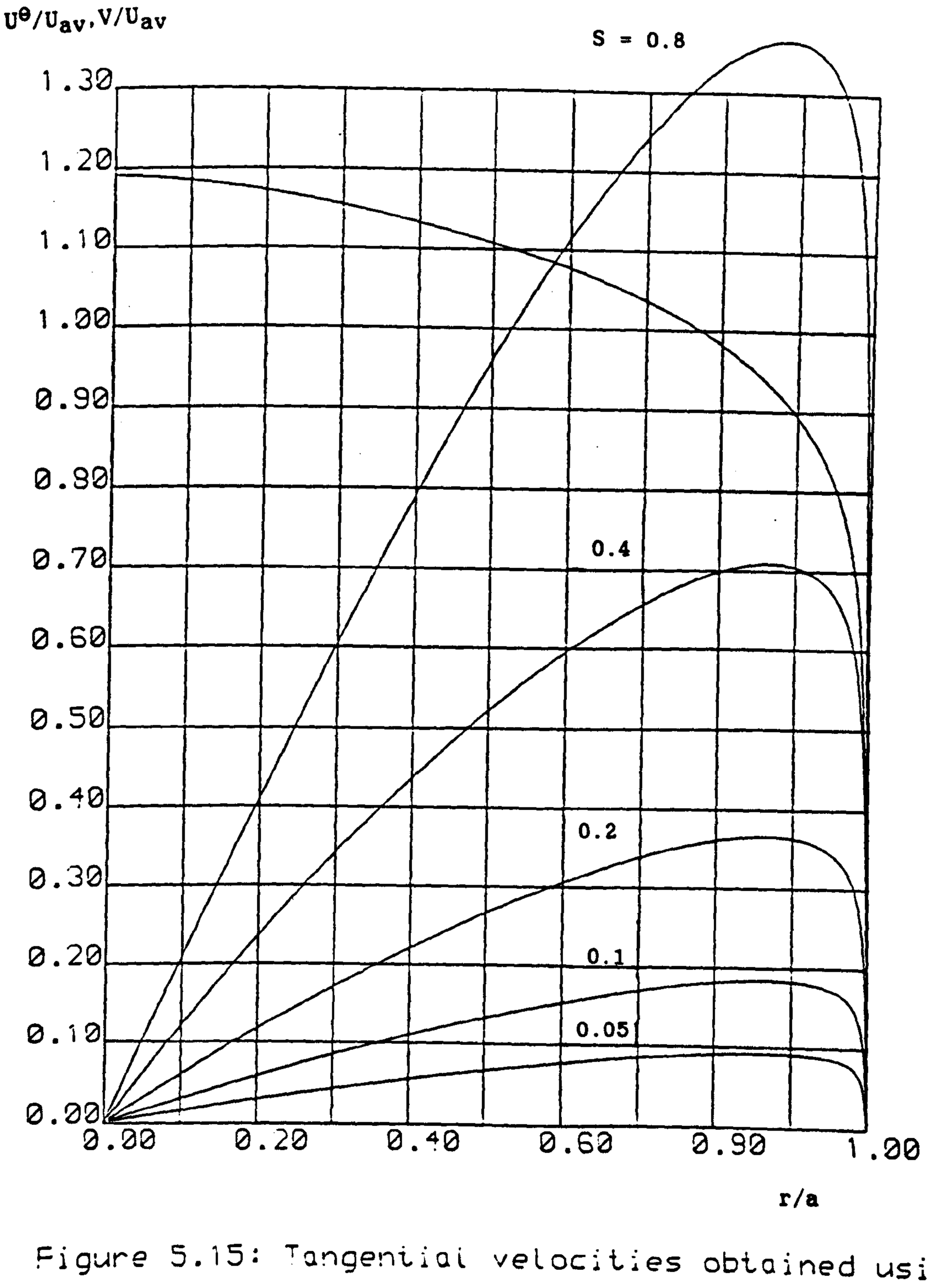

Figure 5.15: Tangential velocities obtained using the similarity theory at Re = 100000 with Method B smooth

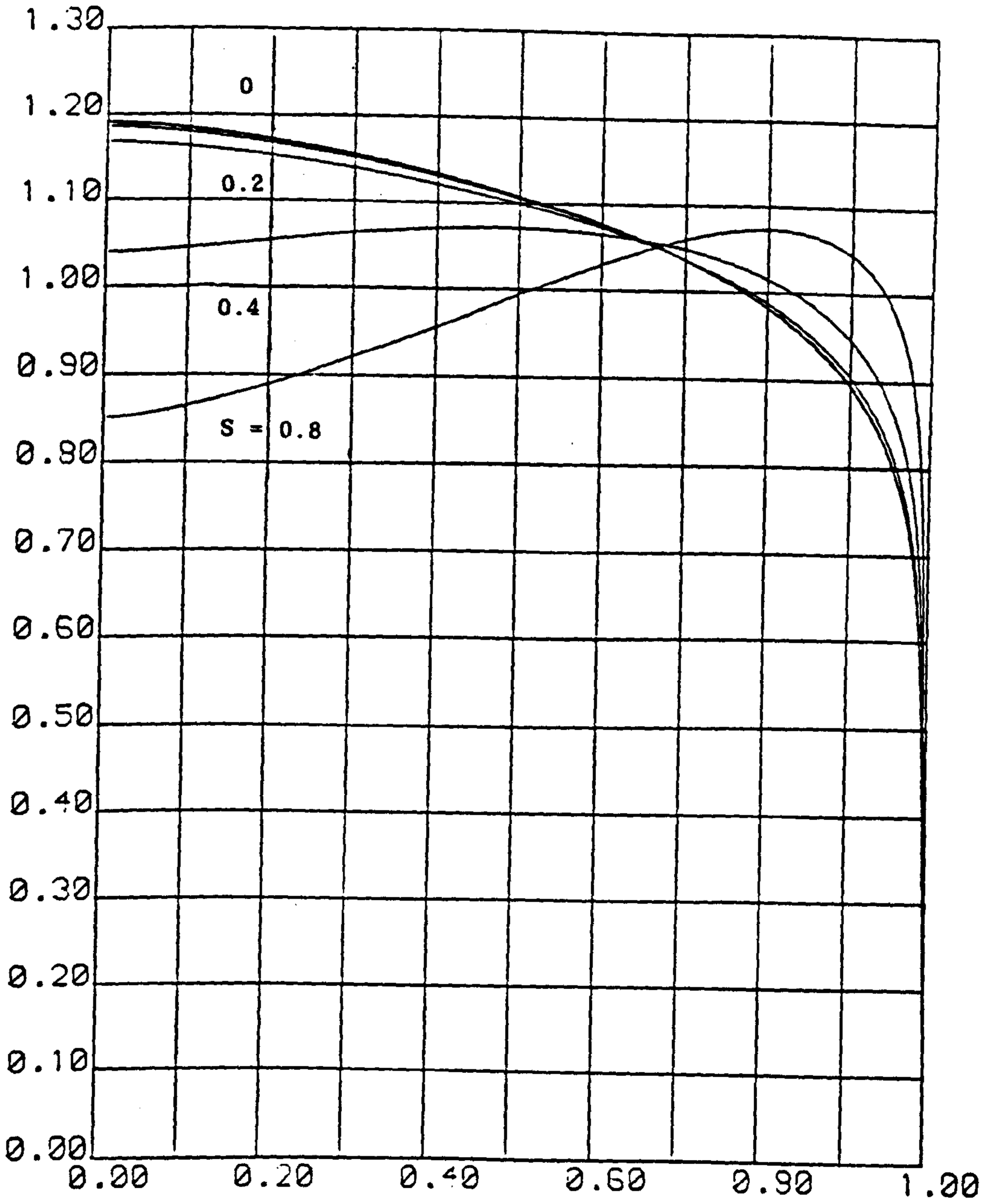

Figure 5.16: Axial velocities obtained using the similarity theory at Re = 100000 with Method B smooth

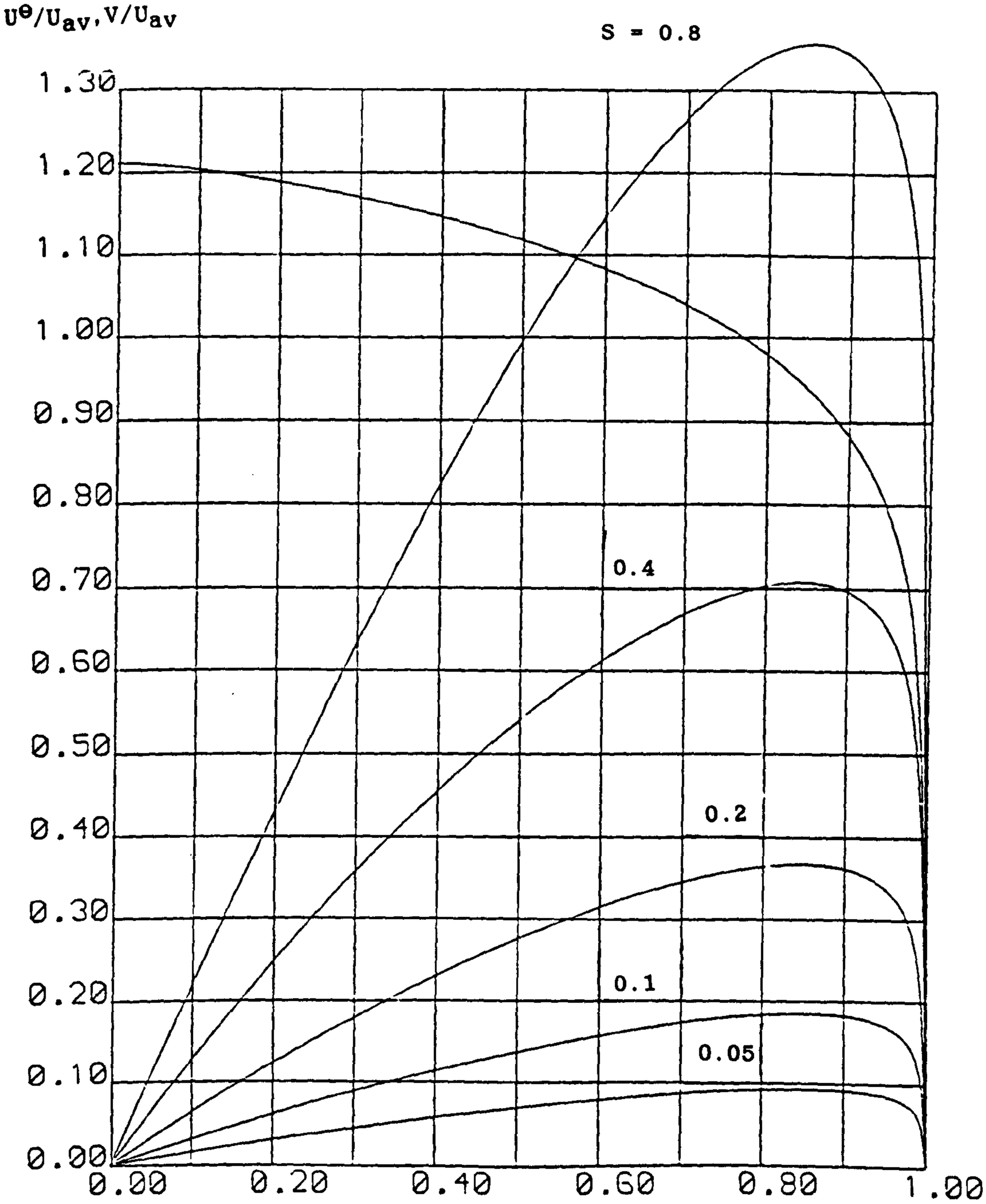

Figure 5.17: Tangential velocities obtained using the similarity theory at Re = 100000 with Method B rough

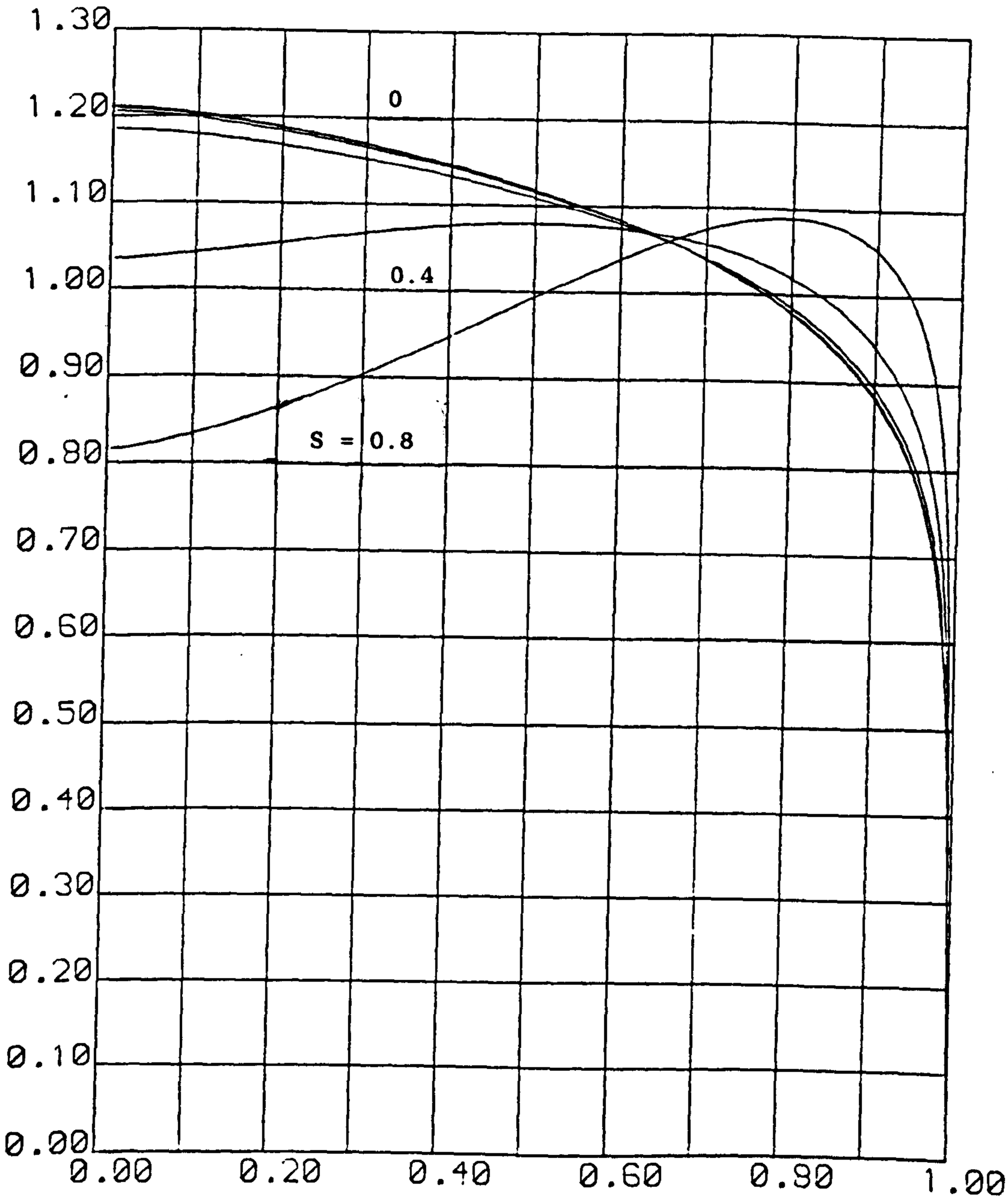

Figure 5.18: Axial velocities obtained using the similarity theory at Re = 100000 with Method B rough

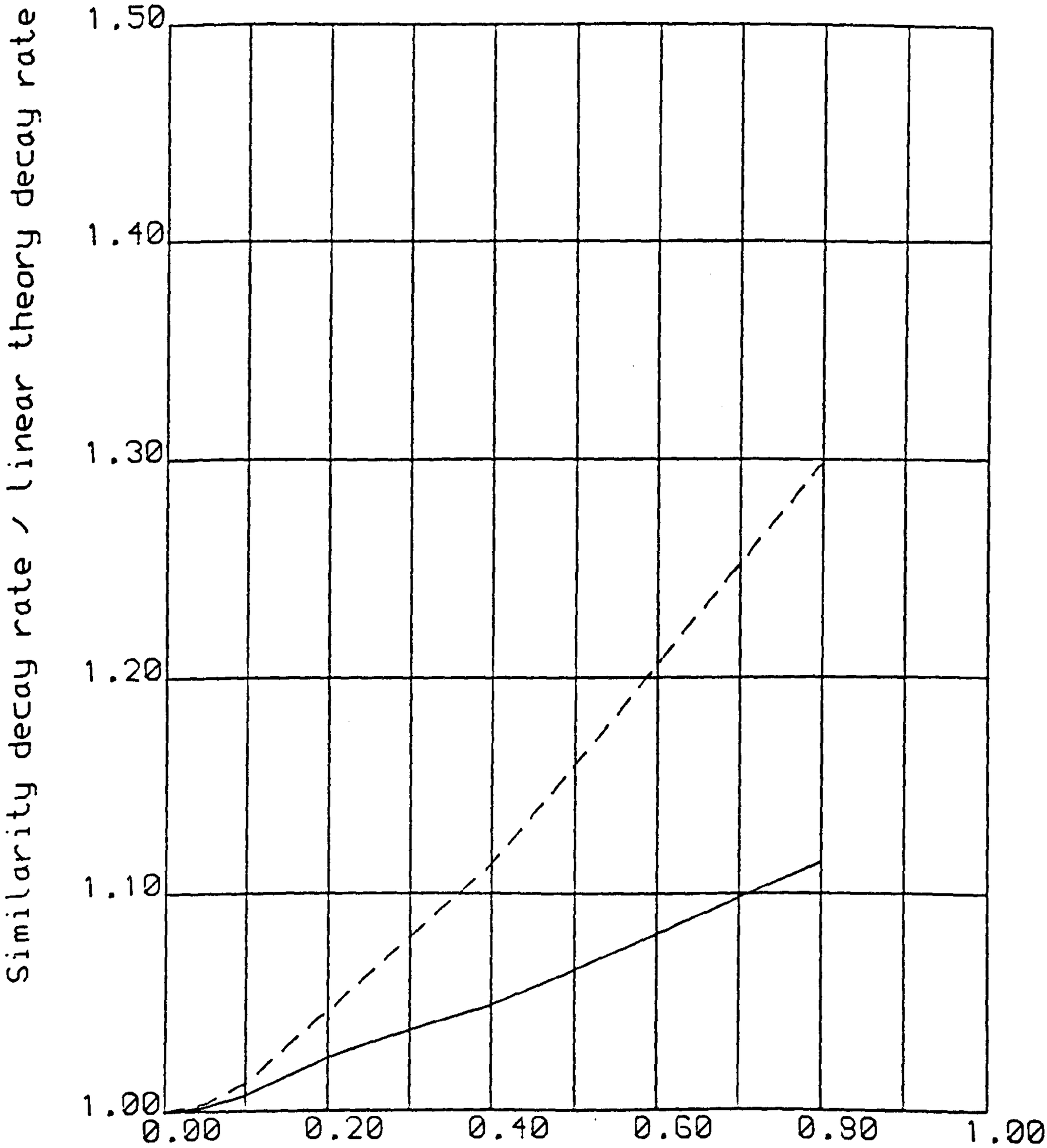

Figure 5.19: Ratio of the decay rates of the similarity and linear theory at Re = 100000

_____ Method B smooth

_ _ _ _ Method B rough

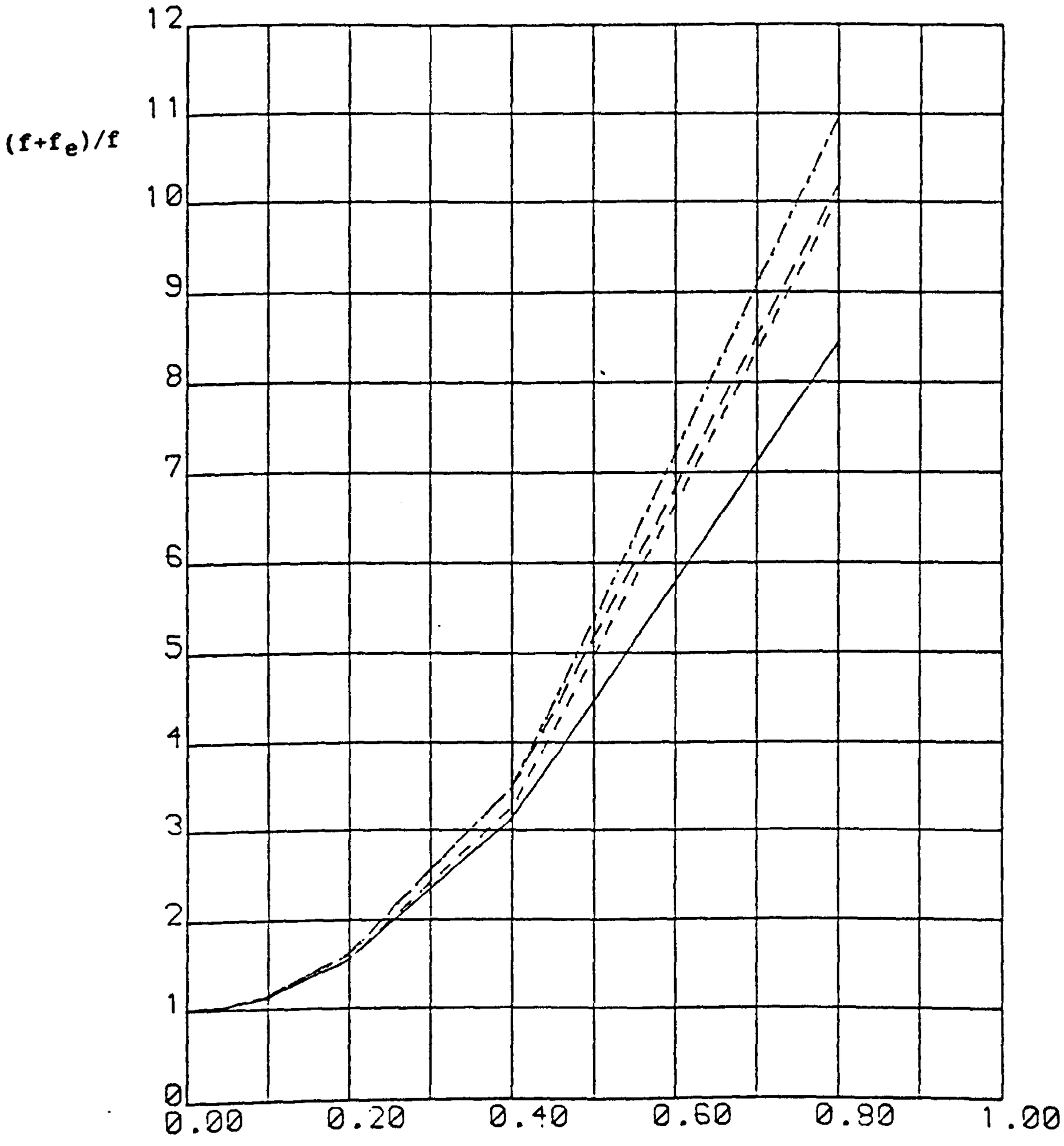

Figure 5.20: Friction Factors at Re = 100000

_____ Similarity theory, Method B smooth

_ _ _ _ Similarity theory, Method B rough

_ _ _ _ _ Second order linear theory, Method B smooth

_ _ _ _ _ _ Second order linear theory, Method B rough

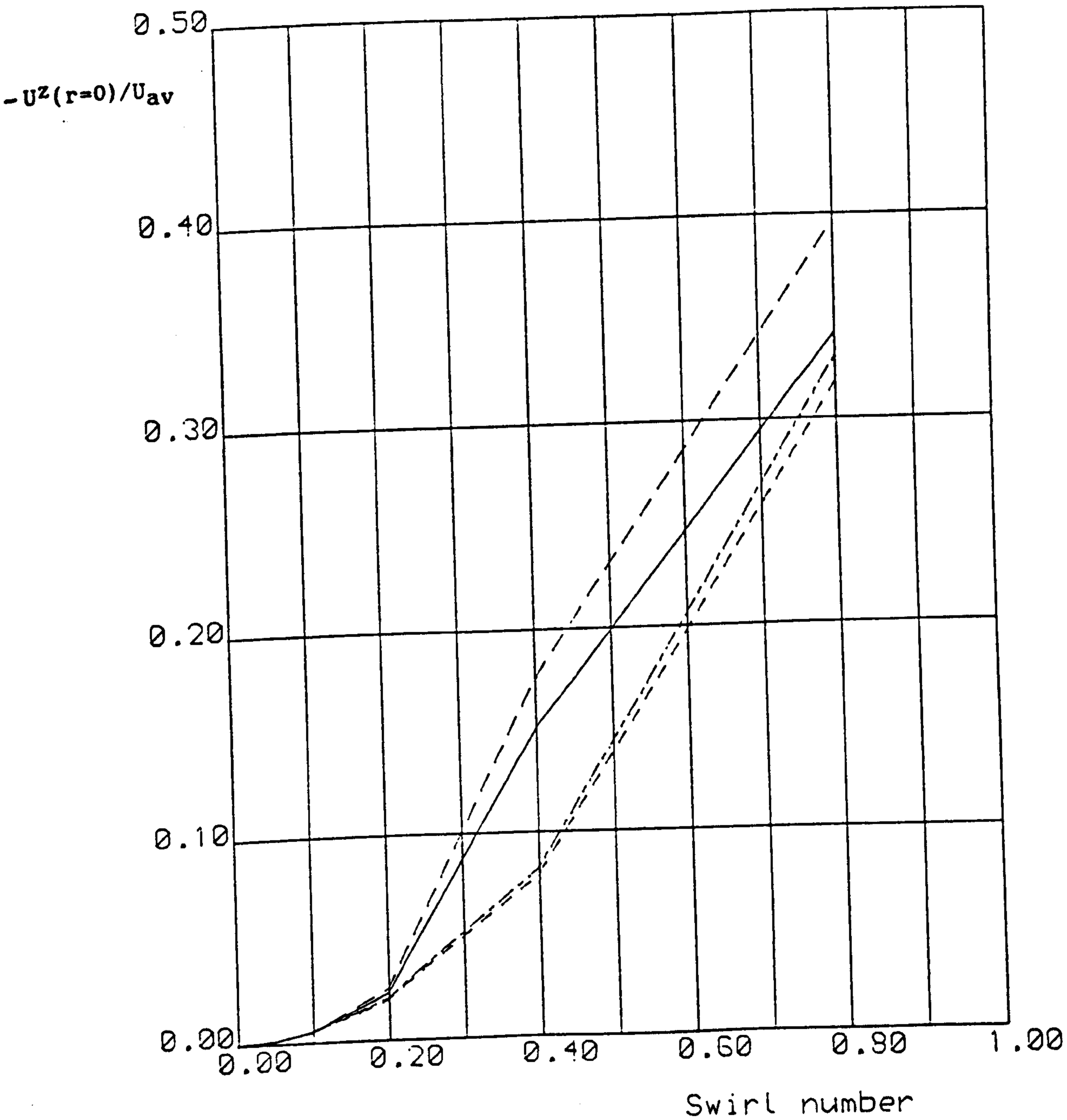

Figure 5.21: Axial velocity on r=0 at Re = 100000

———— Similarity theory, Method B smooth

– – – – Similarity theory, Method B rough

– – – – – Second order linear theory, Method B smooth

– – – – – – Second order linear theory, Method B rough

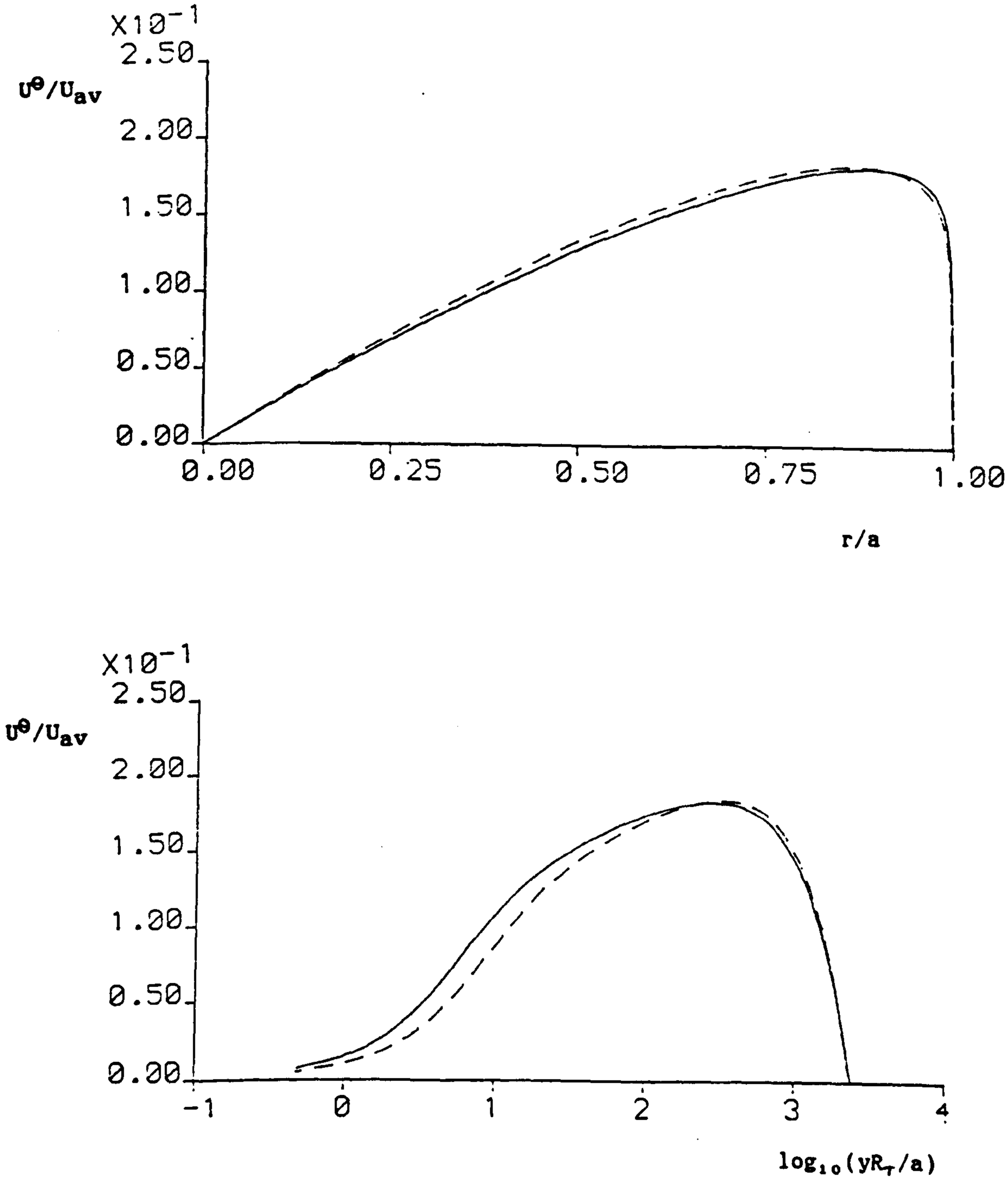

Figure 5.22: Tangential velocity profiles at Re = 100000 and S = 0.1, using Method B smooth

———— Similarity theory

– – – – Linear theory

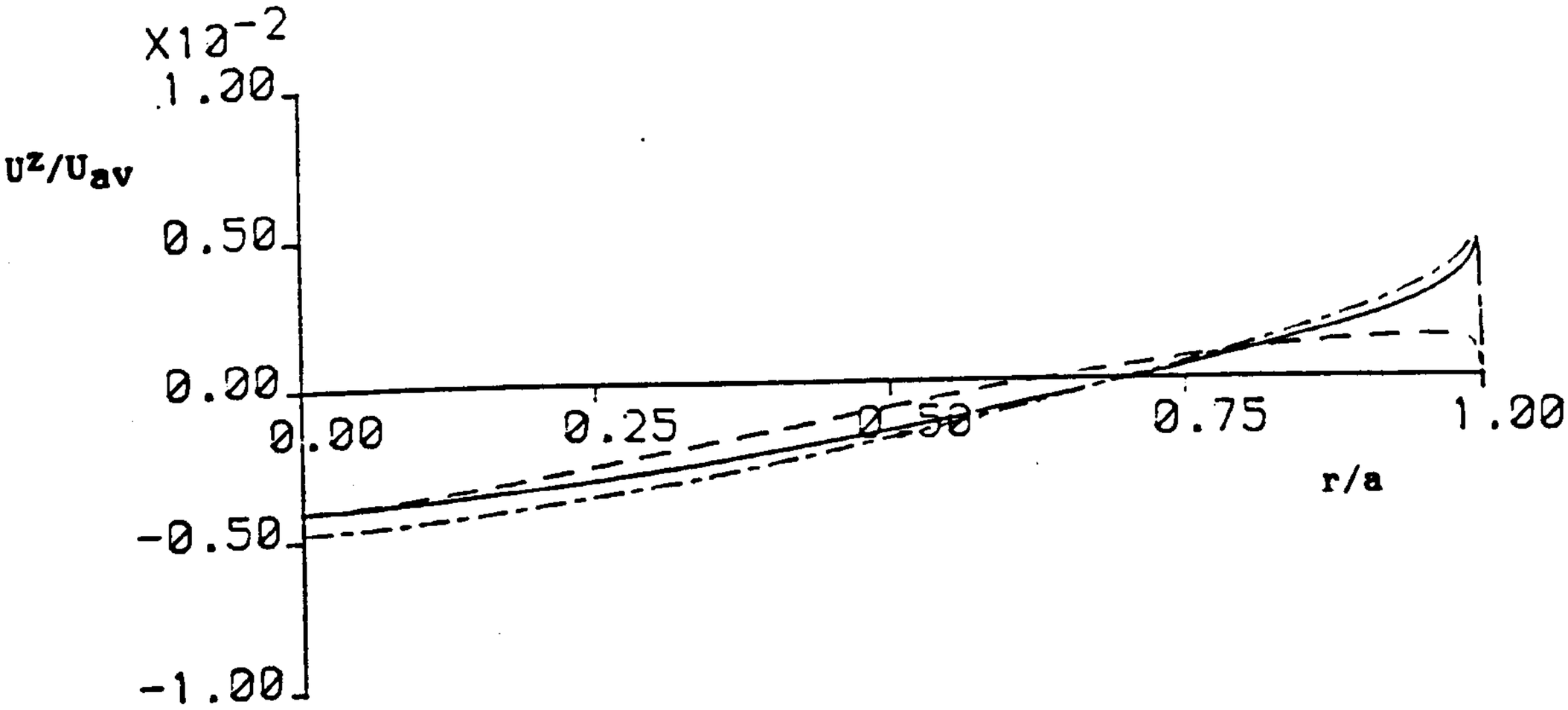

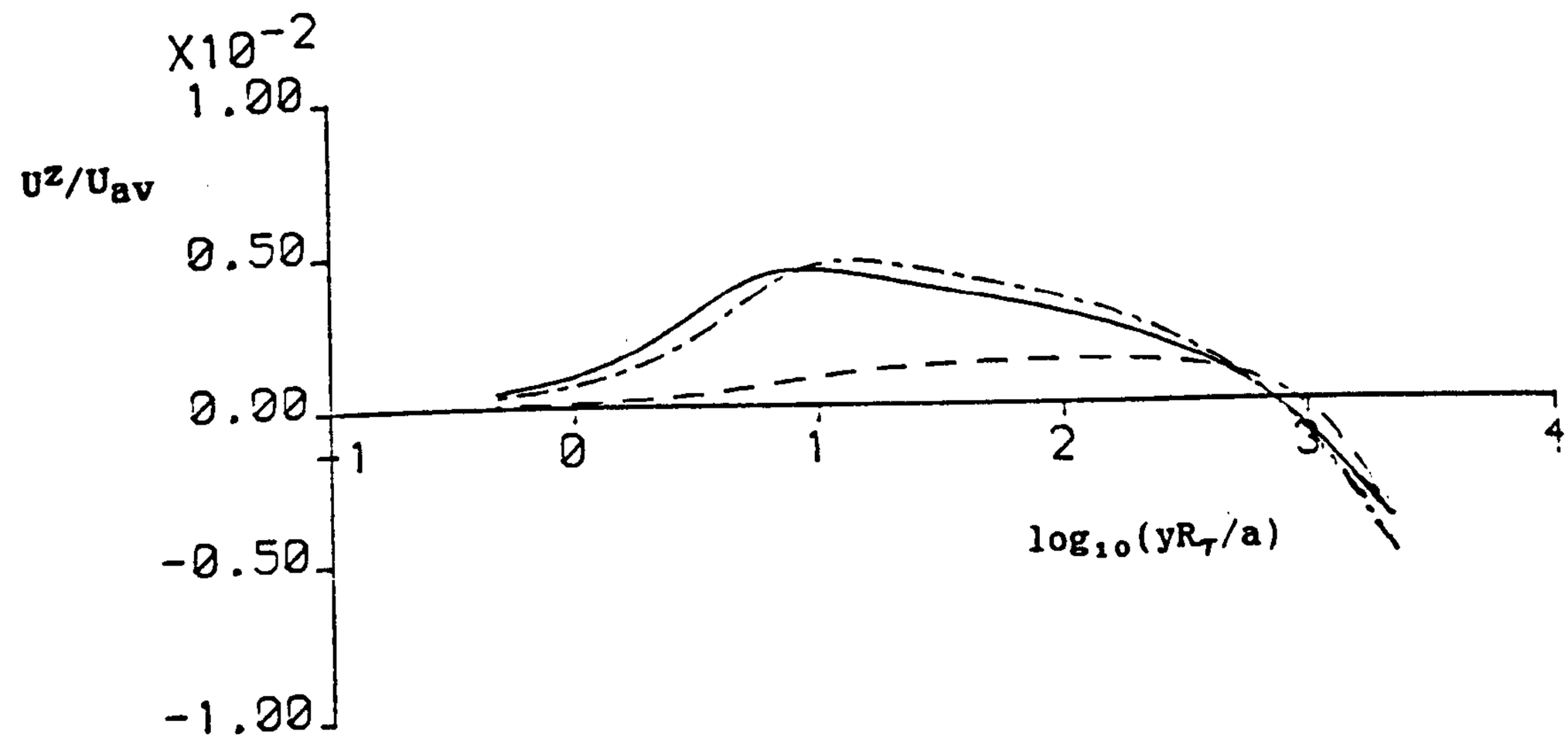

Figure 5.23: Axial velocity profiles at Re = 100000 and S = 0.1, using Method B smooth

———— Similarity theory

— — — — Linear theory

—·—·— Second-order linear theory

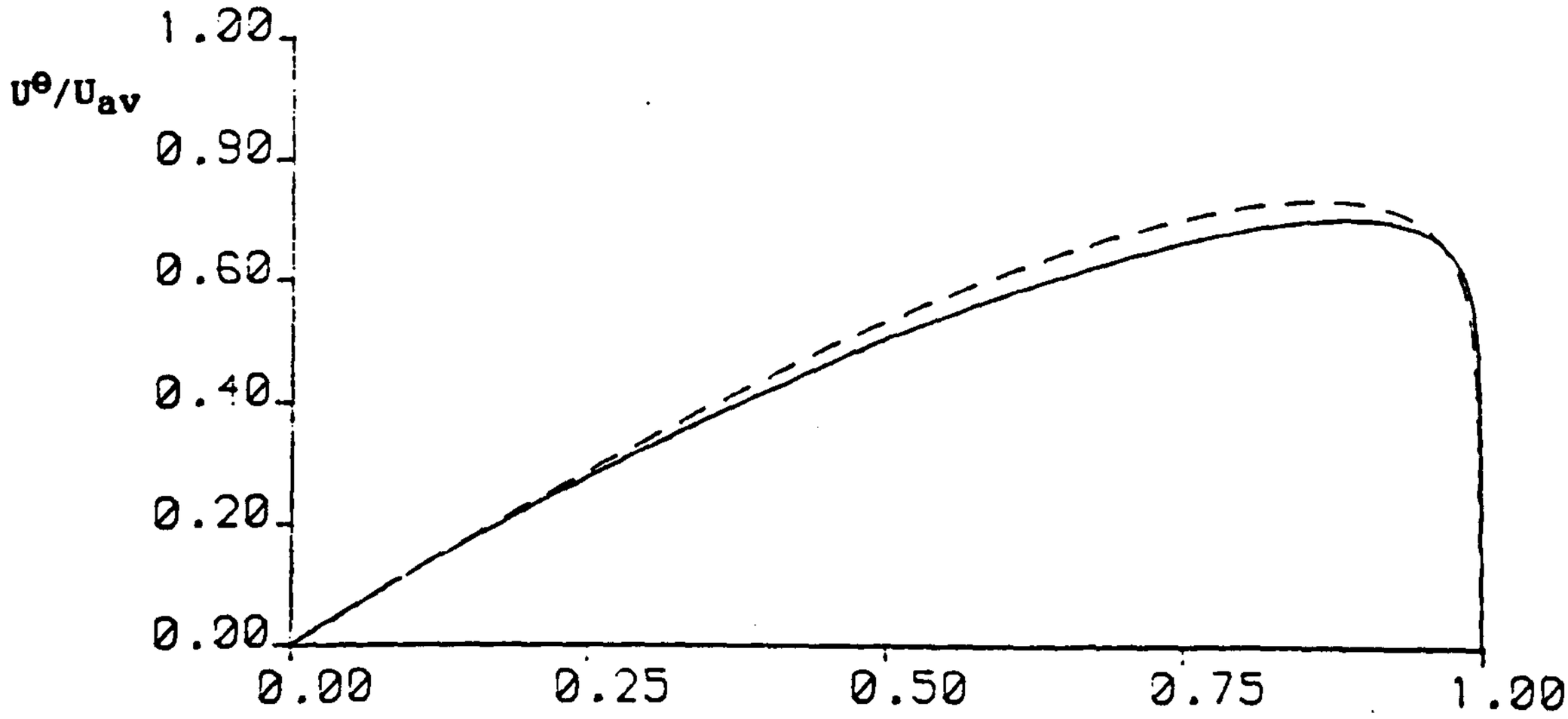

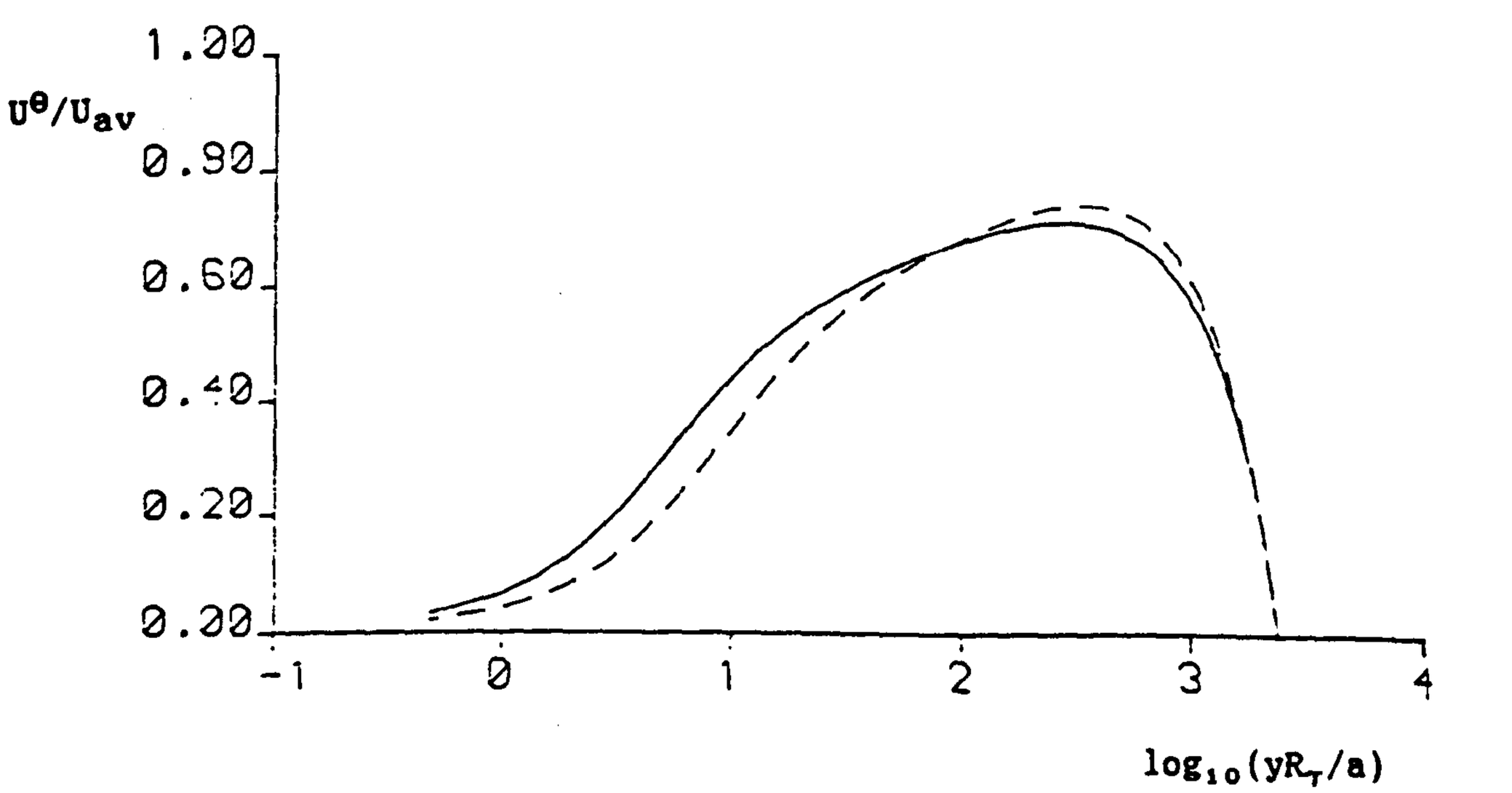

Figure 5.24: Tangential velocity profiles at Re = 100000 and S = 0.4, using Method B smooth

———— Similarity theory

– – – – Linear theory

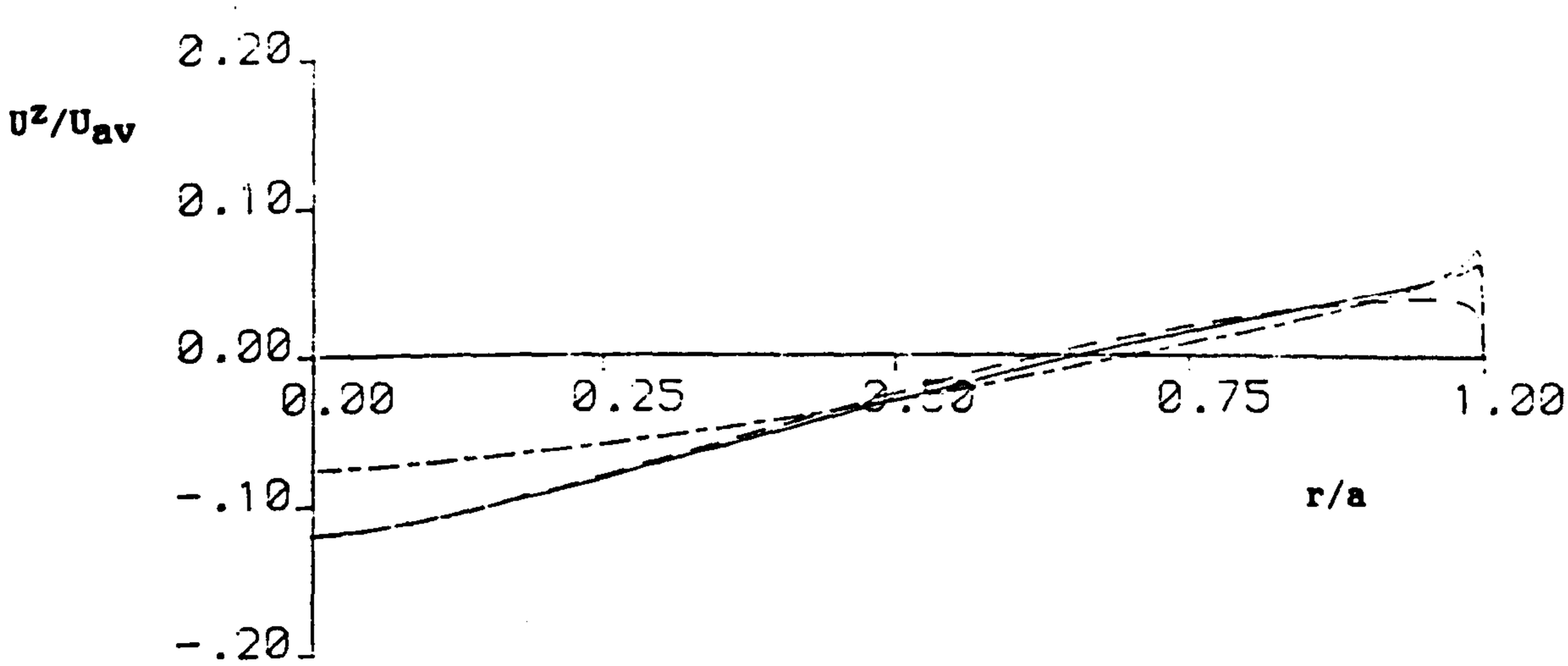

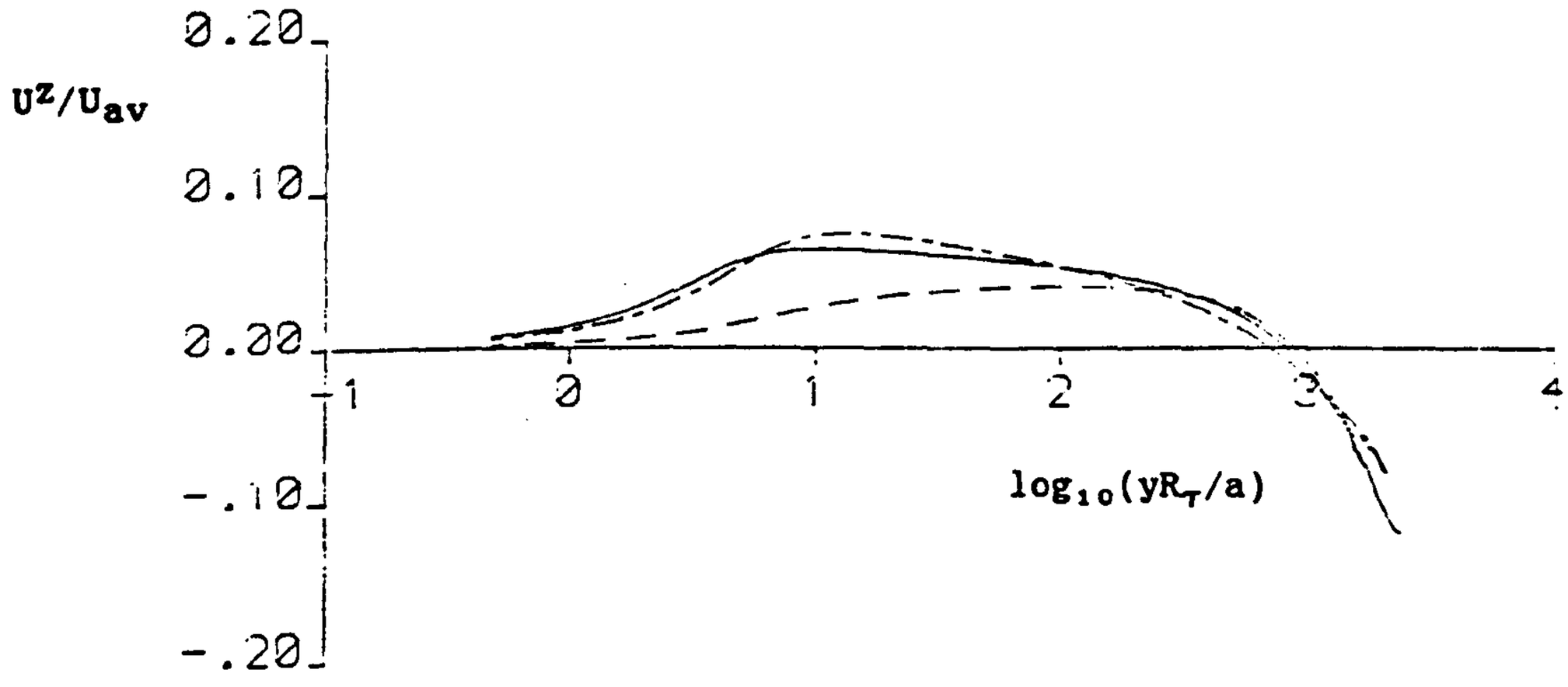

Figure 5.25: Axial velocity profiles

at Re = 100000 and S = 0.4, using Method 3 smooth

———— Similarity theory

— — — — Linear theory

—— —— Second-order linear theory

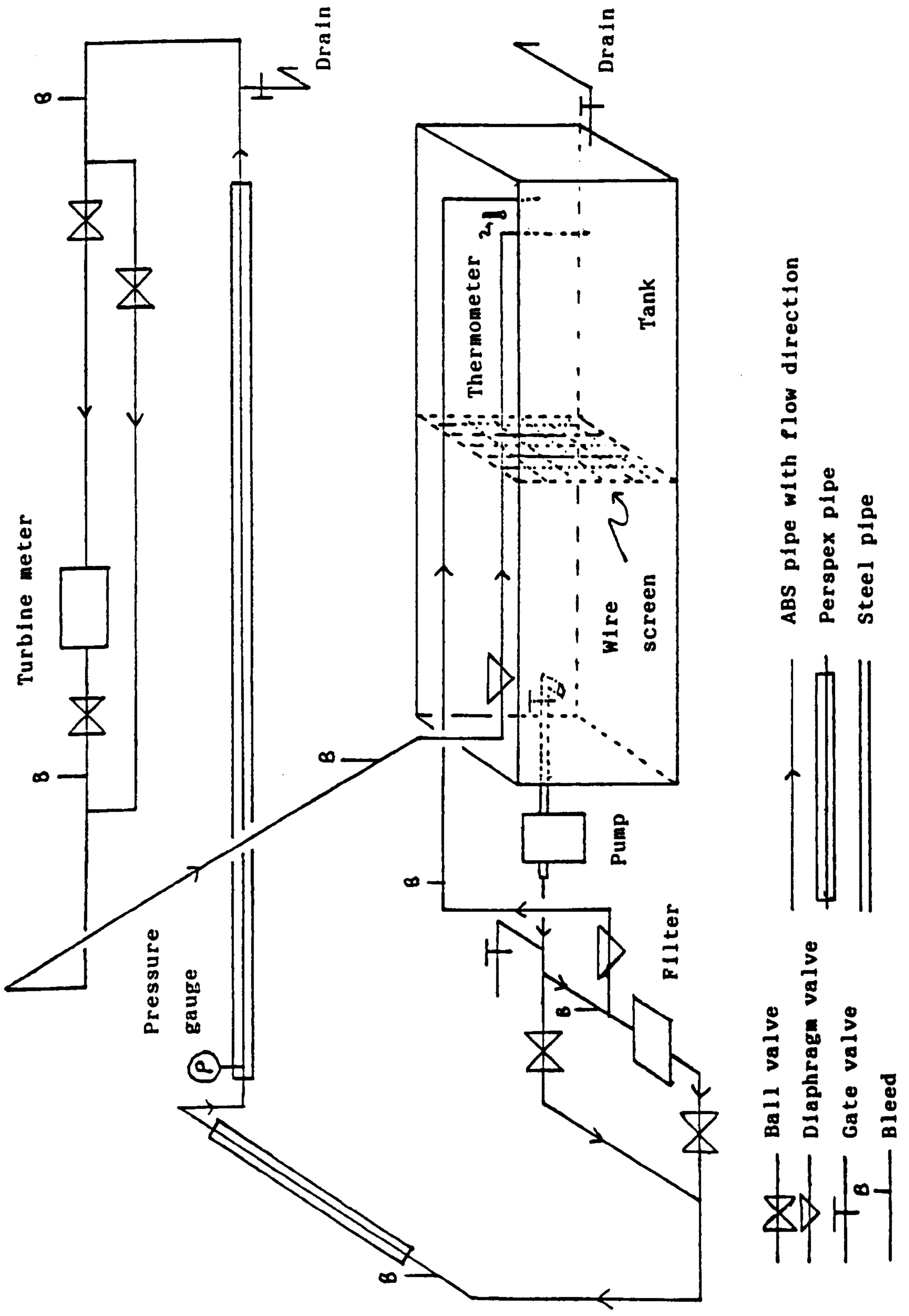

Figure 6.1: Schematic diagram of the flow loop

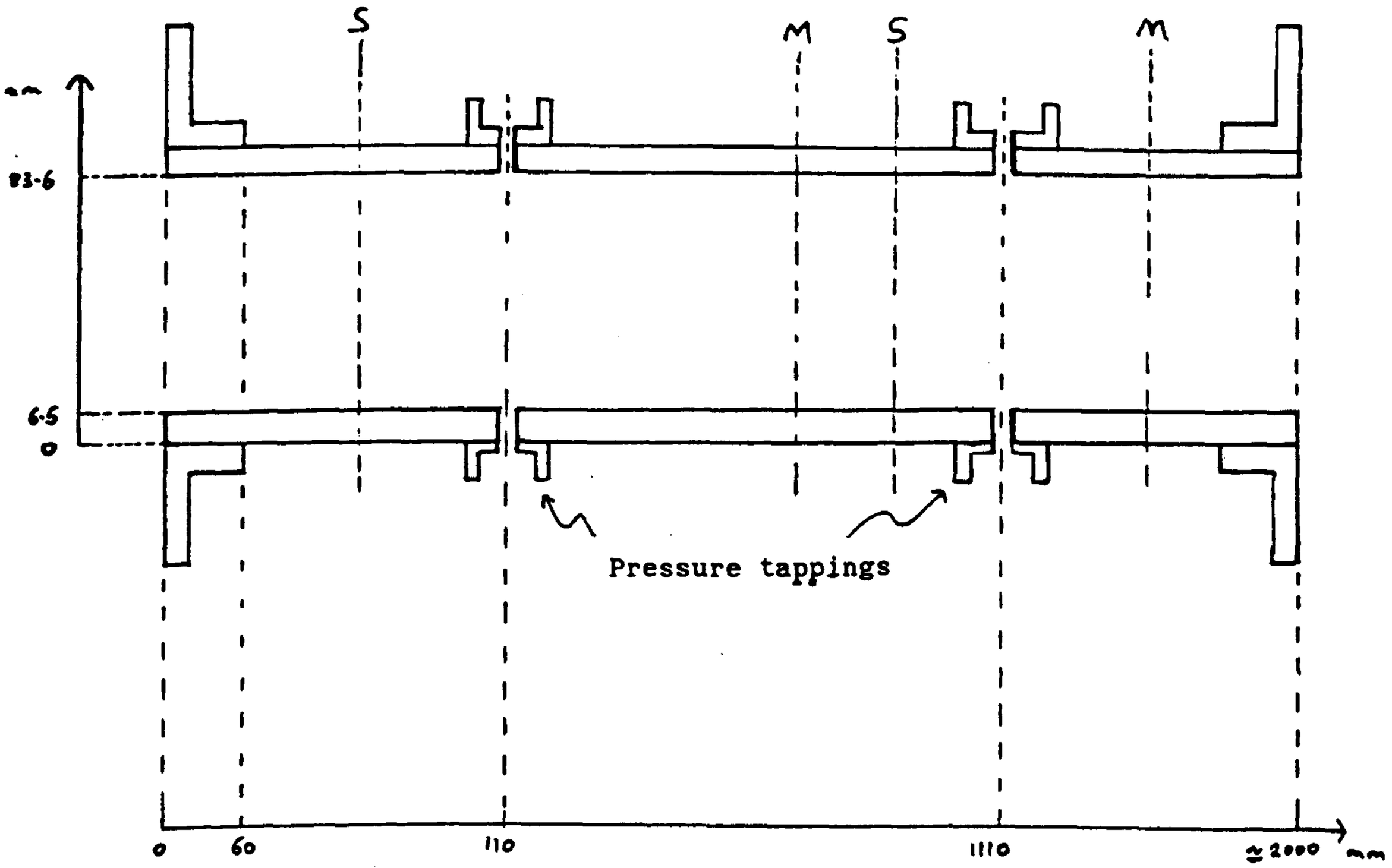

S Positions of support stands

M Positions where velocity measurements could be made

Figure 6.2: Detail of the construction of a test section

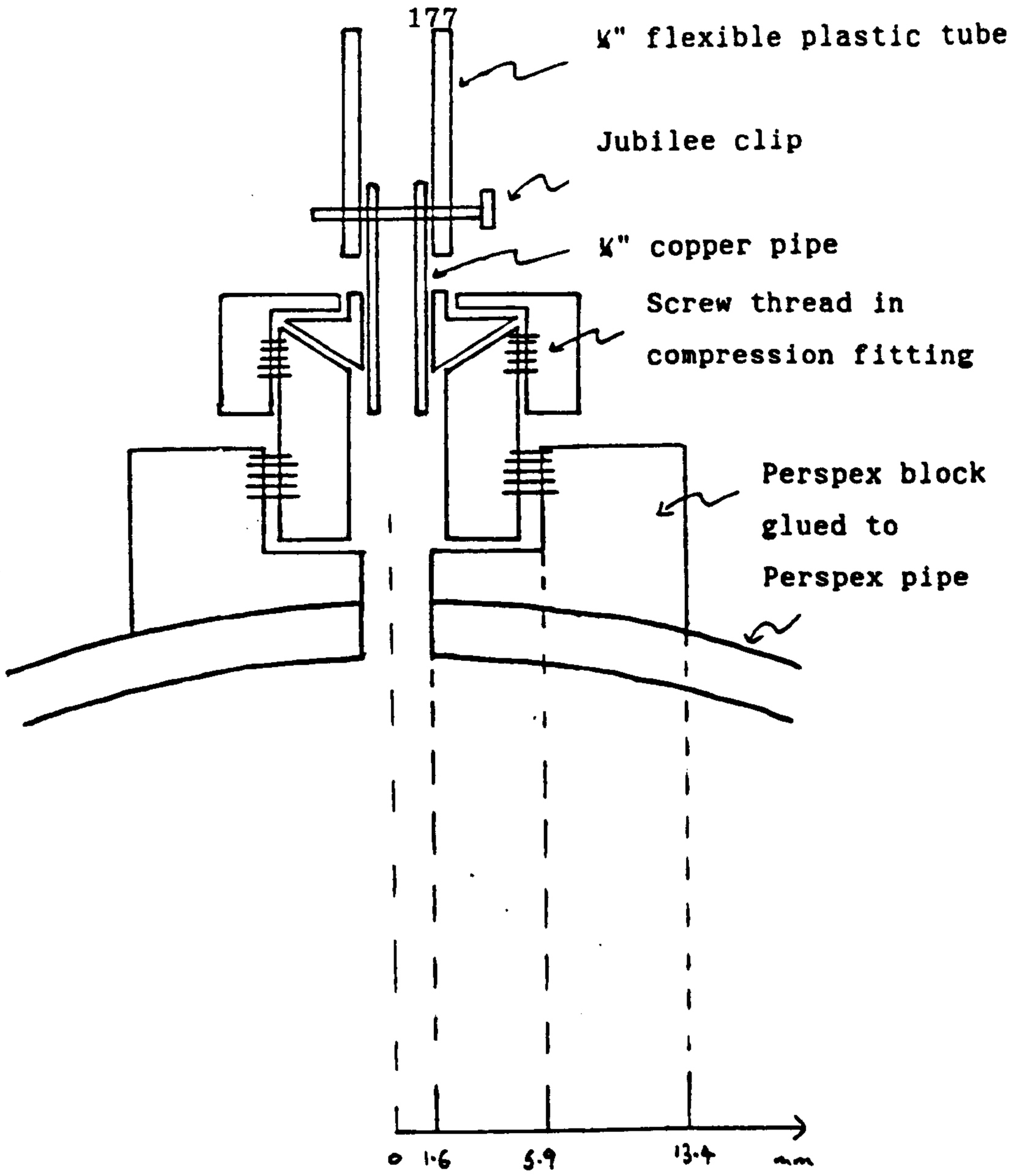

Figure 6.3: Detail of a pressure tapping

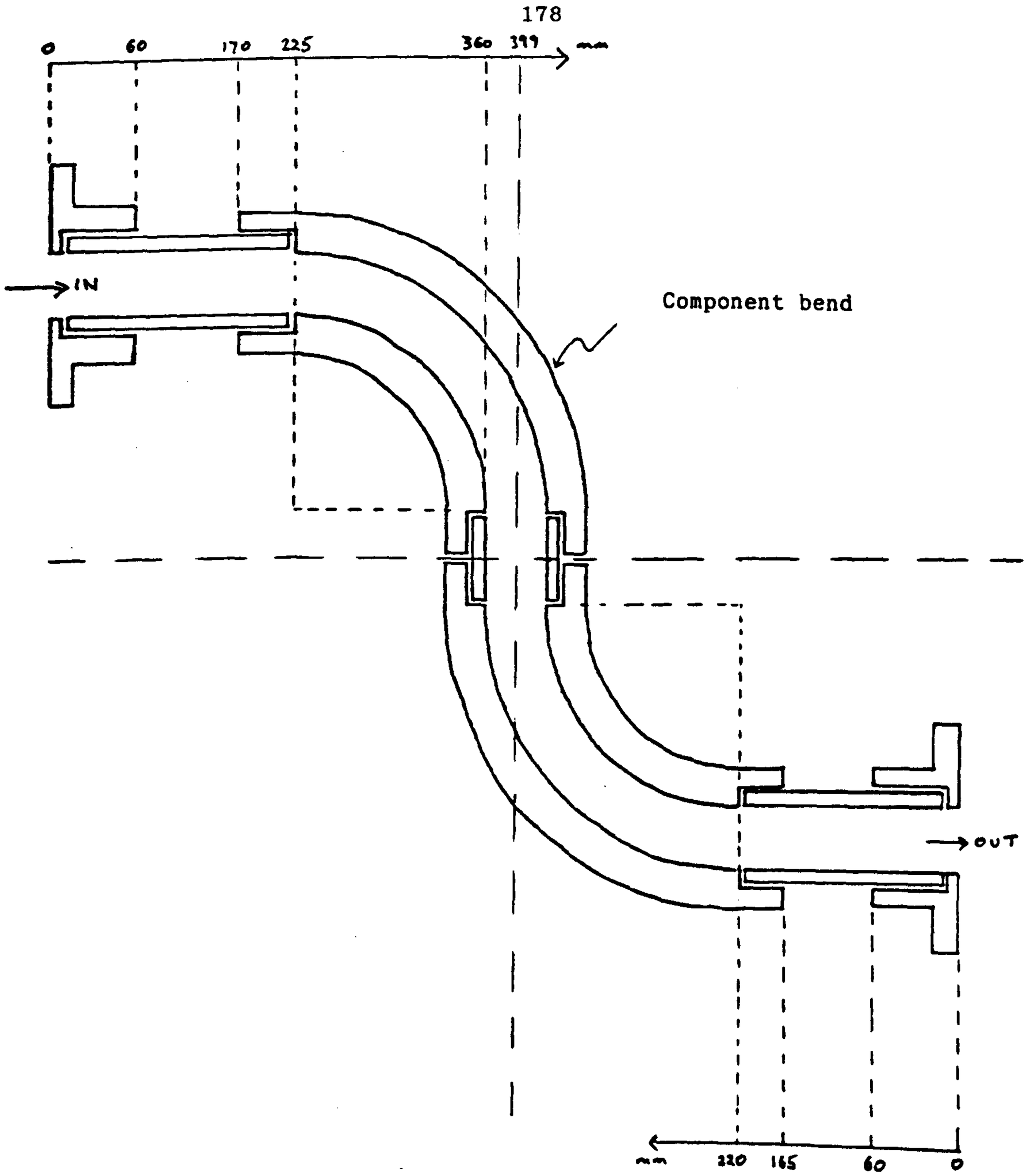

Figure 6.4: Detail of the construction of the double bend

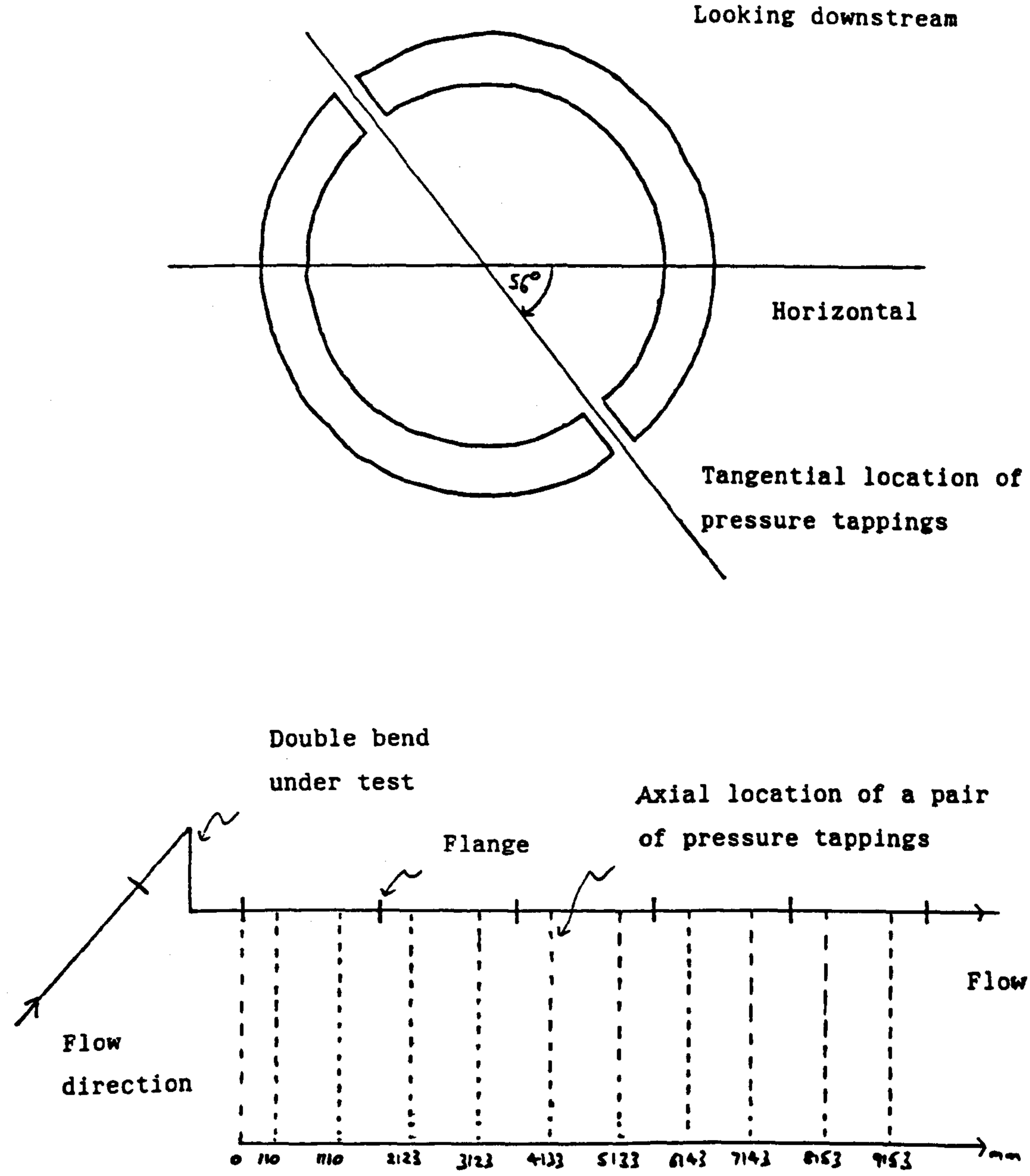

Figure 6.5: Locations of the pressure tappings

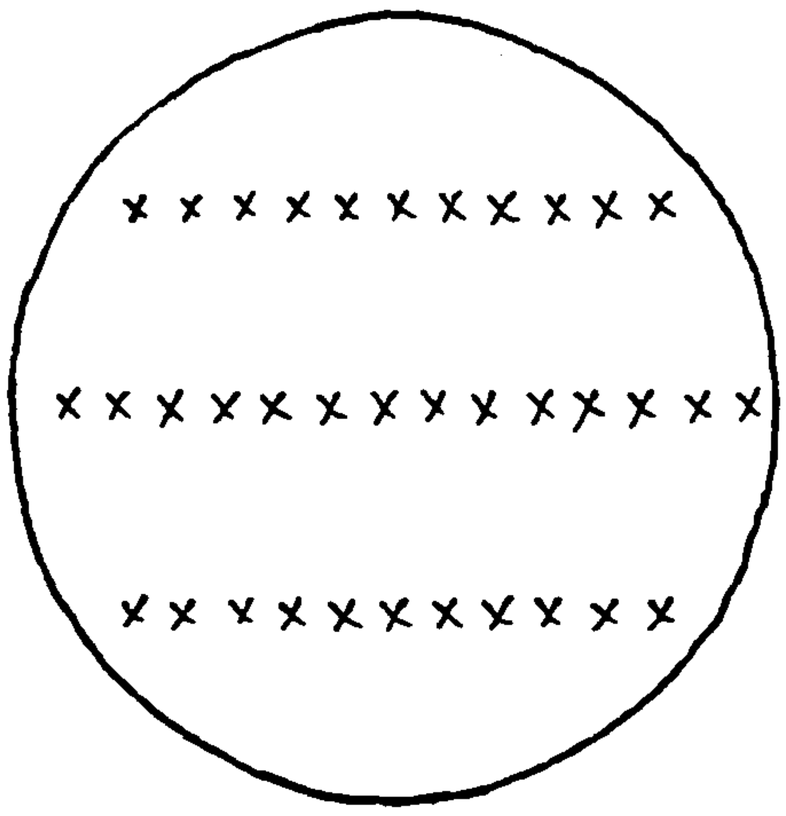

Figure 6.6: Postions of the axial velocity measurements.

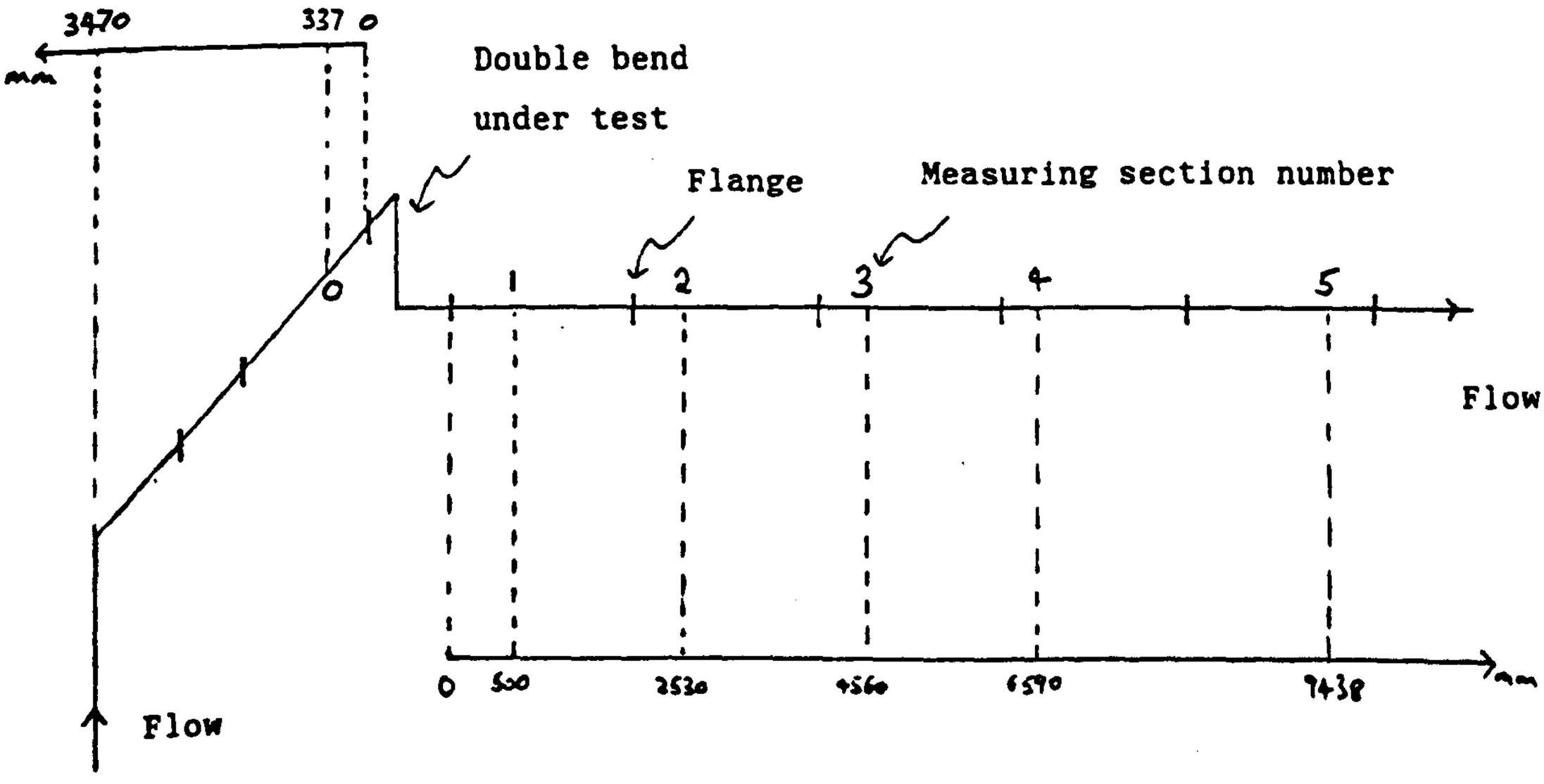

Figure 6.7: Locations of the velocity measurement sections

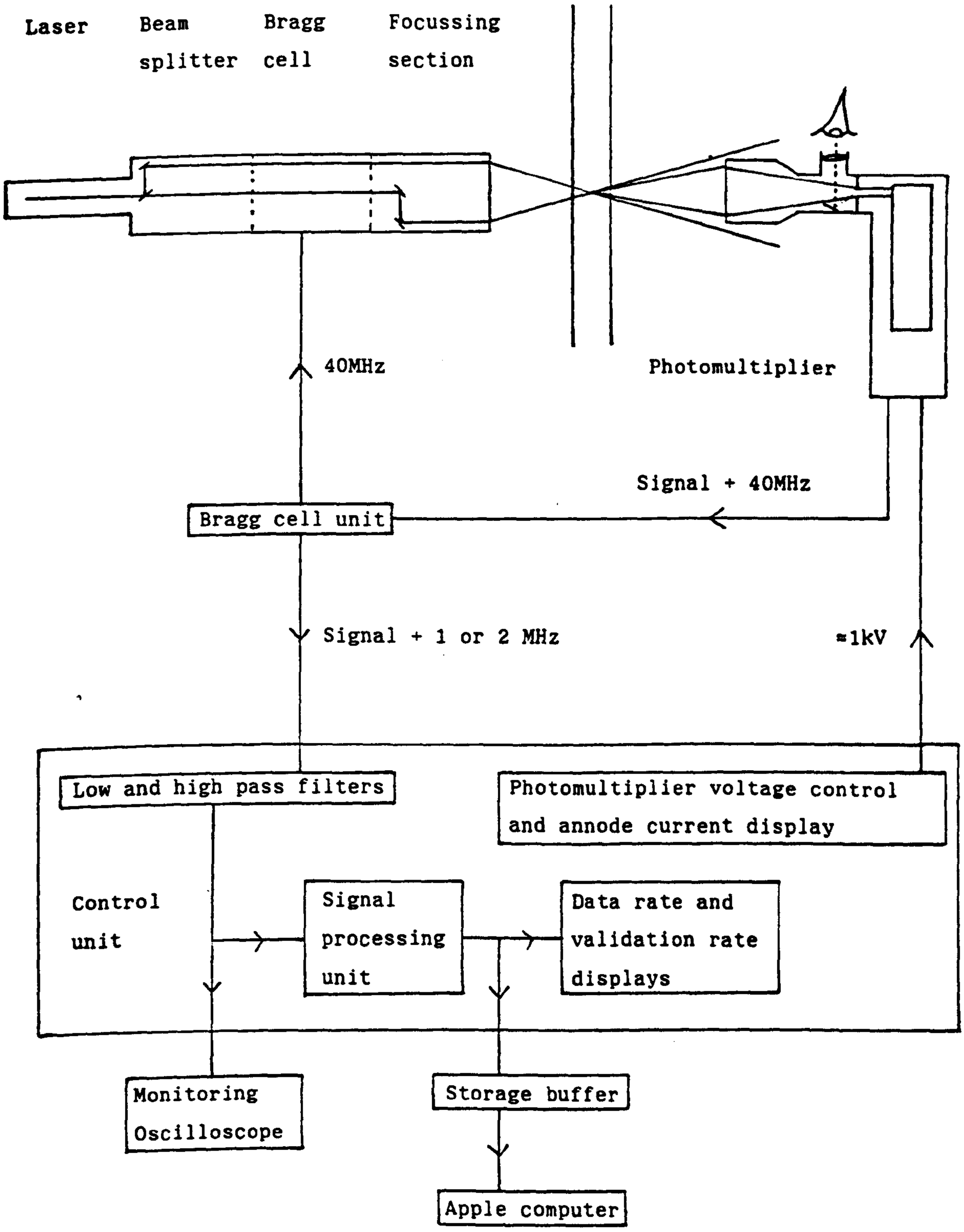

Figure 6.8: Schematic diagram of the LDA apparatus

Screw holes for fastening the two halves of the box together

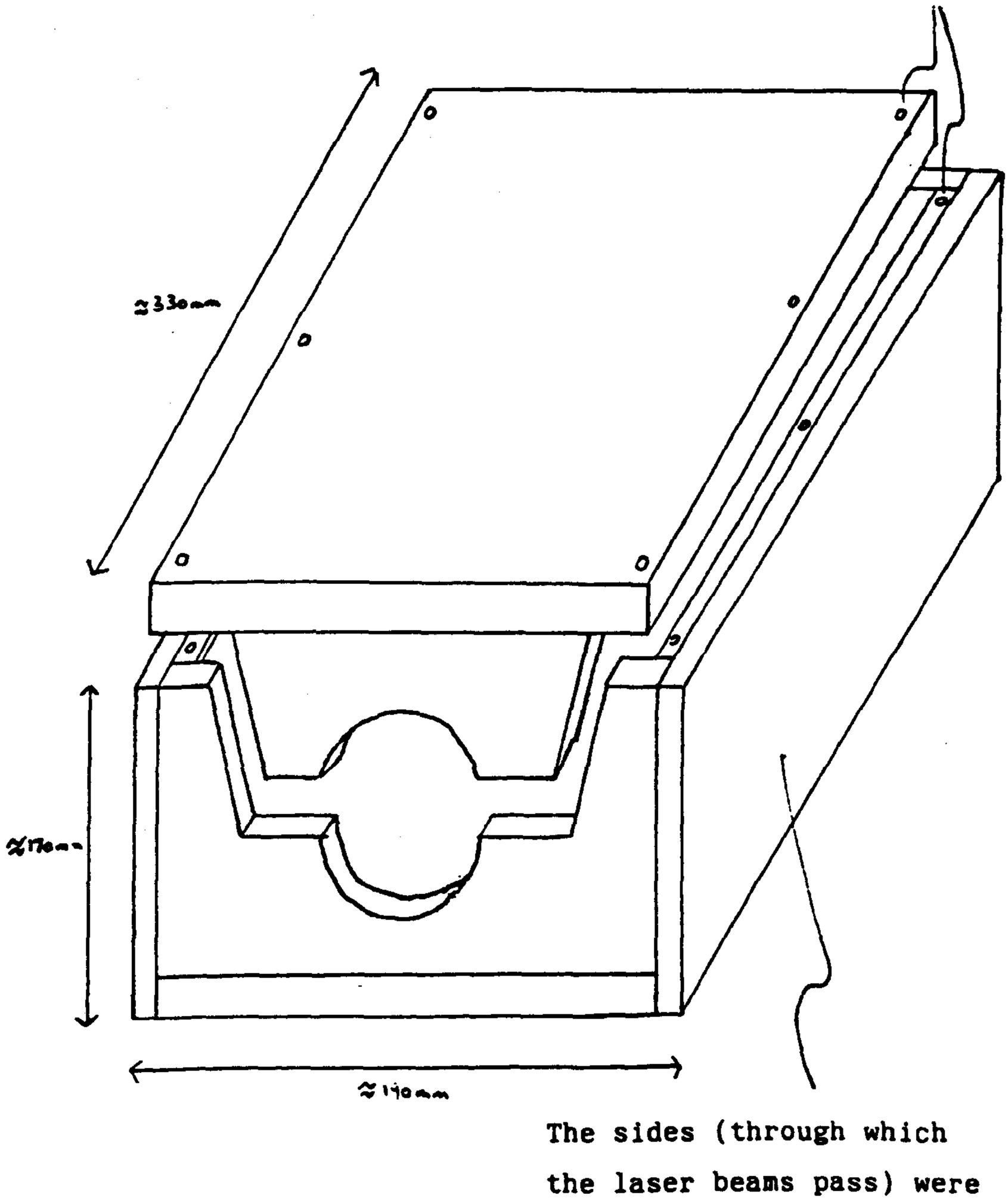

The sides (through which the laser beams pass) were 5mm thick. All other pieces were 13mm thick.

Figure 6.9: Detail of the construction of the perspex box

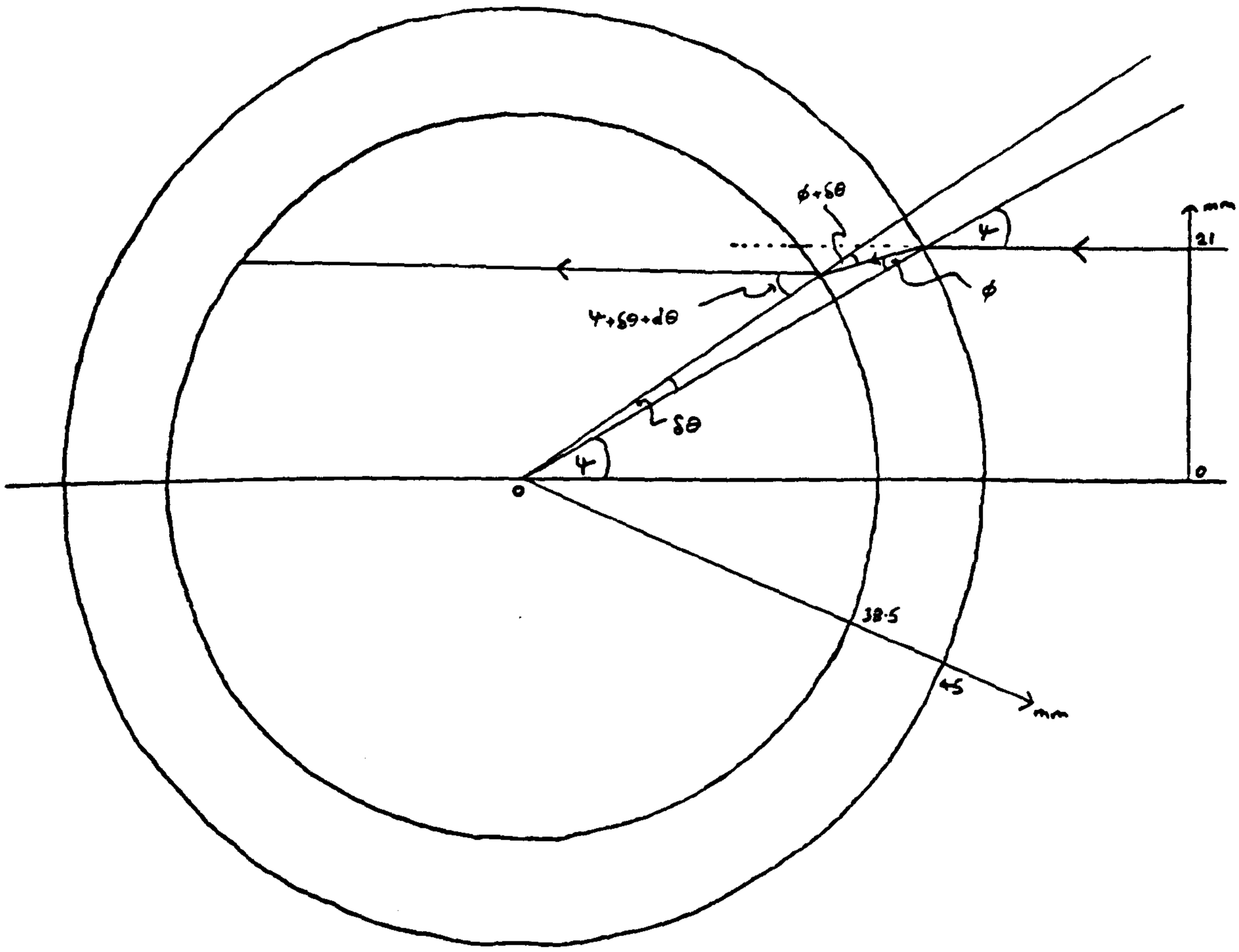

Figure 6.10: Definition sketch for considering the effects of refraction when measuring axial velocity on the offset chords

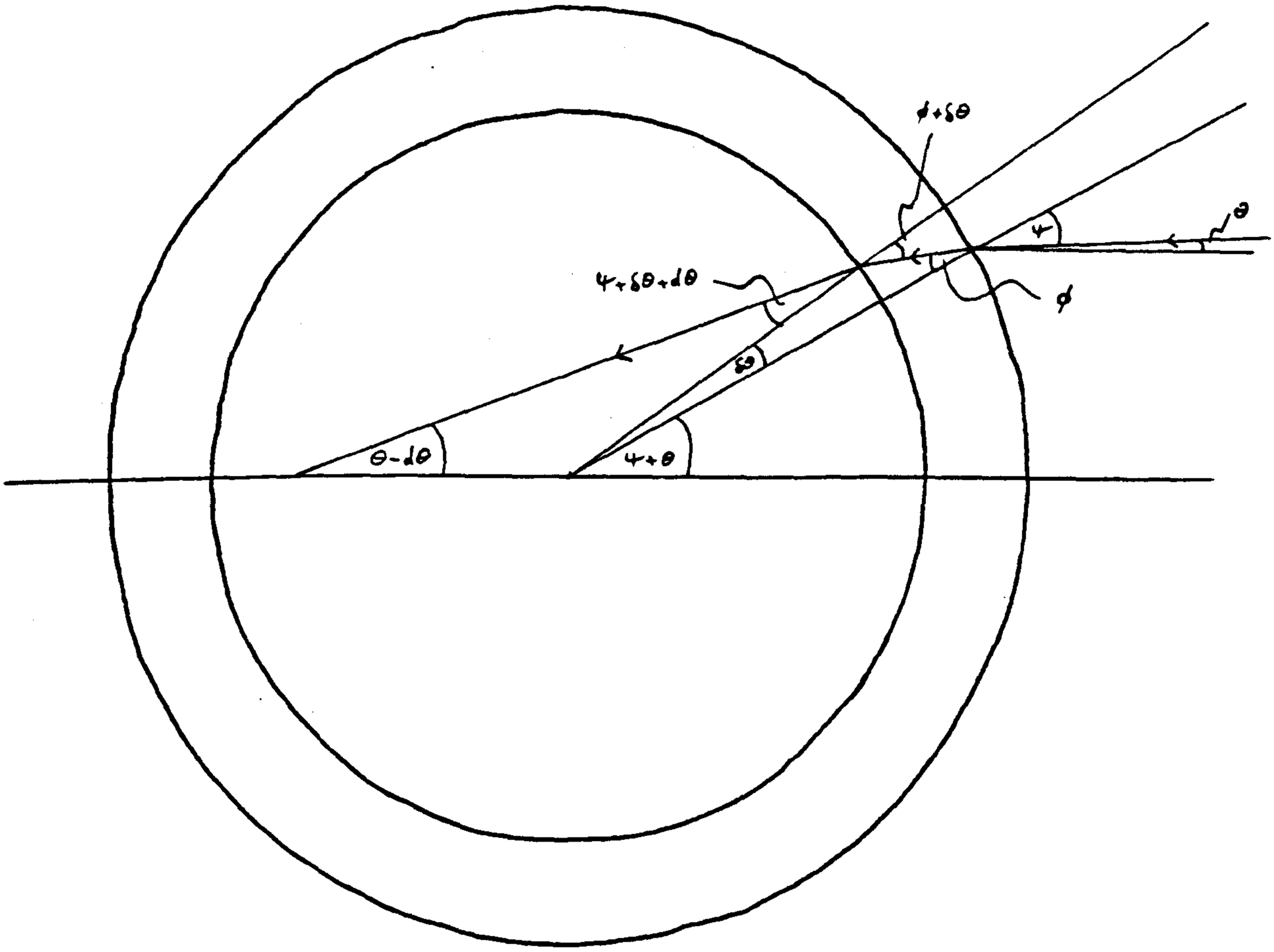

Figure 6.11: Definition sketch for considering the effects of refraction when measuring tangential velocity

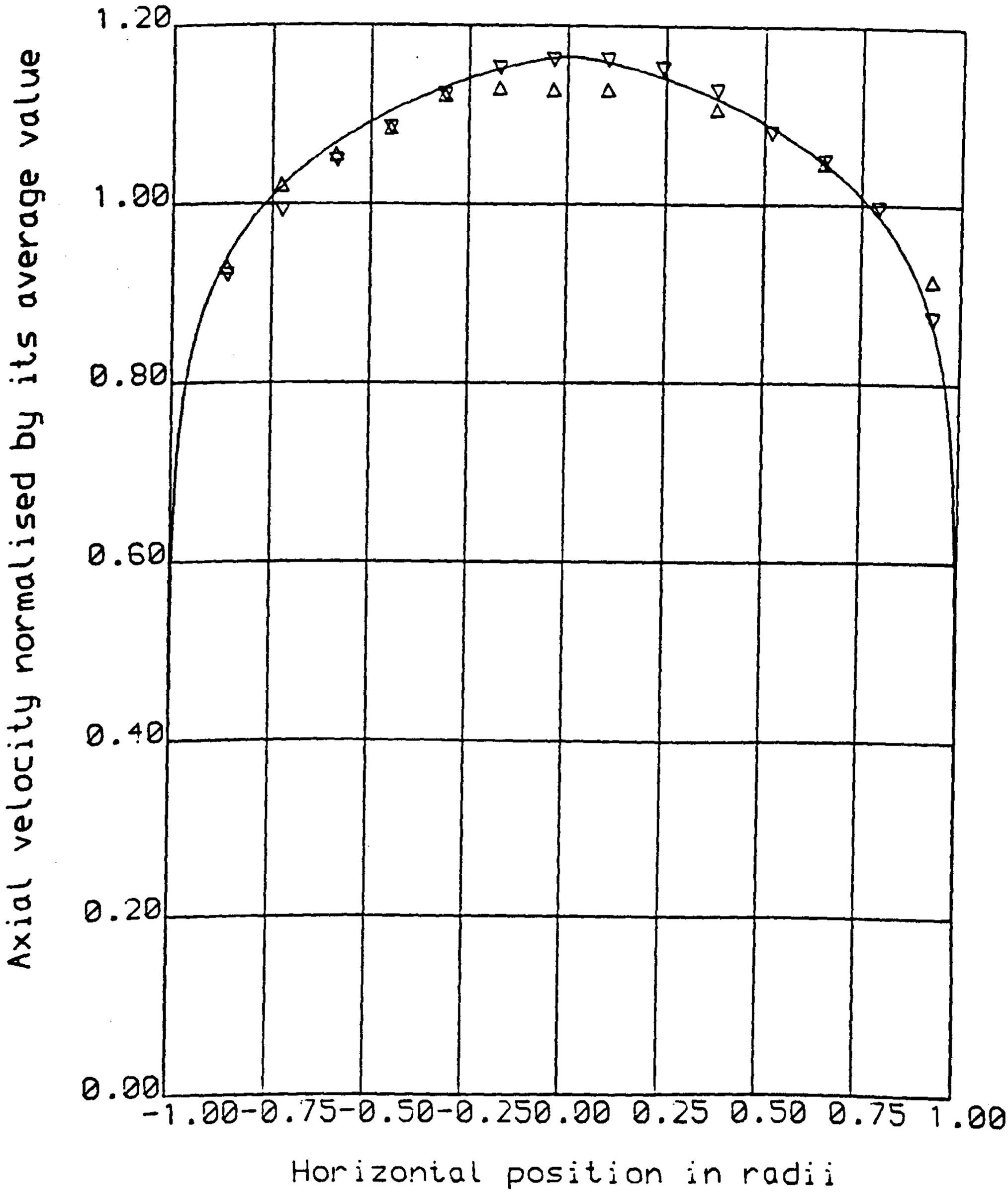

Figure 6.12: Axial velocity measurements on sections 0 and 5 at Re = 413000

——— Theory △ Section 0 ▽ Section 5

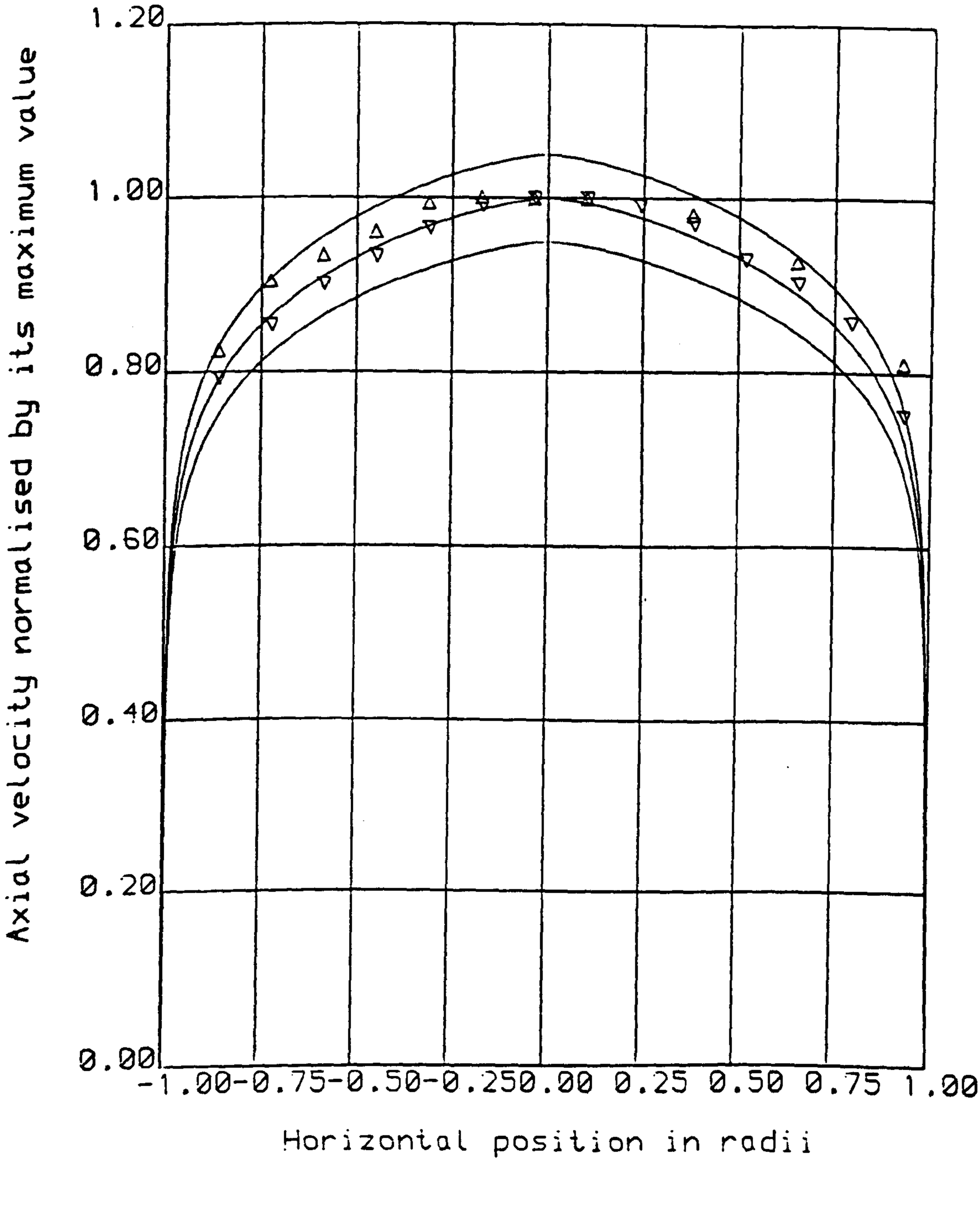

Figure 6.13: Axial velocity measurements on sections 0 and 5 at Re = 413000

——— Theory △ Section 0 ▽ Section 5

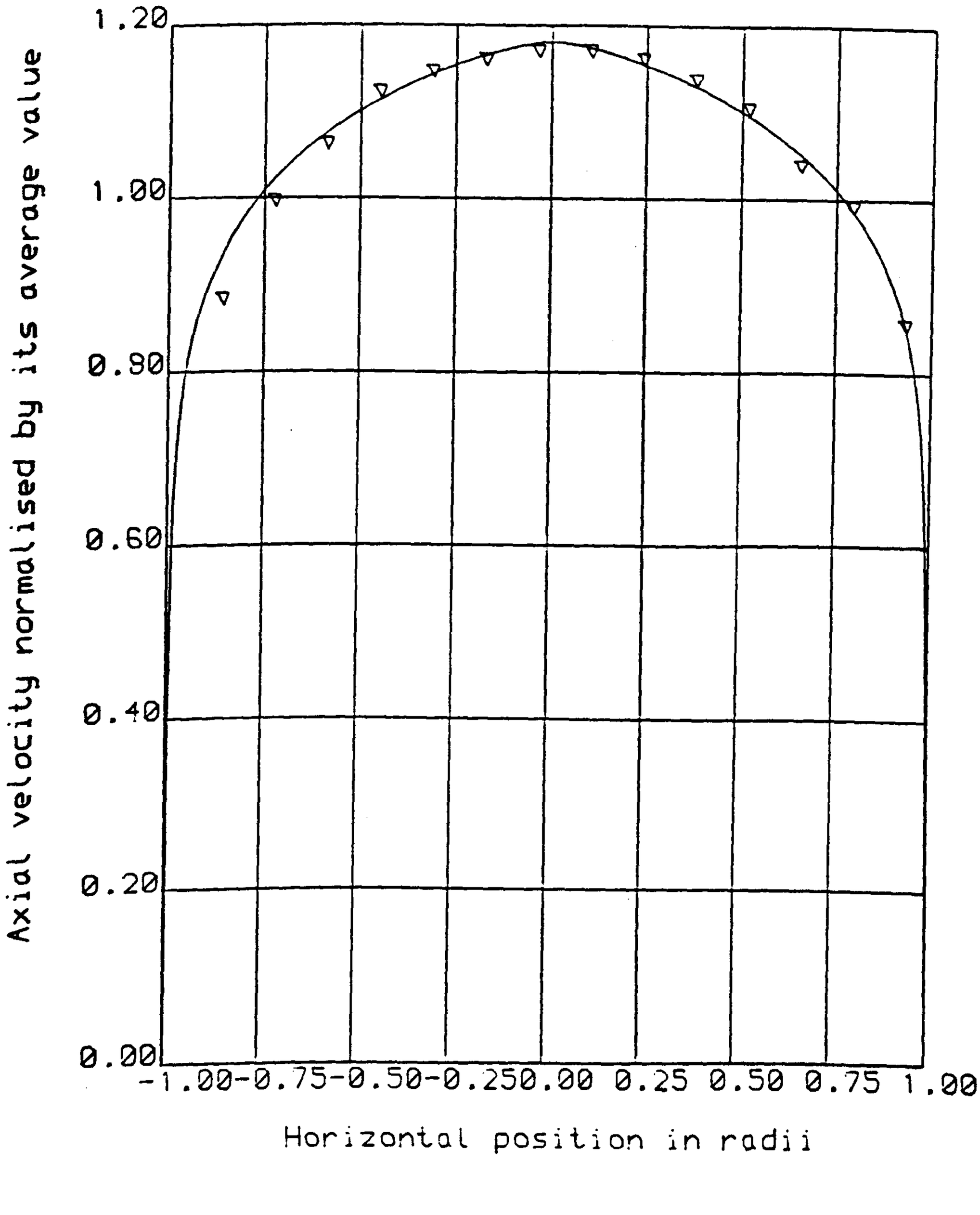

Figure 6.14: Axial velocity measurements on section 5 at Re = 165000

_____ Theory ▽ Section 5

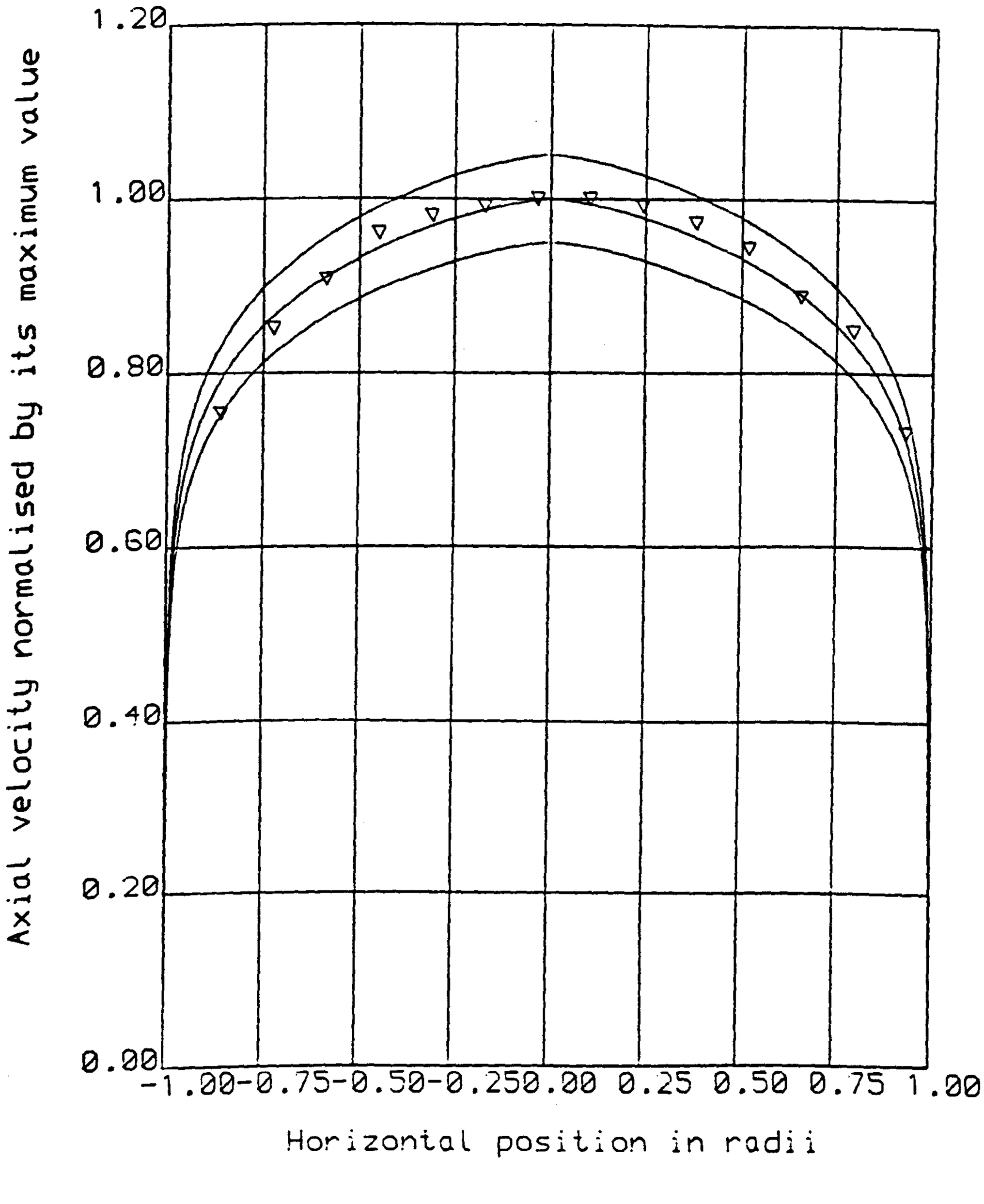

Figure 6.15: Axial velocity measurements on section 5 at Re = 165000

——— Theory ▽ Section 5

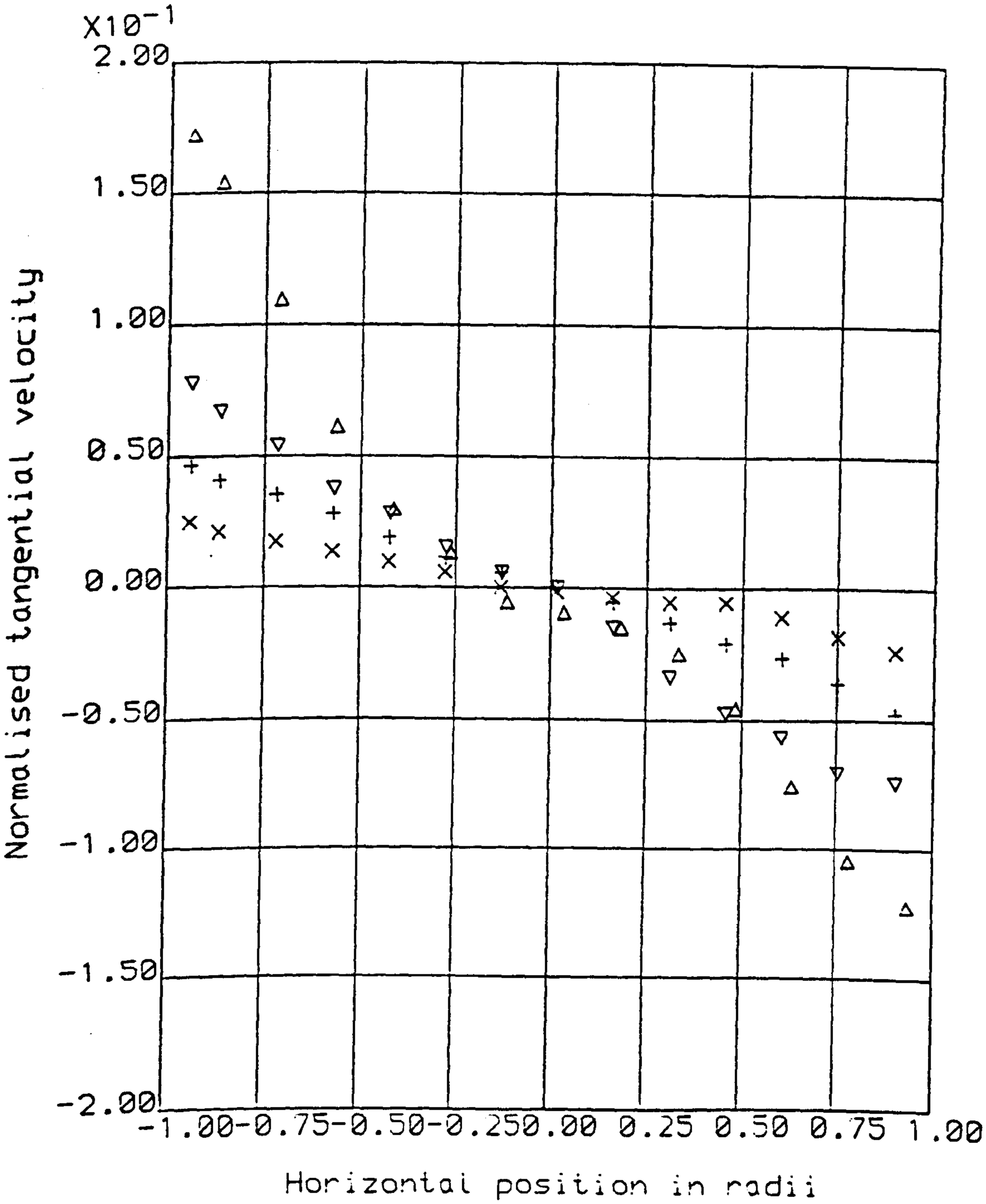

Figure 6.16: Tangential velocity measurements on sections 1 to 4 at Re = 413000

Symbol	△	▽	+	×
Section	1	2	3	4
S	0.071	0.042	0.025	0.013

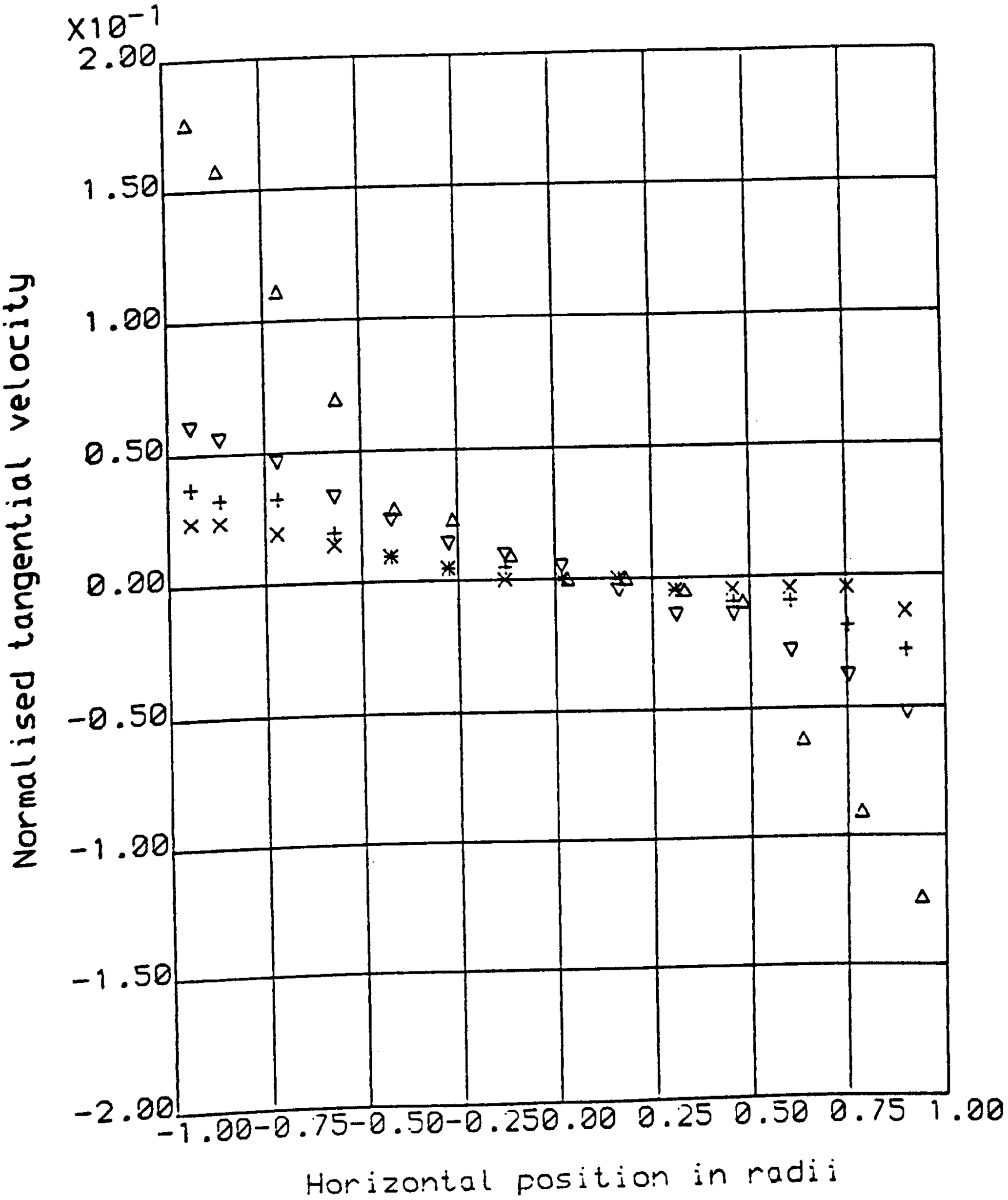

Figure 6.17: Tangential velocity measurements on sections 1 to 4 at Re = 165000

Symbol	△	▽	+	×
Section	1	2	3	4
S	0.069	0.029	0.016	0.009

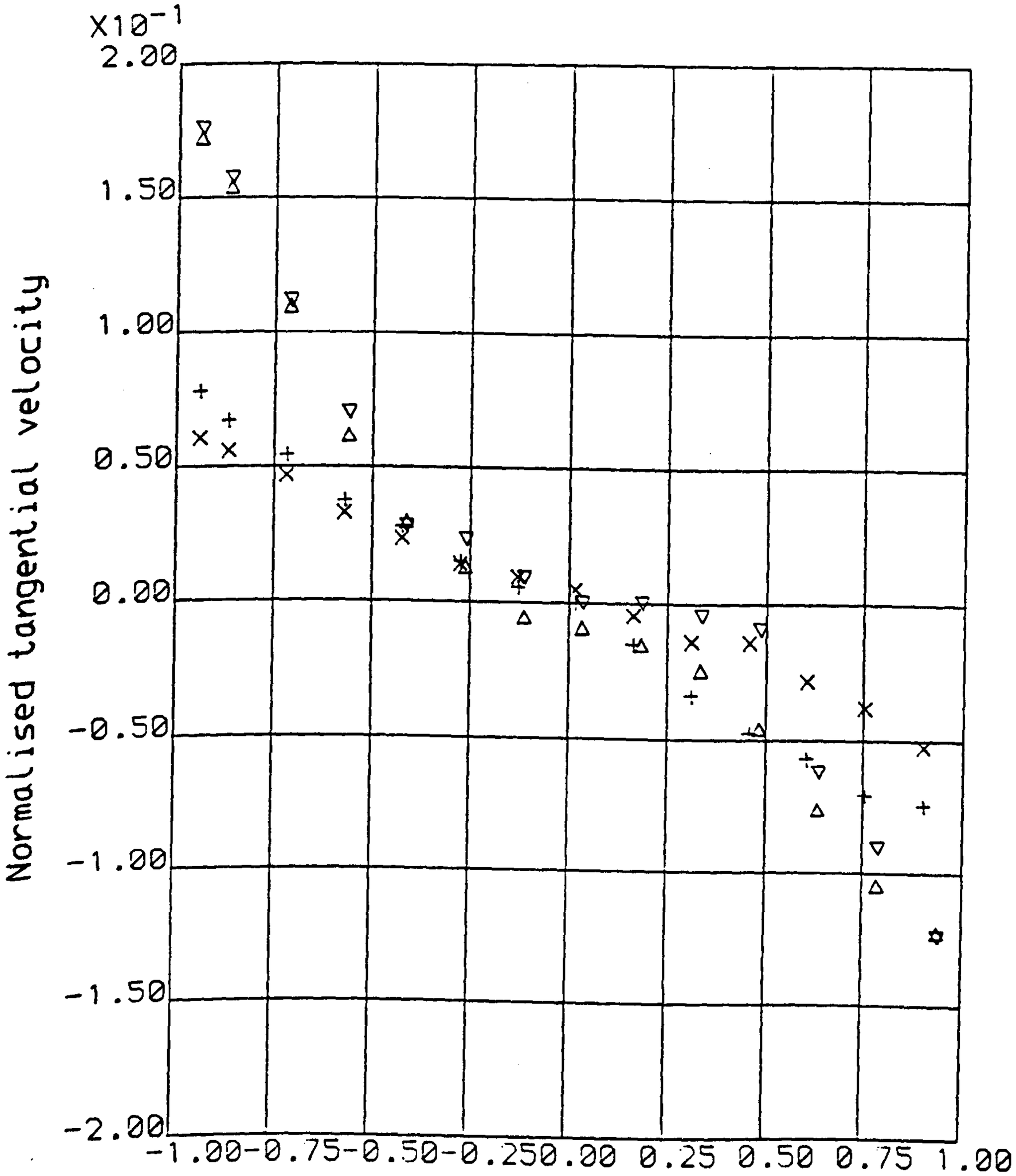

Figure 6.18: Tangential velocity measurements on sections 1 and 2

Symbol	△	▽	+	×
Section	1	1	2	2
Re	413000	165000	413000	165000

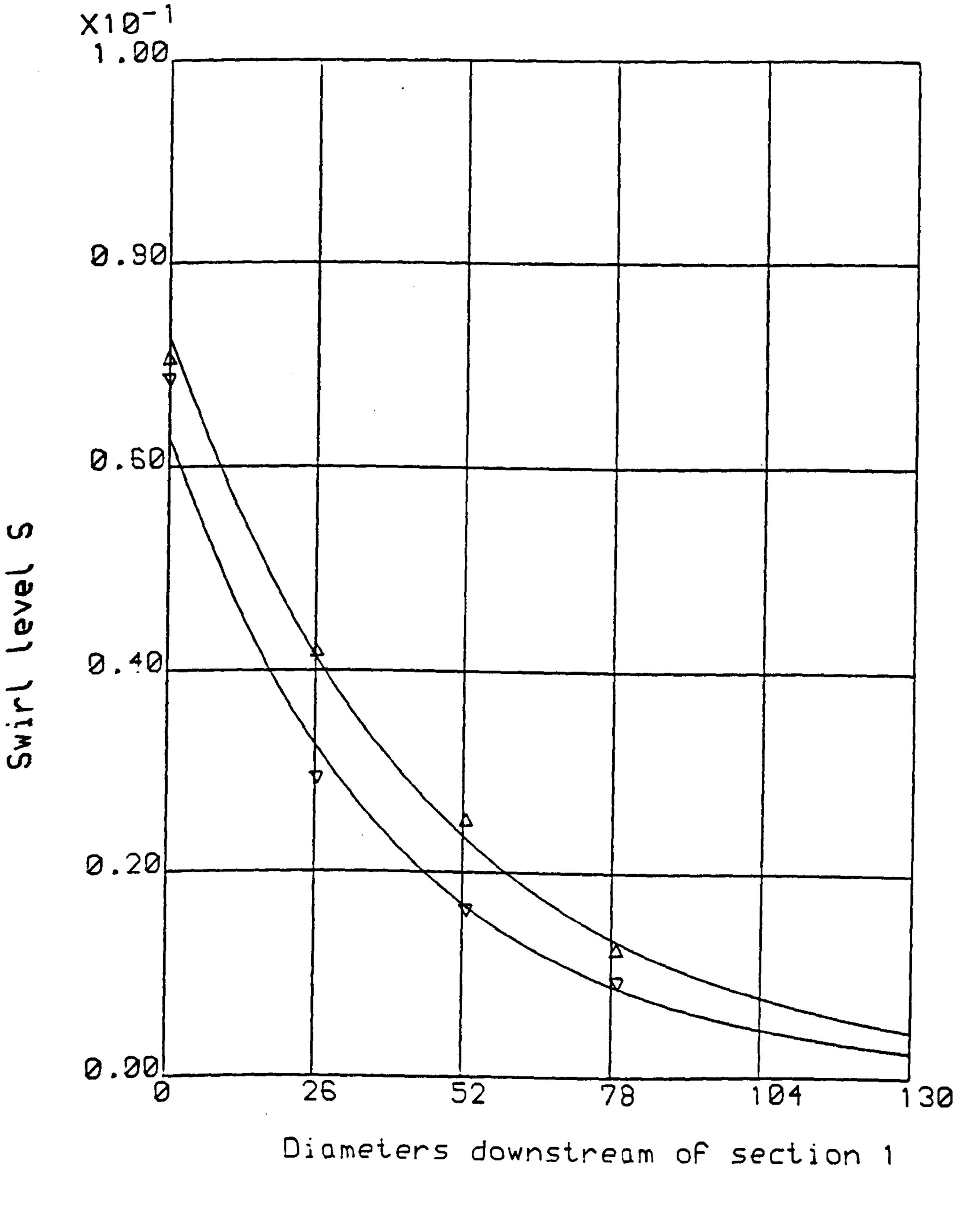

Figure 6.19: Measured swirl levels

Symbol	△	▽
Re	413000	165000

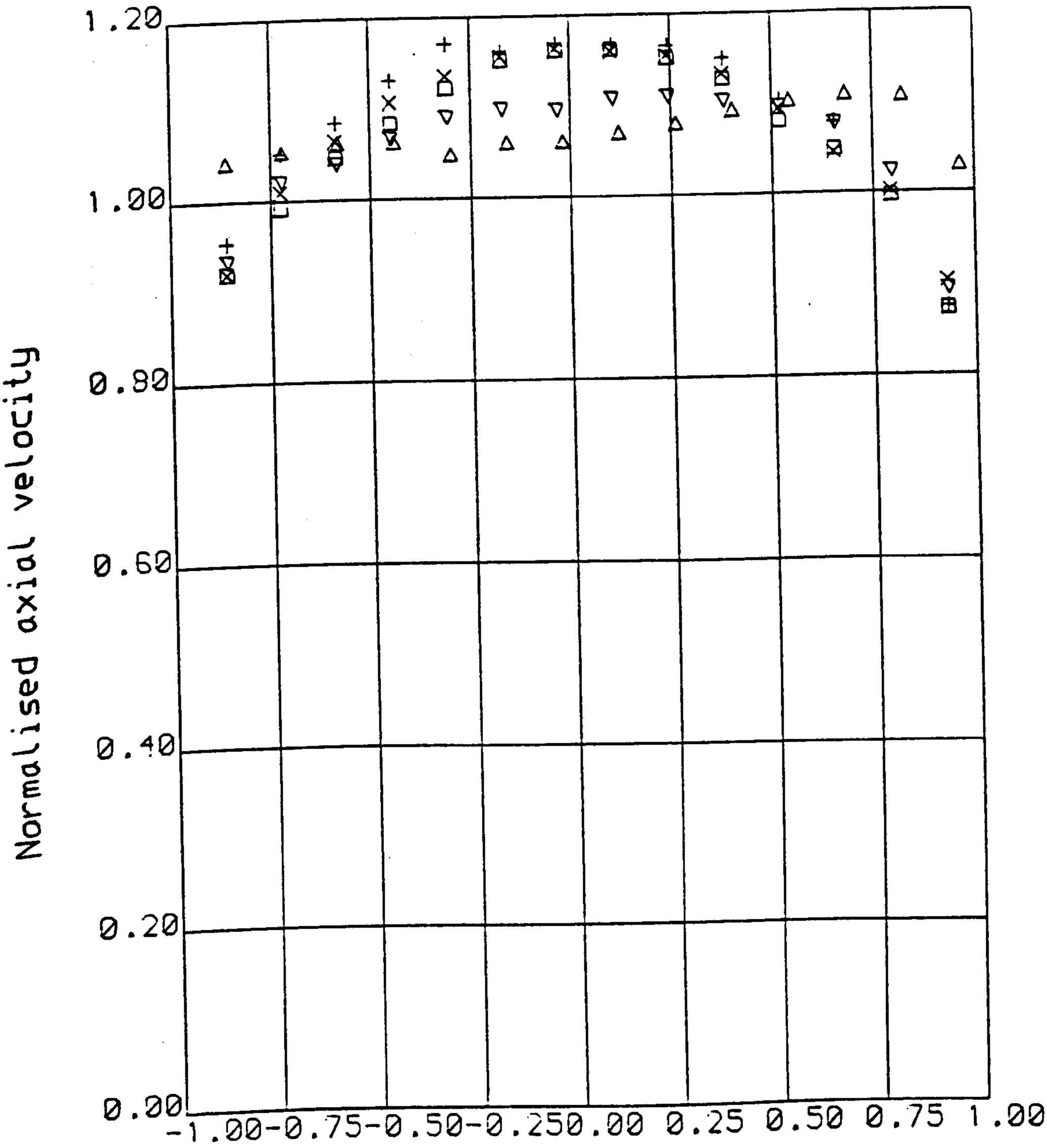

Figure 6.20: Axial velocity measurements on sections 1 to 5 at Re = 413000

Symbol	△	▽	+	×	□
Section	1	2	3	4	5

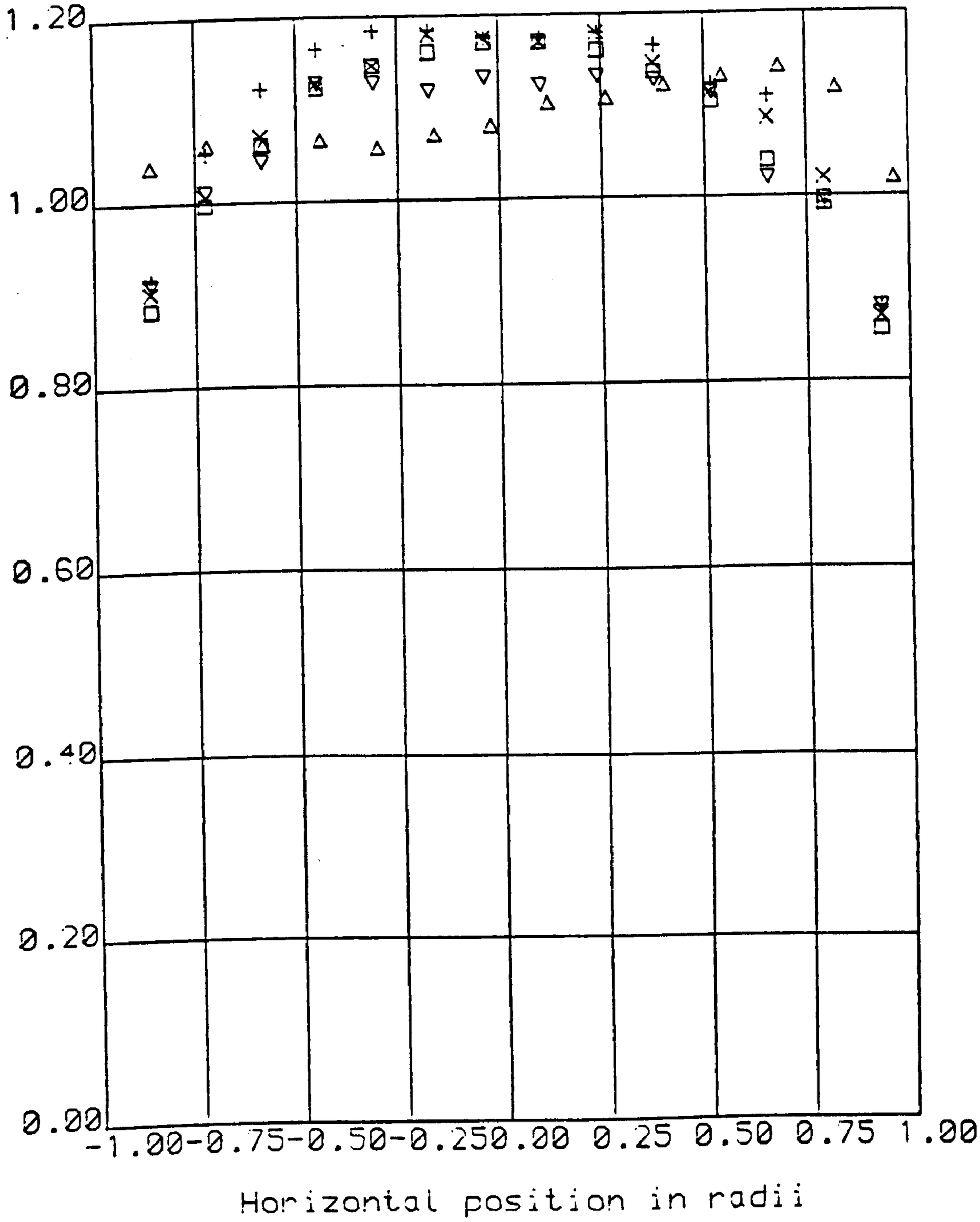

Figure 6.21: Axial velocity measurements on sections 1 to 5 at Re = 165000

Symbol	△	▽	+	x	□
Section	1	2	3	4	5

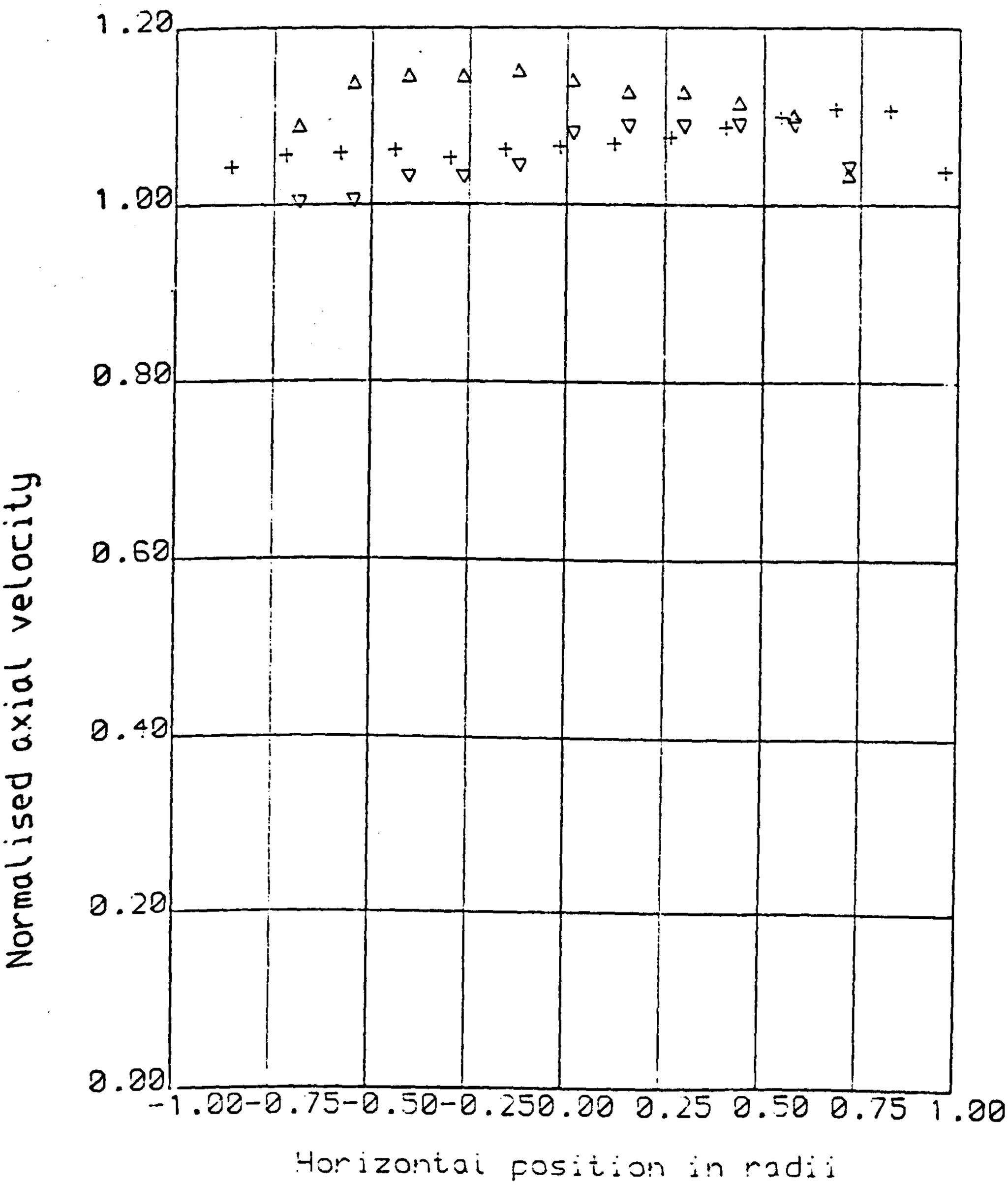

Figure 5.22: Axial velocity measurements

on section 1 at Re = 413000

△ Upper chord + Horizontal diameter ▽ Lower chord

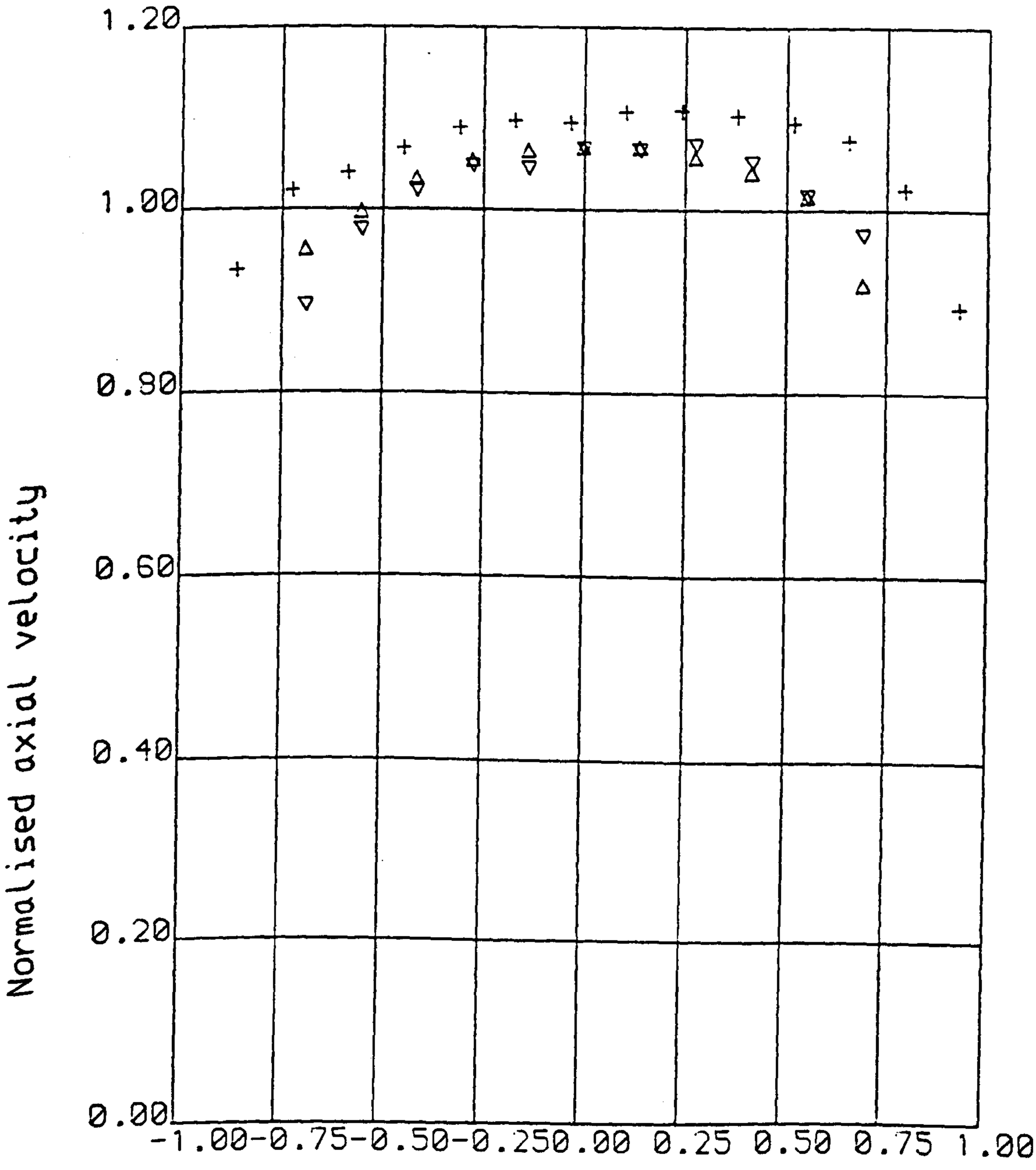

Figure 6.23: Axial velocity measurements

on section 2 at Re = 413000

△ Upper chord + Horizontal diameter ▽ Lower chord

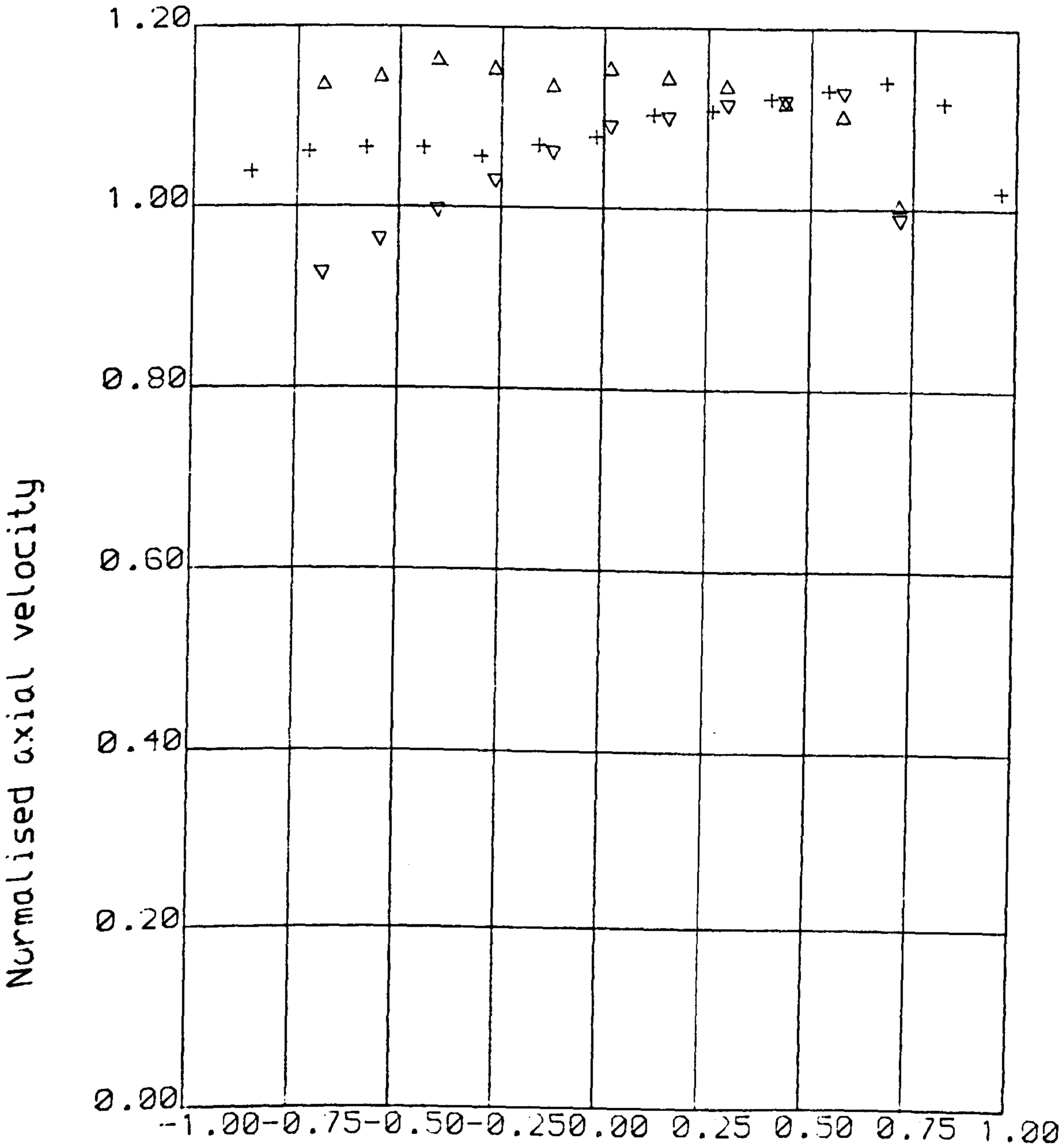

Figure 6.24: Axial velocity measurements on section 1 at Re = 165000

△ Upper chord + Horizontal diameter ▽ Lower chord

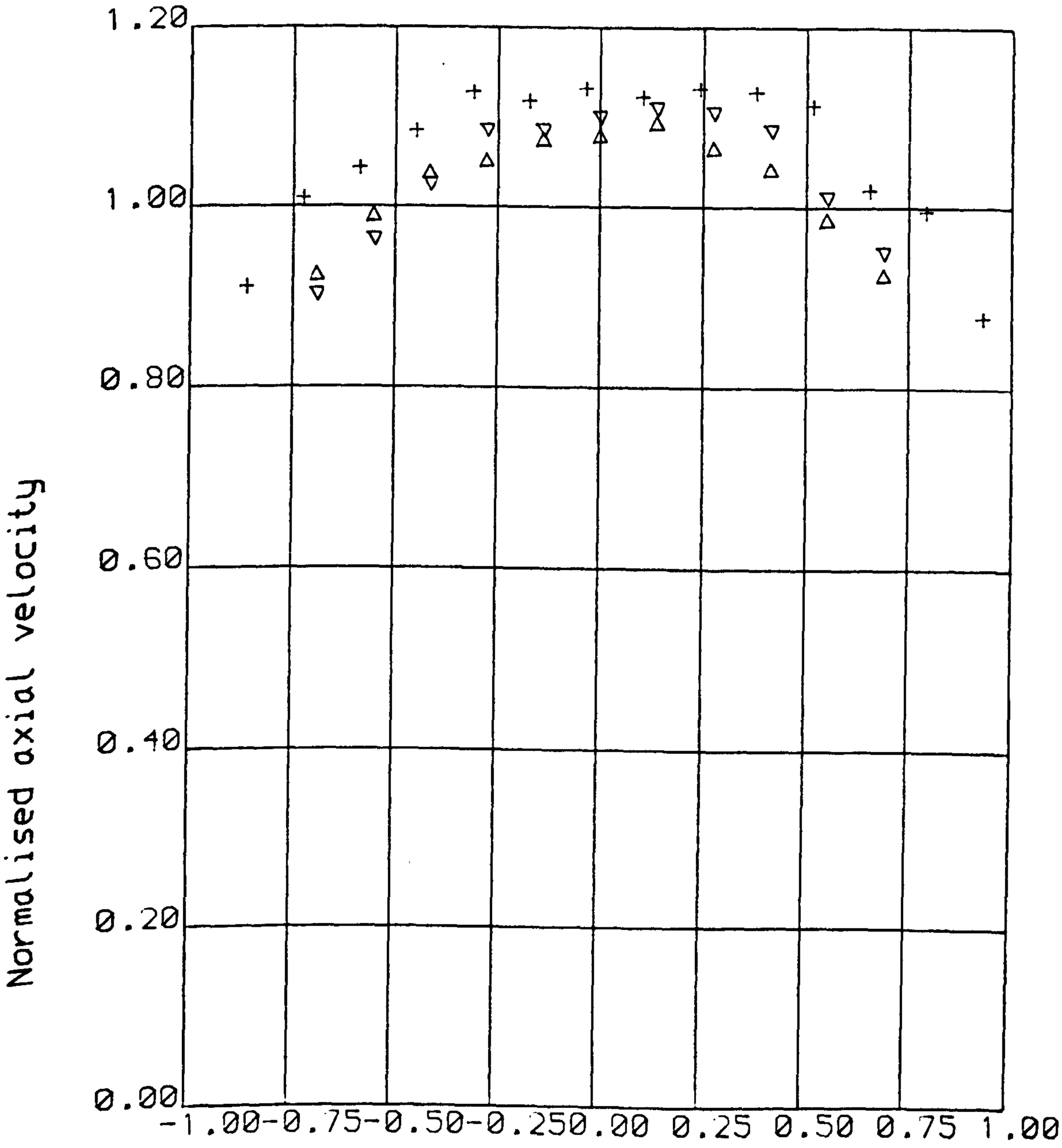

Figure 6.25: Axial velocity measurements on section 2 at Re = 165000

△ Upper chord + Horizontal diameter ▽ Lower chord

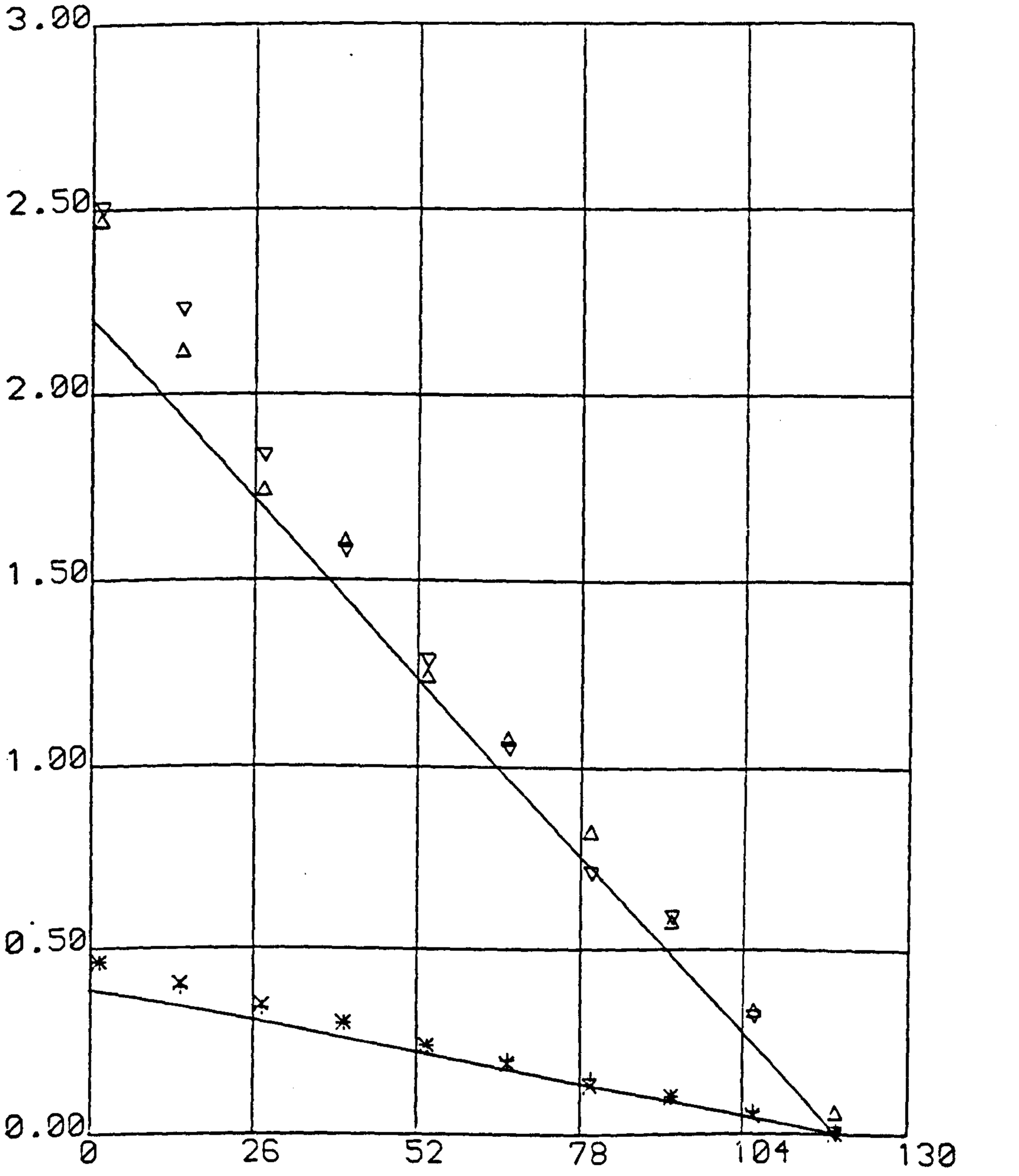

Figure 6.26: Pressure measurements

Re = 413000 △ Upper tapping ▽ Lower tapping

Re = 165000 + Upper tapping × Lower tapping

_____ Fully developed flow theory

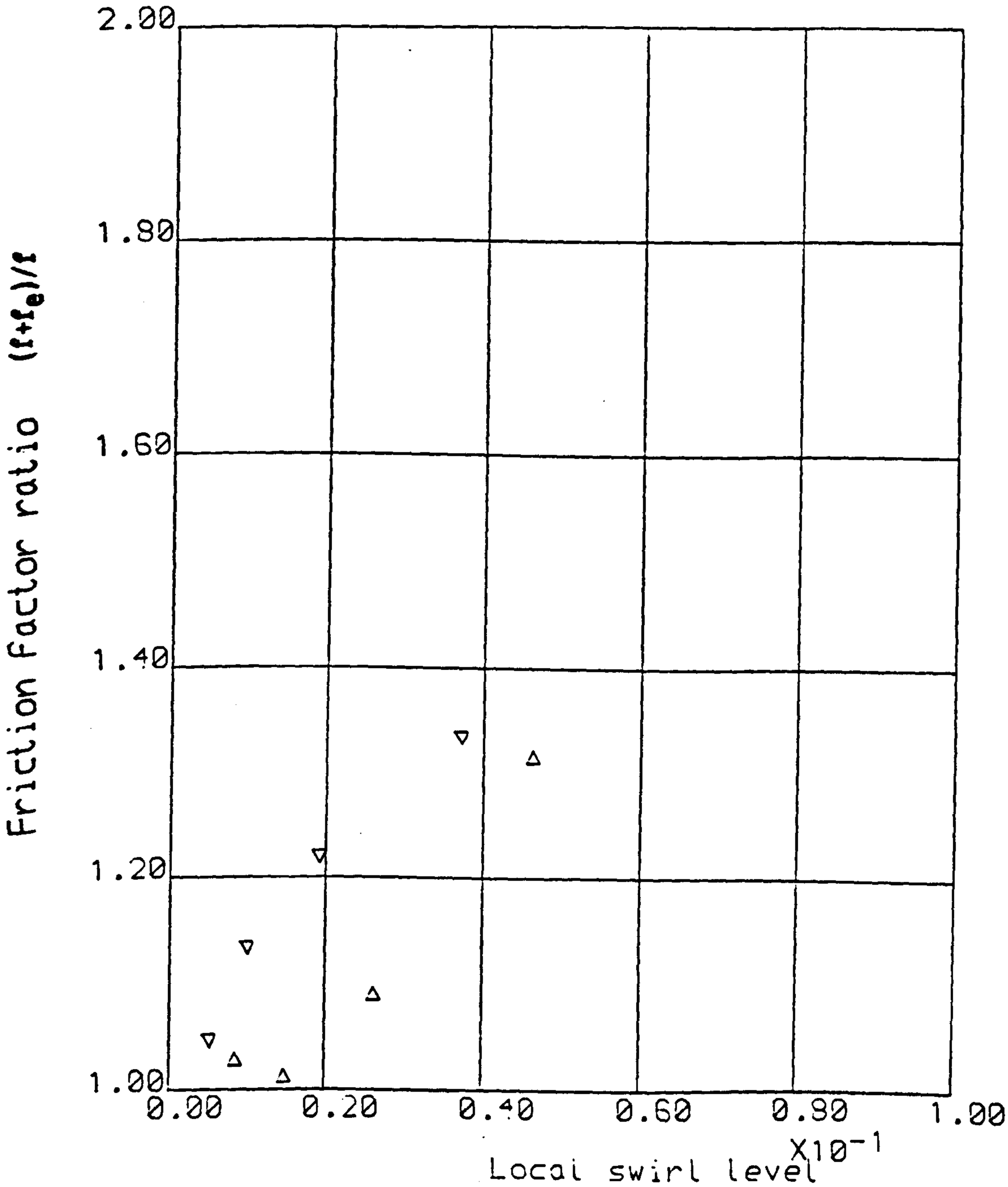

Figure 6.27: Experimental Friction Factors

△ Re = 413000 ▽ Re = 165000

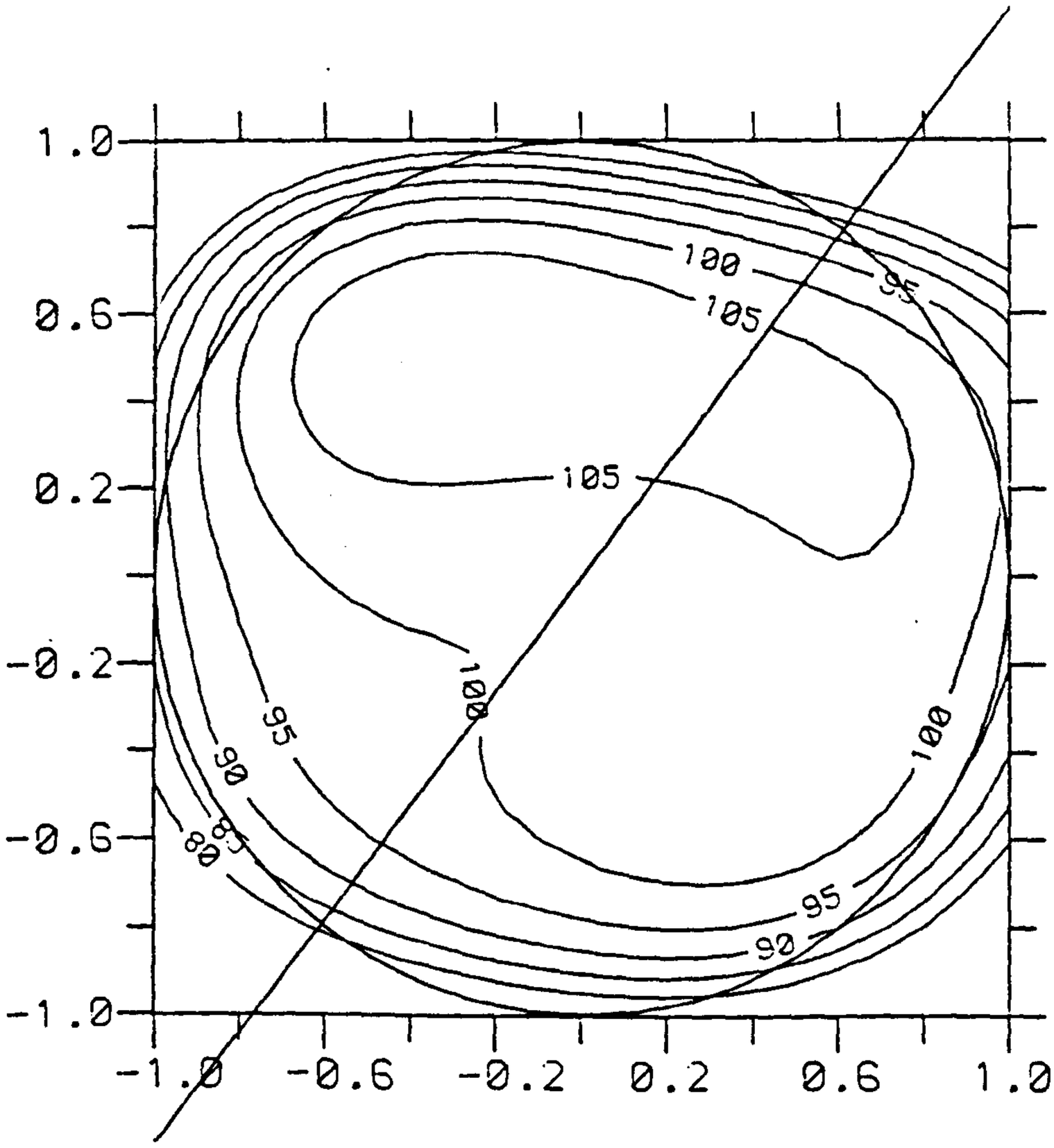

Figure 7.1: Axial velocity contours on section 1 at Re = 413000

——— Line of bulk flow symmetry

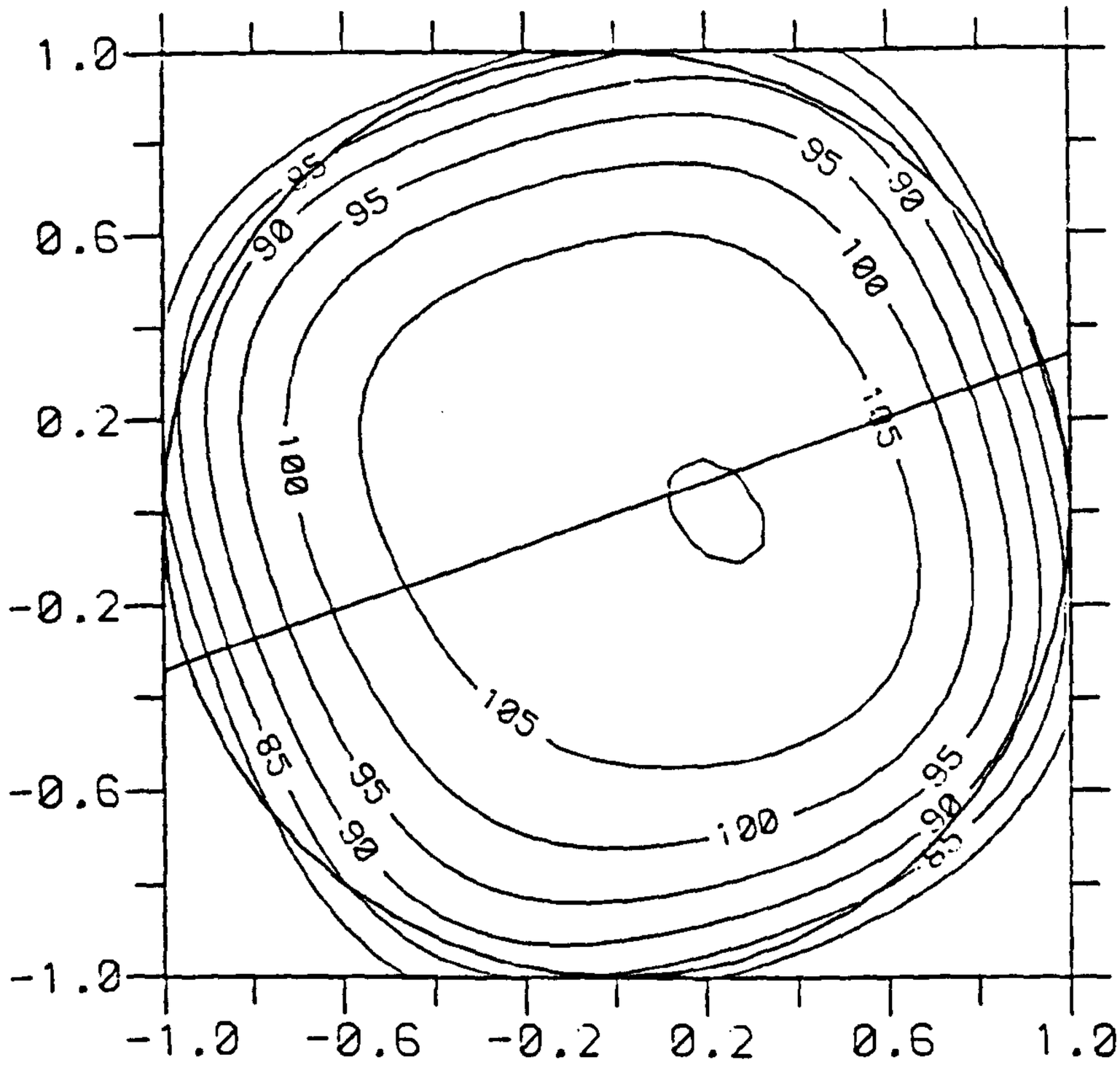

Figure 7.2: Axial velocity contours on section 2 at Re = 413000

_____ Line of bulk flow symmetry

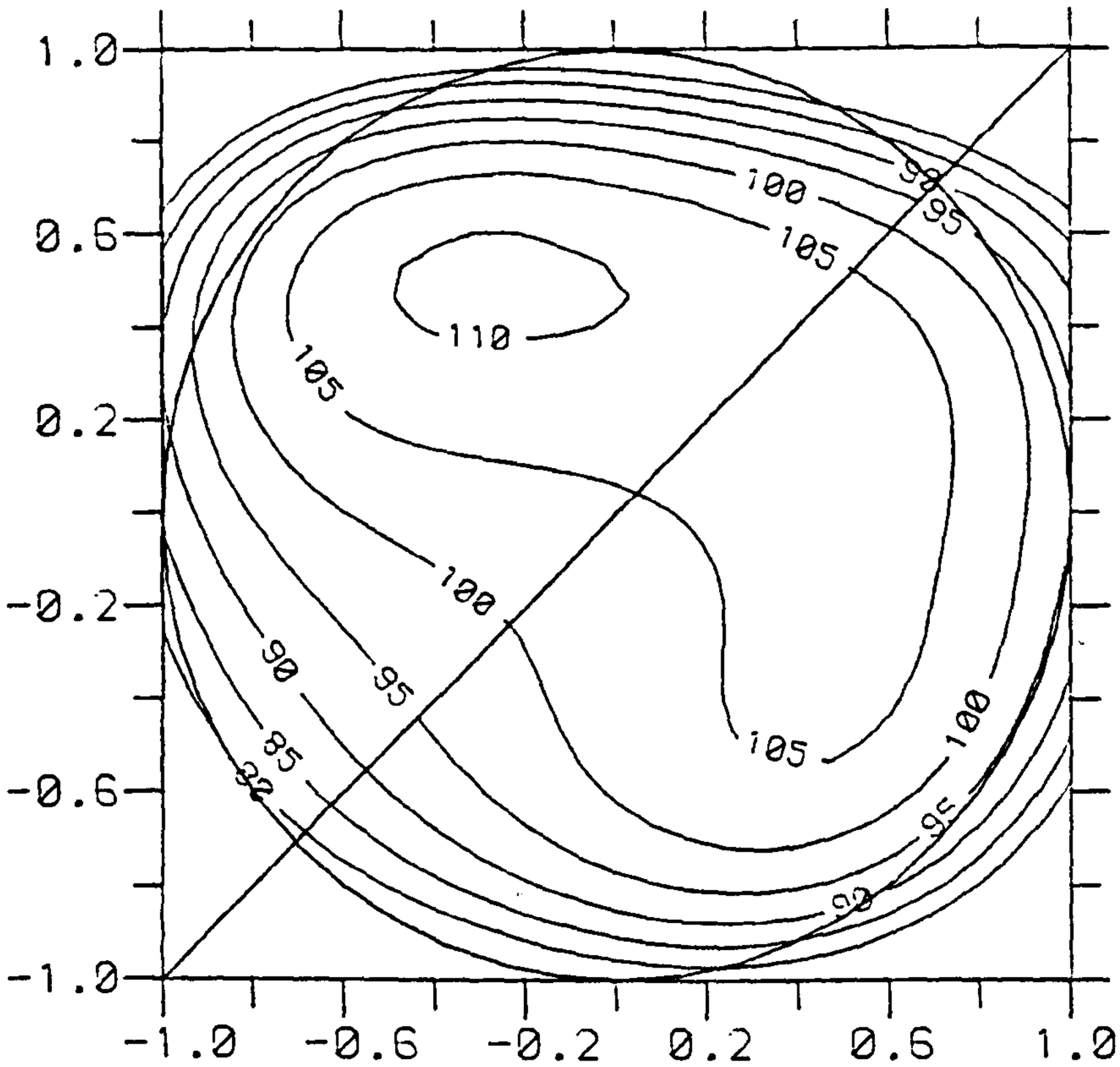

Figure 7.3: Axial velocity contours on section 1 at Re = 165000

_____ Line of bulk flow symmetry

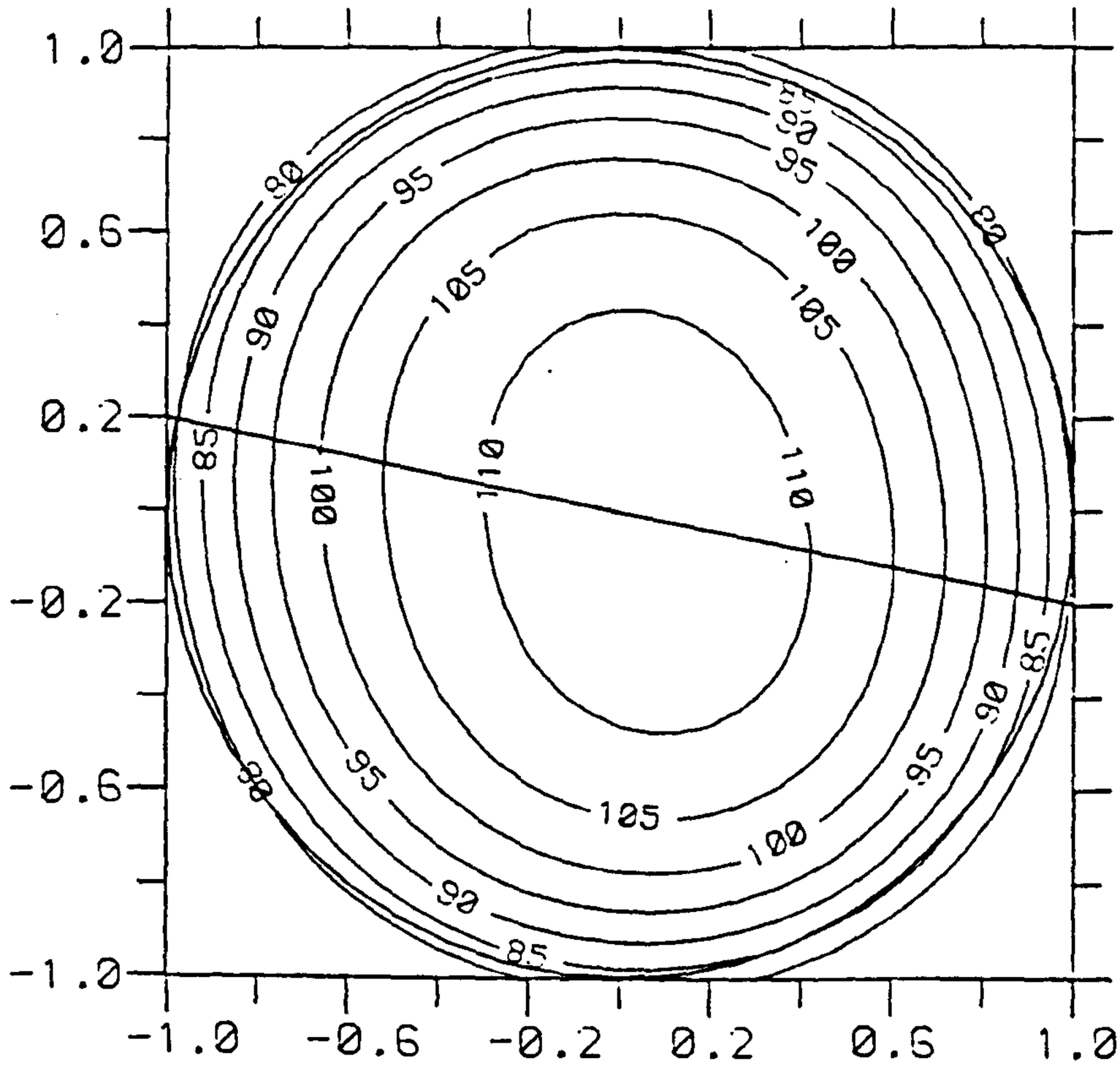

Figure 7.4: Axial velocity contours on section 2 at Re = 165000

_____ Line of bulk flow symmetry

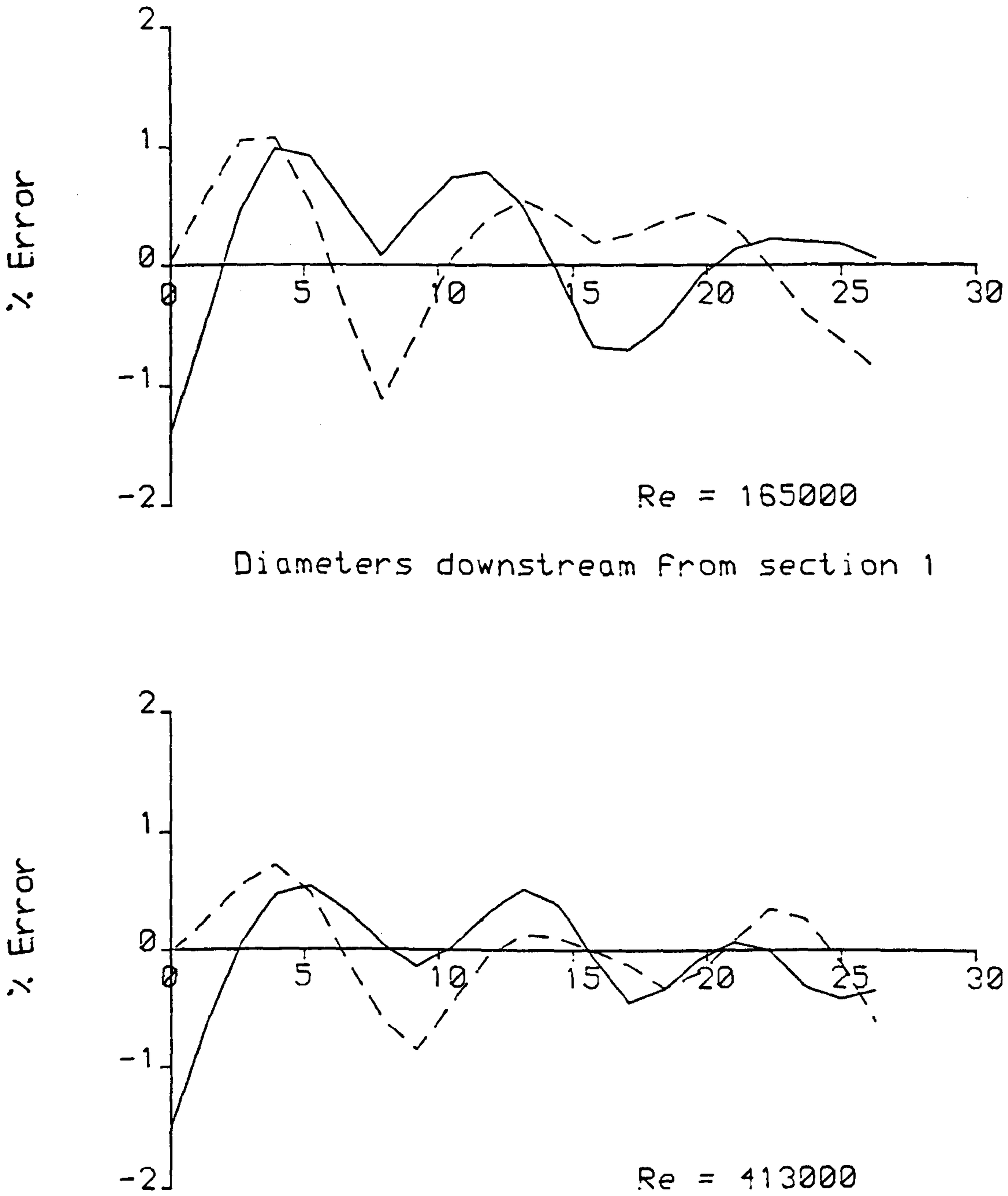

Figure 7.5: Errors of an electromagnetic Flowmeter

_____ Electrodes in vertical plane

_ _ _ _ Electrodes in horizontal plane

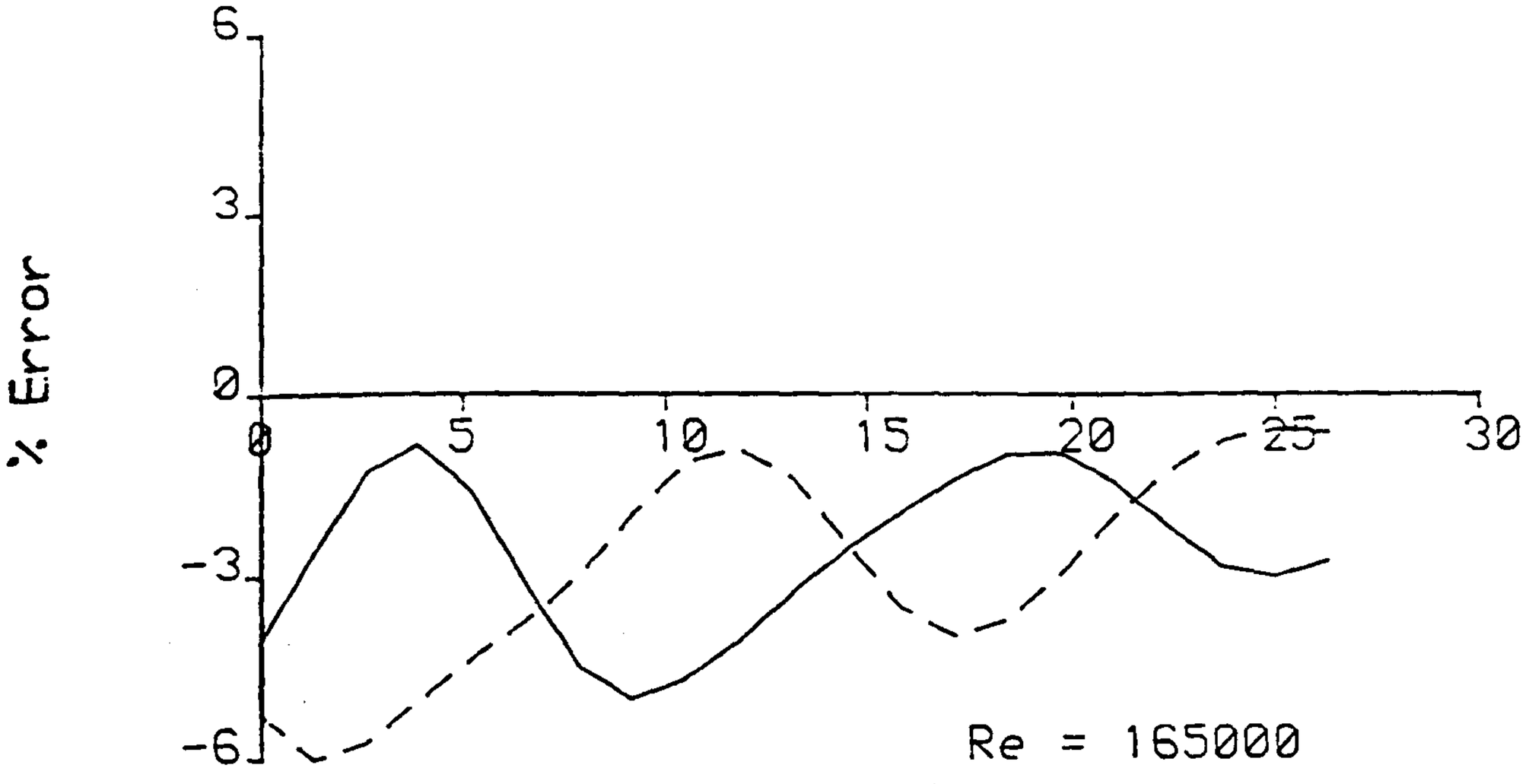

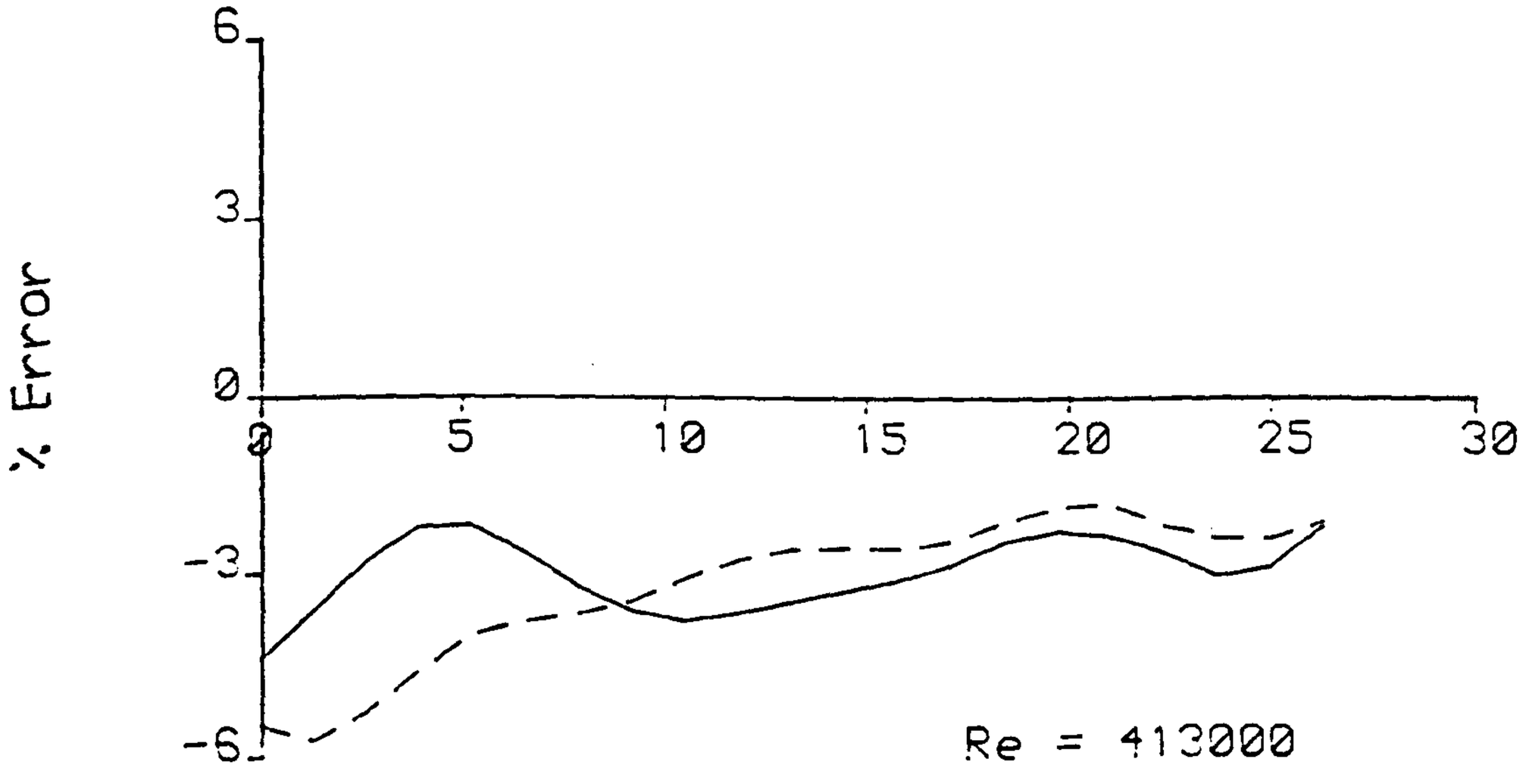

Figure 7.6: Errors of a

single beam ultrasonic flowmeter

_____ Beam in vertical plane

_ _ _ _ Beam in horizontal plane

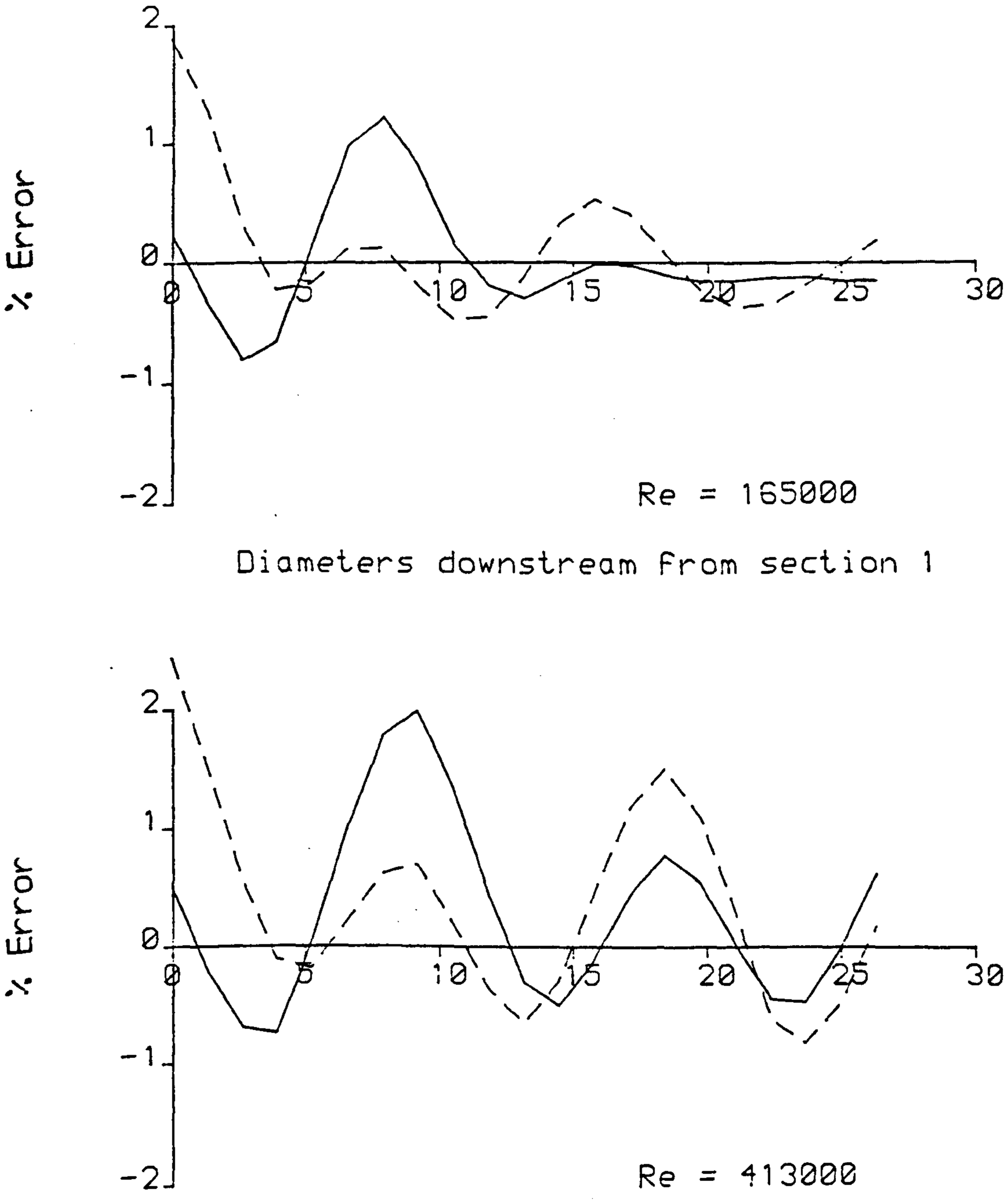

Figure 7.7: Errors of a

dual beam ultrasonic flowmeter

_____ Beams in vertical plane

_ _ _ _ Beams in horizontal plane

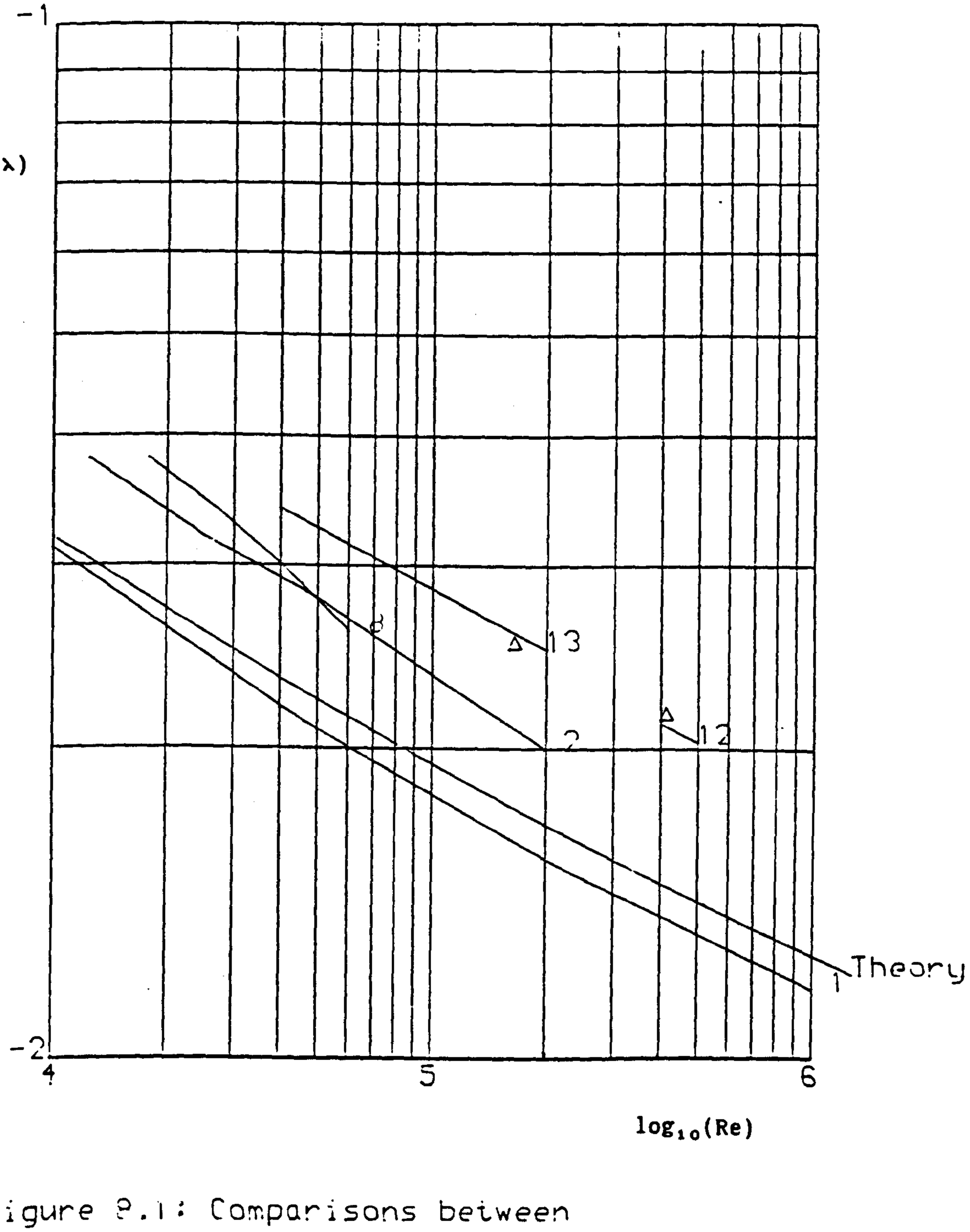

Figure 9.1: Comparisons between
the values of the decay rate obtained from
the theory, experiments and literature

Δ Experimenial points

1,2,9,12,13 As referred to in Figure 9.3

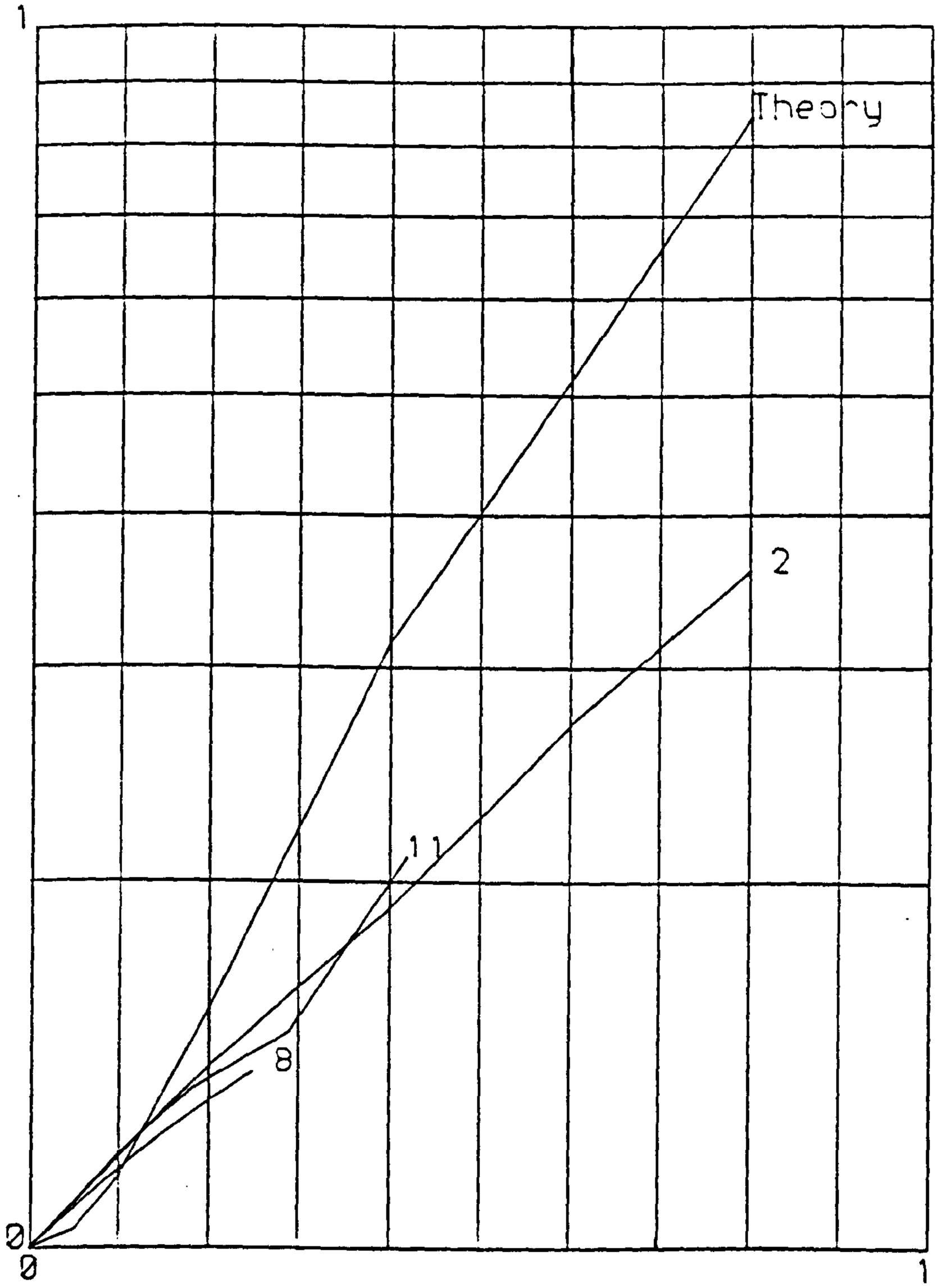

Figure 8.2: Friction factor comparison

2,8,11 As referred to in Figure 3.3

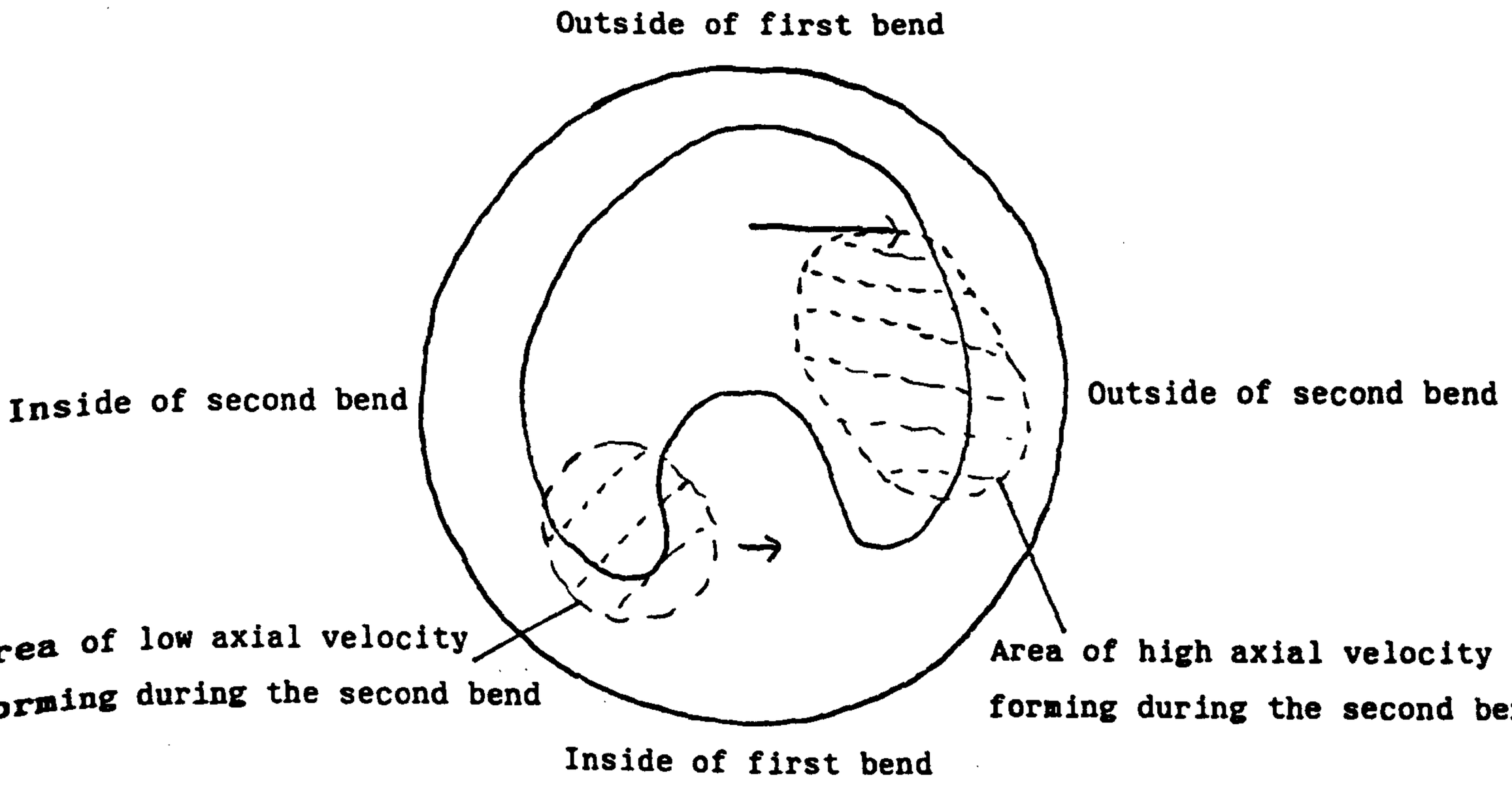

Figure 8.3: The formation of asymmetric profiles after a double bend

Return line

Control valve

Bypass line

Flow direction

Filter

Tank

Bleed

Pump

Inlet section

Flow direction

Tubes connected to pressure tappings

Flow direction

Gate valves

The double bend

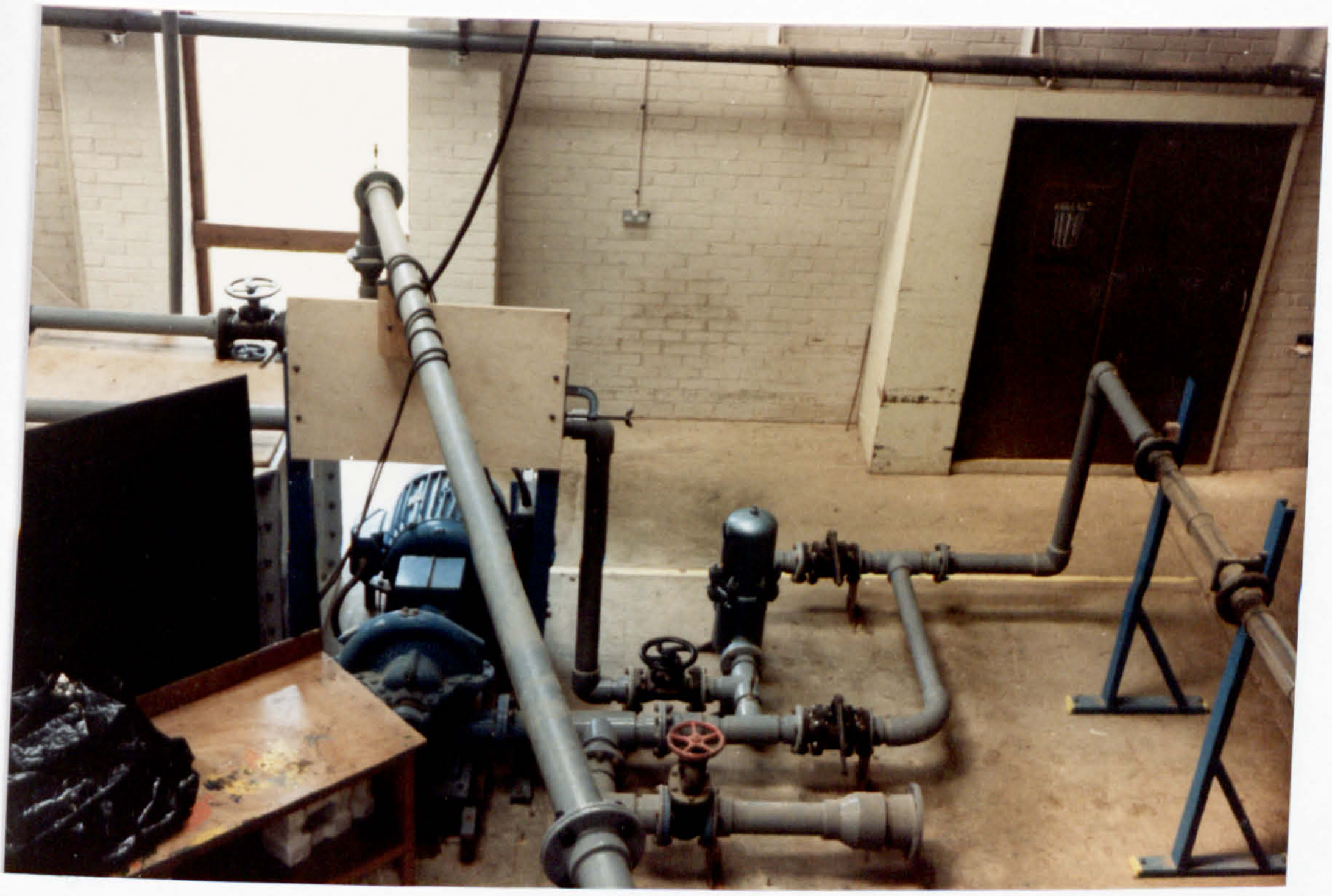

Plate 1: An overhead view of the area near the pump

Plate 2: View from 'behind' the double bend

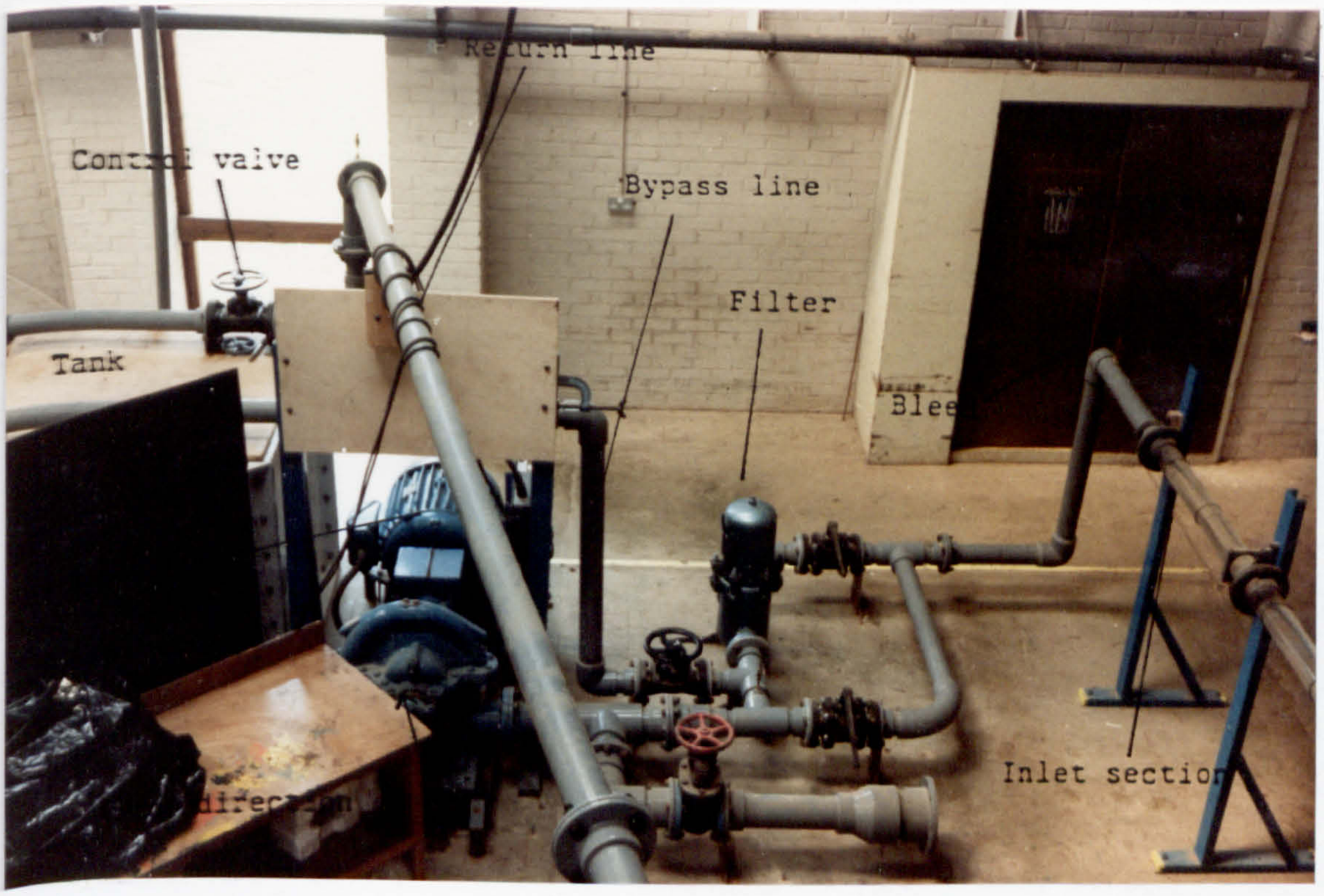

Plate 1: An overhead view of the area near the pump

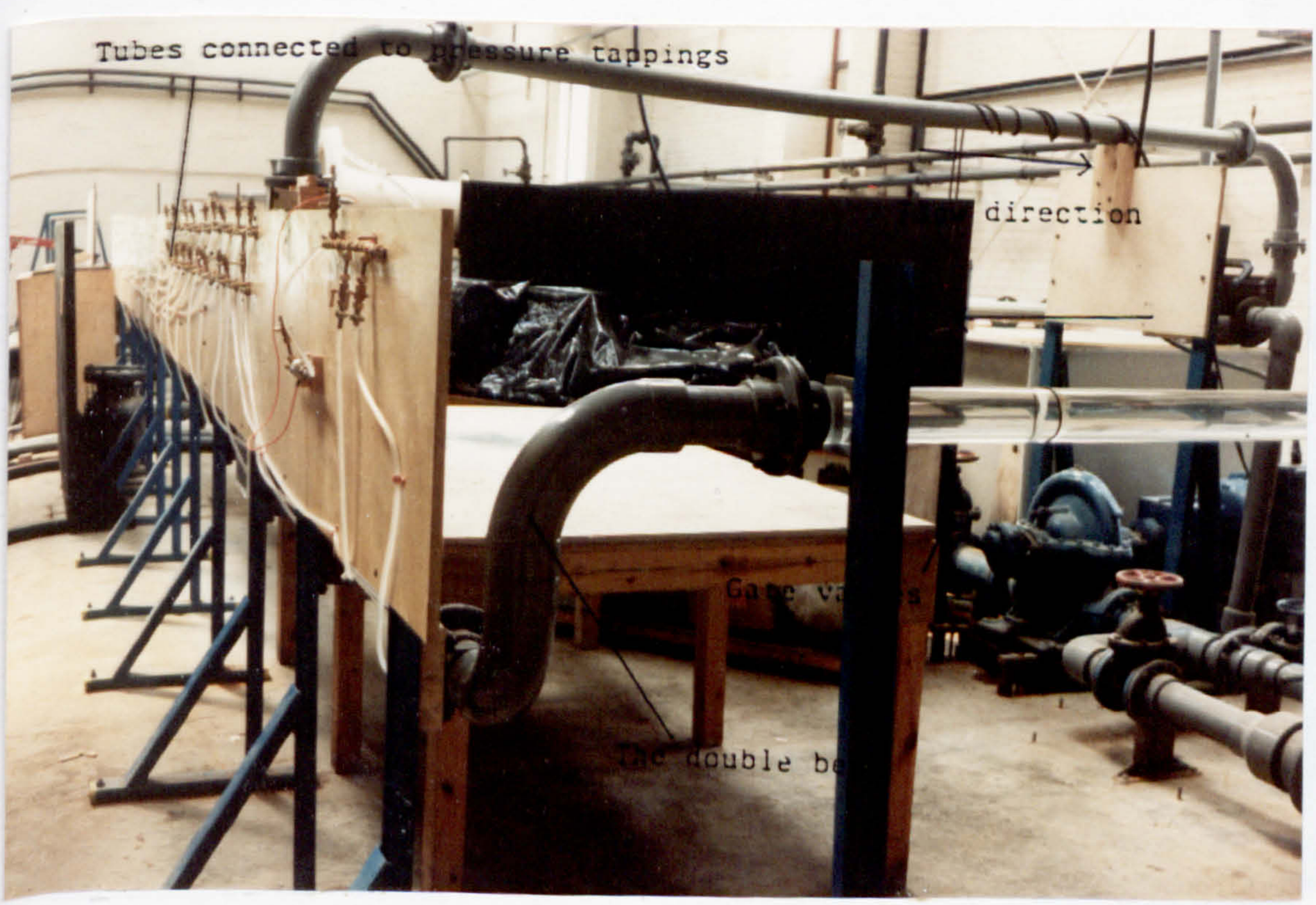

Plate 2: View from 'behind' the double bend

Flow direction

Perspex box

Flow direction

Measurement section 5

Drain

Flow direction

Measurement section 0

Double bend

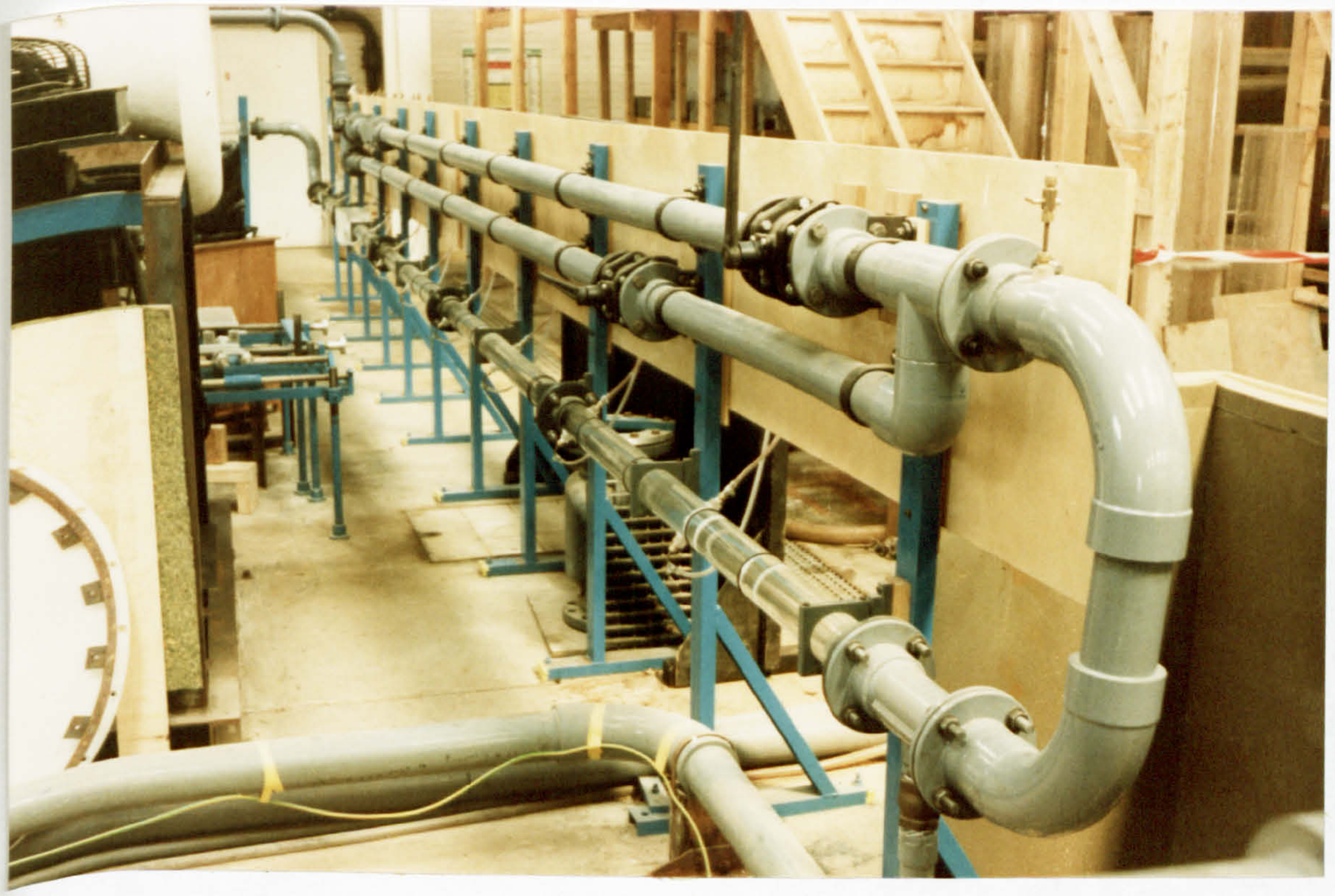

Plate 3: View looking along the test section

Plate 4: The inlet section

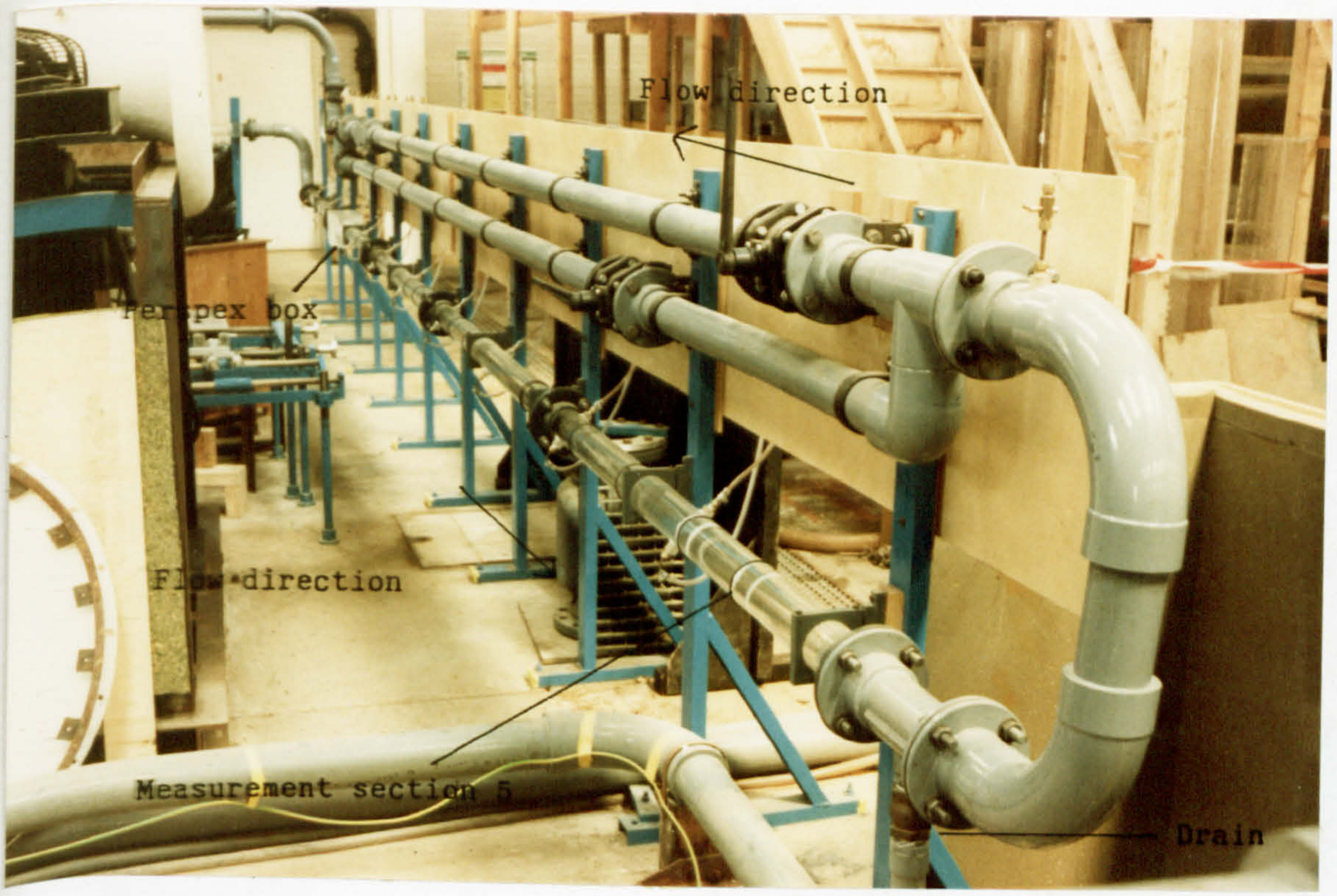

Plate 3: View looking along the test section

Plate 4: The inlet section

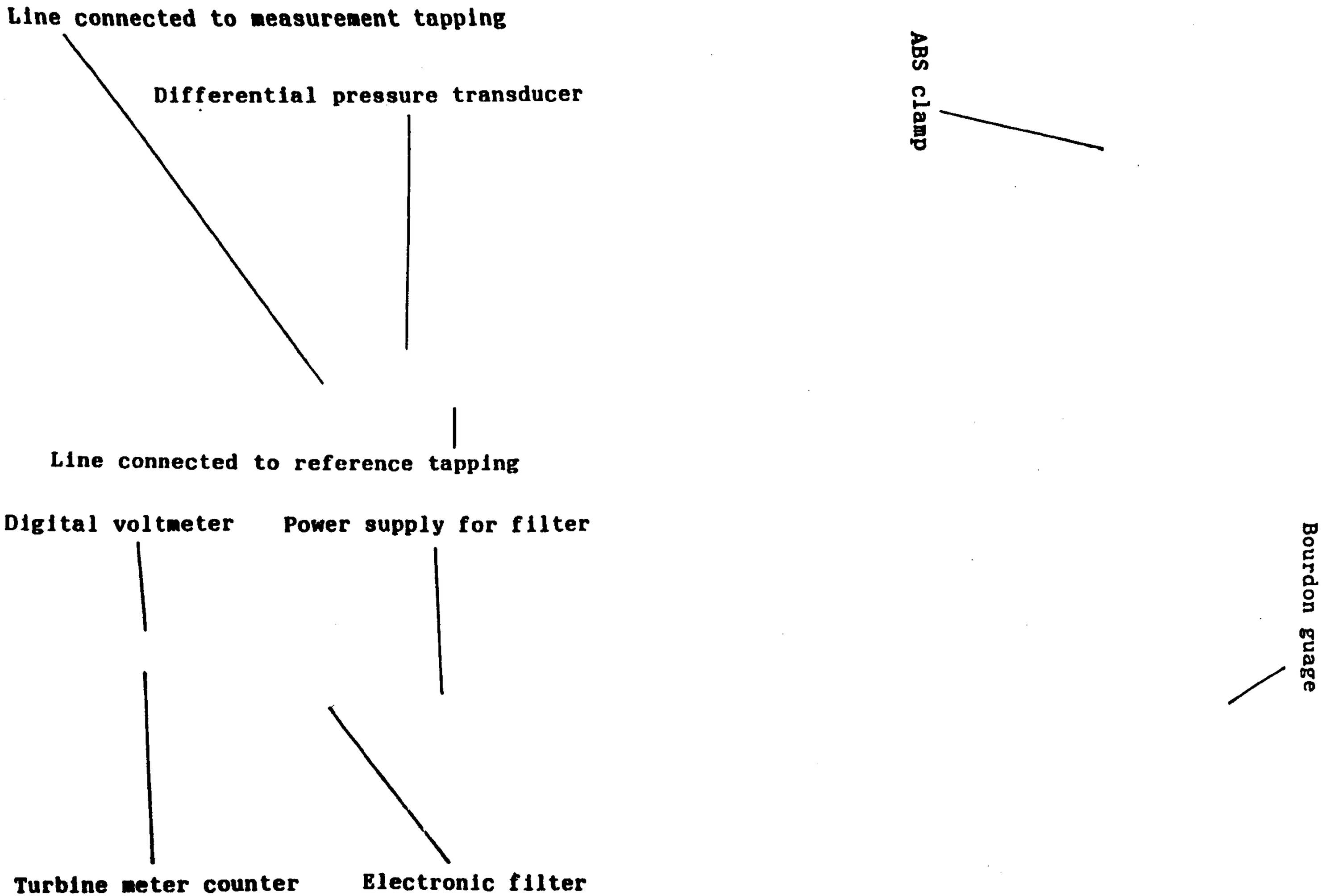
Line connected to measurement tapping
Differential pressure transducer
Line connected to reference tapping
Digital voltmeter
Power supply for filter
Turbine meter counter
Electronic filter
ABS clamp
Bourdon guage

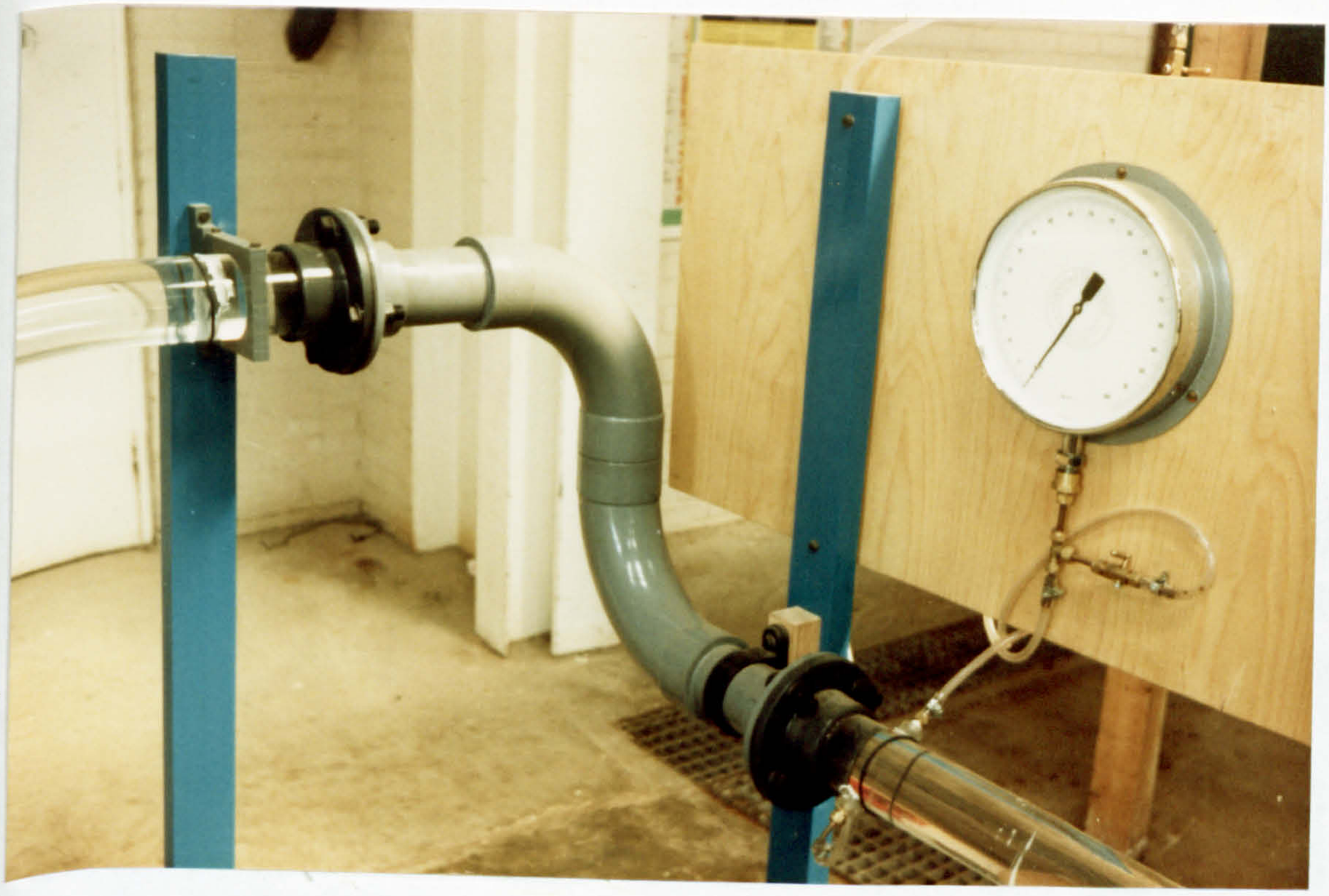

Plate 5: The double bend

Plate 6: The differential pressure measurement apparatus in use

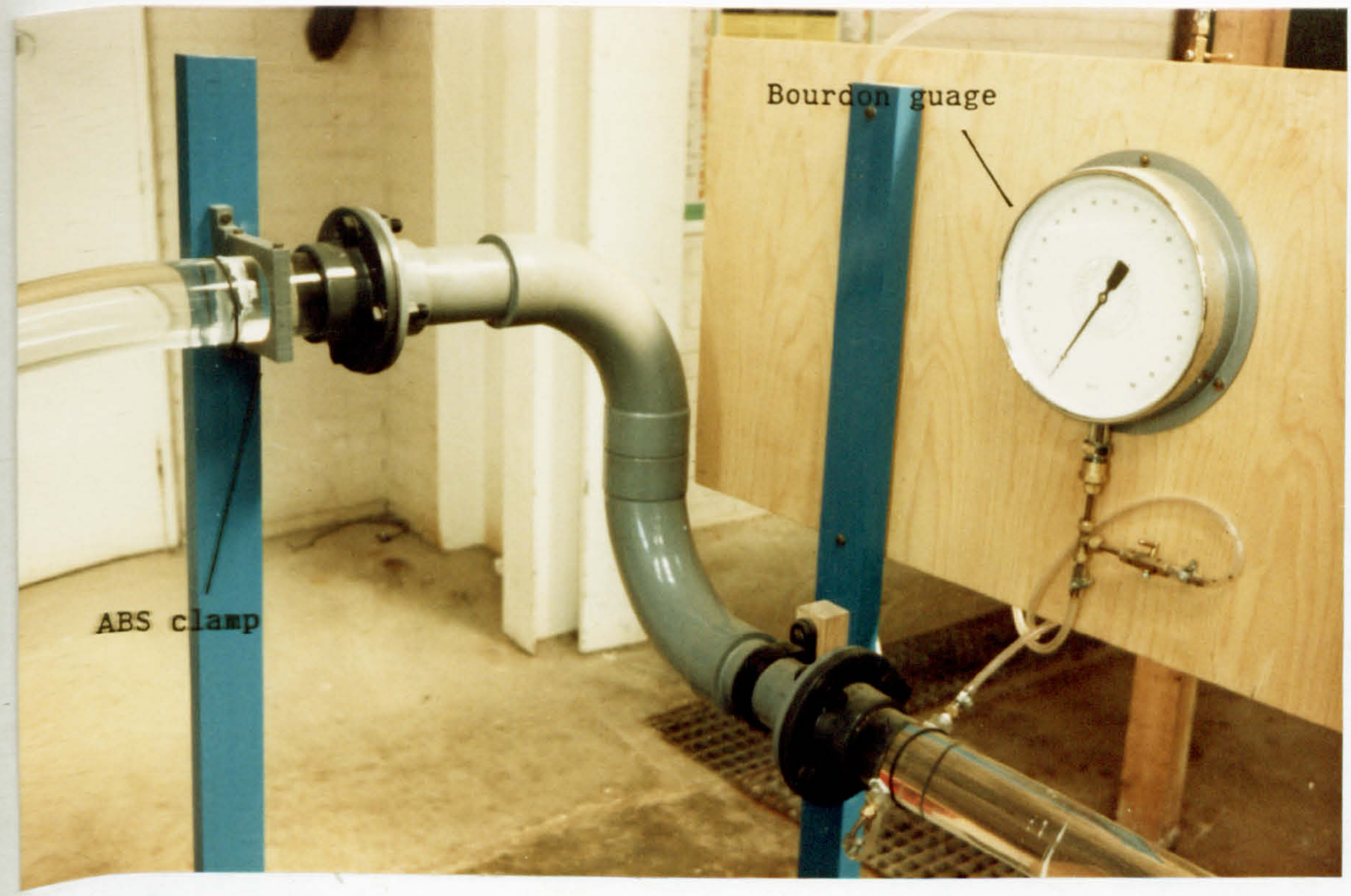

Plate 5: The double bend

Plate 6: The differential pressure measurement apparatus in use

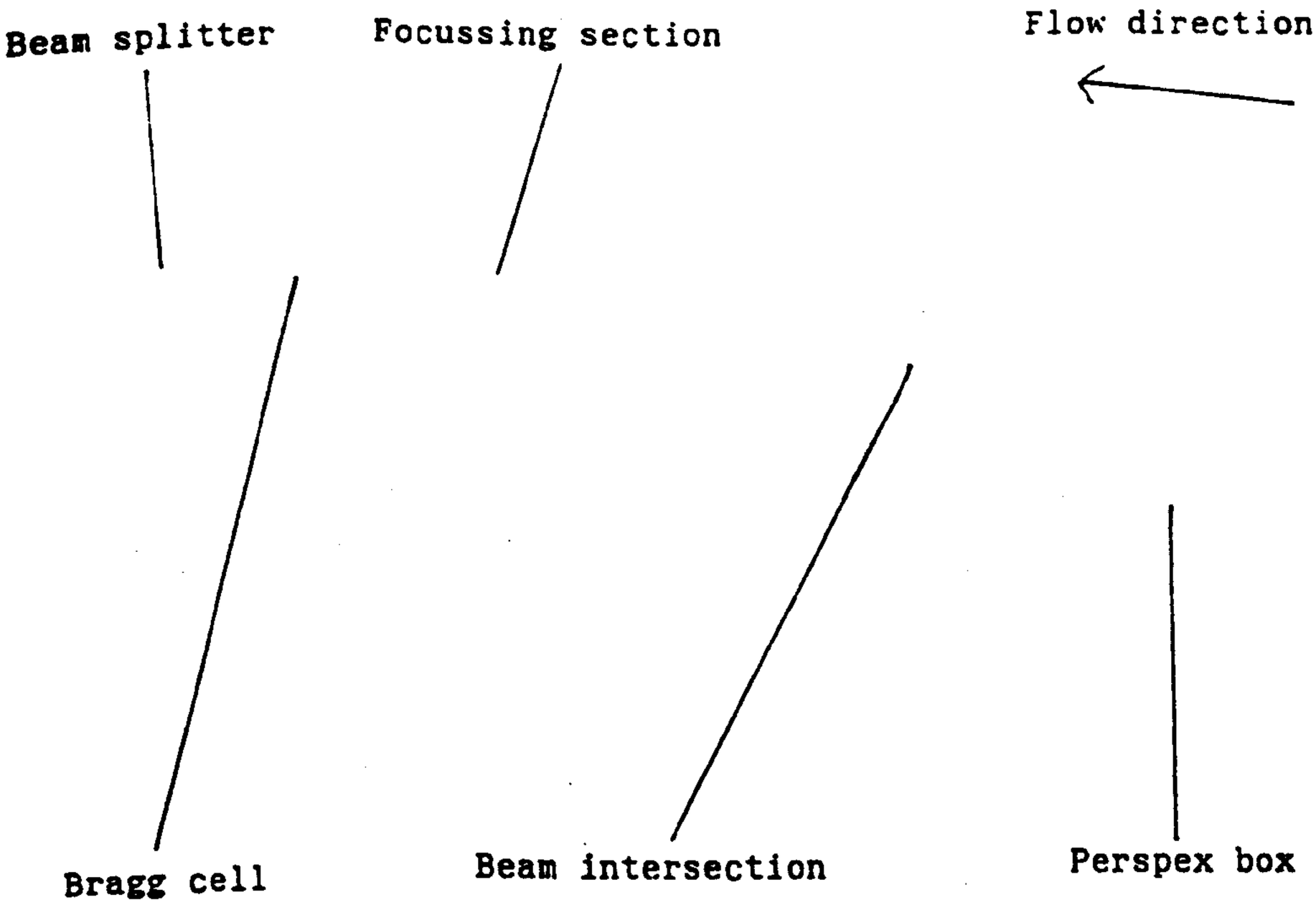
Beam splitter
Focussing section
Flow direction
Bragg cell
Beam intersection
Perspex box

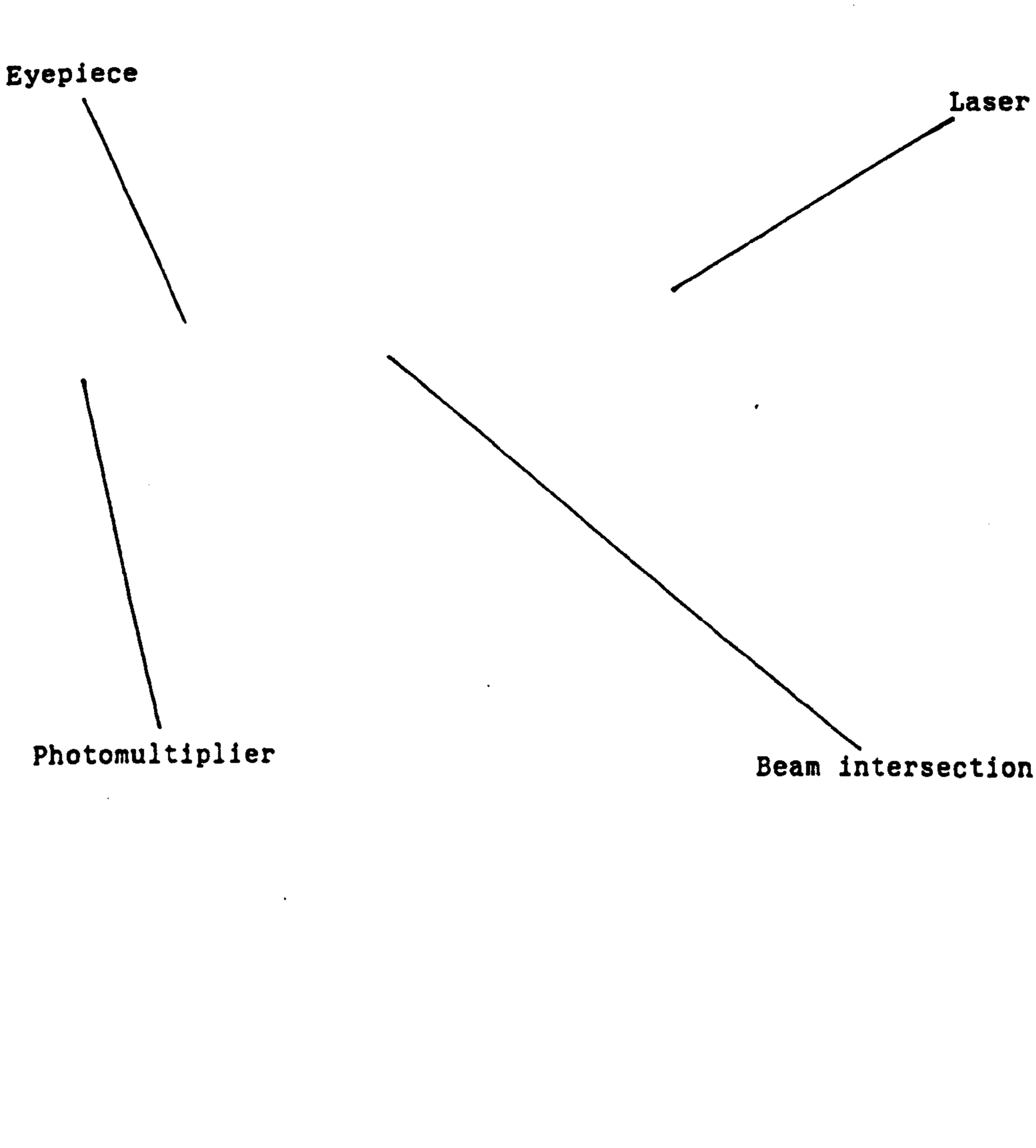
Eyepiece
Laser
Photomultiplier
Beam intersection

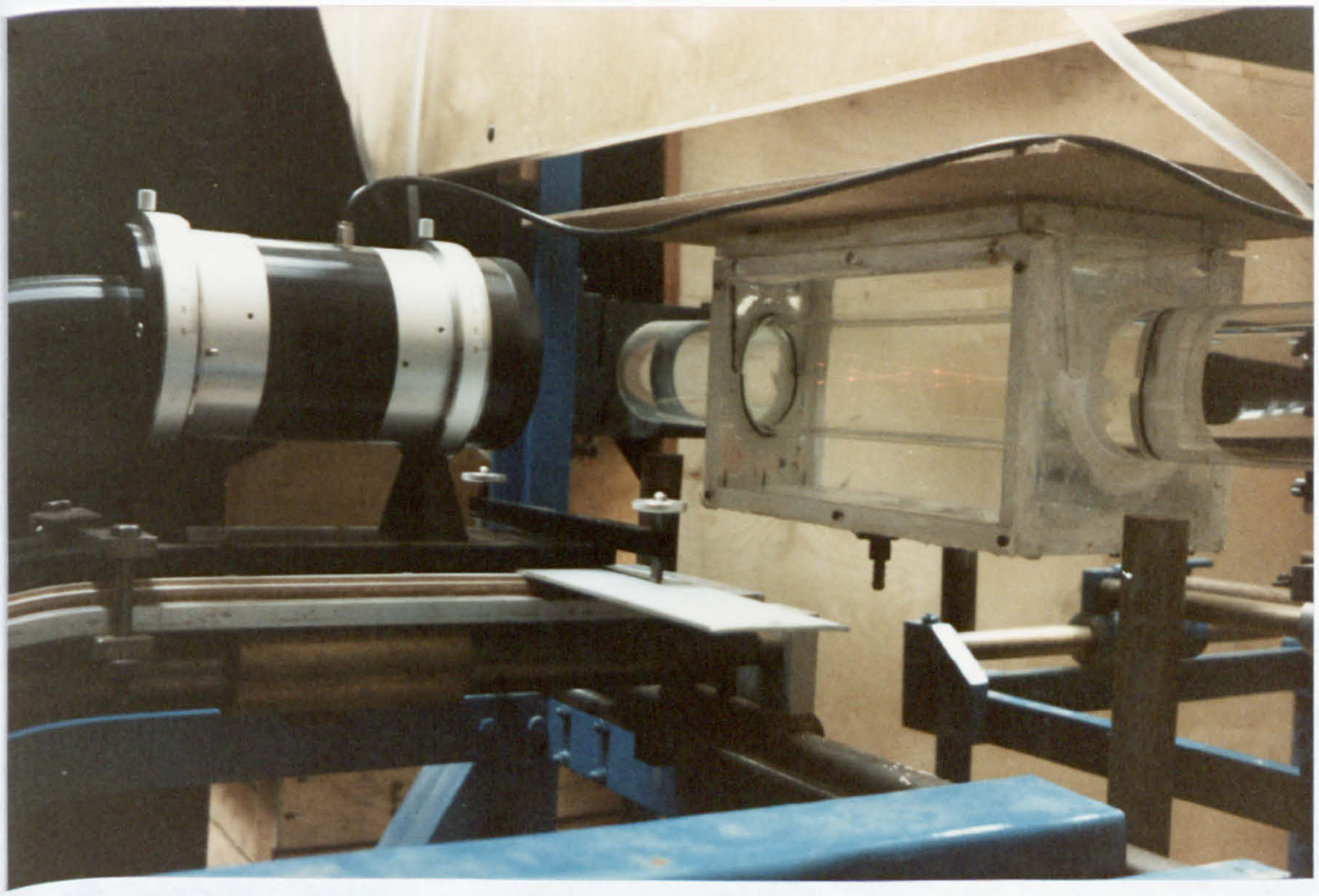

Plate 7: The laser with the beams in the vertical plane

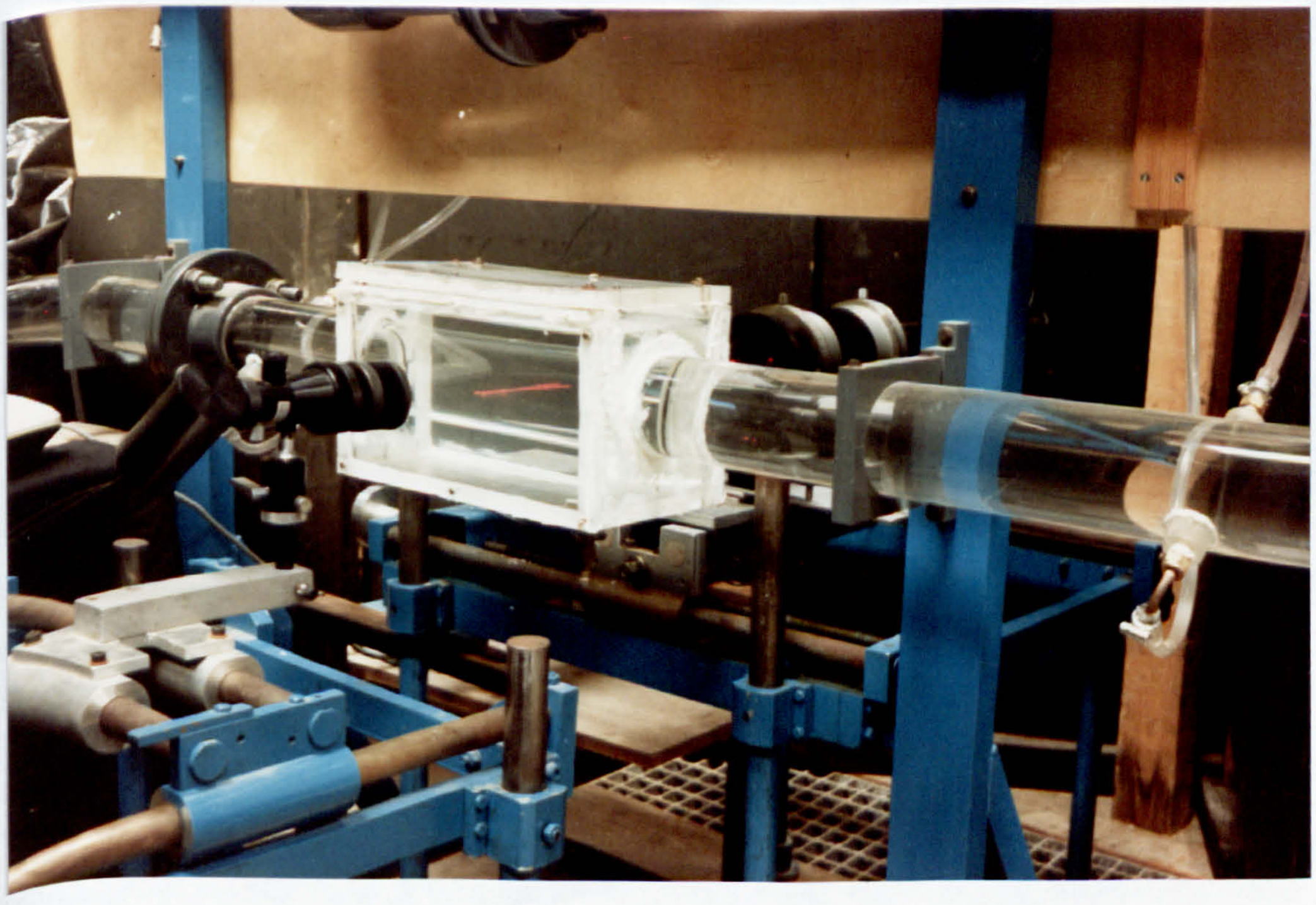

Plate 8: The optical apparatus (laser beams in the horizontal plane)

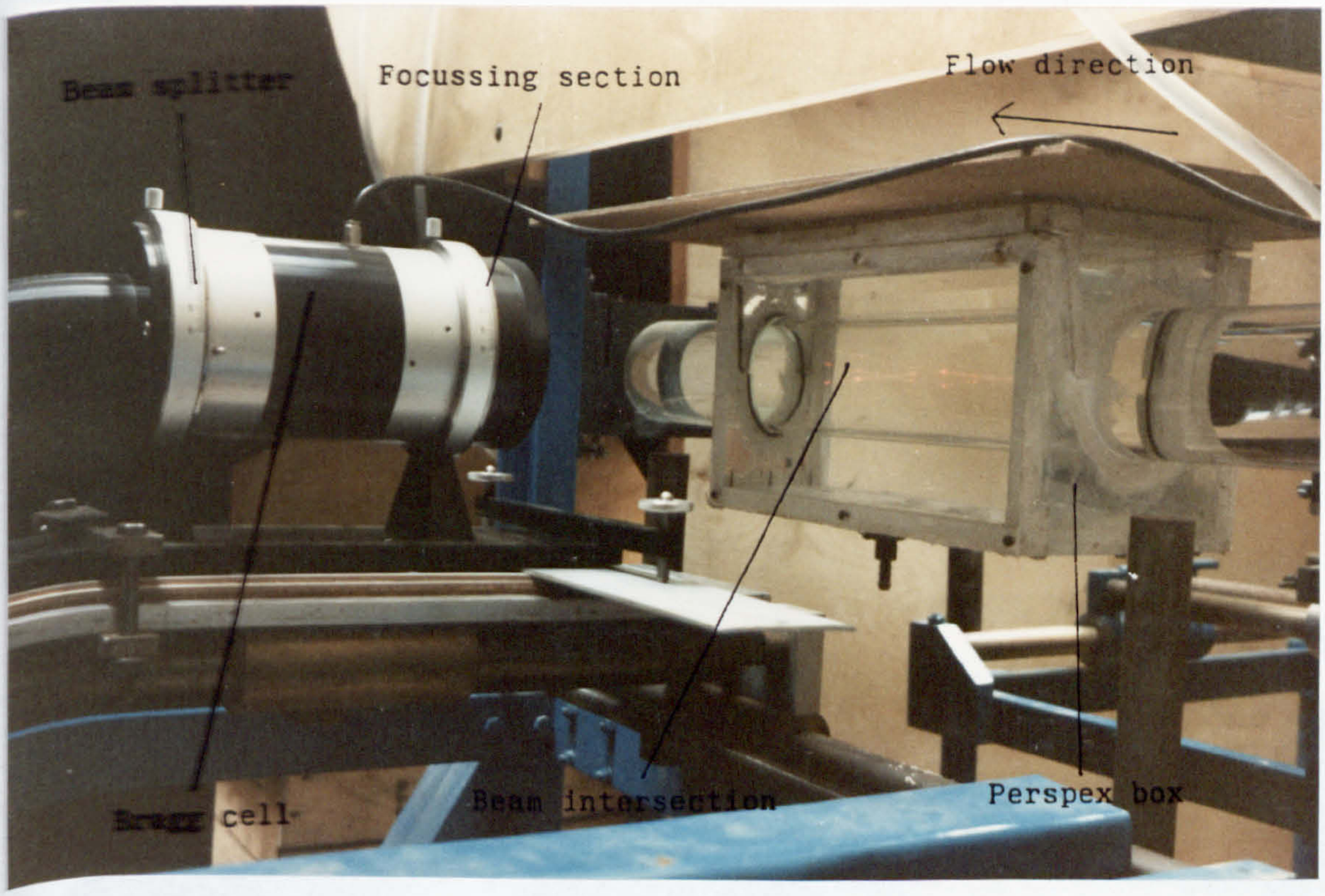

Plate 7: The laser with the beams in the vertical plane

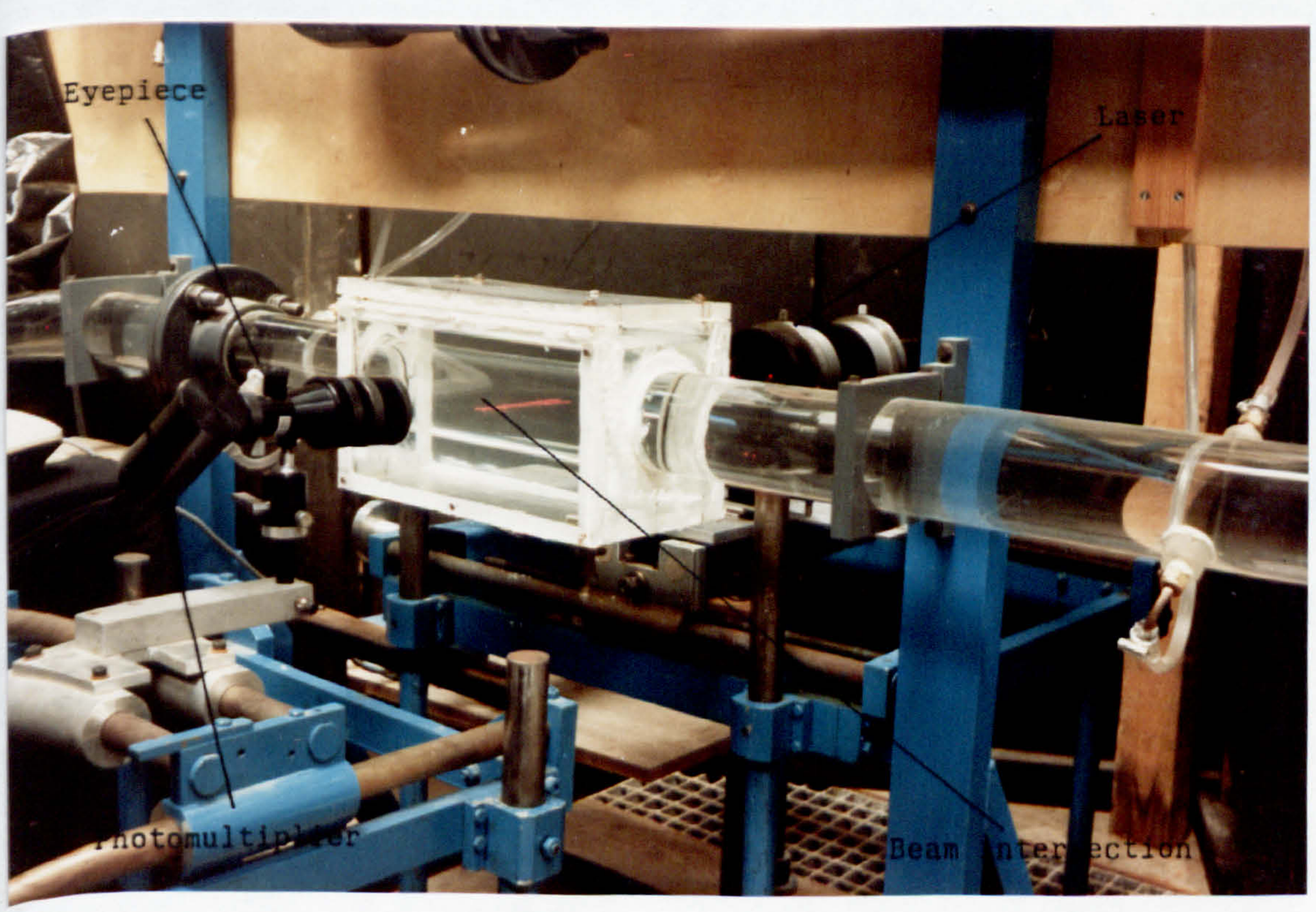

Plate 8: The optical apparatus (laser beams in the horizontal plane)

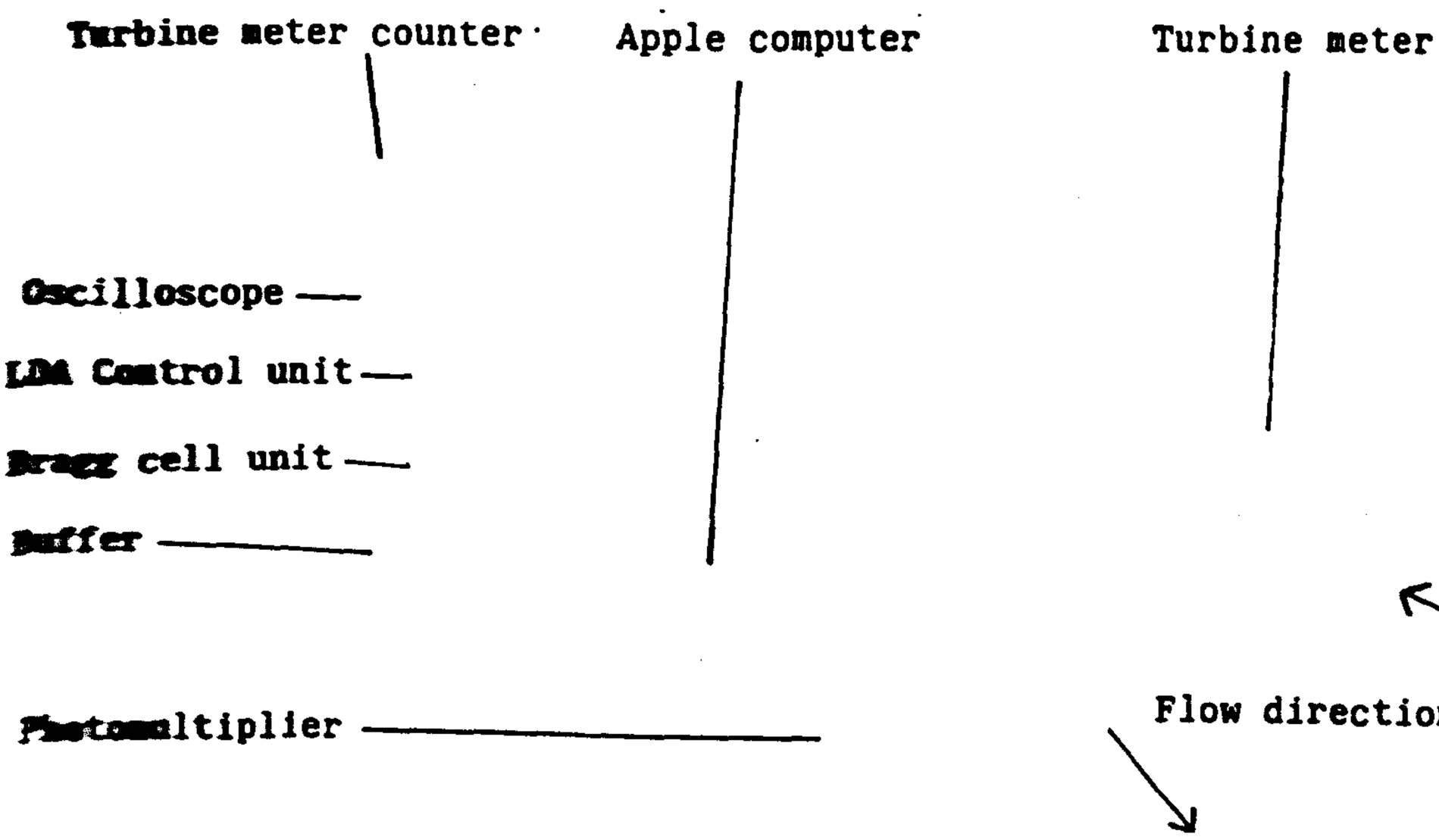
Turbine meter counter
Apple computer
Turbine meter
Oscilloscope
LDA Control unit
Bragg cell unit
Buffer
Photomultiplier
Flow direction

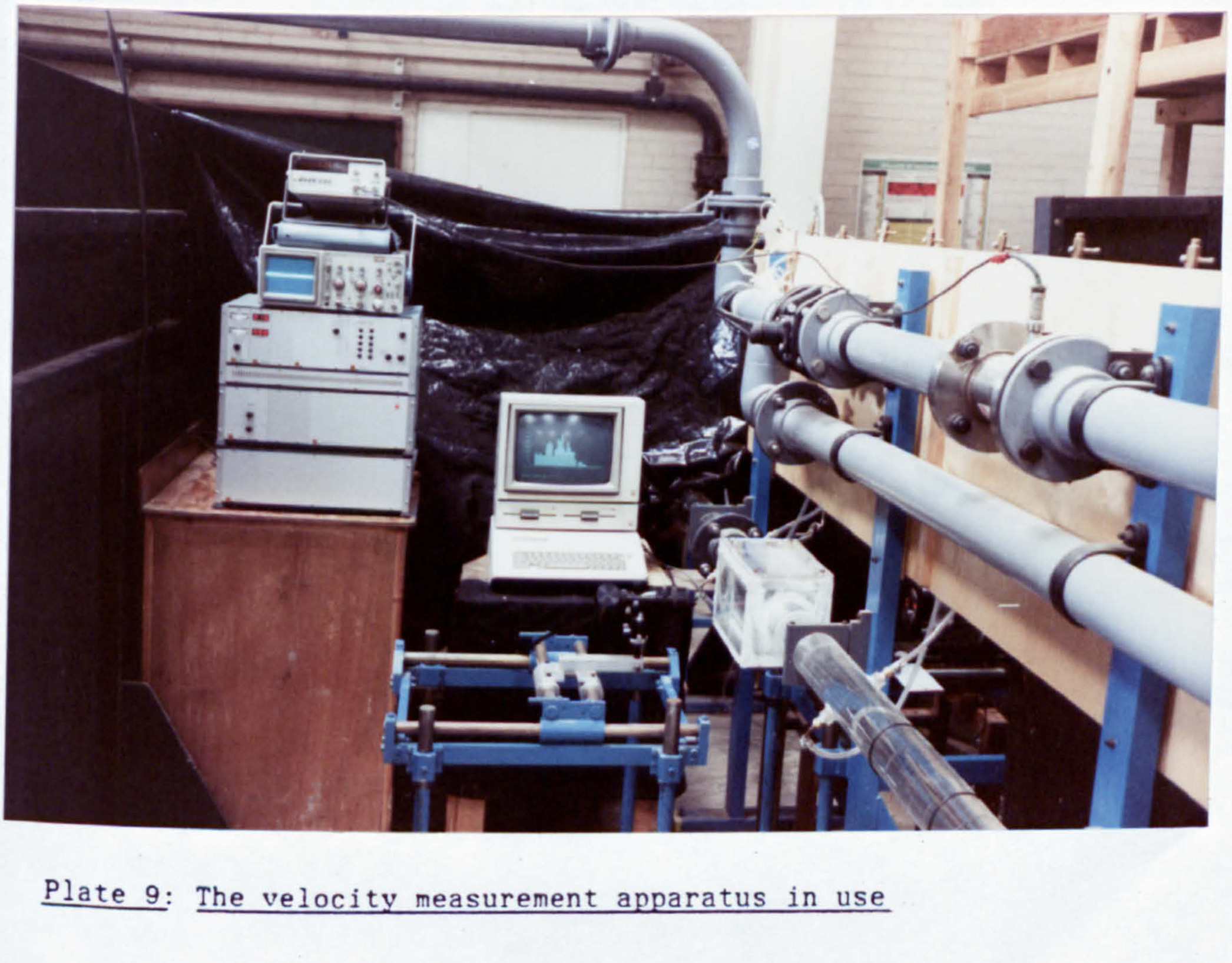

Plate 9: The velocity measurement apparatus in use

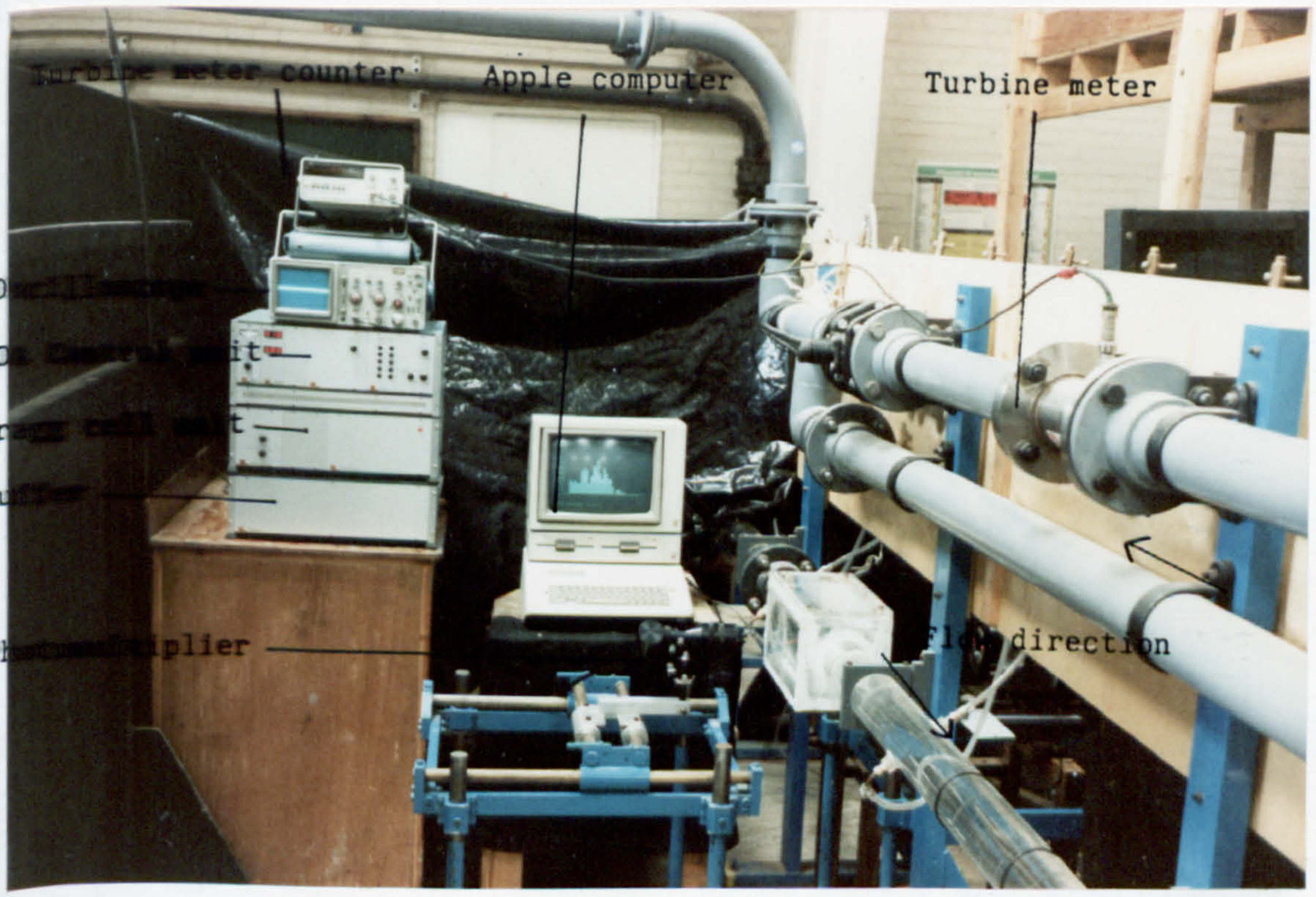

Plate 9: The velocity measurement apparatus in use